

# Modifications of Highway Air Pollution Models for Complex Site Geometries, Volume II: Wind Tunnel Test Program

FHWA-RD-02-037

SEPTEMBER 2002



U.S. Department of Transportation  
**Federal Highway Administration**

Research, Development, and Technology  
Turner-Fairbank Highway Research Center  
6300 Georgetown Pike  
McLean, VA 22101-2296



**Technical Report Documentation Page**

1. Report No. FHWA-RD-02-037	2. Government Accession No.	3. Recipient's Catalog No	
4. Title and Subtitle - Modifications of Highway Air Pollution Models for Complex Geometries-Volume II: Wind Tunnel Test Program		5. Report Date <b>September 2002</b>	
		6. Performing Organization Code:	
7. Author(s) R.E. Hayden, W.D. Kirk, G.P. Succi, T. Witherow, I. Boudierba, et. al.		8. Performing Organization Report No. R 8806-002-RD	
9. Performing Organization Name and Address Technology Integration and Development Group, Inc., Billerica, MA 01821 Subcontractors: Boston University, Boston, MA. 02215 Sigma Research Corp, Westford, MA -01886		10. Work Unit No.	
		11. Contract or Grant No. DTFH61-84-C-00104	
12. Federal Highway Administration, HRDI-09 TFHRC 6300 Georgetown Pike, Mc Lean, VA, 222101-2296 or Federal Aviation Administration, AEE300 800 Independence Avenue, SW, Washington D.C. 20591		13. Type of Report and Period Covered Final Report Vol. II - September 1984-July 1989	
		14. Sponsoring Agency Code	
15. Supplementary Notes Acknowledgements-- State Highway Agencies of Minnesota, New York, Texas, and Washington and New York City Department of Environmental Protection. FHWA Monitor-Howard A. Jongedyk HRDI-09, FAA Technical Monitor-Howard M. Segal, AEE-300			
16. Abstract This is volume II of a two-volume report of a study to increase the scope and clarity of air pollution models for depressed highway and street canyon sites. It presents the atmospheric wind tunnel program conducted to increase the data base and improves physical concepts of pertinent movements and mixing of air and its contaminants. Wind tunnel measurements are less costly than field measurements and are sensitive to controlled input variables. The first wind tunnel operations assured geometric, vortex structure, and upstream flow similarity and correct building wake and moving vehicle effects. Tracer gases from point, line, and moving vehicle sources were used appropriately. For wind tunnel models of depressed roads or street canyons hot-wire anemometer velocity and turbulence, pressure distribution and receptor point concentration measurements were made. Using a selected standard road model which had two dimensions and a width/ height (W/H) ratio of one effects of wind angle, local source location, added upwind cuts, vehicle speed, ambient wind speed, and the presence of upwind wall canopy were observed. Other two-dimensional tests involved changing the w/H ratios from 0.25 to 6.0, sloping the walls, slotted walls, walls of unequal heights, and curved roads. Three dimensional tests included end effects, intersections, and an added taller structure along one side of the road. Test results gave qualitative evaluations, concise tables, graphic illustrations, and qualitative concepts of wind flows and dispersion. Some findings include: (1) Wind flows and air pollution impacts are affected by W/H ratio, road curvature, and slope of walls, vehicle movements, and source locations. Slotted buildings upwind reduce impacts. (2) Air contaminant concentrations are reduced near intersections due to vertical vortices at corners (3) Simulations of five field sites by wind tunnel tests were satisfactory. Volume I is publication FHWA-RD-02-036, " Data Analyses and Model Development"			
17. Key Words: Air pollution, Street canyons, Highway Cut, Urban dispersion Models, Wind tunnel, turbulence		18. Distribution Statement No restrictions. This document is available to the public through the National Technical Information Service, Springfield, VA 22161.	
19. Security Classif. (Of this report) <b>Unclassified</b>	20. Security Classif. (of this Page) <b>Unclassified</b>	21. No of Pages <b>166</b>	22. Price

## SI\* (MODERN METRIC) CONVERSION FACTORS

APPROXIMATE CONVERSIONS TO SI UNITS					APPROXIMATE CONVERSIONS FROM SI UNITS				
Symbol	When You Know	Multiply By	To Find	Symbol	Symbol	When You Know	Multiply By	To Find	Symbol
<b>LENGTH</b>					<b>LENGTH</b>				
in	inches	25.4	millimeters	mm	mm	millimeters	0.039	inches	in
ft	feet	0.305	meters	m	m	meters	3.28	feet	ft
yd	yards	0.914	meters	m	m	meters	1.09	yards	yd
mi	miles	1.61	kilometers	km	km	kilometers	0.621	miles	mi
<b>AREA</b>					<b>AREA</b>				
in <sup>2</sup>	square inches	645.2	square millimeters	mm <sup>2</sup>	mm <sup>2</sup>	square millimeters	0.0016	square inches	in <sup>2</sup>
ft <sup>2</sup>	square feet	0.093	square meters	m <sup>2</sup>	m <sup>2</sup>	square meters	10.764	square feet	ft <sup>2</sup>
yd <sup>2</sup>	square yards	0.836	square meters	m <sup>2</sup>	m <sup>2</sup>	square meters	1.195	square yards	yd <sup>2</sup>
ac	acres	0.405	hectares	ha	ha	hectares	2.47	acres	ac
mi <sup>2</sup>	square miles	2.59	square kilometers	km <sup>2</sup>	km <sup>2</sup>	square kilometers	0.386	square miles	mi <sup>2</sup>
<b>VOLUME</b>					<b>VOLUME</b>				
fl oz	fluid ounces	29.57	milliliters	mL	mL	milliliters	0.034	fluid ounces	fl oz
gal	gallons	3.785	liters	L	L	liters	0.264	gallons	gal
ft <sup>3</sup>	cubic feet	0.028	cubic meters	m <sup>3</sup>	m <sup>3</sup>	cubic meters	35.314	cubic feet	ft <sup>3</sup>
yd <sup>3</sup>	cubic yards	0.765	cubic meters	m <sup>3</sup>	m <sup>3</sup>	cubic meters	1.307	cubic yards	yd <sup>3</sup>
NOTE: Volumes greater than 1000 l shall be shown in m <sup>3</sup> .									
<b>MASS</b>					<b>MASS</b>				
oz	ounces	28.35	grams	g	g	grams	0.035	ounces	oz
lb	pounds	0.454	kilograms	kg	kg	kilograms	2.205	pounds	lb
T	short tons (2000 lb)	0.907	megagrams (or "metric ton")	Mg (or "t")	Mg	megagrams (or "metric ton")	1.103	short tons (2000 lb)	T
<b>TEMPERATURE (exact)</b>					<b>TEMPERATURE (exact)</b>				
EF	Fahrenheit temperature	5(F-32)/9 or (F-32)/1.8	Celsius temperature	EC	EC	Celsius temperature	1.8C + 32	Fahrenheit temperature	EF
<b>ILLUMINATION</b>					<b>ILLUMINATION</b>				
fc	foot-candles	10.76	lux	lx	lx	lux	0.0929	foot-candles	fc
fl	foot-Lamberts	3.426	candela/m <sup>2</sup>	cd/m <sup>2</sup>	fl	candela/m <sup>2</sup>	0.2919	foot-Lamberts	fl
<b>FORCE and PRESSURE or STRESS</b>					<b>FORCE and PRESSURE or STRESS</b>				
lbf	poundforce	4.45	newtons	N	N	newtons	0.225	poundforce	lbf
lbf/in <sup>2</sup>	poundforce per square inch	6.89	kilopascals	kPa	kPa	kilopascals	0.145	poundforce per square inch	lbf/in <sup>2</sup>

\* SI is the symbol for the International System of Units. Appropriate rounding should be made to comply with Section 4 of ASTM E380.

(Revised March 2002)

## TABLE OF CONTENTS

### Volume II: Wind Tunnel Test Program

<u>Section</u>	<u>Title/Content</u>	<u>Page</u>
1.	<b>INTRODUCTION &amp; SUMMARY</b>	1
2.	<b>WIND TUNNEL MODELING APPROACH</b>	7
A.	<b>Criteria</b>	7
B.	<b>Experimental Procedures, Limitations, Precautions</b>	10
	Geometric Similarity	11
	Upstream Flow Field Similarity	11
	Building Wakes	12
	Moving Vehicles	12
	Vortex Structure	12
C.	<b>Test Facility and Test Procedures</b>	13
	Overview	13
	Boundary Layer Profile	15
	Instrumentation	18
	Definition of Flow Field Parameters	19
	Tunnel Velocity Calibration	19
	Dispersion Comparability Tests and Normalization Procedures	24
	Flow Visualization Procedure	25
D.	<b>Results of Initial Fluid Dynamic &amp; Parametric Tests</b>	25
	Overview	25
	Upstream Canyon Influence	26
	Reynolds Number Sensitivity	29
	Effect of Wind Directions	35
	Effect of Vehicle Speed	35
	Comparison of Line Source and Vehicle Source	38
3.	<b>OBSERVATIONS AND RESULTS RELATED TO DISPERSION IN 2-D STRAIGHT CANYONS</b>	41
A.	<b>Overview</b>	41
B.	<b>Analysis of Selected 2-D Straight Canyons</b>	41
	Standard Canyon, Width-to-Height Ratio = 1 (W/H = 1)	41



**TABLE OF CONTENTS (continued)**

<u>Section</u>	<u>Title/Content</u>	<u>Page</u>
	Standard Canyon with Canopy.....	52
	Slotted Canyons.....	56
	Different Width-to-Height Ratio Canyons.....	59
	Stepped Configurations.....	66
	Open Highway.....	74
	Uneven Height Canyon.....	74
	Isolated Tall Building above an Otherwise 2-D Block.....	79
	Sloping Canyons.....	79
	<b>C. Summary of 2-D Straight Canyon Results.....</b>	<b>87</b>
	Comparison of "Hot Spots" and "Averages".....	87
	Comparison of Vertical and Sloping Walls.....	89
	Trends of Different Width to Height Ratios.....	89
	Comparison of Open Highway and Stepped Terrain.....	93
<b>4.</b>	<b>OBSERVATIONS AND RESULTS RELATED TO DISPERSION IN STRAIGHT CANYON WITH CROSSCUTS AND INTERSECTIONS..</b>	<b>97</b>
	<b>A. Overview.....</b>	<b>97</b>
	<b>B. Analysis of Selected Crosscut Cases.....</b>	<b>97</b>
	2-D Canyons with Crosscuts.....	97
	Influence of Vehicle Speed.....	101
	Effect of Crosscut Width.....	101
	Effect of Cross Flows on Crosscut Intersections.....	101
	Effect of a Three-Way ("T") Intersections.....	106
	<b>C. Summary of Crosscut Results.....</b>	<b>109</b>
<b>5.</b>	<b>OBSERVATIONS AND RESULTS RELATED TO DISPERSION IN CURVED CANYONS.....</b>	<b>111</b>
	<b>A. Overview.....</b>	<b>111</b>
	<b>B. Analysis of Selected Curved Canyon Data.....</b>	<b>111</b>
	Narrow Curved Canyon (W/H = 1.0): 0° Wind Direction.....	111
	Narrow Curved Canyon (W/H = 1.0): 180° Wind Direction.....	121
	Wide Canyon (W/H = 2.43): 0° Wind Direction.....	121
	Wide Canyon (W/H = 2.43): 180° Wind Direction.....	122

TABLE OF CONTENTS (continued)

<u>Section</u>	<u>Title/Content</u>	<u>Page</u>
	<b>C. Comparison of Curved Canyon Results.....</b>	<b>122</b>
	Effect of Canyon Width:	
	0' Wind Direction.....	122
	Effect of Canyon Width:	
	180' Wind Direction.....	125
	Effect of Slotted Airport Terminal:	
	0' Wind Direction.....	125
	Effect of Slotted Airport Terminal:	
	180' Wind Direction.....	125
	<b>D. Summary of Curved Canyon Results.....</b>	<b>129</b>
<b>6.</b>	<b>OBSERVATIONS AND RESULTS RELATED TO DISPERSION IN SPECIFIC URBAN SITES.....</b>	<b>130</b>
	<b>A. Overview of Tests on Nonspecific Urban Sites...</b>	<b>130</b>
	<b>B. Analysis of Urban Sites.....</b>	<b>130</b>
	University Avenue Site, St. Paul, Minnesota.....	130
	Warren Street Site, Syracuse, New York.....	137
	Park Avenue and 52nd Street Site, Manhattan, New York.....	140
	<b>C. Summary of Trends in Dispersion Measurements at Urban Sites.....</b>	<b>140</b>
<b>7.</b>	<b>SUMMARY .....</b>	<b>150</b>
	<b>A. Conclusions.....</b>	<b>150</b>
<b>8.</b>	<b>REFERENCES.....</b>	<b>155</b>



## LIST OF FIGURES

<u>Figure No.</u>	<u>Page</u>
1. Schematic of typical test setup.....	2
2. Schematic views of Boston University Atmospheric Boundary Layer Wind Tunnel.....	14
3. Dimensions of model vehicles used on moving-belt source.....	16
4. Plan view of wind tunnel test section.....	20
5. Side view of wind tunnel test section.....	21
6. Probe layout for velocity test with typical urban canyon in place.....	22
7. Results of mean flow and turbulence survey above model urban setting $W/H = 1$ .....	23
8. Coordinate system for 2-D and 3-D canyons.....	27
9. Geometry for tests of upstream canyon effect.....	28
10. Dispersion results for number of upstream block variations of a model urban setting, $W/H = 1$ .....	30
11. Configuration for Reynolds number tests with line source.....	31
12. Results for Reynolds number study with line source.....	32
13. Configuration for Reynolds number test with moving vehicles.....	33
14. Dispersion results for Reynolds number test with moving vehicles.....	34
15. Test setup for studying effect of wind direction, $W/H = 1$ .....	36
16. Results of wind direction effects for two different vehicle speeds.....	37
17. Test setup for source comparison.....	39
18. Dispersion results of wind direction effects or two different vehicle speeds.....	40
19. Test setup and probe locale for standard canyon configurations, $W/H = 1$ .....	48
20. Results of standard canyon configurations, $W/H = 1$ .....	49
21. Flow structure of a standard 2-D canyon.....	50
22. Effect of vortex rotational frequency with increasing gradient velocity, $W/H = 1$ .....	51
23. Effect of vehicle speed at different wind directions in a standard canyon, $W/H = 1$ .....	53
24. Test setup for canopy configurations.....	54
25. Effect of a canopy placed at half height.....	55
26. Effects of a porous walled canyon, $W/H = 1$ .....	57
27. Combined effects of porous walled canyon vs. standard canyon.....	58

**LIST OF FIGURES (continued)**

<u>Figure No.</u>	<u>Page</u>
28.	Flow visualization of width/height ratios from 0.25 to 1.0.....60
29.	Flow visualization of width/height ratios from 1.0 to $\infty$ .....62
30.	Test setup and point locale for different width/height ratios.....63
31.	Effect of different width/height ratios.....64
32.	Effect of a deep canyon (W/H = 0.25) at different wind directions.....65
33.	Effect of vehicle in a wide canyon configuration W/H = 2.....67
34.	Test setup and point locale for stepped terrain.....68
35.	Effect of stepped terrain configurations.....69
36.	Effect of vehicles near a downstream facing step.....70
37.	Vertical dispersion trends for a downstream facing step.....71
38.	Lateral dispersion trends for a downstream facing step.....72
39.	Effect of vehicles near an upstream facing step.....73
40.	Pollution dispersion downwind of an open highway.....75
41.	Test setup and point locale for uneven height walled canyons.....76
42.	Effect of uneven height walled canyons.....77
43.	Effect of vehicles on a taller downstream walled canyon.....78
44.	Flow visualization of a tall building placed with a standard canyon configuration.....80
45.	Plan view of cross sections behind a tall building at 0 and 30° wind direction.....81
46.	Comparison center and wall receptors at 0 and 30° wind direction for a tall building configuration (4H above W/H = 1 canyon).....82
47.	Concentration levels in a 2-D canyon near a tall building at 0°.....83
48.	Concentrations of a 2-D canyon near a tall building at 30°.....84
49.	Test setup and point locale for sloping canyon configuration.....85
50.	Effect of sloping canyon configurations at 0 and 30° wind direction.....86
51.	Comparison of "hot spots" and "averages" in different 2-D canyon configurations.....88
52.	Test setup and probe locale for vertical and sloped walled canyon configuration.....90



LIST OF FIGURES (continued)

<u>Figure No.</u>	<u>Page</u>
53. Comparison of vertical and sloped walled canyon configurations.....	91
54. Comparison of different width to height ratios.....	92
55. Comparison of open highway and downstream steps.....	95
56. Comparison of open highway, downstream step and standard canyon.....	96
57. Flow visualization of an intersected canyon with crosscut twice the canyon height and width, $C/H = 2.0$ .....	99
58. Concentration in a 2-D canyon with vehicles near a crosscut, $C/H = 1.00$ .....	100
59. Effect of vehicle speed near a crosscut.....	102
60. Effect of distance from a crosscut intersection, $C/H = 0.5, C/H = 2.0$ .....	103
61. Comparison of cross section for crosscuts at 0 degrees, $C/W = 0.5, 2.0$ .....	104
62. Concentration in 2-D canyon at $45^\circ$ wind direction near a crosscut.....	105
63. Flow visualization of a "T" intersection, $C/W = 1.00$ .....	107
64. Comparison of cross sections in a "T" intersection.....	108
65. Concentration levels near a "T" intersection at 0 and $30^\circ$ .....	110
66. Plan view of different curved canyon configurations at $0^\circ$ .....	114
67. Coordinate system for curved canyons.....	115
68. Concentrations in a curved canyon, $W/H = 1.0$ , wind azimuth = $0^\circ$ .....	116
69. Concentrations in a curved canyon, $W/H = 1.0$ , wind azimuth = $180^\circ$ .....	117
70. Concentrations in a curved canyon. $W/H = 2.43$ , wind azimuth = $0^\circ$ .....	118
71. Concentrations in a curved canyon. $W/H = 2.43$ , wind azimuth = $180^\circ$ .....	119
72. Flow visualization for narrow and wide curved canyons at $0^\circ$ wind direction.....	120
73. Flow visualization for narrow and wide curved canyons at $180^\circ$ wind direction.....	123
74. Concentration mapping for narrow and wide curved canyons at $0^\circ$ wind direction.....	124
75. Concentration mapping for narrow and wide curved canyons at $180^\circ$ wind direction.....	126
76. Concentration mapping for slotted and solid walled airport terminals at $0^\circ$ wind direction.....	127

LIST OF FIGURES (continued)

<u>Figure No.</u>		<u>Page</u>
77.	Concentration mapping for slotted and solid walled airport terminals at 180° wind direction..	128
78.	Perspective view of University Avenue, St. Paul, MN.....	131
79.	Perspective view of Warren Street, Syracuse, NY..	132
80.	Perspective view of Park Avenue, New York, NY....	133
81.	Plan view of St. Paul, MN with receptor concentrations and location.....	134
82.	Plan view of Syracuse, NY with receptor concentrations and location.....	138
83.	Plan view of Manhattan with receptor concentrations and location.....	141
84.	Comparison of concentration hot spots and averages in 2-D canyons and urban sites.....	142
85.	Concentration levels near source in St. Paul at 0 and 30° wind directions.....	146
86.	Concentration levels near source in Syracuse at 0 and -30° wind direction.....	147
87.	Concentration levels near source in Manhattan at 0 and 30° wind direction.....	149



**LIST OF TABLES**

<u>Table No.</u>		<u>Page</u>
1.	Vehicle spacing.....	17
2.	Data file cross reference for 2-D straight canyons (canyons of different widths).....	42
3.	Data file cross reference for 2-D straight canyons (standard canyons with variations).....	43
4.	Data file cross reference for 2-D straight canyons (stepped topography) (sloping canyons).....	44
5.	Data file cross reference for 2-D straight canyons (slotted canyons).....	45
6.	Table of x, z, coordinates for straight canyon test configuration, Standard canyon height (H) = 3.50 in (8.89 cm).....	46
7.	Data file cross reference for data from crosscut and intersection tests.....	98
8.	Data file cross reference for data from curved canyon configurations.....	112
9.	Table of x, z coordinates for curved canyon test configuration(s) curved canyon height (H) = 3.50 in.....	113
10.	Urban city configurations.....	135
11.	University Avenue site, St. Paul, MN (10 highest concentrations).....	136
12.	Warren Street site, Syracuse, NY (10 highest concentrations).....	139
13.	Park Avenue site, New York, NY, (10 highest concentrations).....	143
14.	"Hot spot" summary.....	145

## 1. INTRODUCTION AND SUMMARY

The dispersion of vehicular emissions in complex urban sites involves complex fluid mechanical interactions, which are dominated by the flow fields of wind interaction with buildings, highway cuts, bridges, etc., which comprise the urban landscape. These flow fields can be simulated in properly-designed atmospheric boundary layer wind tunnels.

This wind tunnel test program was designed to provide measurements of tracer gas concentrations around a wide variety of idealized urban street canyons and highway cuts, as well as measurements of those parameters which affect dispersion of vehicular pollutants, in sufficient detail to allow analytical or computational predictions to be made using modifications of existing algorithms.

The test program was intended to first resolve several open issues (from the literature and other related model and full scale tests), and then proceed with studies of the effects of configuration variations on dispersion of vehicular pollution. A schematic of the wind tunnel model apparatus and sensors is shown in figure 1. Buildings which create "canyons" were simulated by two- and three-dimensional (2-D and 3-D) blocks whose height and separation could be easily changed. The apparatus included means for changing the relative direction of the incoming wind with respect to the simulated urban configurations. Provision for injecting small concentrations of tracer gas (simulating emissions) was made through a movable point source, a 2-D slot (line source) in the floor of the instrumented canyon, and through scaled vehicles on a moving belt. Sensors included single wire hot wire probes, which could be located near the canyon floor or elsewhere, and numerous concentration sampling tubes, all connected to a multichannel gas sample acquisition system.

Configuration variables included:

### 2-D straight canyons:

- Width-to-height ratio.
- Standard canyon with canopy.
- Porosity of one block (simulating a parking garage).

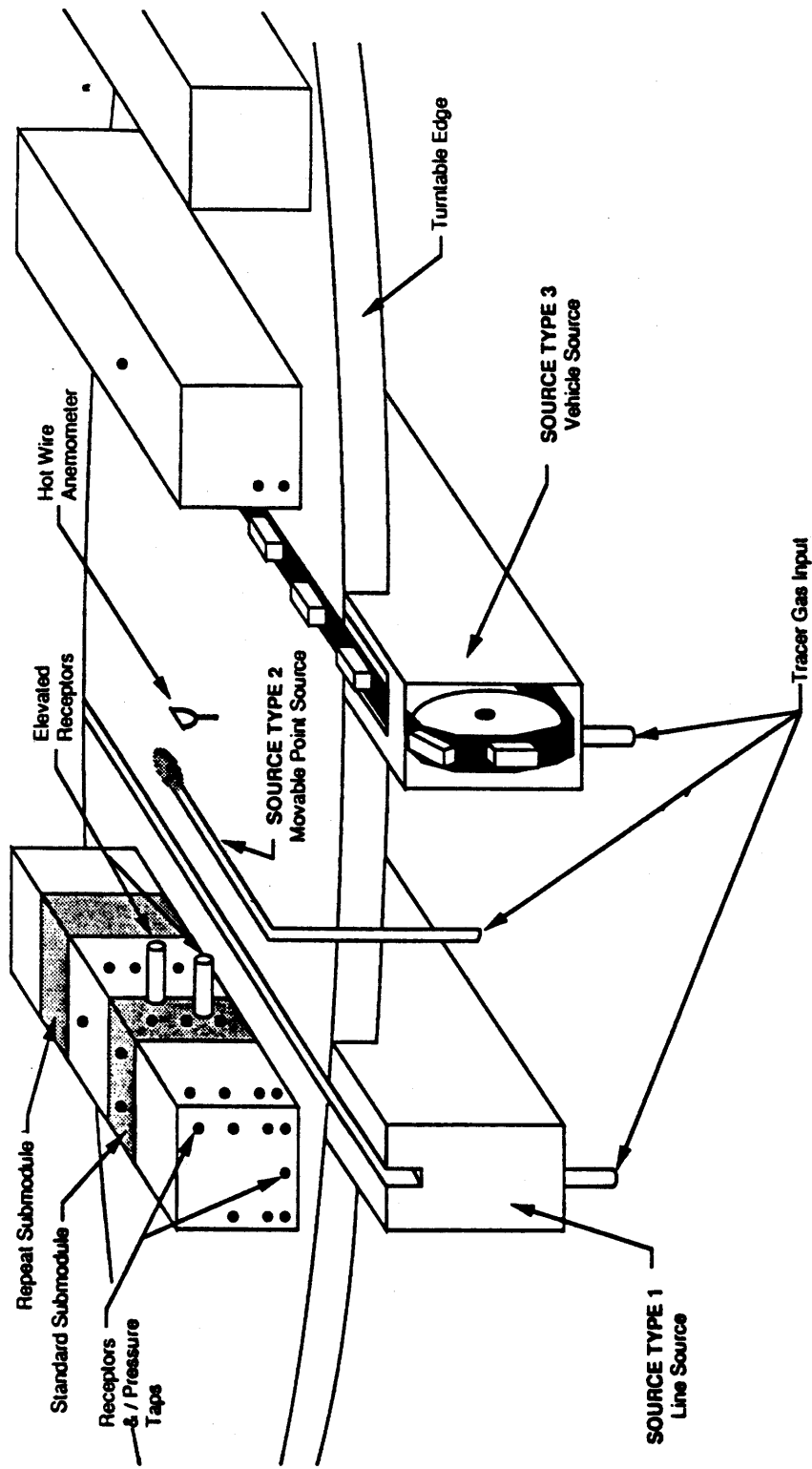


Figure 1. Schematic of typical test setup.

- Sloping walls (cut sections).
- Uneven height buildings.
- Stepped terrain.

**3-D rectangular canyons:**

- Intersections of various widths.
- Intersections with cross wind.
- Isolated tall building in a 2-D block.

**Semicircular canyons:**

- Width-to-height ratio.
- Porous inner wall simulating a typical airport terminal/parking garage configuration.

**Specific urban sites accurately modeled:**

- Katy Freeway cut section, Houston, Texas.
- Warren Street Area, Syracuse, New York.
- St. Paul, Minnesota.
- Midtown Manhattan, New York City.

This data was taken and analyzed for geometries of increasing complexity. The interpretation of this data, in the context of the relevant physical parameters is included in a predictive model. This model is contained in volume I of the report. Volume II of this report provides a graphic exploration of important characteristics of the flow fields and the effects of the primary configuration variables on the resultant concentration levels and distributions. Turbulence and mean flow data is also reported: this data is of primary use in developing and applying the CPB-3 model described in volume I.

This report refers to several data bases which provide the detailed description of each configuration tested, the exact sensor locations, tabular data, and graphic summaries. These data bases provide the reader a resource if additional clarification is needed, a means of checking calculations, and an empirical means of estimating pollution concentrations for specific cases which might be beyond the capabilities of the CPB-3 or other models.

Some key findings of this test program are as follows:

**2-D Canyons:**

- Concentration levels and distribution depend upon source location within the canyon.

- Maximum concentrations occur in the lowest velocity zones, such as near the street level on the upwind side of the canyon.
- Vehicle movements may have a significant effect upon the maximum concentration levels, especially in canyons with  $W/H > 1.0$ .
- Wind direction changes  $\pm 30^\circ$  from the crosswind condition reduce concentrations roughly in proportion to the cosine of the crosswind direction.
- Width-to-height ratio has a profound effect on concentration levels and distributions.
- Sloping canyon (or cut) walls create substantial ventilation of the "canyon" leading to concentration patterns characteristic of open highways.
- The presence of a slotted (or porous) wall or building on the upstream or downstream side of a line source leads to "communicated" pollutants through the slotted building; when the slotted building is on the upwind side of the source, emissions travel through the upwind slotted building (if there is another canyon upwind); while when the slotted building is on the downwind side of the line source, there is relatively little communication of the emission from one canyon to the other (relative to the case where both buildings are solid).
- A "canopy" on the upwind building increases concentration levels in the canyon center. When the wind has longitudinal velocity components the concentrations are reduced along the upstream as well as the downstream canyon walls.

### **3-D Rectangular Canyons:**

- Intersections are well ventilated, and thus have lower normalized concentration levels than their 2-D counterparts.
- The effect of an intersection on the concentrations in the intersecting crosswind 2-D canyons is "felt" for a distance of approximately four canyon widths back from the intersection in a  $90^\circ$  crosswind; in nonperpendicular crosswinds, the effect on the intersecting canyons is more complex, but still substantial



- An isolated tall building in an otherwise 2-D block creates a "hotspot" at its base on the downwind side, and mitigates concentrations in the upwind canyon near its face.

#### **Semicircular Canyons:**

- Pollution dispersion pattern is highly 3-D with location of peaks being a function of wind direction and width-to-height ratio.
- At the apex of the curves, the canyon dispersion resembles the 2-D straight canyon dispersion patterns.
- Along the curved canyons, the flow turns to the direction parallel to the oncoming flow where clean air mixes and reduces the concentrations.

#### **Specific Urban Sites:**

- Katy Freeway, Houston, Texas, has an open sloping wall cut section and experiences low pollution levels relative to straight walled sections.
- St. Paul, MN is characterized by wide canyons with downwind-facing steps. The city blocks are long with relatively few crosscuts. The concentration hot spots occur in areas where 2-D-like flow occurs.
- Syracuse, NY is characterized by variations of the  $W/H=1$  canyon, with height ratios among buildings in the 0.5 to 1.5 range. The canyons have relatively long blocks which promote local 2-D flow behavior, and associated concentration patterns.
- Midtown Manhattan, New York is characterized by tall buildings and "slab" buildings with frequent crosscuts; the city blocks are relatively short, which reduces the extent of 2-D flow and promotes 3-D flows.

#### **Organization of the Balance of This Report**

Section 2 describes the criteria and procedures for wind tunnel modeling of urban winds and pollution dispersion, the wind tunnel facility used, and a survey of the initial tests performed to define the effects of certain key parameters.

Sections 3-6 describe highlights of the concentration data taken for each of the above classes of urban geometries. The

aforementioned included: section 3, detailing 2-D straight canyons; section 4, detailing 3-D intersected canyons; section 5, detailing curved canyon with simulated airport terminal/garages configurations; and section 6, detailing three specific urban site configurations. In addition, drawings from the flow visualization are included to further clarify the flow dynamics.

Section 7 provides a summary and includes findings and conclusions of this study, especially as it deals with the wind tunnel test program. Volume I results also reflect findings of the wind tunnel test program.

There are five data-related collections of data for volume II. These contain detailed descriptions and summaries of each test performed. These data bases include: I, straight and intersected canyon data; II, curved canyon geometries; III, urban city configurations; IV, wind velocity data for straight and curved canyons; and V, parametric and initial studies.

References are given at the end of this volume.

## 2. WIND TUNNEL MODELING APPROACH

### A. Criteria

Physical or analytical modeling of dispersion processes must replicate or account for all-important physical phenomena. The primary justification for wind tunnel fluid modeling is that it provides the most effective means for simulating flow field phenomena associated with atmospheric boundary layer interaction with complex structures and topography. Furthermore, the wind tunnel allows one to control and vary parameters which are not independently or conveniently controllable in full scale, thus providing a means for systematic sensitivity studies, which is indeed the appropriate characterization of the present study.

However, as wind tunnels can only provide approximate and partial replication of full scale conditions, the most important physical similarity parameters must be preserved. Among the important parameters are:

- (1) Geometric similarity of building and terrain topography features.
- (2) Average surface roughness length and resultant vertical distributions of mean velocity, turbulence intensity and length scales, and Reynolds stress.
- (3) Reynolds number;  $Re = U_R L/\nu$  where  $U_R$  is a reference flow velocity,  $L$  is the characteristic geometric length scale, and  $\nu$  is the fluid's kinematic viscosity (momentum diffusivity).
- (4) Rossby number;  $Ro = U_R /L\Omega_R$  where  $U_R$  and  $L$  have their previous meanings and  $\Omega_R$  is a reference angular velocity.
- (5) Froude number;  $Fr = U_R (gL \sigma T_R/T_0)^{-0.5}$  where  $g$  is the gravitational constant,  $T_0$  is the temperature of the adiabatic atmosphere, and  $\sigma T_R$  is the temperature deviation from  $T_0$ .
- (6) Peclet number;  $Pe = U_R Lk$ , where  $k$  is the fluid's thermal diffusivity.
- (7) Reynolds-Schmidt number;  $Re-Sc = U_R L/\alpha$  where  $\alpha$  is the molecular diffusivity.

The modeling of these similarity parameters has been the subject of extensive analytical laboratory and field studies. There is now a reasonable consensus on the relative importance

of most parameters in the context of the type of study described herein. A detailed review of the trade-offs is summarized in the so-called Environmental Protection Agency (EPA) Fluid Modeling Guidelines, which were derived through extensive consultation with and input from a broad spectrum of research professionals and application specialists (Snyder, 1981). Some essential conclusions are discussed below:

#### **Reynolds Number**

In their "Fluid Modeling Guidelines," the EPA has established that, for sharp-edged geometries, the flow over significant elevated terrain and buildings near the source is Reynolds number independent if the Reynolds number.  $Re = U_H L / \nu$  is greater than 11,000.  $U_H$  is the mean velocity upstream at the height of the obstacle  $H$ ,  $L$  is the lesser dimension of the obstacle, and  $\nu$  is the kinematic viscosity of the air.

#### **Rossby Number**

Rossby number is not a critical modeling parameter since the extent of this study represented typical full-scale distances of 1 km (1.62mi) or less.

#### **Froude Number**

For adiabatic (neutral) atmospheric flows, the Froude number is infinite, corresponding to negligible buoyancy forces. Adiabatic atmospheric flows are adequately modeled by maintaining isothermal flow in the test facility. The atmospheric boundary layer wind tunnel used for this study is an open circuit one placed in a large room. Hence, isothermal flow can be readily established. However, finite Froude numbers exist locally due to the elevated temperature of automotive exhausts. Thus a correction for the mean temperature and buoyancy of the canyon flow may be appropriate in the analytical model (volume I). However, for this wind tunnel study, the overriding concern was to develop a heretofore unavailable set of detailed flow and dispersion data consistent with the analytical model requirements, and to explore as many basic configuration variables as possible. Therefore, heated exhausts were not simulated, although the techniques for doing so are well known.

#### **Peclet Number and Reynolds-Schmidt Number**

Molecular and thermal diffusion are believed to contribute negligibly to dispersion within the simulated atmospheric boundary layer, provided the Reynolds number is sufficiently high. The Peclet number and the Reynolds-Schmidt number are then unimportant.

Thus, we are left with a shorter list of similarity parameters to consider; namely items (1), (2), (3), and (5) from the above list. Among these, only the model scale Reynolds number will be far from its full-scale value. However, with appropriate care, the gross flow field features of the atmospheric boundary layer and building wakes can be replicated in model scale. Buoyancy effects in street canyons have not been systematically studied, but Kitahayashi, et al. (1976) found that ambient stability had little effect on street canyon dispersion.

In terms of the canyon flow itself, we should further impose the criterion that the structure of the microscale flow therein replicate full-scale conditions. This raises the issue of moving vehicle effects, canyon surface detail, and vortex structure (primary and secondary). It has already been shown that for some situations, moving vehicle effects are important in determining maximum concentrations and concentration distribution in and about street canyons (Lombardi, 1978, Kitahayashi, et al., 1976, Skinner and Ludwig, 1976, Chock, 1982, Leisen and Sobottka, 1980, and Builtjes, 1984). The locally-energetic flow fields generated by vehicles cause significant initial mixing of the emissions and presumably disrupt the secondary vortex flows. Concentration reduction by a factor of two has been consistently observed when vehicles exceed a certain speed relative to the superimposed wind speed. However, it is difficult to generalize vehicle flow mixes and speeds.

Simulating the detailed structure of the coherent canyon flow ("vortex") presents a difficult problem if the model scale vortices do not replicate full-scale conditions. In general, coherent vortices at low Reynolds number are much more compact and less turbulent than their full-scale counterparts. This is common experience in aircraft and helicopter tip vortex studies and can also be deduced from flow visualizations of model scale urban environments. The consequences of this effect will be high concentrations in the vortex core in the scale model and unrealistically low concentrations elsewhere in the flow field. Such effects could seriously limit the quantitative utilization of model results. Factors which are known to minimize the tendencies of low Reynolds vortices to "roll-up" too tightly are upstream turbulence and local roughness.

Thus, as a minimum, it is vital to include an appropriate simulation of the upstream flow field and local roughness before proceeding with detailed parametric studies. Vortex similarity can be inferred indirectly by observing velocities or concentrations at a large number of locations while varying Reynolds number.



A limited study of that nature was reported by Hoydysh, et al. (1974) in which they deduced that the street flow pattern was independent of Reynolds number when the Reynolds number  $UH/v$  was greater than 3400 ( $H$  = building height). This value is a factor of 3.2 lower than subsequently recommended by EPA (Snyder, 1981). Subsequent studies (such as Builtjes, 1984), show variations in concentration and flow patterns for certain situations (configurations) which suggest that the Hoydysh, et al. result may not be generally applicable. What is clearly needed is a more definitive look at the scaling effects on the all-important canyon flow structure so that one may utilize results of configuration variation studies with a known degree of confidence. In this program, we conducted an initial study phase which explored Reynolds number effects by varying gradient velocity and, as mentioned above, other issues related to the accurate modeling of street canyon flows in the presence of moving vehicles.

In summary, street canyon dispersion modeling in wind tunnels must provide:

- (1) Geometric similarity.
- (2) Upstream flow field similarity.
- (3) Correct building wake effects (i.e., high enough Reynolds number to produce flow fields similar to full scale).
- (4) Simulation of moving vehicle effects, where appropriate.
- (5) Vortex structure similarity.

Second order effects which can be omitted include simulation of ambient stabilities other than neutral Rossby number similarity, and explicit replication of the Peclet and Reynolds-Schmidt numbers with the stipulation that requirements (2) and (3) above are satisfied. The principal concern arising from experience to date and other related disciplines is the possible dissimilarity in the street canyon vortex structure due to Reynolds number effects. This issue was explored at the outset of the test program and is discussed below.

#### **B. Experimental Procedures, Limitations, Precautions**

Procedures for satisfying the above modeling requirements are now briefly described.

### Geometric Similarity

Geometric similarity is achieved when the scaled topography and buildings are constructed in correct proportions to their full-scale counterparts. For this study, the only constraint is that the penetration of the building models into the scaled boundary layer be realistic; i.e., if the model scaled boundary layer has a thickness of 1 m (3.3 ft), which is representative of 200-400 m (656-1312 ft) if full scale, then the dimensions of scaled canyons should be 1/300 to 1/400 times their typical full-scale values so that the structure of the turbulent flow approaching the canyon is realistic. Using a scale factor of 1/400, the minimum velocity required to meet the EPA criterion of a minimum Reynolds number of 11,000 can be estimated for typical urban block heights:

<u>Height</u>	<u>Minimum Velocity</u>
4 story	4.2 m/s (14 ft/s)
10 story	1.9 m/s ( 6 ft/s)
30 story	0.7 m/s ( 2 ft/s)

This constraint may be relaxed a bit, if necessary, to facilitate flow visualization and insertion of dense arrays of instrumentation.

### Upstream Flow Field Similarity

Rigorous procedures for establishing for field similarity have been established by the EPA (Snyder, 1981). The test facility utilized in this study complies with those requirements. Upstream flow field similarity is achieved by a long, slowly diverging duct which has roughness elements distributed along the floor of the tunnel. The roughness elements may be varied in size and spatial density in accordance with the scale of the model and the profile which one is attempting to replicate. In some cases, where a thick boundary layer is needed, spires are placed at the entrance of the tunnel to provide an initial thickening of the boundary layer and introduction of large scale turbulence. The model may be mounted on a motorized turntable to simulate changes in wind direction; roughness elements can be seen upstream of the turntable, with spires placed at the entrance to the flow conditioning section. A check of the pressure gradient down the tunnel is made to ensure that no regions of strong gradients exist. The roughness distribution or the position of the roof of the tunnel can be adjusted to give zero pressure gradient along the tunnel axis.

To establish that flow field similarity exists, mean velocity and turbulence profiles are taken with multiple hot-wire anemometers along the centerline of the tunnel and at several spanwise locations just upstream of the test section, across the test section and downwind of the test section. Shear stress ( $-uw$ ) profiles are generally measured at the upstream locations and, if required, at other locations. For dispersion measurements, a "dispersion comparability" test is carried out in which an isokinetic point release of tracer gas is made at several heights in the boundary layer just ahead of the test area. Downwind Y-Z cross sections of concentration are measured with an array of receptors to establish that the dispersion characteristics are appropriate to the stability selected (Pasquill Gifford categories, C-D, in this case).

In the Boston University facility, an 80-channel simultaneous gas sampling system was available for rapid acquisition of samples from large arrays of sensors.

If the above measurements demonstrate that the flow simulation is appropriate, experiments proceed; otherwise, adjustments in roughness may be necessary. Once satisfactory flow field modeling has been achieved, velocity and temperature sensors are positioned at several locations in the test section for monitoring of reference velocity and temperature uniformity during testing.

#### Building Wakes

If the upstream flow similarity conditions are met throughout the velocity range of the proposed tests, building wakes are usually satisfactorily replicated if sharp-edged models are used; occasionally, the addition of surface roughness or trip wires may be appropriate when rounded and/or smooth surfaces exist. In this study, sharp-edged blocks were used.

#### Moving Vehicles

For some tests, moving vehicles were simulated with a moving belt upon which scale model vehicles were placed at various spacings. A variable speed reversible drive facilitates speed changes and direction reversals. The apparatus was integrally-mounted in the turntable along with the emission apparatus and sensor arrays so that wind direction changes can be simply and quickly carried out.

#### Vortex Structure

Vortex structure was explored over the range of Reynolds numbers available in the wind tunnel. A 2-D configuration was

selected which is representative of the range of width-to-height ratios to be tested. Flow visualization was used to observe the vortex structure and a rotation speed ratio was measured through frame-by-frame timing of the vortex rotations.

Additional methods to measure vortex strength include pressure distribution and hot-wire studies. Wise, (1971) showed that the characteristic velocity above the ground in a stable street canyon vortex could be correlated ( $R = 0.93$ ) with the pressure differential between the lee upwind face of the downwind building and the luv (downwind) face of the upwind building, and the velocity profile of the approaching flow. This finding is important since the detailed pressure distribution on faces of buildings and the ground is more easily measured than a detailed velocity distribution. This is particularly true when many wind direction or configuration changes are envisioned. Thus, the pressure distribution technique was also used in the preliminary phases of this study. Reynolds number was varied by changing both the free stream velocity and the actual dimensions of the configuration, thus providing a redundant check on the effects observed. The gradient wind speed ranged from approximately 0.5 m/s to 10 m/s (2 ft/s to 33 ft/s). The geometric scale factor cannot be varied over such a wide range without violating the constraint of excessive penetration into the boundary layer and without introducing 3-D effects of the tunnel walls.

### **C. Test Facility and Test Procedures**

#### Overview

The tests were carried out in the Atmospheric Boundary Layer Wind Tunnel at Boston University, Boston, Massachusetts, illustrated in figure 2. This tunnel is 60 ft (18 m) long. The tunnel is designed to develop a boundary layer similar to that of steady airflow over the earth's surface. The variation of mean velocity with height can be determined. The variation of mean velocity with height can be described by  $V/V_g = (Z/Z_g)^\alpha$ , where  $\alpha$  can be set to the desired value. The tunnel is calibrated to ensure flow dispersion characteristics are comparable to field condition described by the EPA (Snyder, 1981). The EPA comparability is designed to ensure that the dispersion of a free plume in the tunnel corresponds to the Pasquill Gifford neutral plume dispersion category C to D. An additional set of tests was done (figure 2) to certify that velocity profile uniformity is acceptable over the entire working test section. A schematic of the test configuration is illustrated in figure 1. The urban canyon is modeled using a set of square section metric blocks (3 1/2 in by 3 1/2 in (8.89 cm by 8.89 cm)) which span the tunnel width.

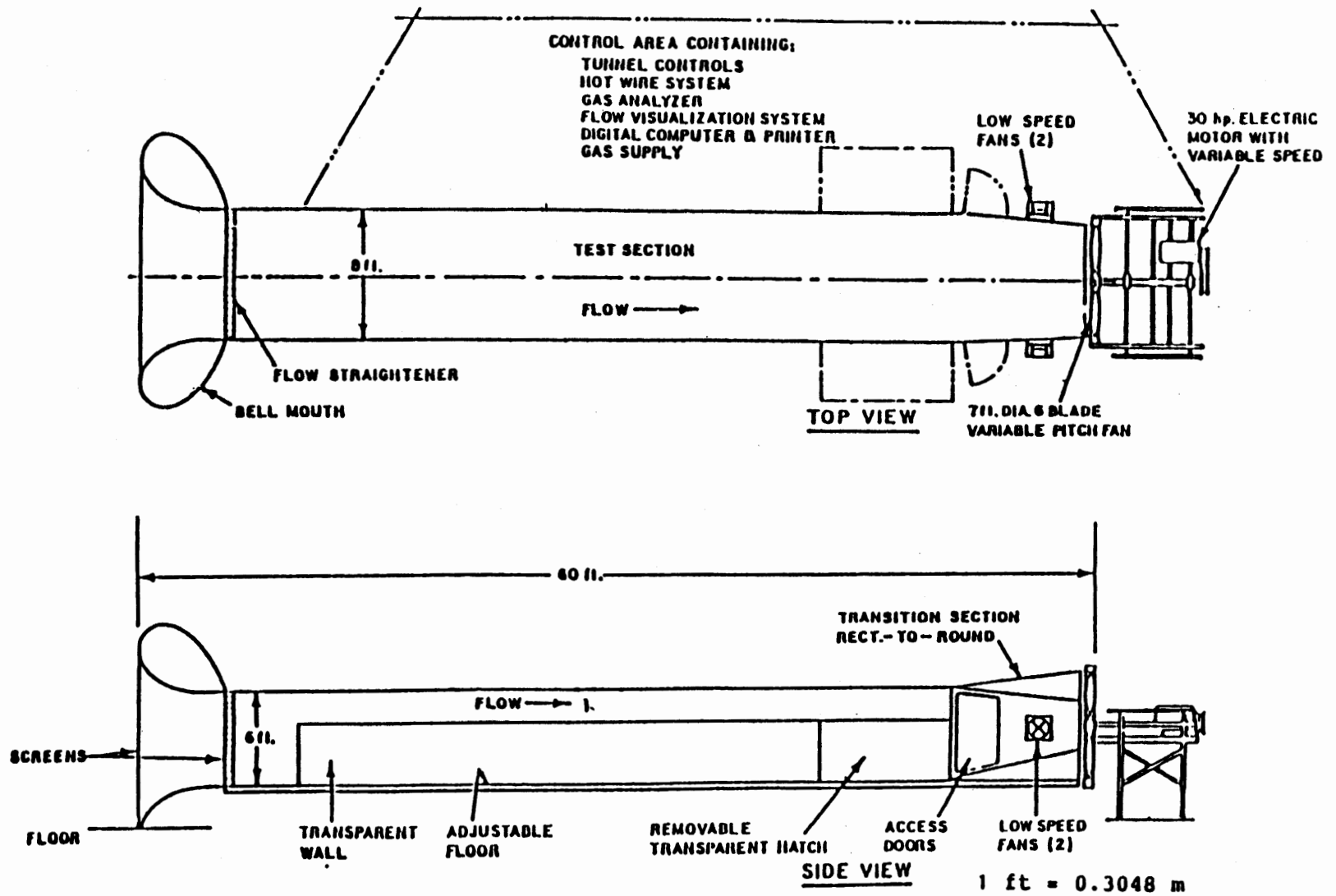


Figure 2. Schematic views of Boston University Atmospheric Boundary Layer Wind Tunnel.



For most tests, enough blocks were placed upstream to provide a limit condition so that the addition of another upstream block does not affect the concentration in the test canyon.

The test canyon is the space between two blocks. Tracer gas is introduced into the channel in three ways: through a movable point source probe, a long (2-D) slot in the tunnel floor, or from the scale model vehicles on a moving belt.

The model roadway consisted of two moving belts.<sup>1</sup> A diagram of the model vehicles are presented in figure 3 and vehicle spacing in table 1.

The preliminary tests can be divided into two categories: fluid dynamical tests and model studies. The fluid dynamical tests were designed to ensure that the tests performed correspond and can be scaled to field conditions. The model tests were designed to show the influence of canyon shape on dispersion characteristics, over a range of generic canyon shapes typically encountered in urban environments.

The concentration of tracer gas is measured using a multichannel sampler. This sampler consists of a set of up to 80 small collector bags, 1 liter volume, connected to a ganged set of positive displacement pumps, driven by a common motor. The bags are connected to the tunnel via a set of receptors, which terminates at the wall, street level, away from the walls and above the model street canyon.

### Boundary Layer Profile

The atmospheric boundary layer is often described by a power law

$$\left[ \begin{array}{c} V_z \\ \overline{V_g} \end{array} \right] = \left[ \begin{array}{c} Z \\ \overline{Z_g} \end{array} \right]^\alpha$$

where  $V_z$  is the velocity at altitude  $Z$  and  $V_g$  is the velocity at the gradient height,  $Z_g$ . In the BU boundary layer wind

<sup>1</sup>Only the upwind belt was used to inject pollutants through a series of scaled vehicles; the downwind belt had no vehicles and did not emit pollutants. The center of the belts where the pollutants are injected were 3/4 in (1.9 cm) from the canyon center.

# MODEL VEHICLE DIMENSIONS AND CONSTRUCTION

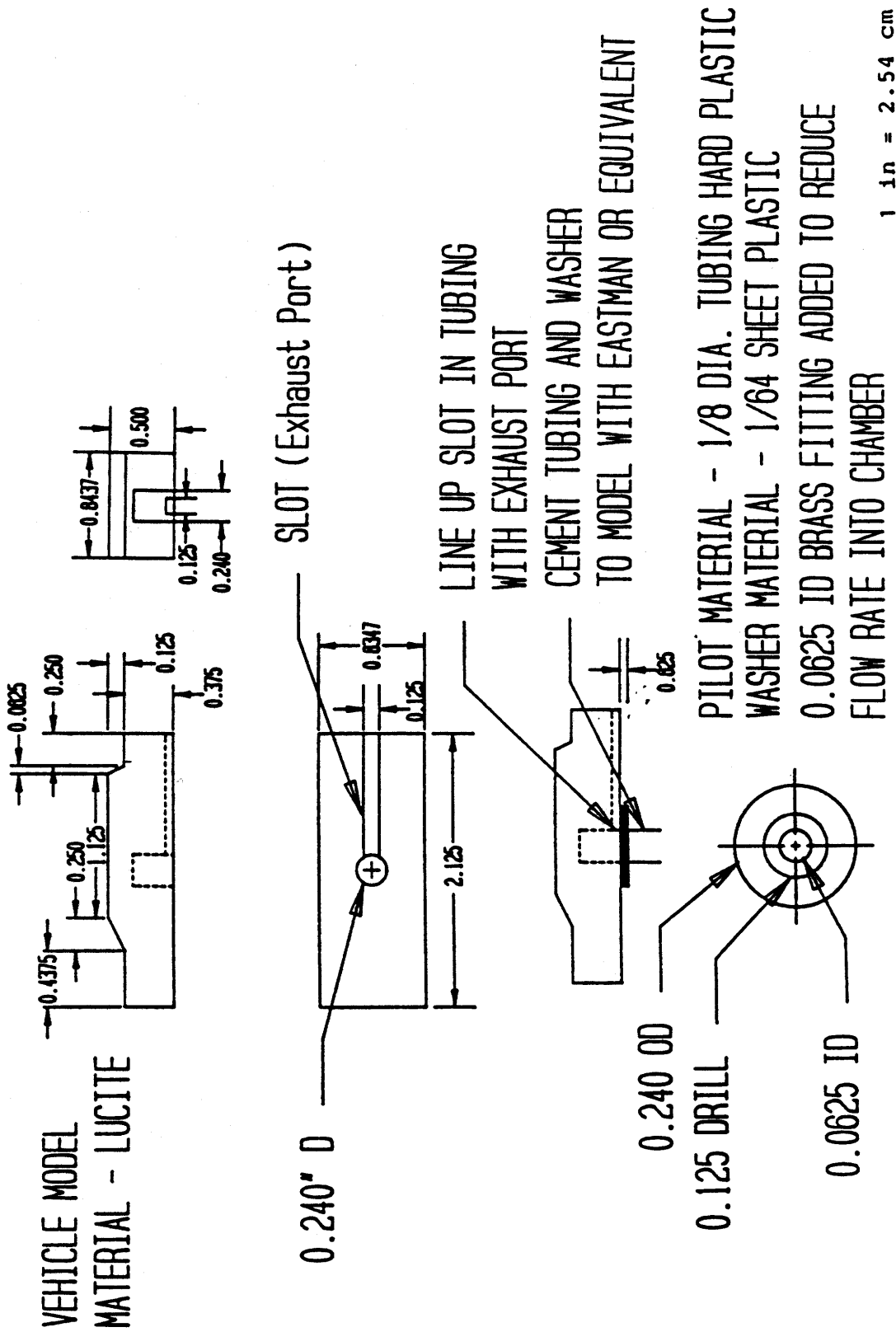


Figure 3. Dimensions of model vehicles used on moving-belt source.

Table 1. Vehicle Spacing

Vehicle Number	Spacing of Large-Scale Vehicles High-Density (Vehicle length)
1	0.68
2	1.35
3	0.90
4	1.58
5	0.23
6	1.58
7	2.25
8	1.58
9	0.90
10	0.68
11	0.45
12	1.13
13	3.83
14	0.68
15	0.68
16	1.58
17	0.90
18	0.90
19	1.13
20	1.35
21	2.93
22	0.45
23	0.90
24	3.60
25	1.35
26	0.90
27	1.35
28	0.90
29	4.28
30	0.90
31	0.90
32	0.90
33	1.13
34	2.03
35	2.03
36	0.90
37	1.13
38	2.25
39	2.70

tunnel,  $Z_g$  has been determined to be approximately 36 in (0.95 m). The exponent  $a$  can be maintained at 0.15 or 0.30 across the tunnel width. To generate these boundary layers, a set of spires is placed at the inlet of the tunnel and sets of surface roughness elements are placed in the upstream section of the tunnel. These surface roughness elements have a 1-in by 1-in (2.54 cm) cross section and are either 1 in (2.54 cm) or 2 3/8 in (6.03 cm) high. By changing the arrangement of the roughness elements, different boundary layers can be developed.

To sustain the boundary layer as the flow passes over the test section, some surface roughness is necessary. This roughness is provided by an artificial grass carpet.

### Instrumentation

The basic instrument used for flow field measurements was a hot wire anemometer made of 1/2-mil diameter and 1/4-in length of platinum wire. This wire was supported on a probe and was connected to a hot wire anemometer signal conditioner. The output signal from the anemometer is connected to a personal computer via an A/D board which provides 16 input channels that can be sampled at a variable rate. Normally 2048 samples at 300 hertz are used, giving a sampling time of 6.8 seconds. Initial tests were performed to establish that the number of samples and sampling time were sufficient to produce accurate mean velocities and turbulent intensities.

The hot wire calibration is ultimately traced to a primary standard through comparison with velocity measured from a pitot tube. The pitot tube calibration is done using a water column. The gradient flow velocity (normally 10 m/s [33 ft/s]) is determined by measuring the difference between dynamic pressure and static pressure indicated by the displacement of the water column with a microdetector. The static and dynamic ports of the pitot tubes were also connected to a differential pressure device.

To calibrate the hot wire probes, the probe is positioned near the pitot, but far enough away so the flow is not affected by the pitot tube. The tunnel flow is then accelerated from 0 m/s to 10 m/s (0 ft/s to 33 ft/s) while voltage output from the probe and the pitot tube is sampled simultaneously. The velocity from the pressure sensor is used as reference, and the voltage output from the hot wire probe is curve fitted to the velocity curve.

### Definition of Flow Field Parameters

To determine the flow characteristics at any point, both mean velocity and turbulence intensity must be calculated. Each voltage reading was converted to a velocity, then the set of velocities was used to calculate mean velocity ( $V_m$ ) and turbulence intensity ( $I$ ). The reduction formulas used herein are:

$$V_m = \sum_i^N V_i / N \quad (1)$$

$$V_{rms} = \sum_i^N [(V_i)^2 - (V_m)^2]^{1/2} / N \quad (2)$$

$$I = V_{rms} / V_m \quad (3)$$

where  $V_m$  is the mean velocity,  $V_i$  is the set of sampled velocities,  $V_{rms}$  is the root mean square fluctuation,  $N$  is the number of samples, and  $I$  is a measure of turbulent intensity based on the local velocity. Note that this data must be reinterpreted when the indicated turbulence intensity is high. The procedure for reprocessing this data is outlined in volume I. In most cases, the local mean flow,  $V_m$ , was normalized by dividing its value by the mean gradient velocity,  $V_g$ ; in this report and the databases, the parameter  $I$  always uses the local values of  $V_{rms}$  and  $V_m$ .

### Tunnel Velocity Calibration

The tunnel was calibrated for the flow profile  $\alpha = 0.30$ . The flow profile was measured at three axial stations at leading edge, center and trailing edge of the test section; the locations are shown in figures 4 and 5. Vertical profiles were taken at the center line at each axial center line at each axial station. Horizontal profiles were taken at heights of 2 1/8 in (.05 m), 6 1/2 in (.17 m), and 30 in (.76 m) above the floor. The data indicate that both mean flow velocity and turbulence intensity profiles can be maintained across the test section. Turbulence intensity,  $I$  (as defined above), near the tunnel floor is approximately 45 percent. Figure 6 shows the measurement setup for a similar survey carried out when the  $W/H = 1$ ,  $0^\circ$  wind direction baseline urban canyon cityscape was in place, and figure 7 illustrates the mean velocity and turbulence profiles above the center of the canyon which was used as the primary test area throughout the study.



TOP VIEW OF TEST SECTION  
AND MEASUREMENT STATIONS

JUNE 6-13, 1985

NB12 P17-33

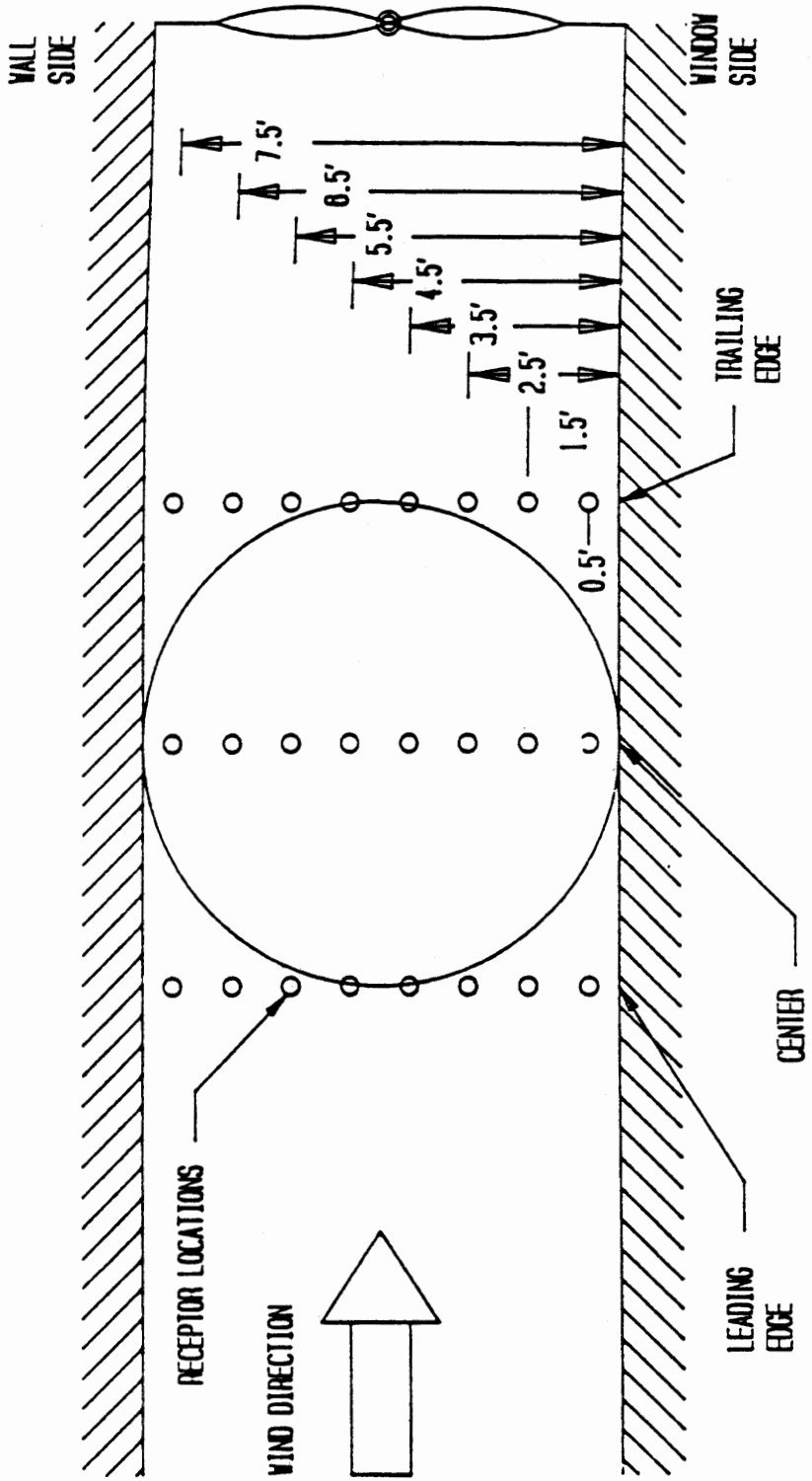


Figure 4. Plan view of wind tunnel test section.

SIDE VIEW OF TEST SECTION  
AND MEASUREMENT STATIONS

JUNE 6-13, 1985

ND12 P17-33

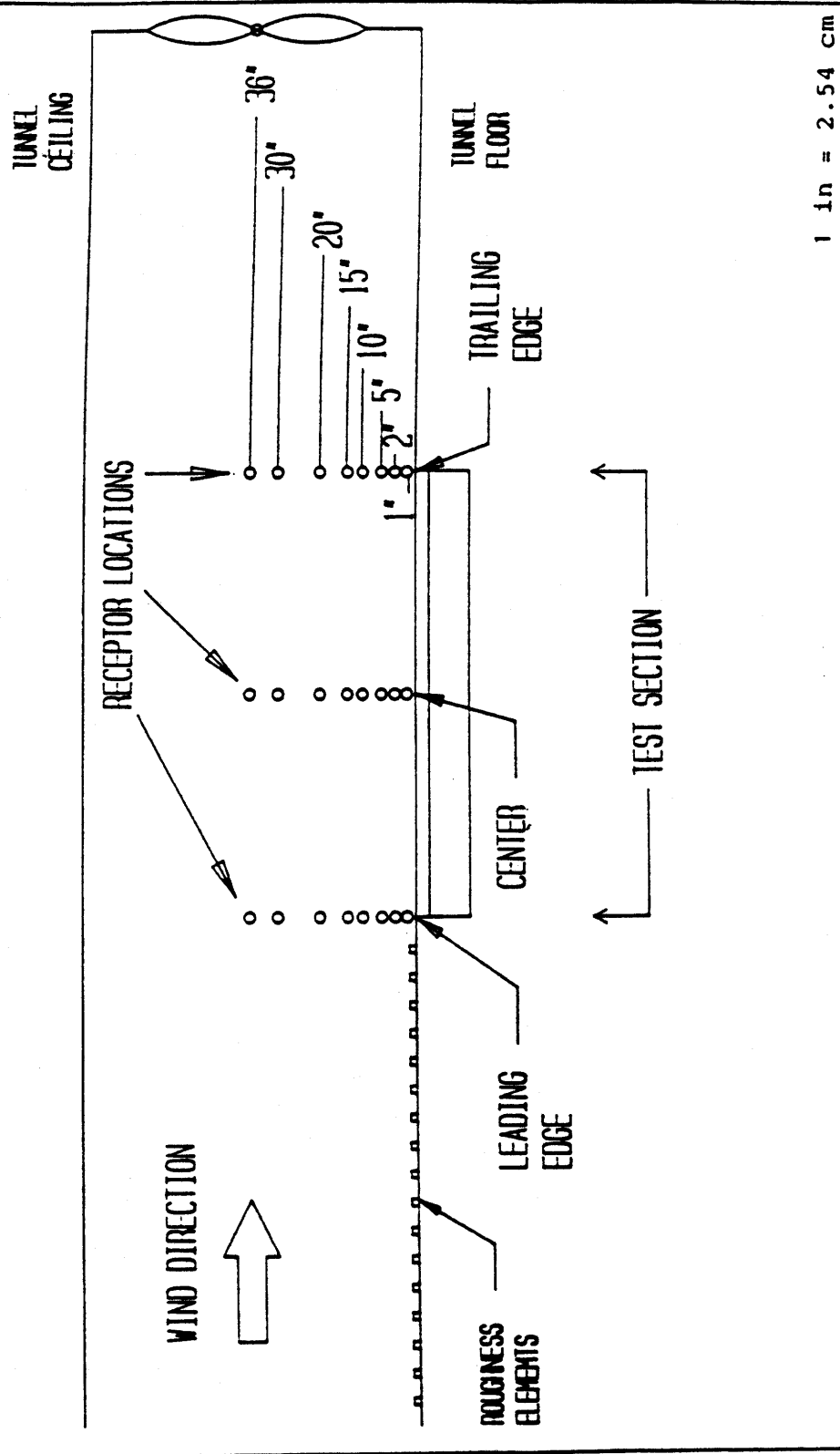


Figure 5. Side view of wind tunnel test section.

HOT WIRE TESTING

JULY 25, 1985

VELOCITY AND TURBULENCE PROFILE

NB13P151

W/H = 1

CROSS SECTION VIEW OF STREET CANYON  
CONFIGURATION (A)

WIND DIRECTION 0 DEGREES



APPROACH FLOW

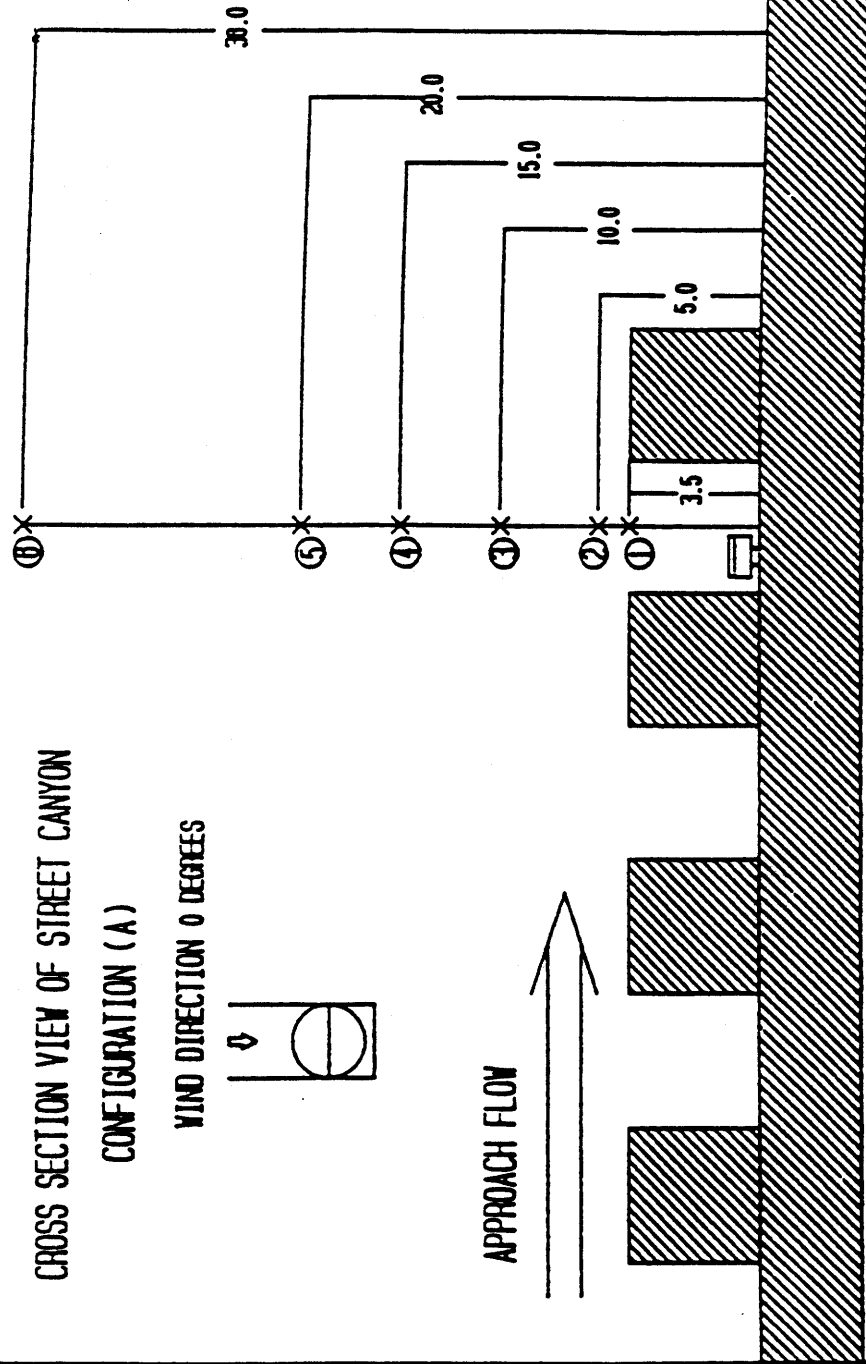
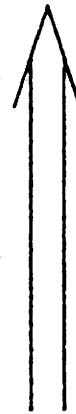


Figure 6. Probe layout for velocity test with typical urban canyon in place.

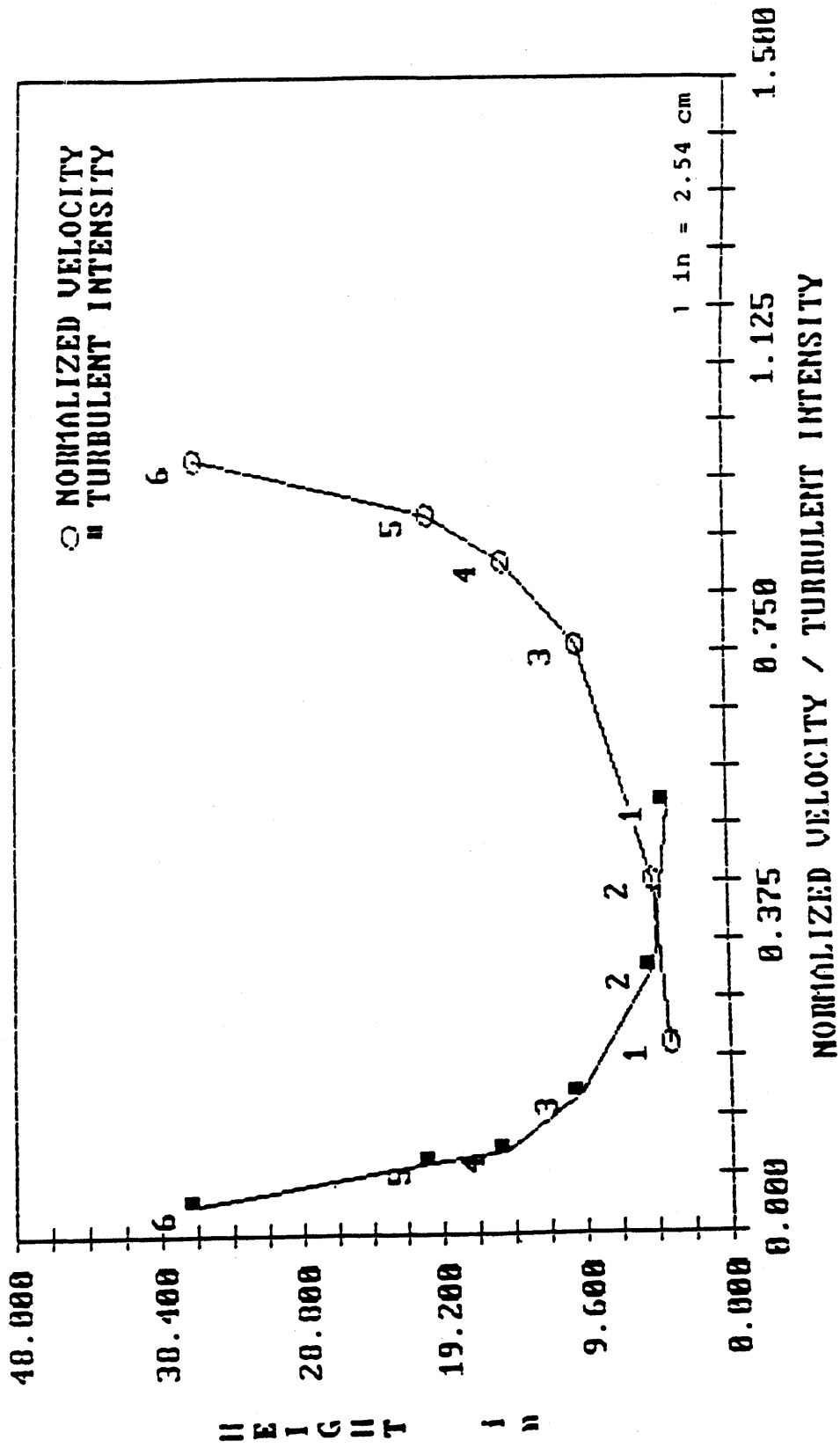


Figure 7. Results of mean flow and turbulence survey above model urban setting  $w/H = 1$ .

## Dispersion Comparability Tests and Normalization Procedures

A set of atmospheric dispersion comparability tests was carried out in strict conformance with the EPA Guidelines (Snyder, 1981). These measurements ensure model flow dispersion characteristics are comparable to field conditions. In these tests, the dispersion from a model stack was compared to that of a neutrally stable plume. The present tests showed that the plume dispersed in a manner between the Pasquill-Gifford category C and D. These data are too voluminous to warrant presentation herein, but are available upon request.

Raw values of the tracer gas concentrations were usually normalized by the formula below, equation (4), unless otherwise indicated.

$$C^* = \frac{X \cdot Vg \cdot H}{Q^*} \quad (4)$$

where:  $C^*$  = normalized concentration (dimensionless)  
 $Vg$  = gradient velocity (10 m/s, unless otherwise indicated)  
 $H$  = block height (0.0889 m, unless otherwise indicated)  
 $X$  = raw concentration value (ppm \* 0.00065 gram/m<sup>3</sup>)

$$X = \frac{\text{PPM}}{10^6} \cdot \frac{10^3 \ell}{\text{m}^3} \cdot \rho_{\text{ch4}}$$

where: ppm = parts per million of tracer gas  
 $\rho_{\text{ch4}}$  = density of methane trace gas (0.65 grams/liter)  
 $Q^*$  = mass flow rate per characteristic length  
(0.01454 \* Rch4/D)

$$Q^* = \frac{\text{Rch4} \cdot \rho_{\text{ch4}} \cdot 1 \text{ minute}}{\text{correction factor} \cdot D \cdot 60 \text{ seconds}}$$

where: Rch4 = flow meter reading in liter/min  
correction factor = converts meter reading to actual volume flow rate (0.745)  
D = characteristic length

These general formulas are presented in terms of this program's specifics to allow readers to un-normalize the data in this report and the addenda if desired.

Example:  $C^* = 0.03974 \bullet \text{PPM} \bullet D / \text{Rch4}$

For point sources:

D = 0.0889 m                      Rch4 = 0.200 L/min                      C\* = 0.017664 \* PPM

For the first line source used in exploratory tests:

D = 2.24 m                      Rch4- 1.732 L/min                      C\* = 0.06879 \* PPM

For the "new" line source in the parametric tests:

D = 1.893 m                      Rch4 = 0.516 L/min                      C\* = 0.14577 \* PPM

For the moving belt vehicle source:

D = 1.70 m                      Rch4 = 0.516 L/min                      C\* = 0.13093 \* PPM

where 1 ft = 0.3048 m and 1 gal = 3.785 L

Flow Visualization Procedure

Flow visualization tests were run on each configuration to identify effective sampling locations for the pollution dispersion tests.

Smoke was generated with titanium-tetrachloride and emitted through an easily moveable point source. By decreasing the wind tunnel gradient velocity to 3 m/s (10 ft/s) and taping in color reversible mode, the smoke clearly outlined the flow patterns.

A video camera with good low light capability was used to generate 2 hours of edited tape containing 31 different canyon geometries. A 6-minute introduction tape is also available, highlighting 12 characteristic flows. The 2-hour videotapes are indexed by test number and are sequenced Tape A (1-21) and Tape B (22-31). Lists of these tests are included in the cross-reference data tables 2, 3, 4, 5, 7, and 8. Sketches made from the videotapes are used throughout the report clarifying the flow dynamics of each configuration.

**D. Results of Initial Fluid Dynamic and Parametric Tests**

Overview

Nine types of fluid dynamics test were performed to establish the flow quality in the tunnel and the required upstream conditions, Reynolds number, and source type comparison.

1. Velocity profiles and turbulence across the tunnel section.
2. Dispersion of a free plume.
3. Velocity profiles above the highway canyon (described above and in data base 4).
4. Effect of the number of upstream blocks on concentrations in test canyon.
5. Influence of Reynolds number on test canyon concentrations with line source.
6. Influence of Reynolds number on test canyon concentration with moving vehicle source.
7. Influence of wind direction on concentration.
8. Influence of vehicle speed on concentration.
9. Comparison of vehicle source to line source.

Because of the volume of data contained in this report, the complete data sets contained in the data bases are in a uniform format. For each test, the data set contains:

1. Description of the test.
2. Schematic of test geometry.
3. Table of receptor locations.
4. Table of measured concentrations and receptor number.
5. Plots of measurements.

The coordinate system used to locate receptors and other test points is illustrated in figure 8. The cartesian coordinates  $x$ ,  $y$ , and  $z$  refer respectively to the cross-canyon, along-canyon, and vertical directions. The origin (0,0,0) is located on the tunnel centerline, on the midline of the canyon floor. The axis system is fixed in the canyon and rotates with wind direction. For example, the receptor coordinates for 0-degree and 30-degree wind direction are identical, even though the canyon has been rotated by 30° clockwise.

#### Upstream Canyon Influence

The model canyon was constructed using a set of wood blocks, 3 1/2 in by 3 1/2 in by 8 ft (.089 m by .089 m by 2.43 m). For the baseline tests, each of these blocks was spaced 3 1/2 in (0.89 m) apart, producing a width-to-height value of one ( $W/H = 1$ ), as shown in figure 9. Because the flow in the canyon is

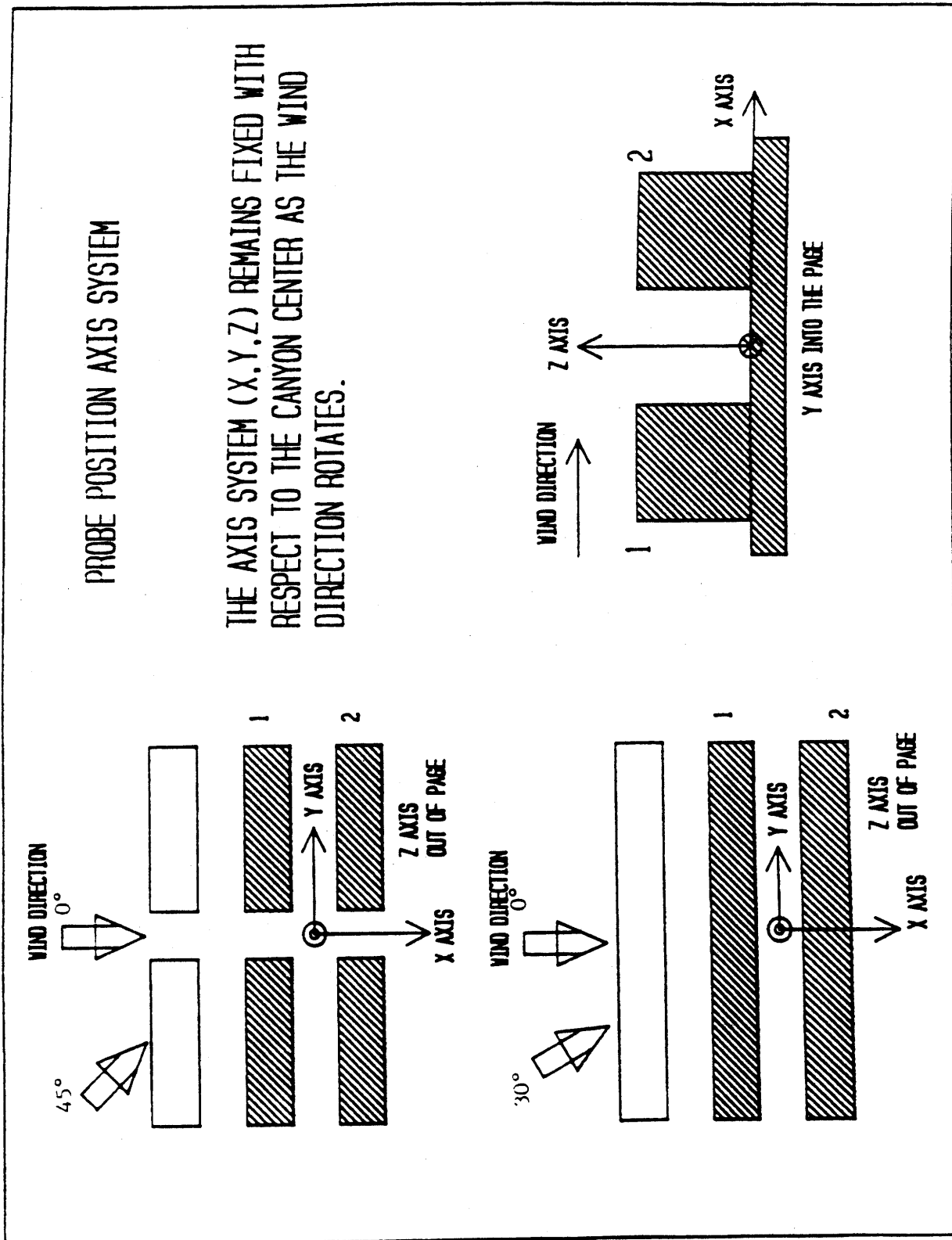


Figure 8. Coordinate system for 2-D and 3-D canyons.



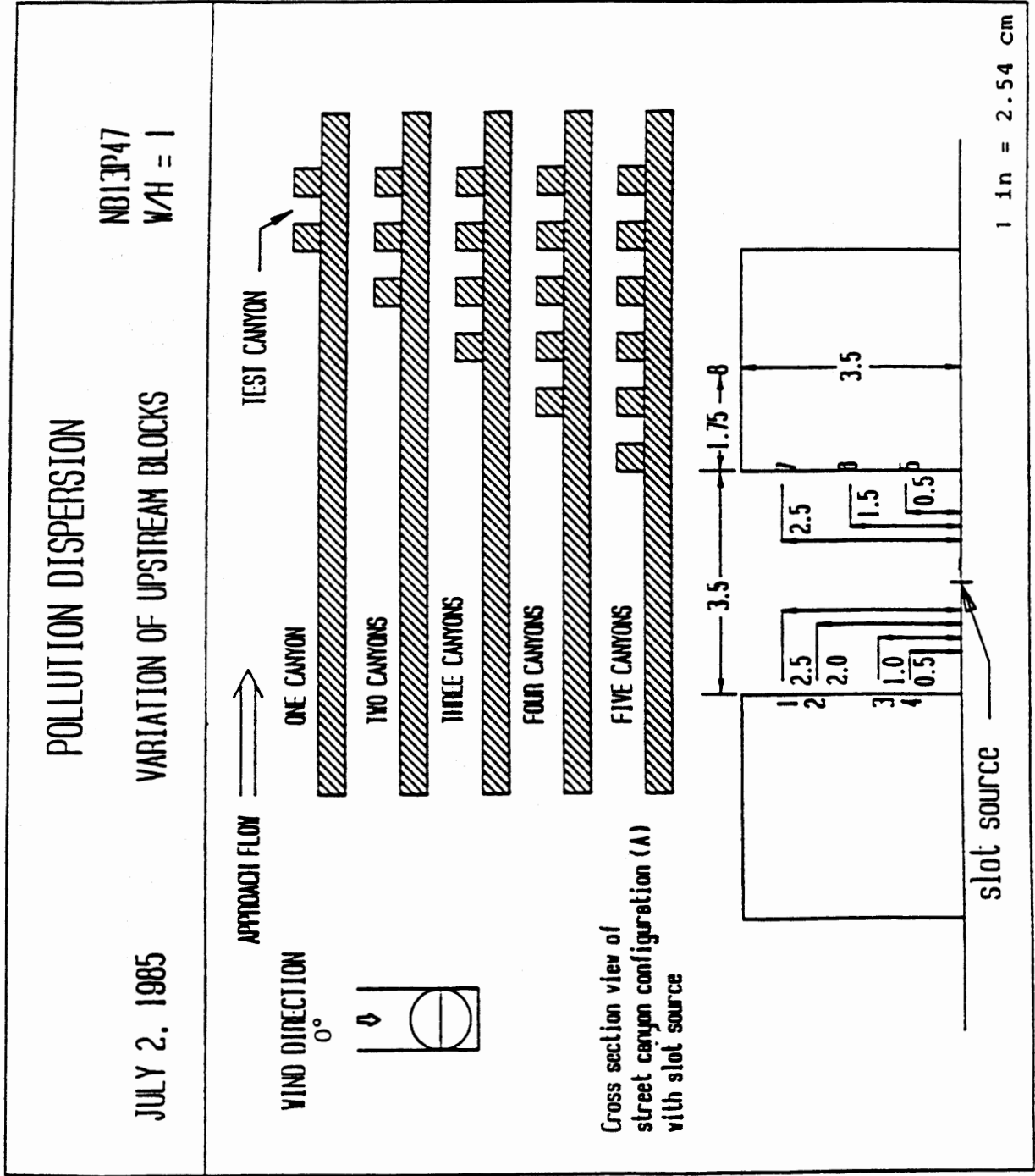


Figure 9. Geometry for tests of upstream canyon effect.

sensitive to the upstream geometry, it is necessary to establish the number of blocks upstream of the test section which will render the test canyon flow insensitive to the upstream conditions. The data in figure 10 shows that after a certain number of rows of blocks are placed upstream, the presence or absence of another row of blocks has little effect on the flow and dispersion characteristics in the model canyon. The results indicate little change in the upstream wall receptors after one block was placed upstream of the test section; however, in order to establish consistency of concentration at the downstream wall receptors, at least four blocks must be placed upstream of the test section canyon. All further tests were done with five blocks upstream of the test section canyon.

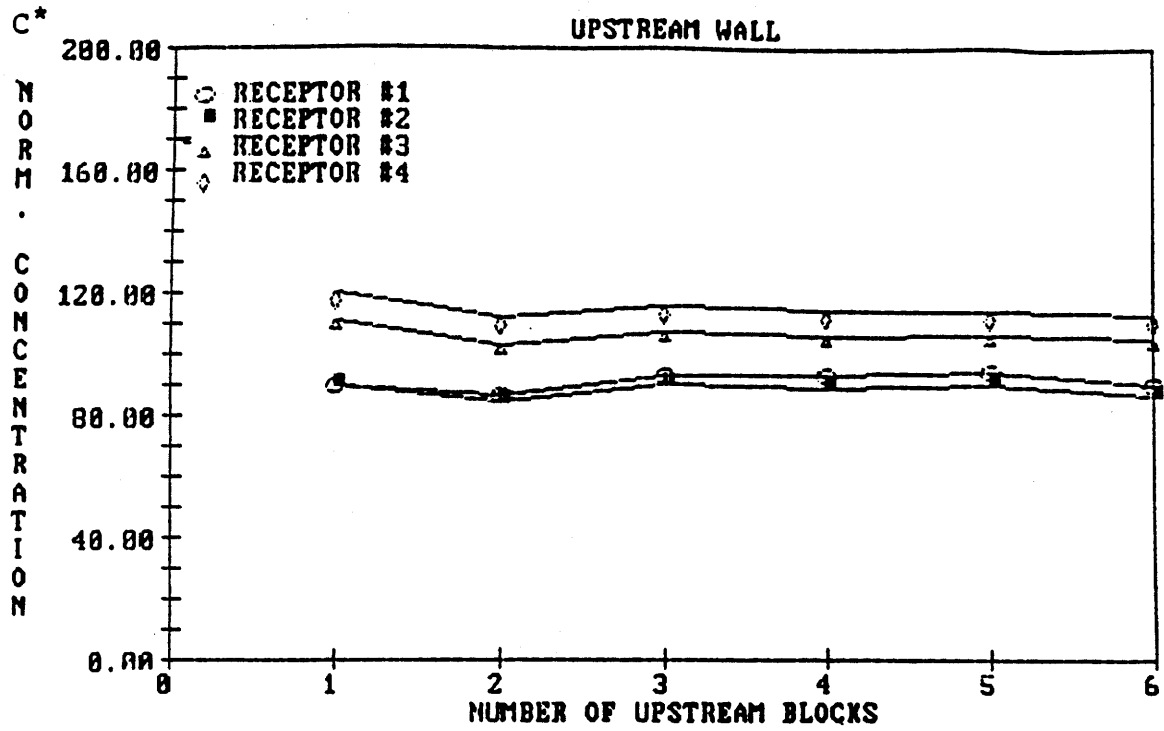
#### Reynolds Number Sensitivity

These tests were designed to determine the effect of Reynolds number on the pollution concentrations. This test was carried out by varying the gradient wind velocity and measuring on the concentration measurements. Two tests were done, one with a line source and another with a vehicle source. Figure 11 shows the line source configuration which produced the results shown in figure 12. A more detailed survey was prepared on the vehicle source, defined by figure 13, which produced the results shown in figure 14. According to the normalization formula,

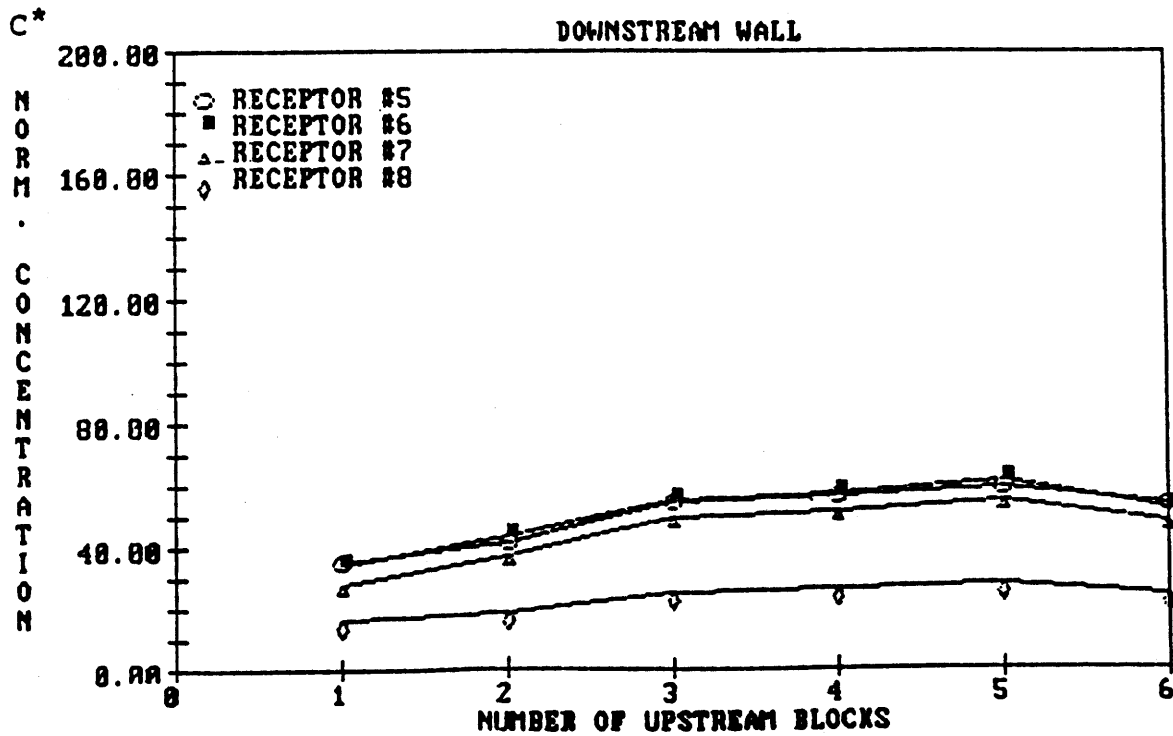
$$C^* = \frac{x * Vg * H}{Q^*}$$

the normalized concentration is linearly proportional to the gradient velocity. The results showed that the normalization formula is effective for gradient velocities above 9.25 m/s (30 ft/s) i.e., Reynolds numbers  $Re_H > 17,900$ . At lower velocities, the concentration values dropped significantly. All further tests were done with gradient velocities near 10.0 m/s (33 ft/s) to ensure flow field similarity.

The configuration shown in figure 13 also tested Reynolds number effect with a moving vehicle stream. The effect of vehicle speed was predominant along the upstream wall for all three gradient velocities (shown in figure 14); the higher vehicle speeds causing lower concentrations. Significantly lower concentrations were found across the canyon and along the downstream wall for  $Vg = 10.0$  m/s (33 ft/s) and 9.25 m/s (30 ft/s); slight changes were found for the case of  $Vg = 8.25$  m/s (27 ft/s). This result may indicate that some of the early reports of the effect of vehicle speed were performed at sub-critical Reynolds numbers, and thus the effect was exaggerated.



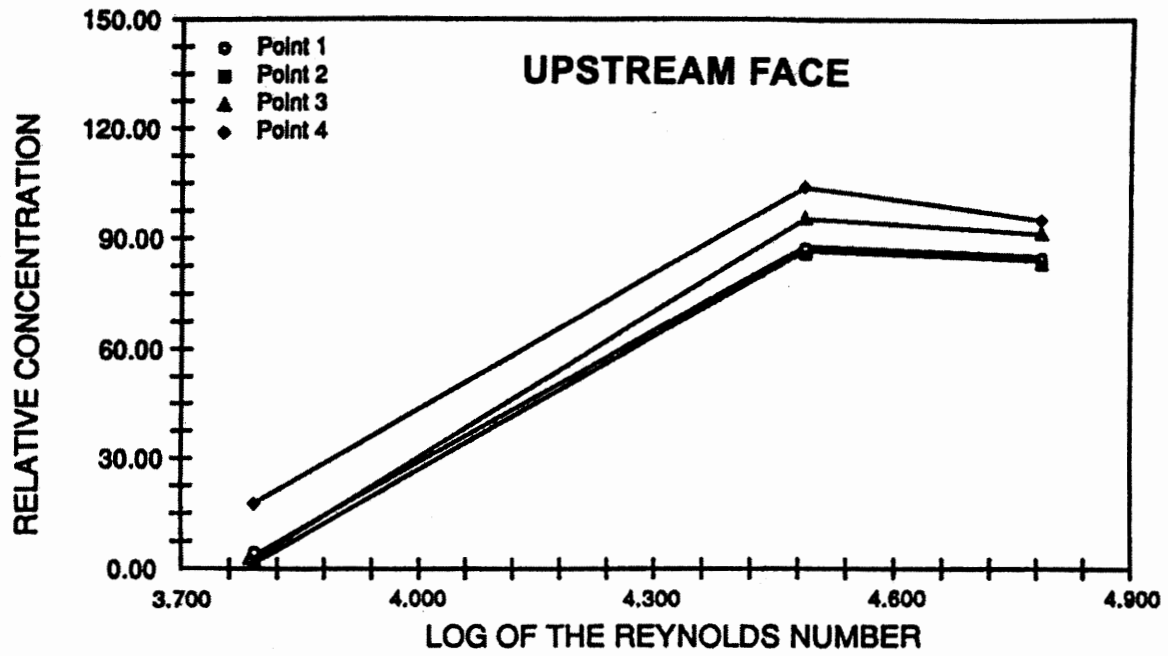
a)



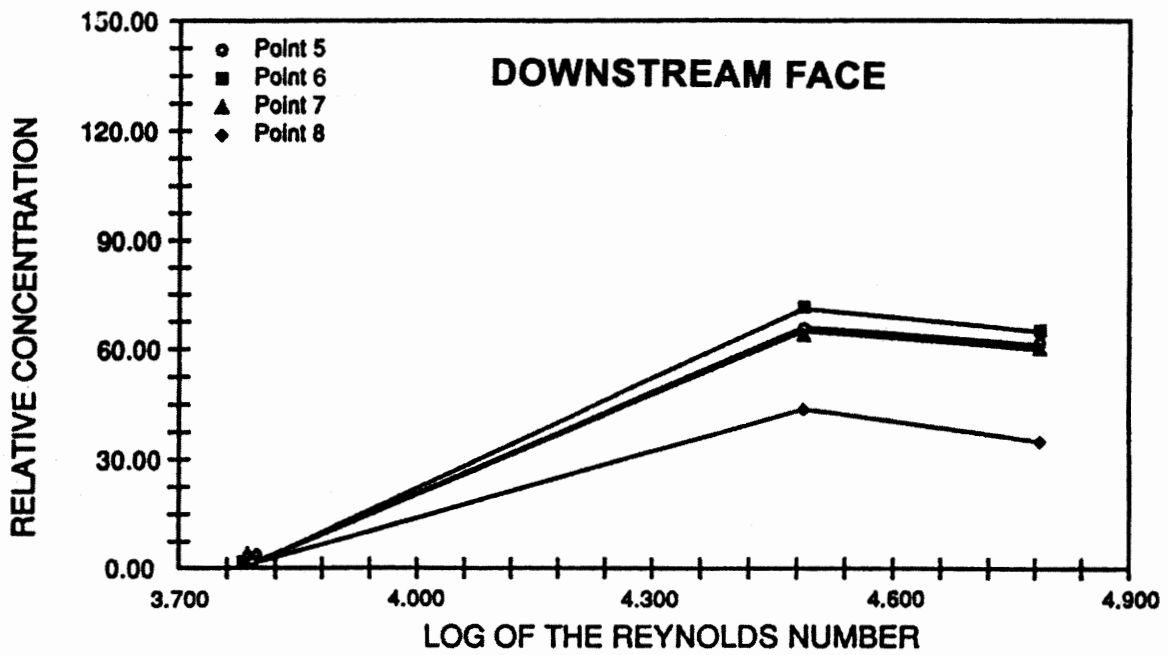
b)

Figure 10. Dispersion results for number of upstream block variations of a model urban setting,  $W/H = 1$ .





a)



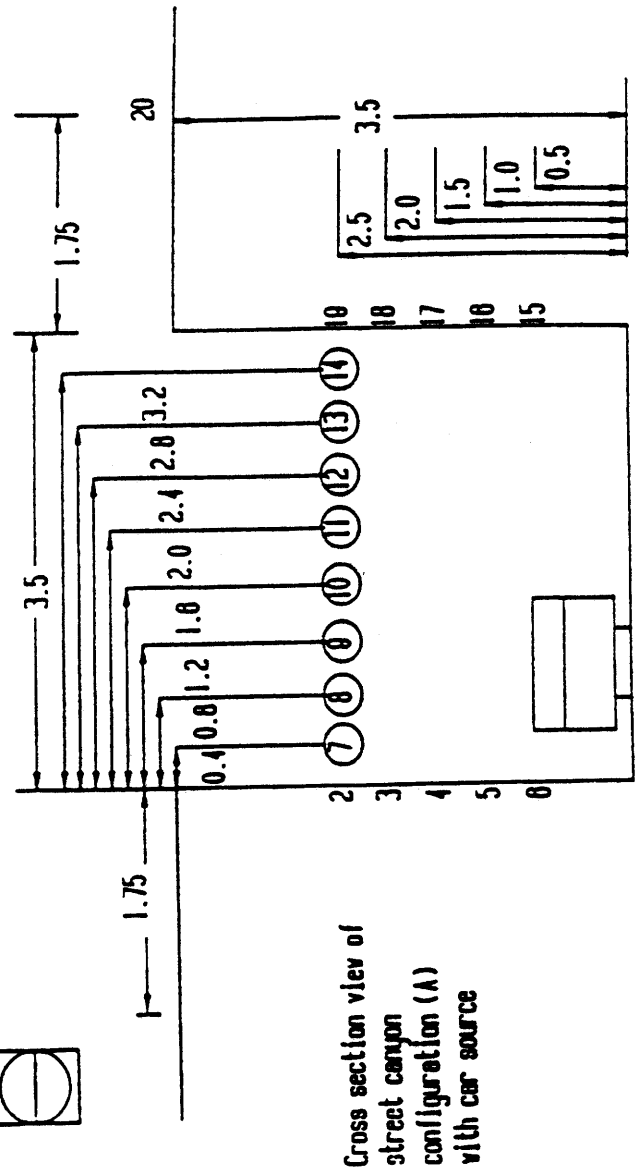
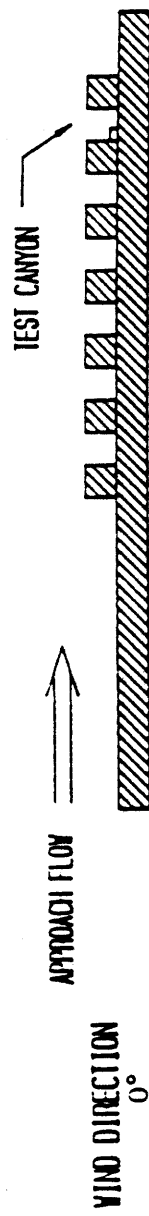
b)

Figure 12. Results for Reynolds number study with line source.

# POLLUTION DISPERSION

NB14P53  
W/HI = 1

JANUARY 1, 1986 INFLUENCE OF GRADIENT WIND VELOCITY



Gross section view of street canyon configuration (A) with car source

1 in = 2.54 cm

Figure 13. Configuration for Reynolds number tests with moving vehicles.

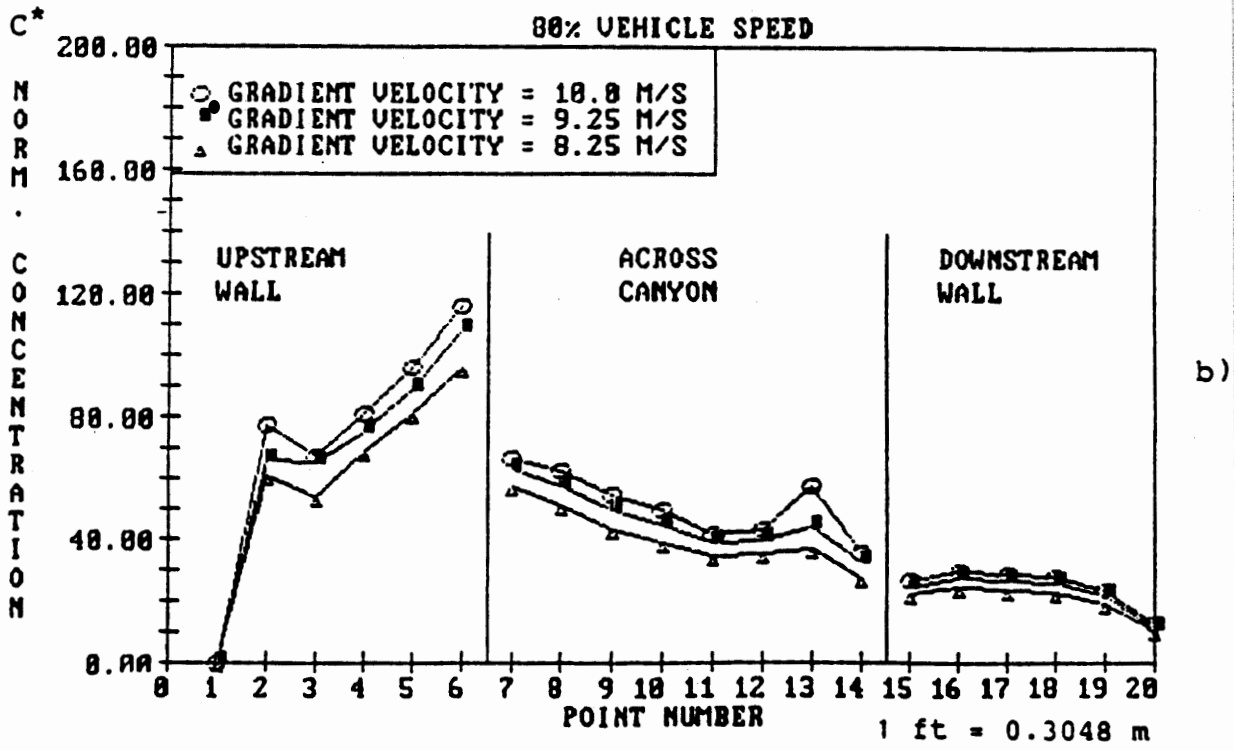
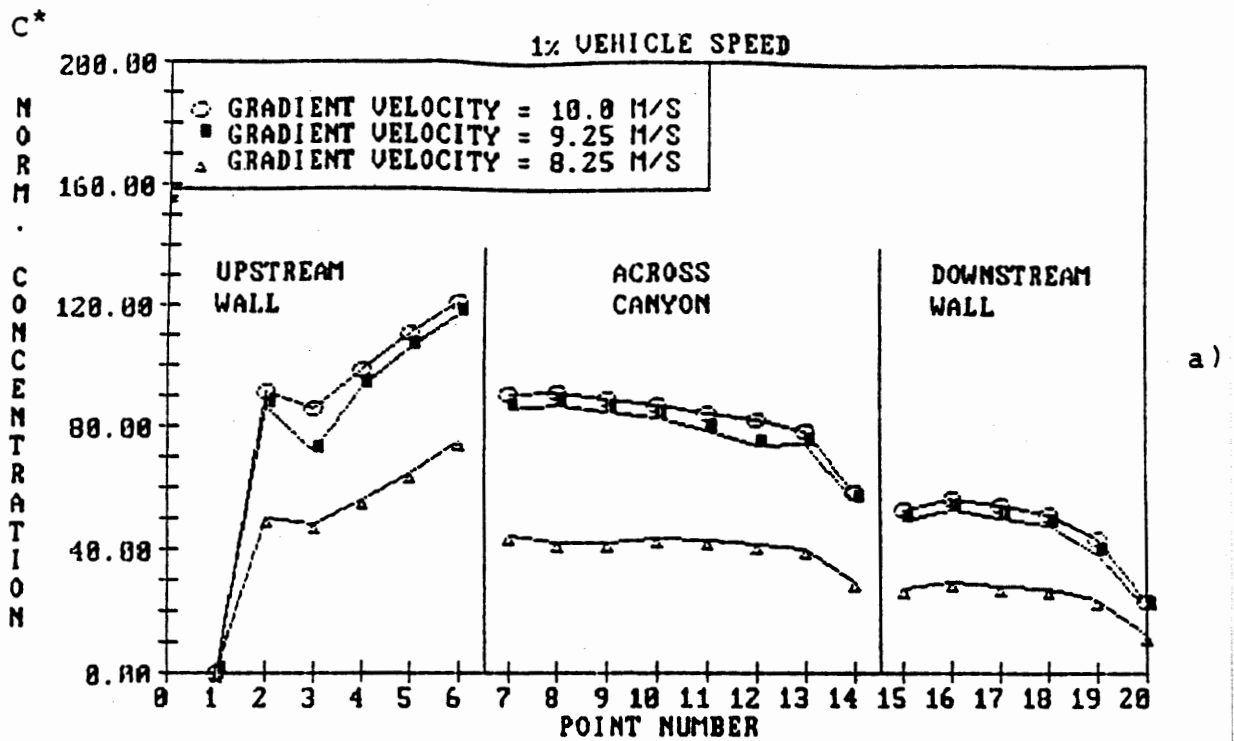


Figure 14. Dispersion results for Reynolds number test with moving vehicles.

It should be noted that the test illustrated in figure 11 used a line source that was later found to have inadequate control over the emission rate of the tracer gas mixture. For that reason, the absolute values of concentration shown in figure 12 are in error.

#### Effect of Wind Direction

This test was performed on the baseline canyon ( $W/H = 1$ ) with closed ends at three different wind directions:  $0^\circ$ ,  $15^\circ$ , and  $30^\circ$ . The test layout is shown in figure 15, and the data are shown in figure 16. For 1.0 percent vehicle speed at  $0^\circ$  and  $15^\circ$ , a strong vortex developed, and the concentration measurements were comparable. Lower values were found in the case of the  $30^\circ$  wind direction where the along-canyon component of the flow increased the rate of transport of the emission from the canyon.

When the vehicle speed was increased to 80 percent of the maximum, the vehicle movement increased the mixing of the flow causing the concentration values for the different wind directions to become closer in value. For  $1.0$  and  $15^\circ$  wind direction, all of the concentrations were lower. For the  $30^\circ$  wind direction, the concentration measurements were slightly greater than those found in the  $0^\circ$  case. The direction of the vehicles opposed the lateral along-the-canyon velocity component. Apparently, when the vehicle mixing motion, opposes the along-canyon flow, the ventilation is decreased. This suggests that the major changes in flow structure were due primarily to vehicle speed for the  $0$  and  $15^\circ$  cases, and due to the combined effects of wind direction and vehicle speed for the  $30^\circ$  case. Apparently, the additional mixing caused by the vehicle does not cause large changes in the concentration values when the flow is already slightly unstable.

Previous tests have shown the concentrations are significantly lower for open-ended canyons as compared to closed-end canyons at corresponding wind directions. An open-ended canyon channels more air through the canyon producing a stronger lateral flow component and increased ventilation. For open-ended canyons, a significant change in the basic trend occurred on the upstream face between  $15$  and  $30^\circ$ ; this change had not yet occurred at  $30$  degrees for the closed-ended case. All subsequent tests were performed with the closed-end geometry.

#### Effect of Vehicle Speed

A series of tests to determine the effect of vehicle speed on concentration measurements were performed on selected canyon geometries. In the Reynolds number range, which had been

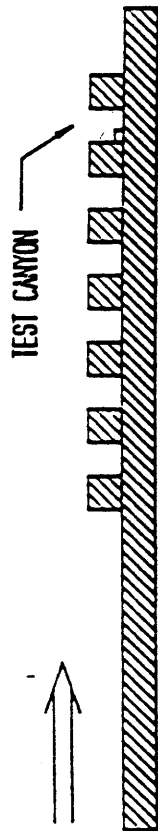


# POLLUTION DISPERSION

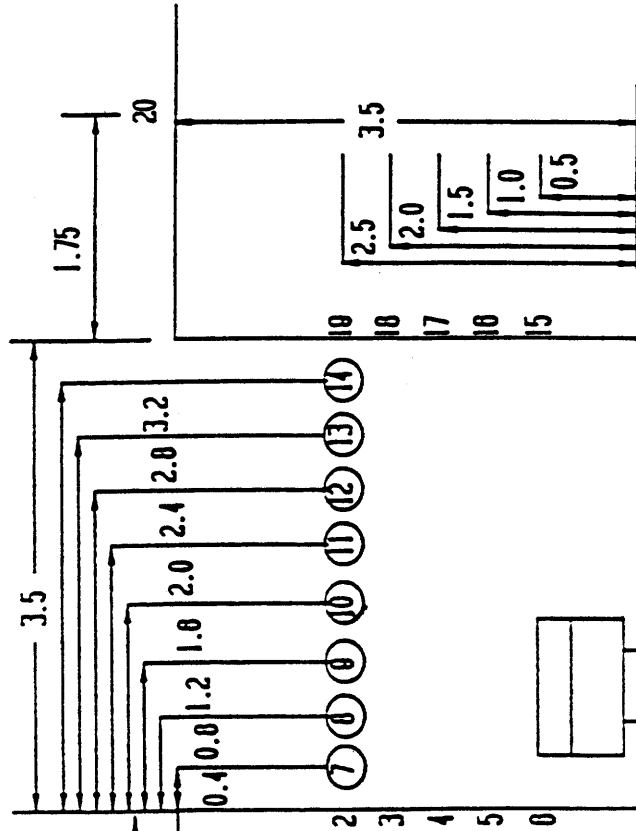
NB14P55  
W/H = 1

VARIATION OF WIND DIRECTION ANGLE

JANUARY 7, 1988



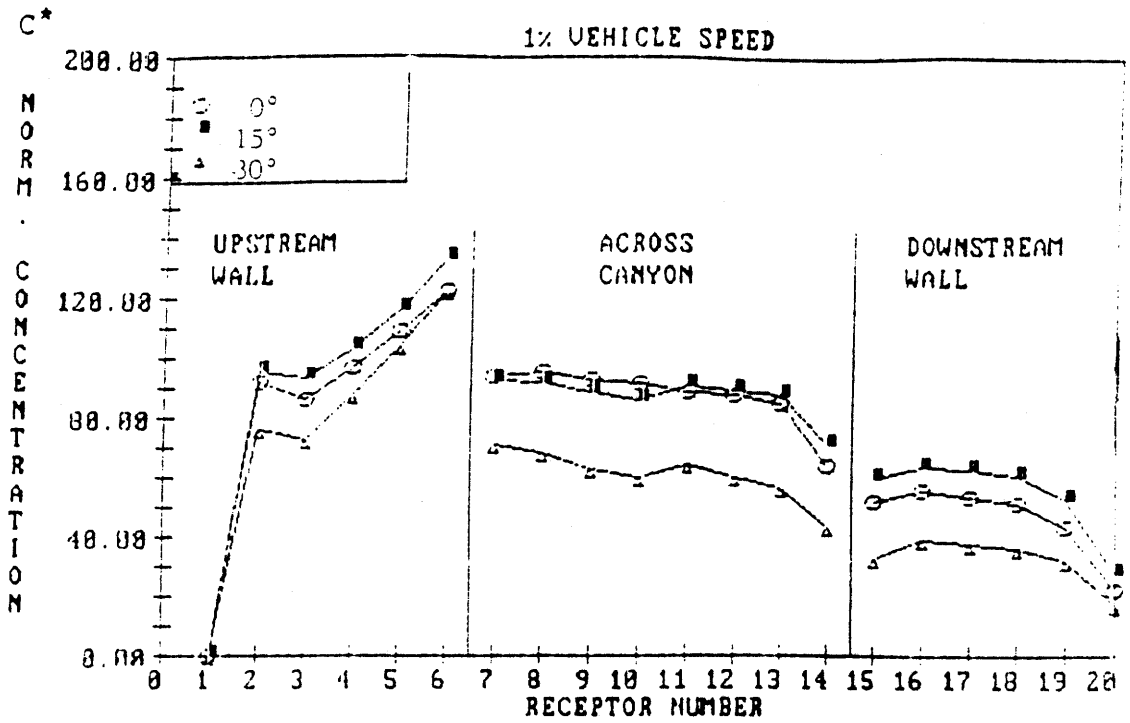
WIND DIRECTIONS : 0°  
15°  
30°



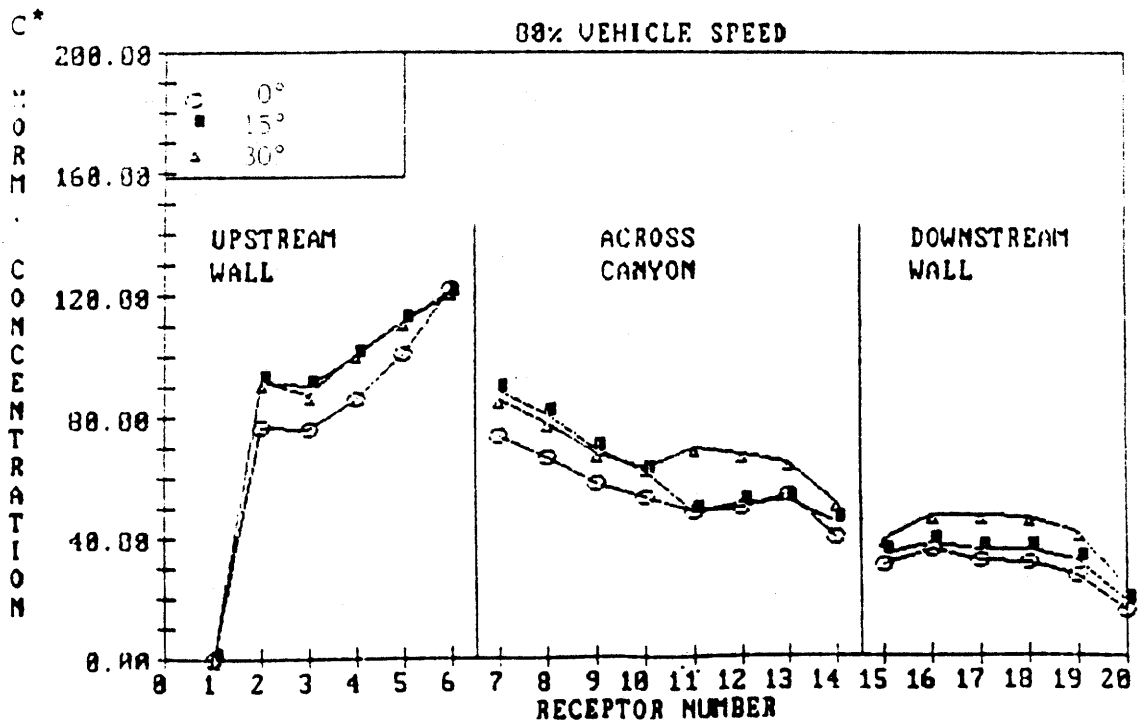
Cross section view of  
street canyon  
configuration (A)  
with car source

1 in = 2.54 cm

Figure 15. Test setup for studying effect of wind direction, W/H = 1.



a)



b)

Figure 16. Results of wind direction effects for two different vehicle speeds.

determined to be proper for the program, large vehicles on the moving belt described earlier were placed  $3/4$  in (1.9 cm) from the upstream side of the canyon where they inject pollutants into the canyon. The test was run at 1 percent and 80 percent of the maximum vehicle speed, where the maximum belt speed is 9.2 ft/s (2.81 m/s). We note that the high vehicle speeds were on the order of  $1/4$  that of the gradient wind velocity. It is clear that one parameter which will determine the relative importance of vehicle-induced mixing is the ratio of vehicle speed to wind speed.

For a given wind speed, the location of the vehicle source with respect to canyon walls determines what effect vehicle speed has on in-canyon concentrations. In general, when the vehicle source is located in stagnant or recirculating flow patterns, the concentrations decrease with vehicle speed; the opposite is true when the vehicles are located in regions of strong non-recirculating flow. Individual cases are discussed within Instrumentation (see figures 23, 33, 36, 37, and 43). These data supported the notion that vehicle motion effects can be important, depending upon the canyon geometry and the location of the vehicle therein. Some of these effects are incorporated into the CPM-3 model (see volume I). Further studies of these effects are warranted in the future.

#### Comparison of Line Source and Vehicle Source

An approximation often used for a line of vehicles has been a line source. In order to demonstrate the comparability of the line and moving vehicle sources, the standard canyon ( $W/H = 1$ ) was used as a baseline for comparison. Figure 17 shows the test layout, and figure 18 illustrates the correlation at two different vehicle speeds and wind directions. As shown, the line source produces results that lie between the values obtained at 1 percent and 80 percent vehicle speed at  $0^\circ$  wind direction, while maintaining the same basic trends. For the  $30^\circ$  case, the line source also exhibited consistently lower concentrations by a factor approximately equal to the cosine of the wind angle.

A caution should be noted when translating vehicle source values to comparable line source values. The position of the vehicle source in relationship to the flow field must be taken into consideration (see Effect of Vehicle Speed) and, therefore, each individual case must be analyzed separately.

Comparison of Vehicle and Line Source: 0 and 30° Wind Direction

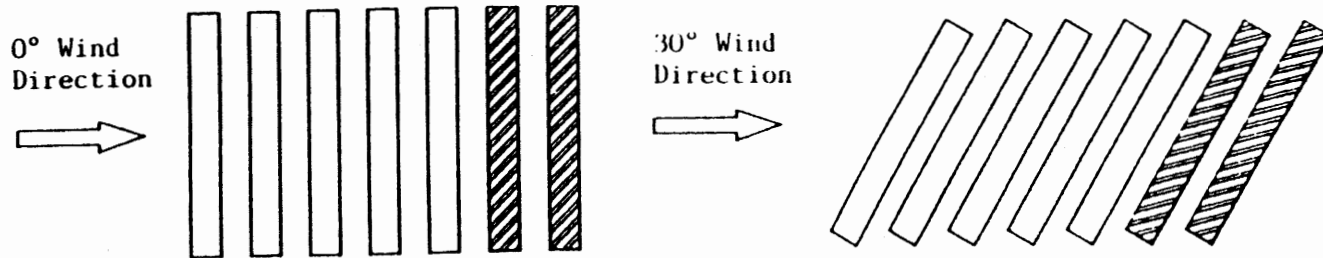
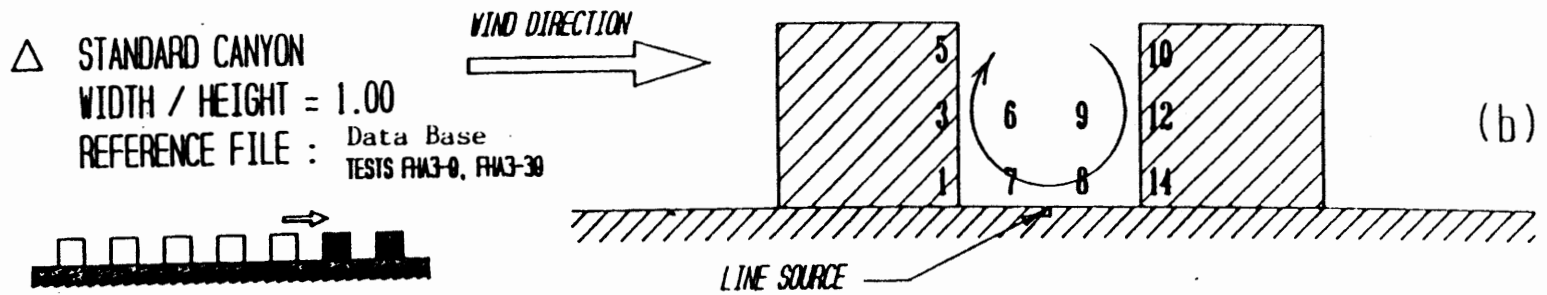
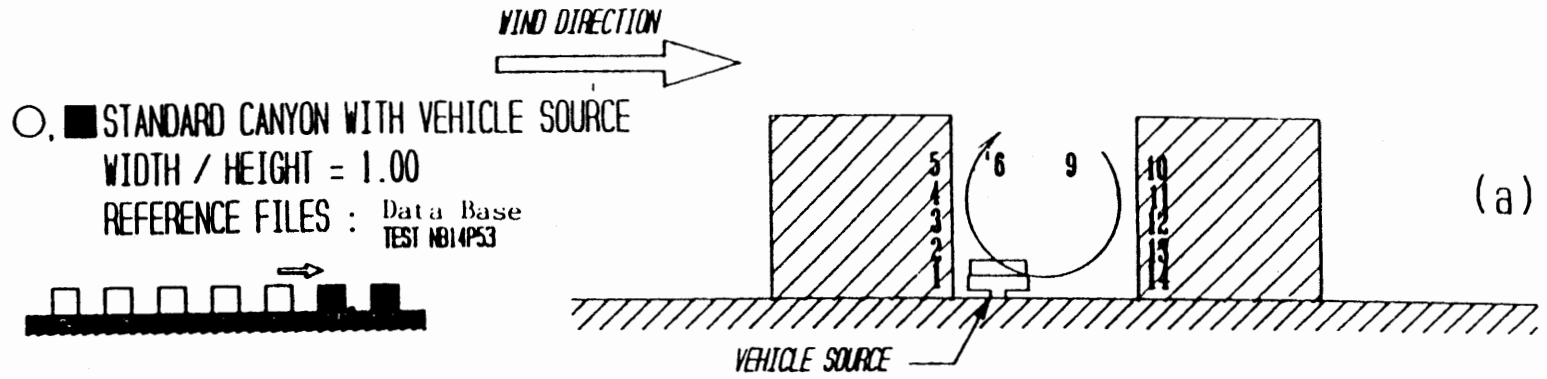
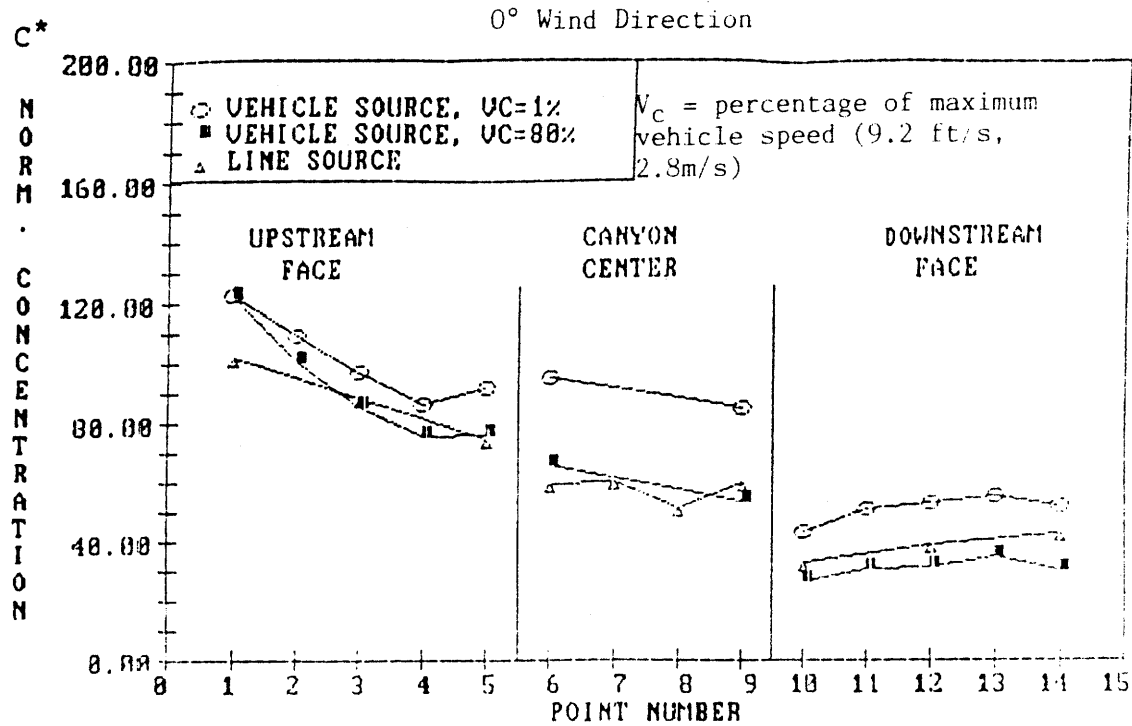
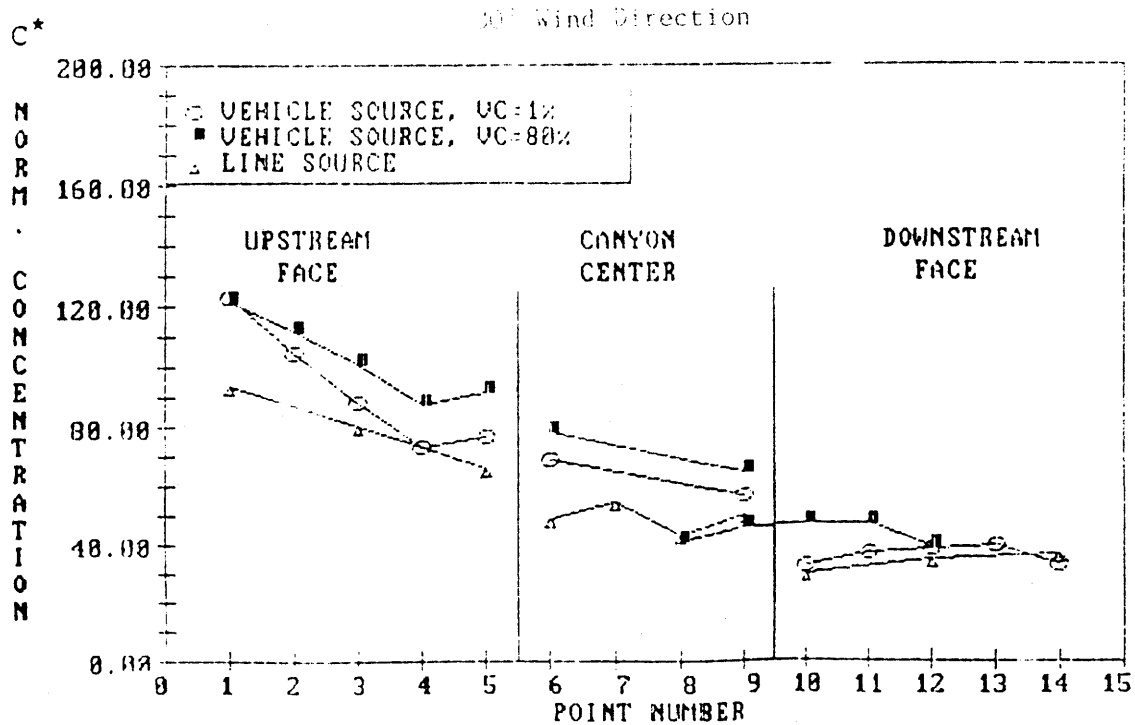


Figure 17. Test setup for source comparison.



a)



b)

Figure 18. Dispersion results of wind direction effects for two different vehicle speeds.

### 3. OBSERVATIONS AND RESULTS RELATED TO DISPERSION IN 2-D STRAIGHT CANYONS

#### A. Overview

Straight 2-D canyons comprise the major class of configurations studied. The baseline canyon was a 2-D canyon of  $W/H = 1$ . Other variations included varying  $W/H$ , adding a canopy to the upstream wall, sloping walls, and slotted canyons which were intended to simulate the effect of a multilevel open parking garage.

Tables 2-5 provide a listing of all the configurations tested and the type of data recorded and analyzed for each. The raw data on 2-D canyons and the sensor layouts for each test are compiled in data base number 1 to volume II of this report.

#### B. Analysis of Selected 2-D Straight Canyons

In this section, we have selected data which, when cross-plotted, provide insight into empirical trends and the types of dispersion conditions which exist in different types of canyon configurations. Table 6 provides a listing of receptor heights. These probe positions are consistent throughout this section.

##### Standard Canyon Width-to-Height Ratio = 1 ( $W/H = 1$ )

The  $W/H = 1$  "standard" canyon is characterized by a strong recirculating vortex. The configurations are shown in figure 19, and data for these cases are plotted in figure 20. Here we compare dispersion conditions for the  $W/H = 1$  canyon, and the immediate downstream neighbor. Flow visualization techniques revealed the strong vortex and intermittent secondary vortex (figure 21) as well as indicating a rotation rate and a rate at which the fluid in the canyon was transported away by the various flow exchange mechanisms ("washout") rate.

Frame-by-frame analysis of the flow visualization clearly demonstrated that the canyon vortex rotates faster as the air speed increases, as is predicted by theory. Figure 22 shows a linear relationship between the wind tunnel gradient velocity (maximum velocity above the test section) and the rotation rate of the vortex.

**Table 2. Data file cross reference  
for straight 2-D canyons  
(canyons of different widths).**

Headings:						
	wind angle	W/H	velocity data file	pollution concen- tration file	flow visualization test #	tape
Wide canyon	0	6	FHA1-29		3	A-3
Wide canyon	30	6	FHA1-31		10	A-16
Wide canyon	0	5	FHA1-143			
Wide canyon	0	4	FHA1-141			
Wide canyon	0	3	FHA1-139			
Wide canyon	0	2.5	FHA1-137			
Wide canyon	0	2	FHA1-41 NB17P23	NB14P63	2	A-2
Wide canyon	30	2	FHA1-33		9	A-17
Wide canyon	0	1.5	NB17P21			
Standard canyon	0	1	FHA1-27	FHA3-9	1	A-1
Standard canyon	30	1	FHA1-35	FHA3-39	11	A-15
Narrow canyon	0	.5	FHA1-49		4	A-6
Narrow canyon	30	.5	FHA1-47		12	A-20
Deep canyon	0	.25	FHA1-73	FHA3-81	42	A-8
Deep canyon	30	.25	FHA1-75	FHA3-83		

**Table 3. Data file cross reference  
for 2-D straight canyons (standard  
canyons with variations).**

Headings:						
	wind angle	W/H	velocity data file	pollution concen- tration file	flow visualization test #	Tape #
Tall building	0	1		FHA3-11, 13	41	B-31
Tall building	30	1		FHA3-41, 43		
Upstream block H=2W	0	1		FHA3-31	17	A-9
Downstream block H=2W	0	1	NB13 P121	NB14P59		
Canopy	0	1		FHA3-33		
Canopy	30	1		FHA3-45		
Canopy - source at W/4	0	1		FHA3-35		
Canopy - source at W/4	30	1		FHA3-47		



**Table 4. Data file cross reference for 2-D straight canyons (stepped topography) (sloping canyons).**

Headings:						
	wind angle	W/H	velocity data file	pollution concentration file	flow visualization test #	tape #
Upwind facing step	0		FHA1-43	NB14P65	6	A-5
Upwind facing step	30		FHA1-37			
Downwind facing step	0		FHA-51	NB14P61	5	A-4
Downwind facing step	30		FHA1-45			
Sloping wall	0	3		FHA3-95	19	A-10
Sloping wall	30	3		FHA3-93		
Katy freeway - source at W/4	0	7		FHA3-85	18	A-11
Katy freeway - source at W/4	30	7		FHA3-91		
Katy freeway - source at 3W/4	0	7		FHA3-87	18	A-11
Katy freeway - source at 3W/4	30	7		FHA3-89		

**Table 5. Data file cross reference  
for 2-D straight canyons  
(slotted canyons).**

Headings:						
	wind angle	W/H	velocity data file	pollution concentration file	flow visualization test #	tape #
<b>Standard canyons with slotted garage:</b>						
upstream canyon	0	1	FHA1-55	FHA3-77	13	A-12
downstream canyon	0	1	FHA1-57	FHA3-79	14	A-13
upstream canyon	30	1	FHA1-67			
downstream canyon	30	1	FHA1-65			
<b>Narrow canyon with slotted canyon:</b>						
upstream garage	0	.5	FHA1-59			
downstream canyon	0	.5	FHA1-63		15	A-14
upstream canyon	30	.5	FHA1-69			
downstream canyon	30	.5	FHA1-71			

Table 6. Table of x,z coordinates for straight canyon test configuration. Standard canyon height (H) = 3.50 in (8.89 cm).

PNT #	STANDARD, CANOPY TALL BUILDING, H1/H2 = 2		SLOTTED GARAGE		DEEP CANYON h = 3.786 H		STEPPED TERRAINE, H2/H1 = 2	
	<b>Along Upstream Wall Receptors</b>							
	X/H	Z/H	X/H	Z/H	X/H	Z/H	X/H	Z/H
1	-0.500	0.143	-0.500	0.143	-0.500	0.144	-0.500	0.143
2	*	*	*	*	-0.500	0.856	-0.500	0.286
3	-0.500	0.500	-0.500	0.500	-0.500	1.571	-0.500	0.429
4	*	*	*	*	-0.500	2.287	-0.500	0.571
5	-0.500	0.857	-0.500	0.500	-0.500	3.642	-0.500	0.714
	<b>Canyon Center Receptors</b>							
	X/H	Z/H	X/H	Z/H	X/H	Z/H	X/H	Z/H
6	-0.214	0.175	-0.214	0.500	-0.500	3.286	-0.171	0.714
7	-0.214	0.143	-0.214	0.143	-0.500	0.143	*	*
8	0.214	0.143	0.214	0.200	0.500	0.143	*	*
9	0.214	0.175	0.214	0.500	0.500	3.286	0.171	0.714
	<b>Along Downstream Wall Receptors</b>							
	X/H	Z/H	X/H	Z/H	X/H	Z/H	X/H	Z/H
10	0.500	0.857	0.500	0.200	0.500	0.143	0.500	0.714
11	*	*	*	*	0.500	0.856	0.500	0.571
12	0.500	0.500	0.500	0.500	0.500	1.571	0.500	0.429
13	*	*	*	*	0.500	2.287	0.500	0.286
14	0.500	0.143	0.500	0.894	0.500	3.642	0.500	0.143
	<b>Additional Receptors</b>							
	X/H	Z/H	X/H	Z/H	X/H	Z/H	X/H	Z/H
15	*	*	0.000	0.323	*	*	0.500	1.000
16	*	*	0.000	0.537	*	*	0.500	1.500
17	*	*	0.000	0.786	*	*	0.500	1.829

Table 6. Table of x,z coordinates for straight canyon test configuration. Standard canyon height (H) = 3.50 in (8.89 cm) (continued).

POINT #	WIDE CANYON W/H = 2		SLOPING CANYON		KATY FREEWAY	
	Along Upstream Wall Receptors					
	X/H	Z/H	X/H	Z/H	X/H	Z/H
1	-1.000	0.143	-0.643	0.143	-4.394	0.251
2	-1.000	0.286	*	*	*	*
3	-1.000	0.429	-1.000	0.500	-5.286	0.500
4	-1.000	0.571	*	*	*	*
5	-1.000	0.714	-1.357	0.857	-6.180	0.751
	Canyon Center Receptors					
	X/H	Z/H	X/H	Z/H	X/H	Z/H
6	-0.429	0.714	-0.500	1.000	-3.500	1.000
7	*	*	*	*	*	*
8	*	*	*	*	*	*
9	0.429	0.714	0.500	1.000	3.500	1.000
	Along Downstream Wall Receptor					
	X/H	Z/H	X/H	Z/H	X/H	Z/H
10	1.000	0.714	1.357	0.857	4.394	0.751
11	1.000	0.5711	*	*	*	*
12	1.000	0.429	1.000	0.500	5.285	0.500
13	1.000	0.286	*	*	*	*
14	1.000	0.143	0.643	0.857	6.180	0.751
	Additional Receptors					
	X/H	Z/H	X/H	Z/H	X/H	Z/H
15	*	*	1.500	1.000	7.071	1.000
16	*	*	1.929	1.214	7.557	1.214
17	*	*	1.929	2.429	7.557	5.286

# EFFECT OF STANDARD CANYON CONFIGURATIONS

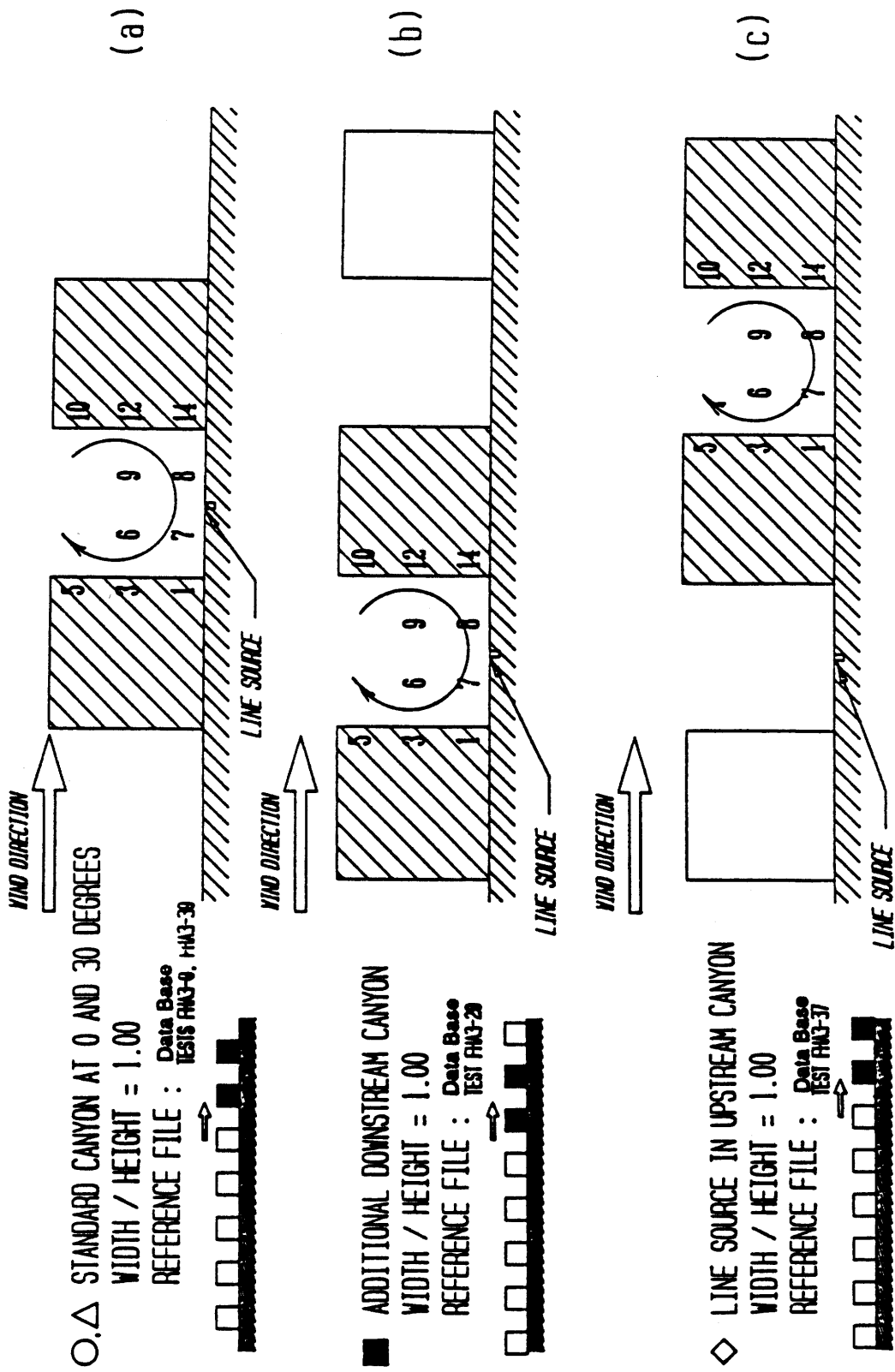


Figure 19. Test setup and probe locale for standard canyon configurations, W/H = 1.

C\*

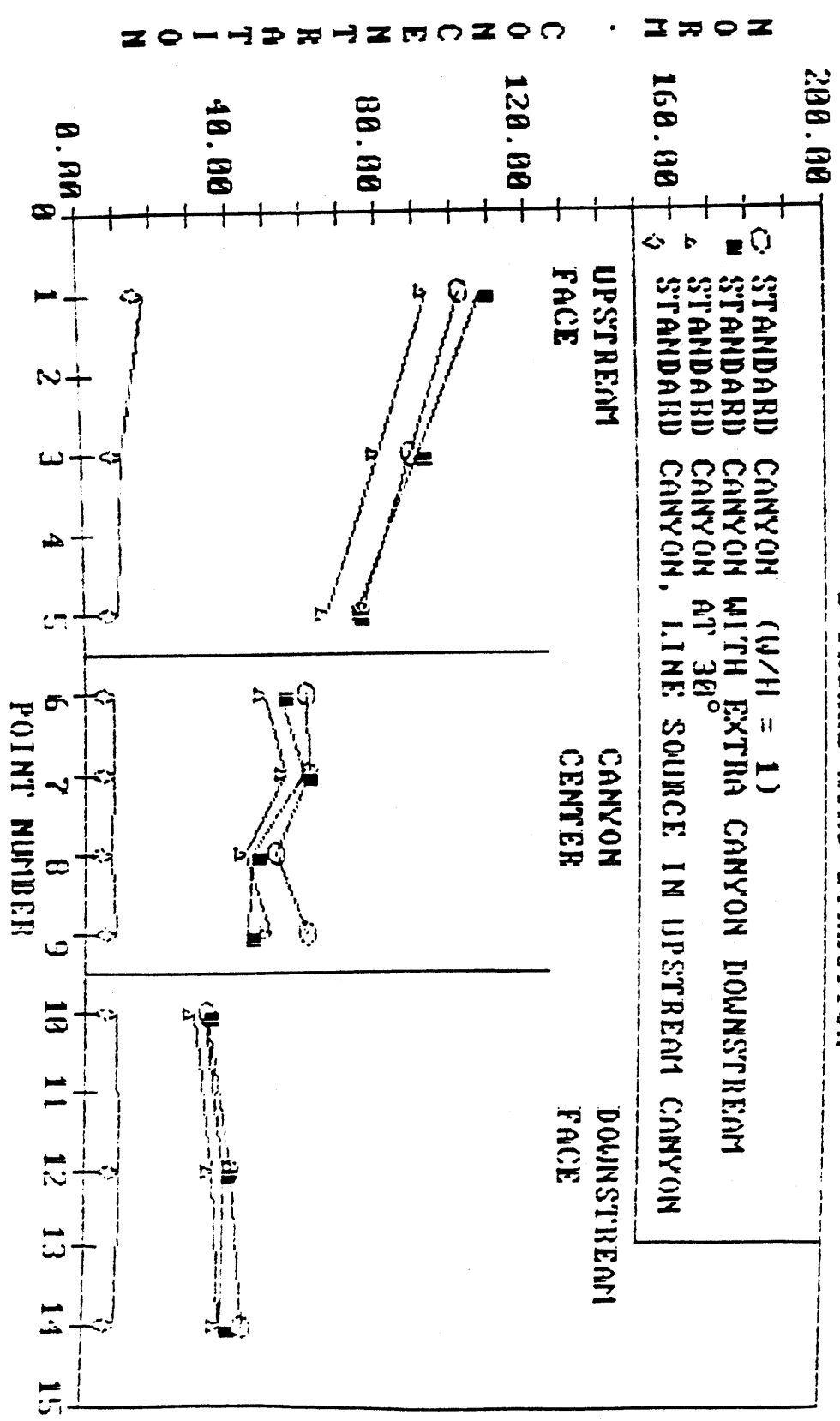


Figure 20 Results of standard canyon configurations, W/H = 1.

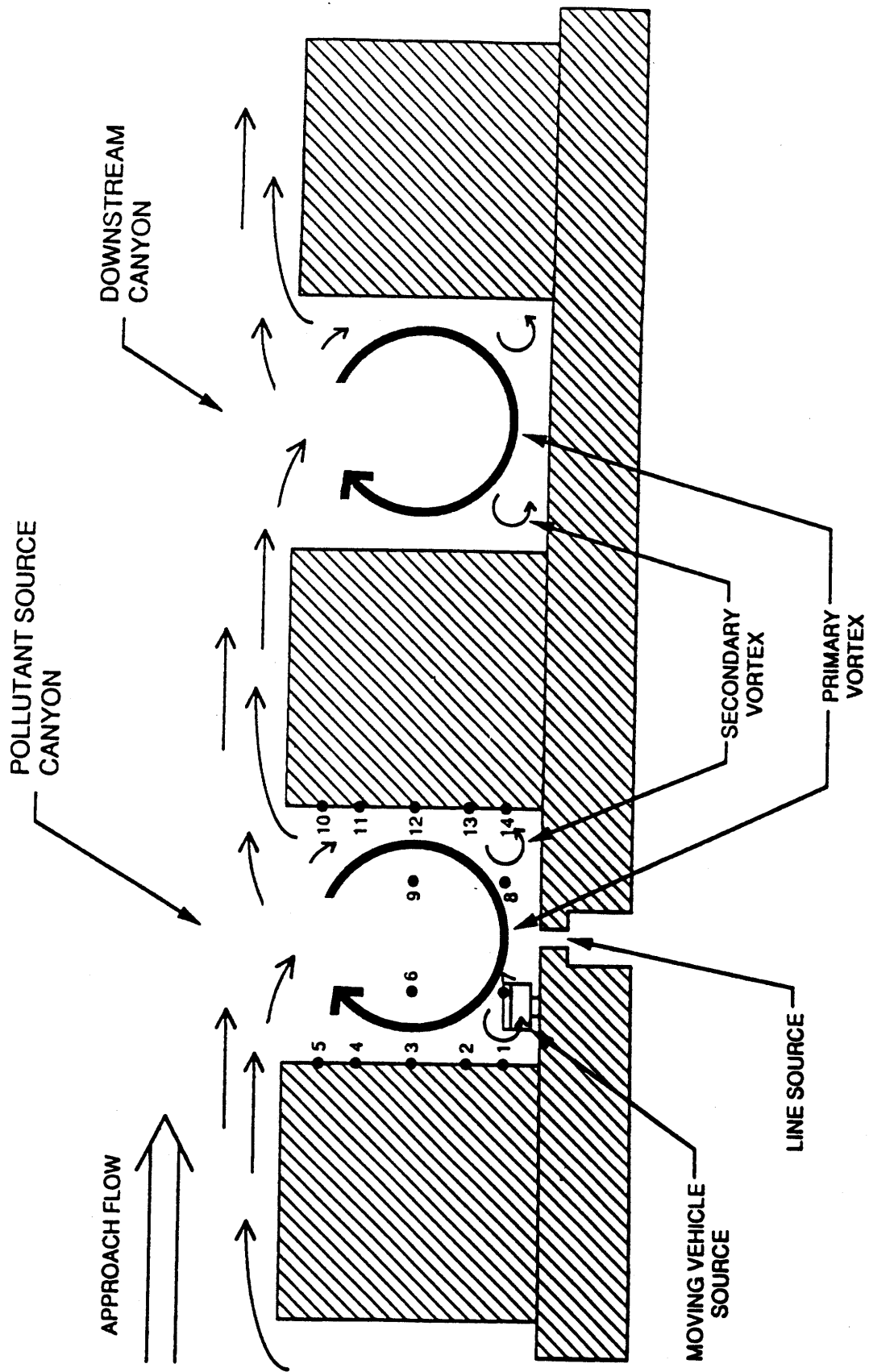


Figure 21. Flow structure of a standard 2-D canyon.

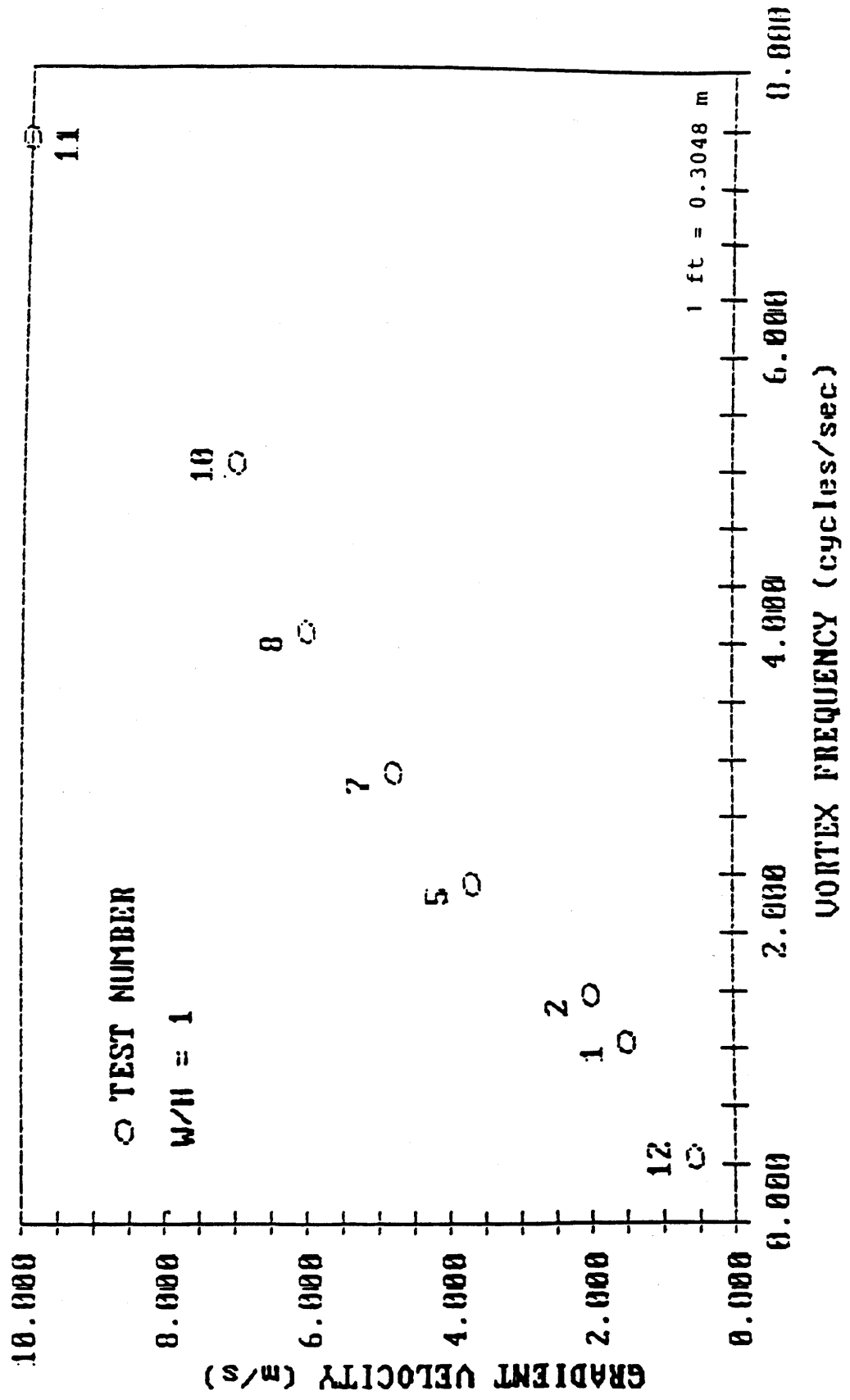


Figure 22. Effect of vortex rotational frequency with increasing gradient velocity,  $W/H = 1$ .



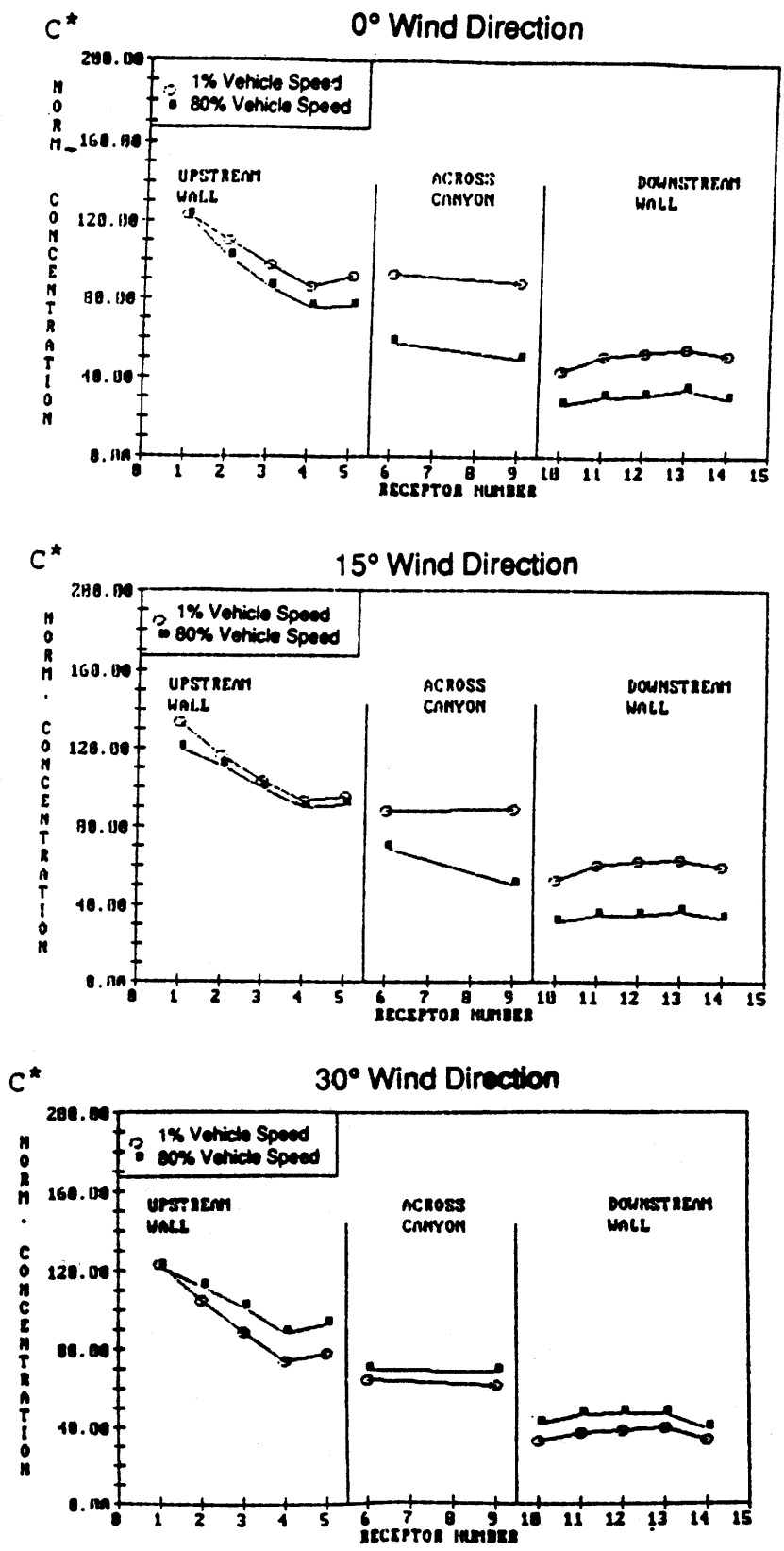
To determine the "washout" rate, the canyon was videotaped with a low gradient velocity, 0.6 m/s (2 ft/s), and the tapes were viewed frame by frame. The rotation rate of the canyon vortex was 27 cycles/min. By allowing the canyon to completely fill with smoke, then removing the source, a 95 percent washout of smoke was observed in 7 seconds. This occurred after three complete vortex rotations.

Figure 19C illustrates a test quantifying the emissions that pass from the source canyon to its downwind neighbor. The concentrations that occur in the canyon immediately downstream are around 15 percent of the source canyon mean concentrations (figure 20), and the receptors indicate nearly uniform dispersion throughout the downstream canyon. This is in sharp contrast to the source canyon dispersion profile with the pollution introduced at street level. A 44 percent lower concentration is consistently found along the downstream wall. The difference in these profiles is a function of where the emissions are introduced since the flow structure is identical in both canyons. Throughout this report the concentration profile for the "standard" canyon in figure 20 will be used as a common case for which all other configurations will be compared. As the approach wind direction is changed to an angle of 30', the concentrations are reduced an average of 10 percent. The "hot spot" at the base of the upstream wall remains. The consistent variation in concentrations with wind angle, for angles less than 30', occur in proportion to the cosine of the wind angle (i.e., in direct proportion to the cross-canyon component of velocity).

For 0' wind direction, the effect of vehicle speed in the standard canyon is a decrease in concentration as the vehicle speed is increased (figure 23). The effect is greatest across the canyon and along the downstream wall. At a wind angle of 30' the effect of car speed is reduced. This is thought to be attributed to the along-canyon velocity component, which in this case is in the opposite direction of the car motion.

#### Standard Canyon with a Canopy

These tests were designed to determine the effect of a canopy attached to the upstream wall of a standard canyon at half height. When a canopy is added (figure 24), the concentration under the canopy increases for a wind angle of 0', but other locations are unaffected (figure 25A). This effect was independent of source position from W/4 to W/2. When the wind direction changes to  $\pm$  30', the canopy effect is largely eliminated, presumably due to along canyon flow, as shown



a)

b)

c)

Figure 23. Effect of vehicle speed at different wind directions in a standard canyon, W/H = 1.

# EFFECT OF A CANOPY ADDED TO A STANDARD CANYON 0 AND 30 DEGREE WIND DIRECTION

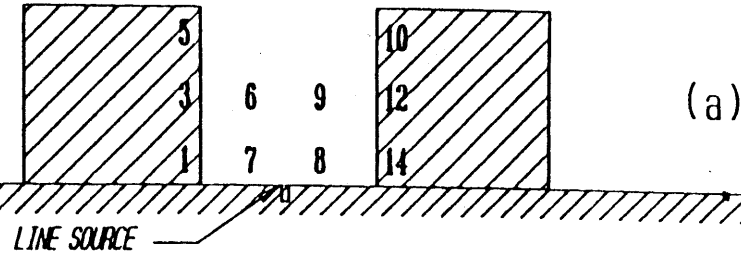
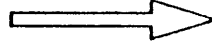
○ STANDARD CANYON

WIDTH / HEIGHT = 1.00

REFERENCE FILE : Data Base  
TEST FHA3-9, FHA3-30



WIND DIRECTION



(a)

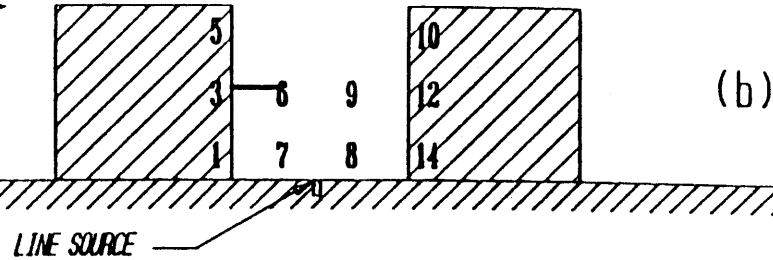
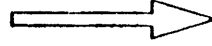
■ CANOPY WITH LINE SOURCE AT W/2

WIDTH / HEIGHT = 1.00

REFERENCE FILE : Data Base 1  
TEST FHA3-33, FHA3-45



WIND DIRECTION



(b)

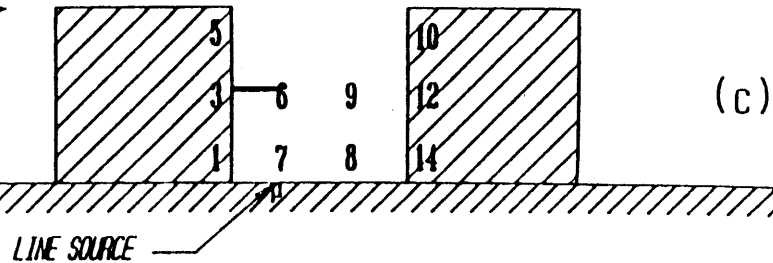
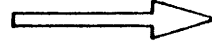
△ CANOPY WITH LINE SOURCE AT W/4

WIDTH / HEIGHT = 1.00

REFERENCE FILE : Data Base  
TEST FHA3-35, FHA3-47

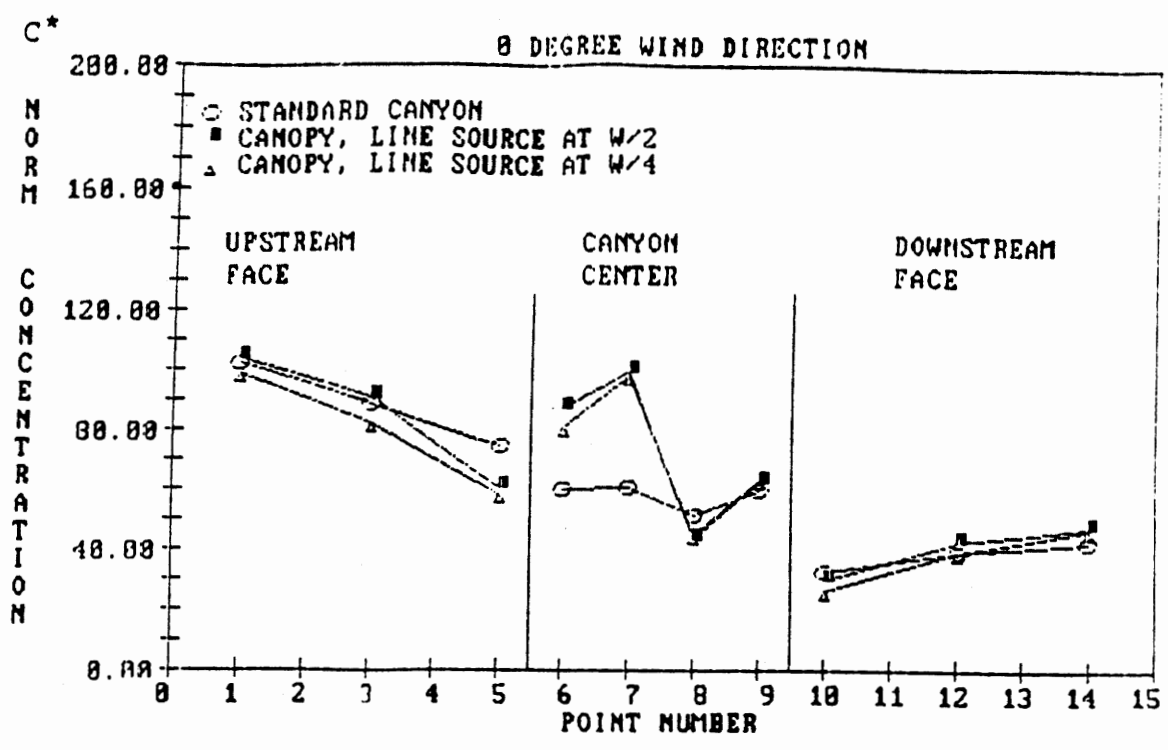


WIND DIRECTION

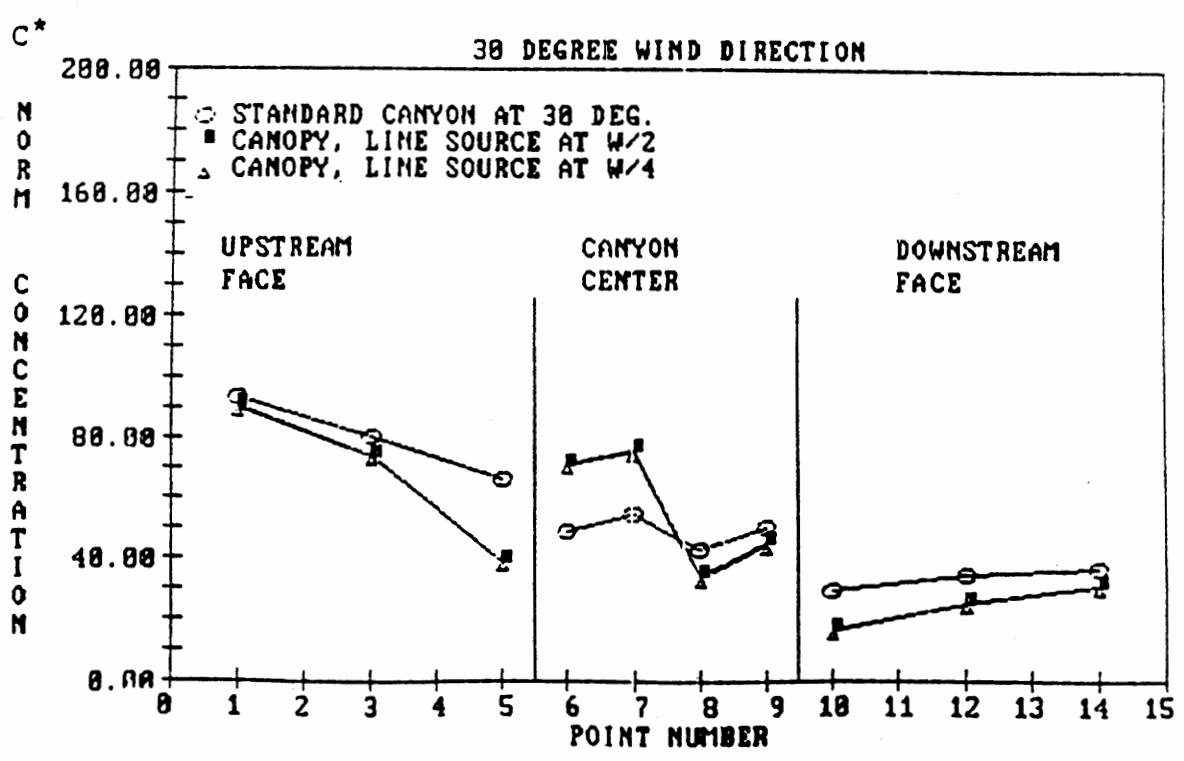


(c)

Figure 24. Test setup for canopy configurations.



a



b)

Figure 25. Effect of a canopy placed at half height

in figure 25B. When the line source was moved from width/2 to width/4 from the upstream wall, little change was observed. For the 30° wind direction case, the decrease in concentration is directly comparable to the change in the standard canyon and is consistent throughout the canyon.

### Slotted Canyons

A canyon was constructed with one side slotted, as a simulation of a typical parking structure. This configuration was tested with the street level source upstream and downstream of the slotted canyon. No emissions were simulated in the "garage" itself. Figure 26 illustrates the configuration and plotted concentrations. In both the cases simulated, the concentrations along the downwind wall were within 20 percent of the baseline (unslotted) canyon concentrations. The concentrations along the upstream wall and at street level varied dramatically. Using the concentration values of the standard canyon ( $W/H = 1$ ) for the upstream wall comparison, the canyon upstream of the slotted building has similar concentrations. When the source is downstream of the slotted building, the upstream wall concentration values are 50 percent lower than the corresponding unslotted canyon ( $W/H = 1$ ) values. When the source is located upwind of the slotted building, the upstream wall concentration values are similar to the corresponding unslotted canyon ( $W/H = 1$ ) values.

Flow visualization shows that the slots in the building connect the high pressure to the low pressure in each canyon. The pressure gradient across the upper slot "favors" the downwind canyon, and the pressure gradient in the lower two slots favors the upwind canyon. This pressure difference creates fluid transfer between the two canyons. This promotes a greater circulation in the upstream canyon, and draws pollutants from the downstream canyon into the upstream canyon.

By superimposing the concentration levels for both source locations, the net effect of a dual source configuration was determined. The combined concentrations found in figure 27 are the results of the addition of the concentrations in figure 26 - heavy lines for the slotted case and thin lines for the unslotted case. For the standard canyon configuration, the combined upwind canyon (canyon "A") levels are identical to the standard canyon values because no backflow of pollutants from canyon "8" occurs. The net pollutant transfer illustrates quantitatively how concentration levels increase in canyon "A" and decrease in canyon "8" when slots are introduced, as compared to the corresponding unslotted configuration.

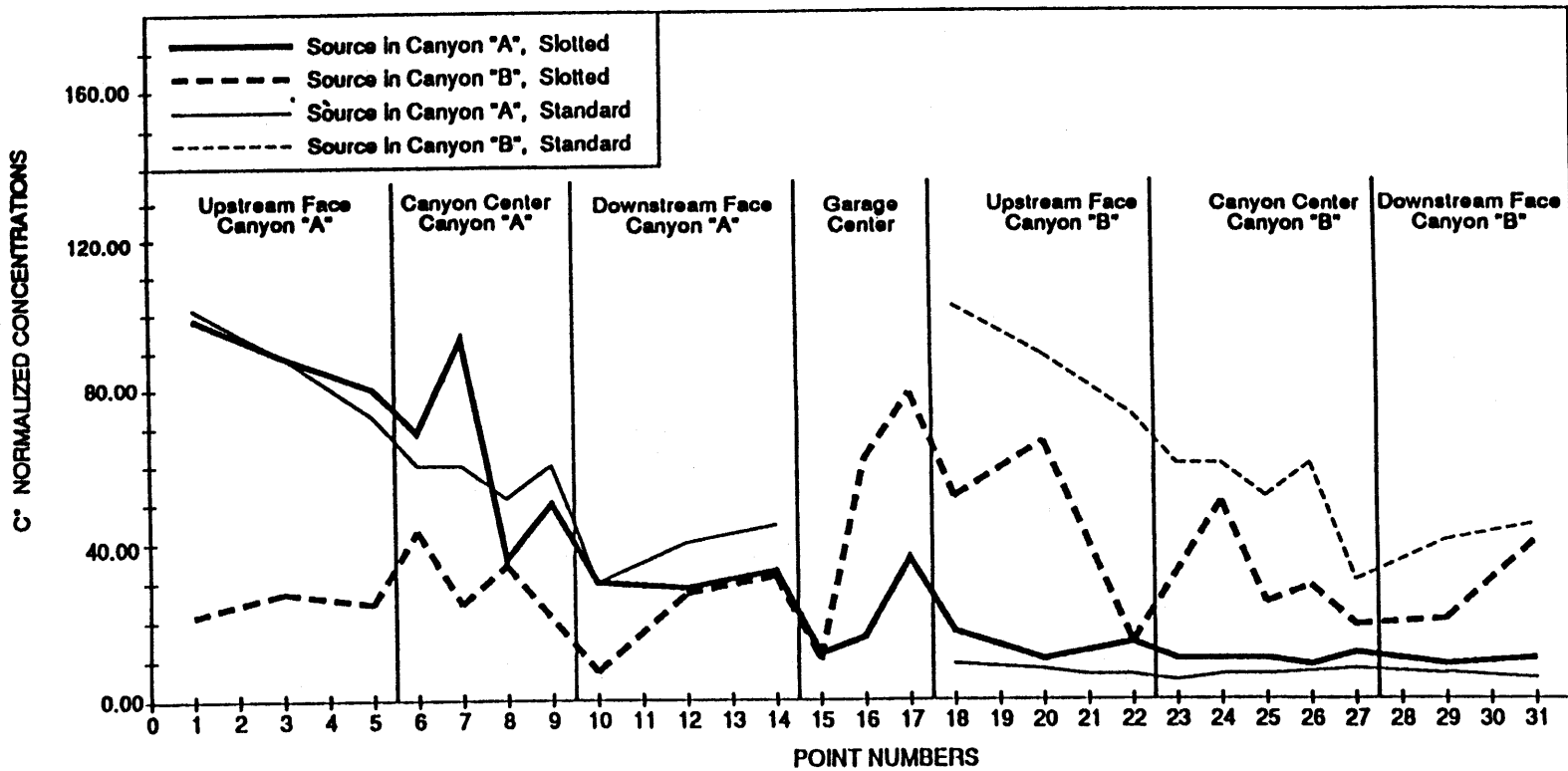
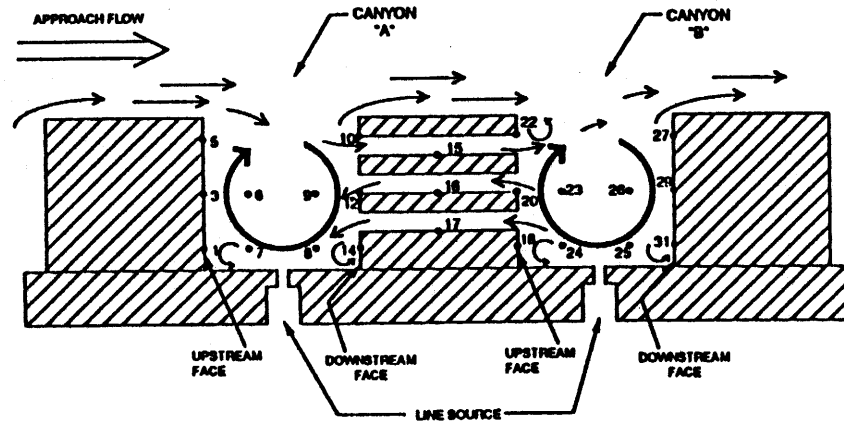
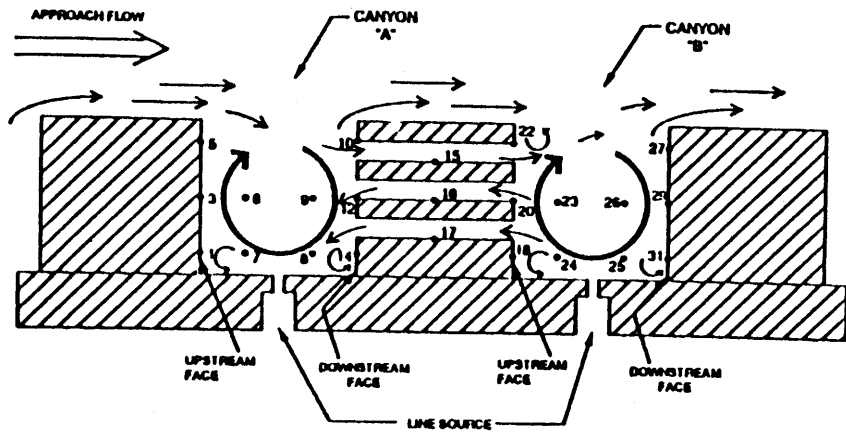


Figure 26. Effects of a porous walled canyon,  $W/H = 1$ .



85

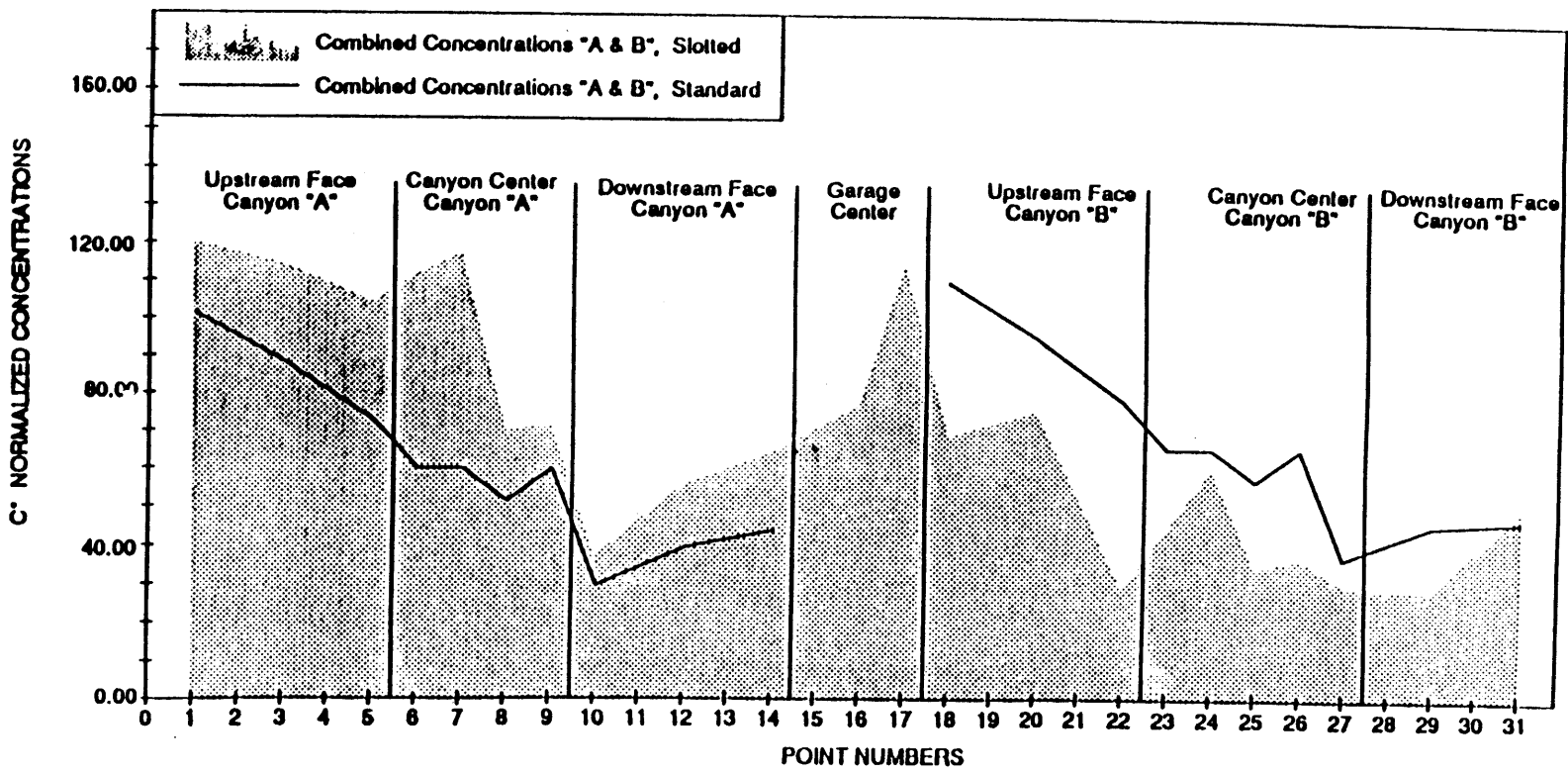


Figure 27. Combined effects of porous walled canyon vs. standard canyon.

### Different Width-to-Height Ratio Canyons

These tests were designed to explore the effect of increasing the W/H ratio from 1 to a limiting case of the downstream facing step. Also, the standard canyon was deepened to study the W/H ratios of less than 1.

Flow visualization for a full range of W/H are illustrated in figures 28 and 29.

- Width-to-Height Ratios Greater than One

The canyon vortex that is typical of the 1:1 canyon appears in almost all canyon geometries. As the canyon widens, the 1:1 vortex will appear where the geometric boundaries allow, and the vortex seems to resist elongation and remain circular in cross section. The remaining canyon space is filled by secondary vortices and random flows. The 1:1 canyon vortex will elongate until a W/H ratio between 1.5 and 2. The flow then changes and maintains a new characteristic pattern until  $W/H = 5$ . The canyons  $W/H = 2, 3, 4$  have a vortex against the downstream wall and have a stagnation pocket along the upstream wall. This flow pattern is similar to the downstream facing step. There is a progression of strengthening vortex and shrinking stagnation pocket as the W/H ratio decreases from  $W/H = 4$  to 2.

The  $W/H = 5$  appears to be a transitional geometry where two repeating flow patterns exist. First, there appear to be two vortices, one centered at  $X \sim 4H$  and the other against the downstream wall. This will change as surges of air will occasionally make the entire canyon act as an elongated vortex.

From  $W/H = 6, 7, 8$ , the dominating flow pattern is located within the upwind  $X \sim 4H$  of the canyon. There is some effect, although slight, from the downstream wall on the flow in the first  $4H$  of the canyon.

At  $W/H = 9$  there is no longer any effect of the downstream wall, and the flow over the upstream wall is identical to a downstream facing step. Likewise, the flow over the downstream wall is identical to the upstream facing step.

- Width-to-Height Ratios Less than One

For the  $W/H$  ratio =  $1/2$  (figure 28B), a strong vortex develops in the top half of the canyon, driving a weak counter-rotating vortex in the lower half of the canyon. For the canyon with  $W/H = 1/4$  (figure 28C), a strong vortex develops in the top of the canyon. This strong top vortex intermittently pushes air



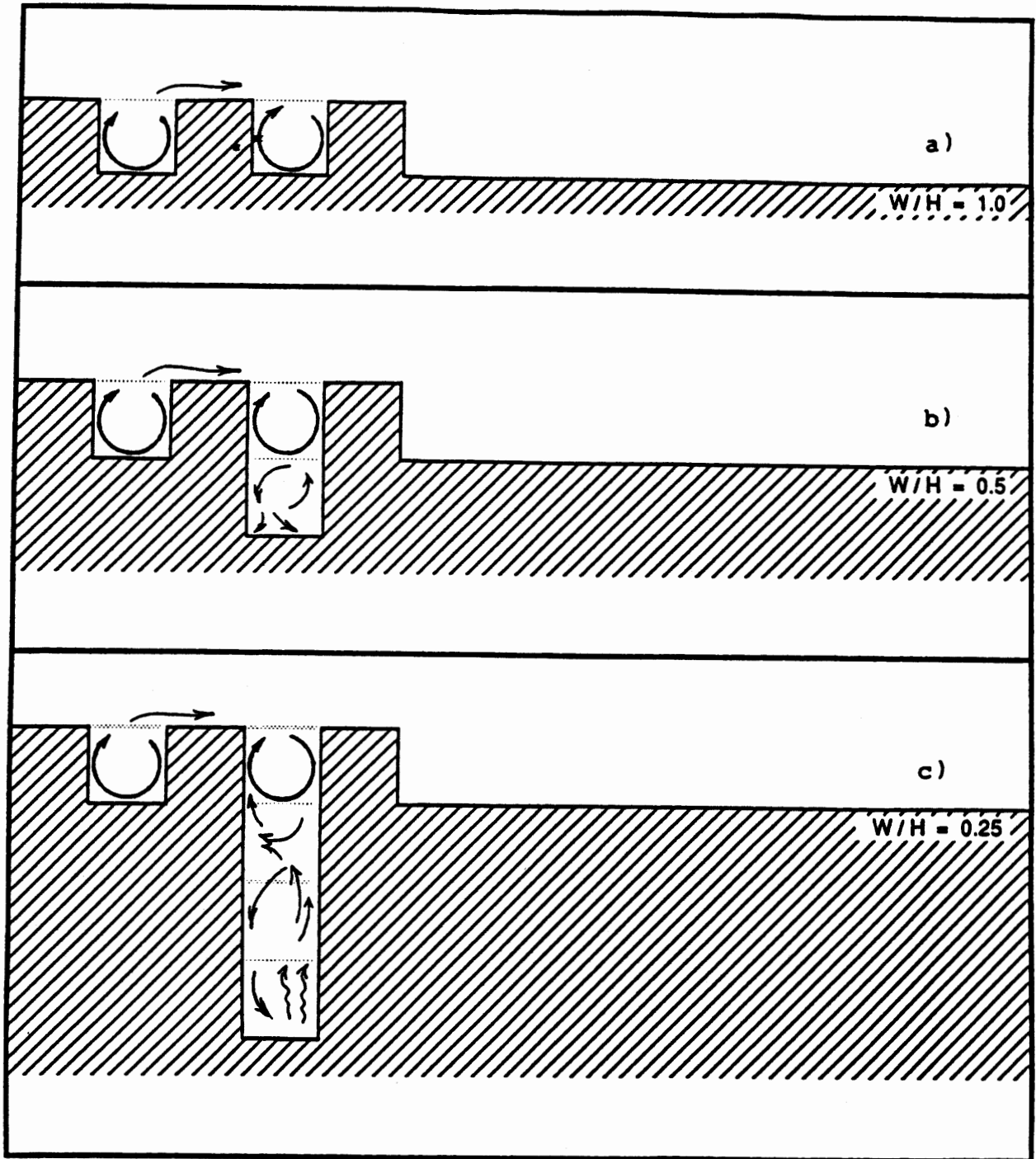


Figure 28. Flow visualization of width/height ratios from 0.25 to 1.0.

into the canyon on the downwind side, and intermittently pulls air up out of the canyon. The exchange process has been observed to be very intermittent. No counter-rotating vortex develops.

- Comparison of Width-to-Height Ratios

Due to meandering flow characteristics of the deep canyon (figure 28C) and the downstream step (figure 29F), the dispersion trends are similar (figure 31). When stagnant air pockets occur, the concentration levels are extremely high at the lower corner and decrease sharply with increased height. The standard canyon and the wide canyon also produced similar trends due to the recirculating nature of the flows. The increase in concentration along the upstream face is less steep, and concentrations on the downstream face are much lower than stagnant flow patterns (figure 31). Figure 30 represents the test set-ups which produced the results in figure 31.

- "Deep" Canyon;  $W/H = 0.25$

This test was developed to determine the effect of a canyon with a width-to-height ratio =  $1/4$  with a line source. As expected, the concentrations at canyon bottom were significantly higher than those found in the standard canyon. The highest values were on the downstream side of the canyon (for a clearer understanding, see figure 30B). The concentration levels decrease as the height increases, thus showing that more mixing of pollutants and fresh air occurs nearer the top of the canyon.

When the wind direction approached from  $30^\circ$ , a sharp decrease in concentration levels occurred throughout the canyon (figure 32). The lateral wind component caused greater mixing and thereby substantially increased the ventilation of the canyon.

- Wide Canyon;  $W/H = 2$

This test was developed to determine the effect of a wider canyon configuration,  $W/H = 2$ , with a vehicle source at  $0.143W$  upstream of the canyon center. To more accurately compare the concentration to those obtained by a line source, see Effect of Vehicle Speed and Comparison of Line Source and Vehicle Source.

The concentration levels peaked at the lower upstream wall and decreased across the canyon (figure 31). The pollutants are drawn towards the upstream wall and then pulled upward by the shear flow near the canyon ceiling. The wider canyon followed the same trends as the standard canyon ( $W/H = 1$ ) but had lower

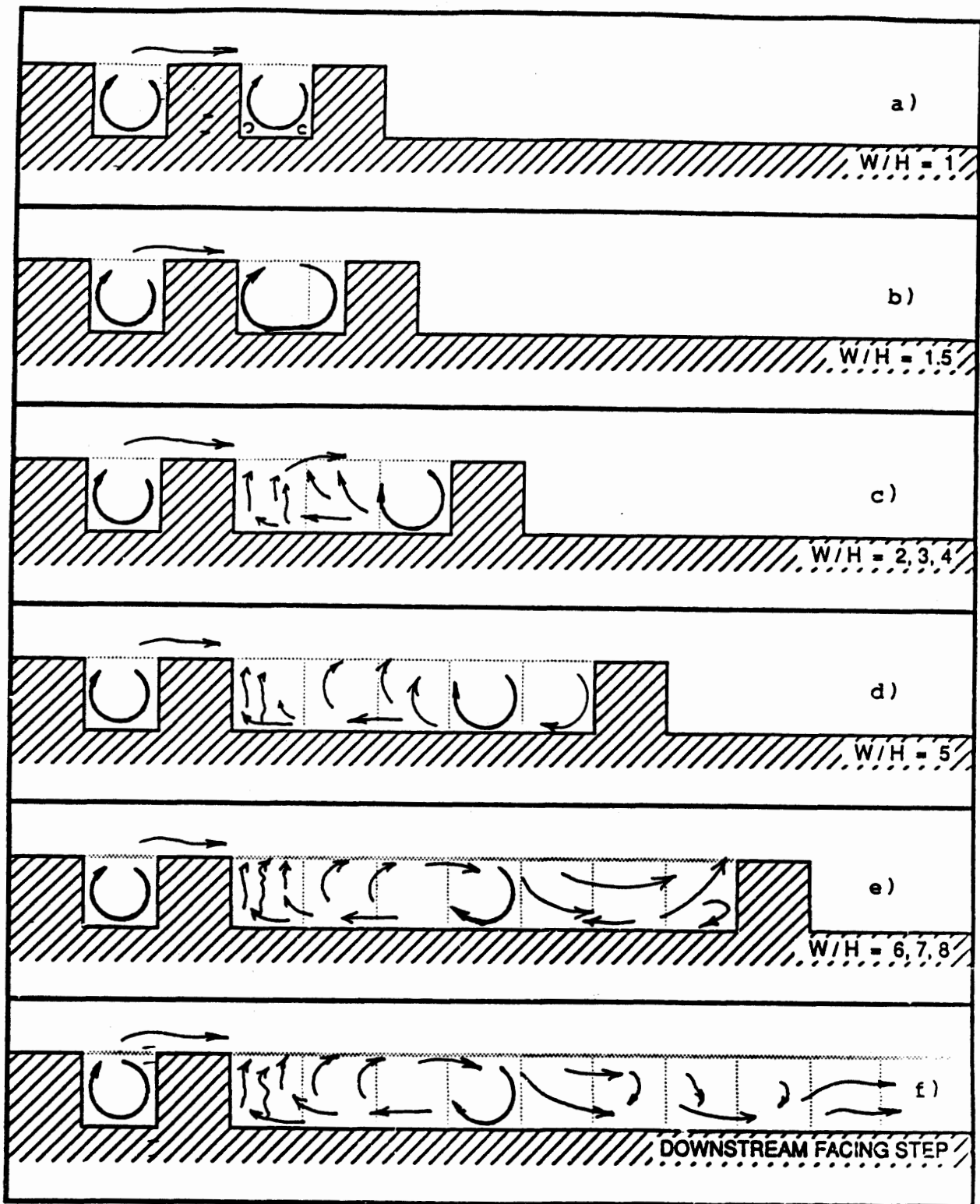


Figure 29. Flow visualization of width/height ratios from 1.0 to  $\infty$ .

# EFFECT OF DIFFERENT WIDTH TO HEIGHT RATIOS

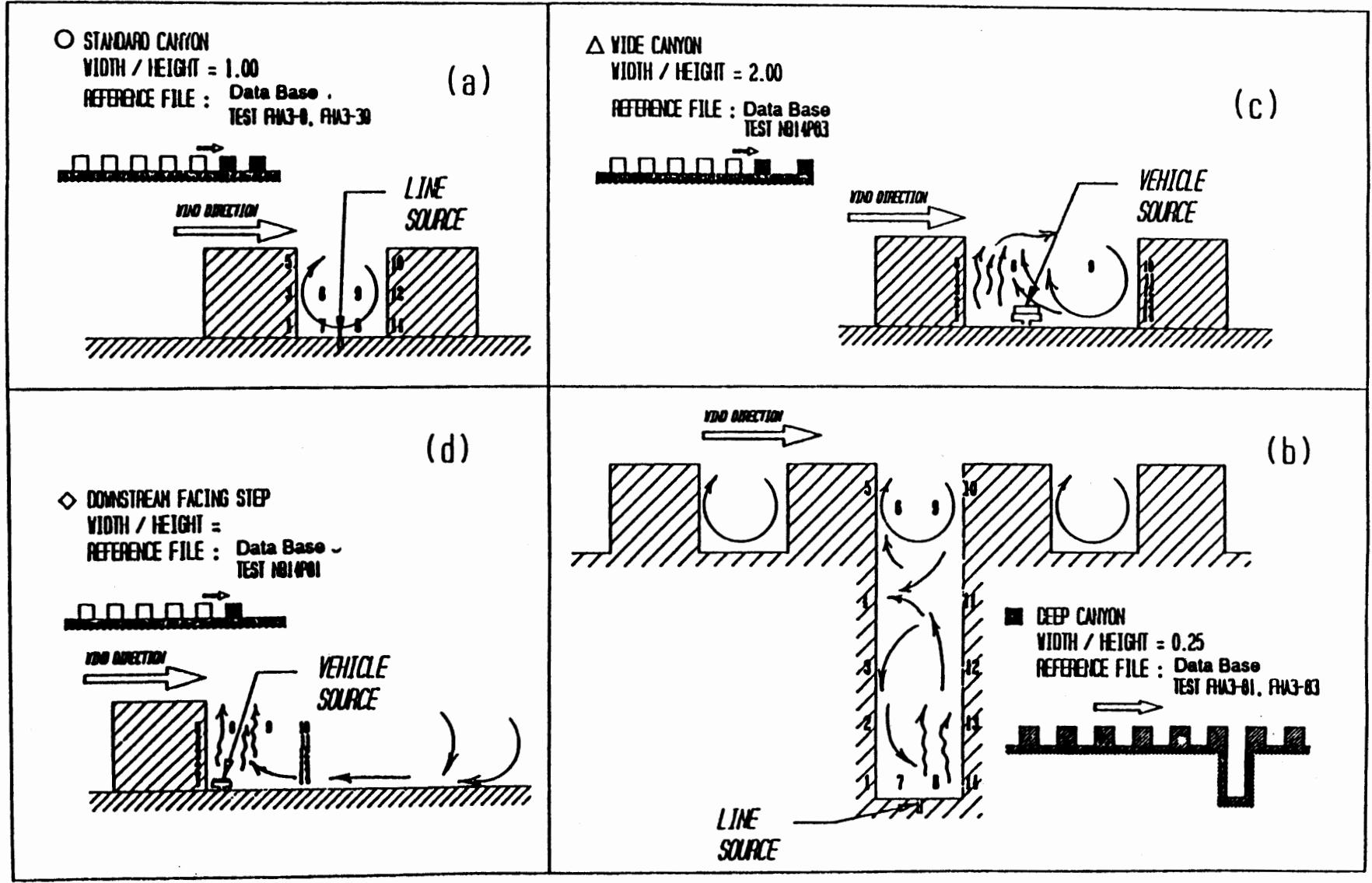


Figure 30. Test setup and point locale for different width/height ratios.

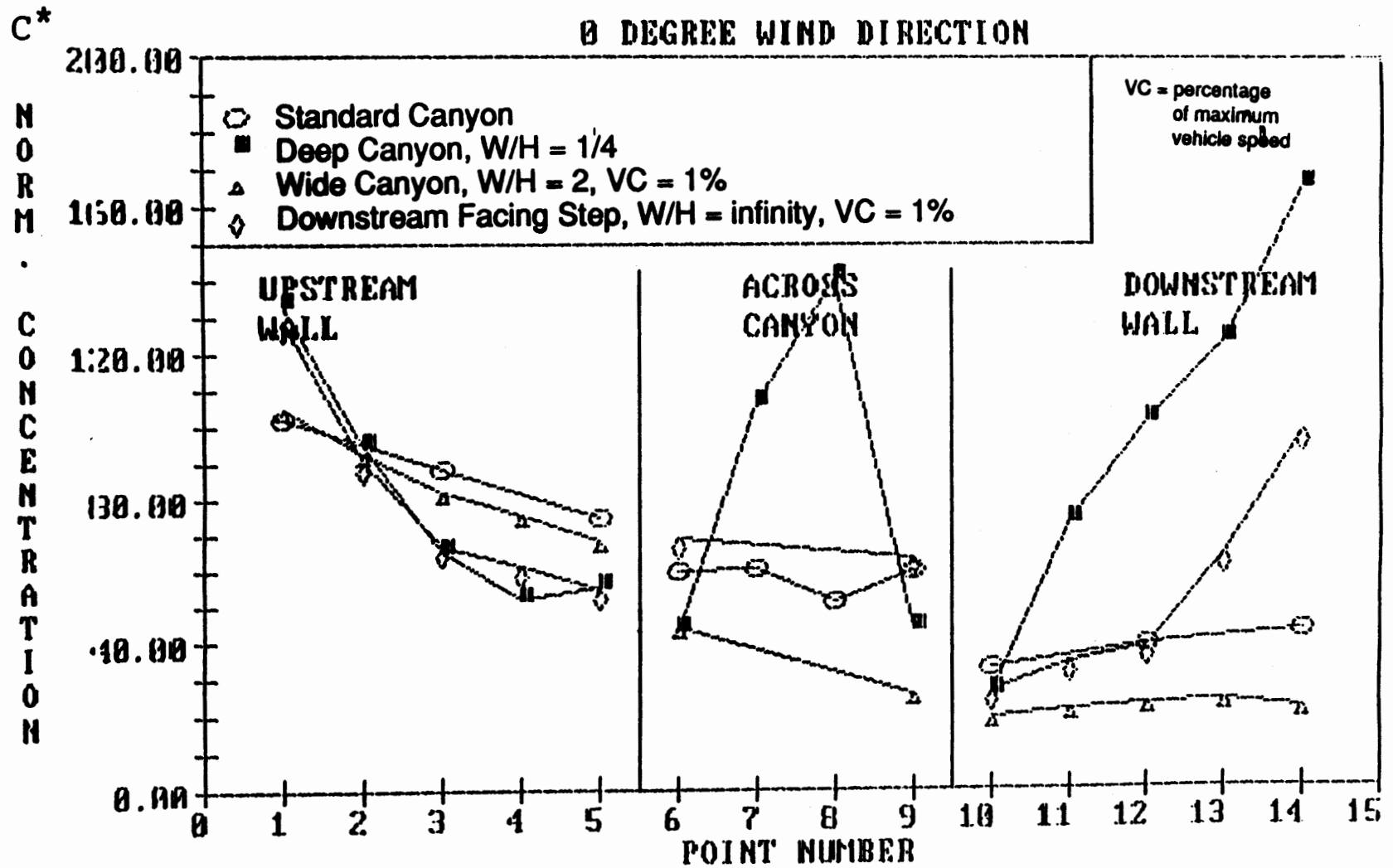


Figure 31. Effect of different width/height ratios.

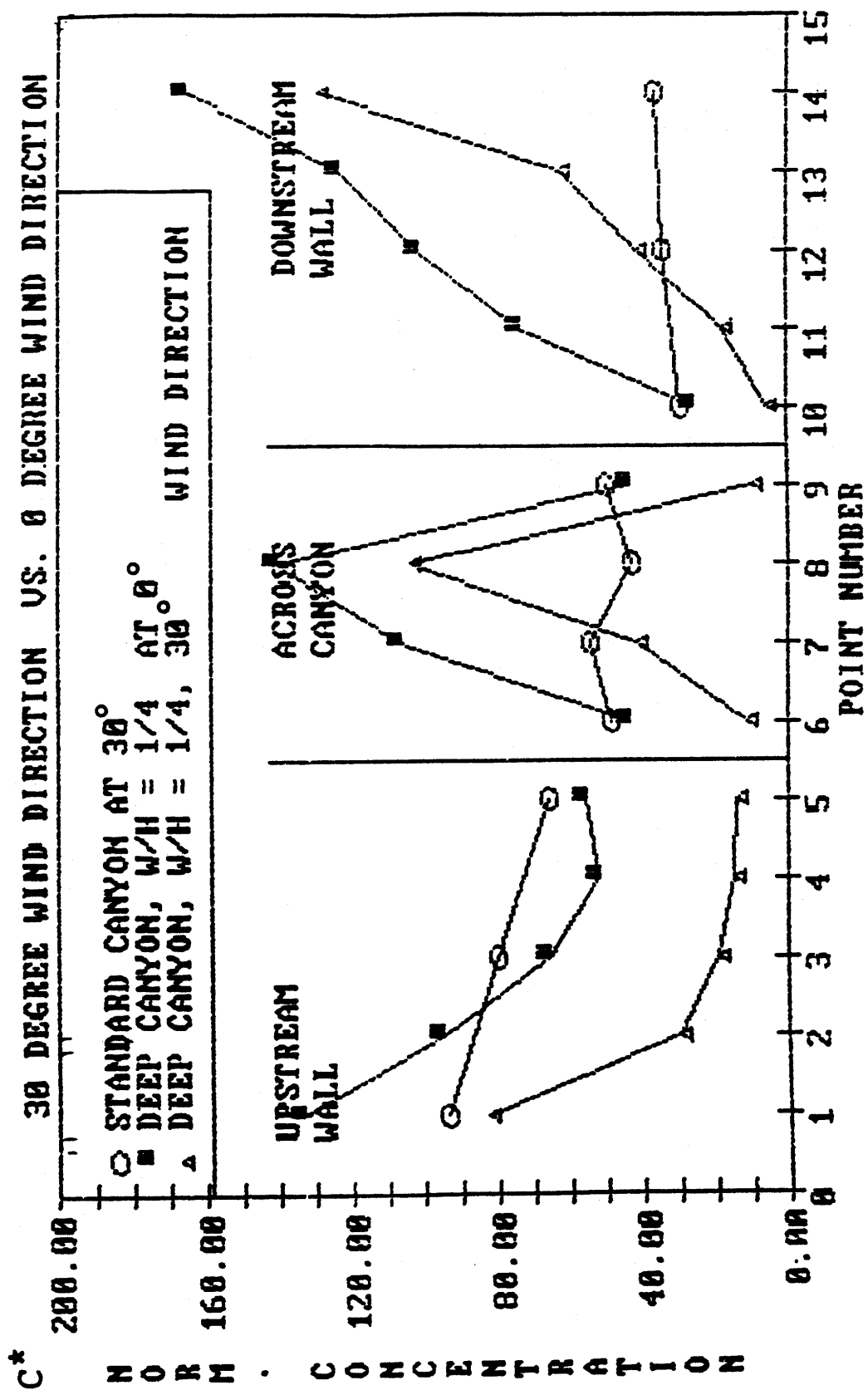


Figure 32. Effect of a deep canyon (W/H = 0.25) at different wind directions.

concentrations throughout the canyon. By increasing the vehicle speed from 1 percent to 80 percent of the maximum, the concentration values drop significantly on the upstream wall and drop slightly across the canyon and along the downstream wall (figure 33). The upstream drop resulted from increased mixing due to the vehicle speed in a relatively inactive flow region.

### Stepped Configurations

- Effect of a Downwind Facing Step

This test was designed to determine the effect of a downstream step, which is a typical urban configuration occurring along rivers, parks, and waterfronts (figure 34B). In this case, the downstream block of a standard canyon was removed, leaving the downstream side of the canyon open. Concentrations peaked in the lower upstream corner and decreased sharply from the bottom to the top of the upstream wall (figure 35). Across the canyon, the concentrations peaked at mid-canyon and were lower on the upstream side than on the downstream side. These results suggest that the local flow does not develop a recirculating vortex, but that the pollutants are in a pocket of lower velocity air, causing lower receptor concentration to be high. When the vehicle speed was increased from 1 percent to 80 percent, all of the receptors recorded lower concentrations. Results are shown in figure 36.

Figure 37 shows vertical concentration profiles made at two different distances,  $1H$  and  $4.43 H$ , downstream from the downwind facing step. As the receptor height increased, the concentration dropped sharply. When the distance from the upstream wall was increased to  $4.43 H$ , the concentrations decreased greatly, as expected. The decrease of pollutants in the plume behind the downstream facing step is illustrated in figure 38. Immediately behind the step at  $Z/H = 0.714$ , a detailed profile shows there is an area of high pollutants within one height back from the wall. Additional data was unavailable at lower heights, but even higher concentrations are expected.

- Effect of an Upstream Facing Step

This test (figure 34C) was designed to determine the effect of an upstream step. In this case, the upstream blocks of the standard canyon were removed, leaving the upstream side of the canyon open. Also, all the upstream canyons were removed, but the tunnel's roughness elements all remained in place. The results (figure 39) show that this configuration produced the lowest concentrations. Vehicle speed variation caused little

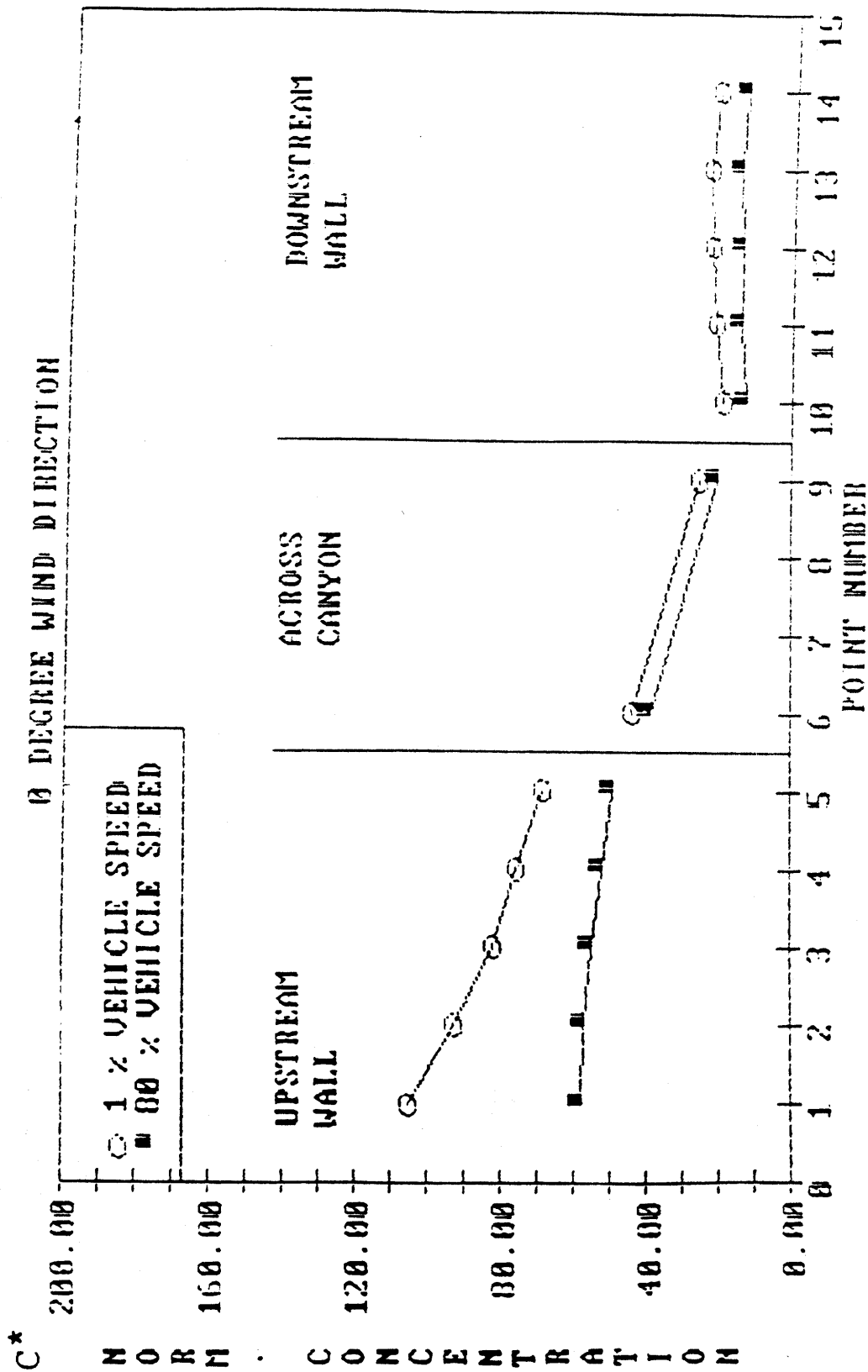



Figure 33. Effect of vehicle in a wide canyon configuration W/H = 2.




# EFFECT OF STEPPED TERRAINE

○ STANDARD CANYON  
 WIDTH / HEIGHT = 1.00  
 REFERENCE FILE : Data Base TEST RW3-9



■ DOWNSTREAM FACING STEP  
 WIDTH / HEIGHT =  
 REFERENCE FILE : Data Base TEST N814P1



△ UPSTREAM FACING STEP  
 WIDTH / HEIGHT =  
 REFERENCE FILE : Data Base TEST N814P6


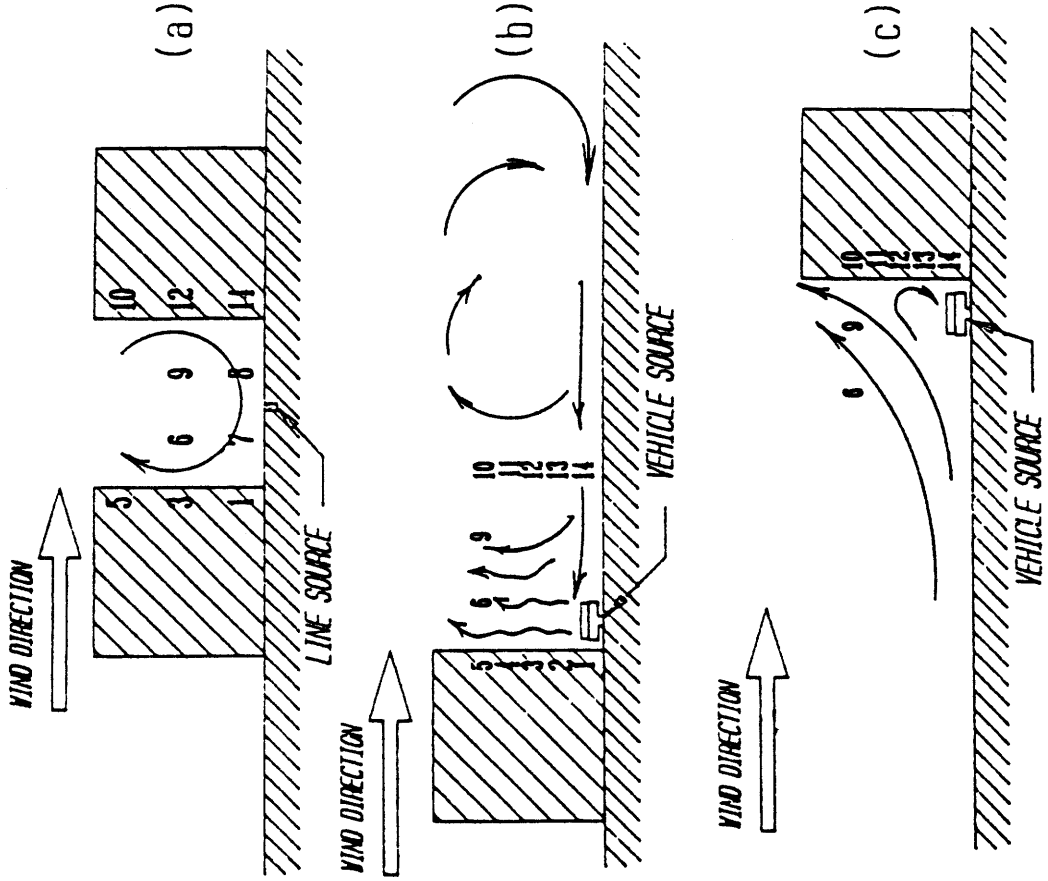



Figure 34. Test setup and point locale for stepped terrain.

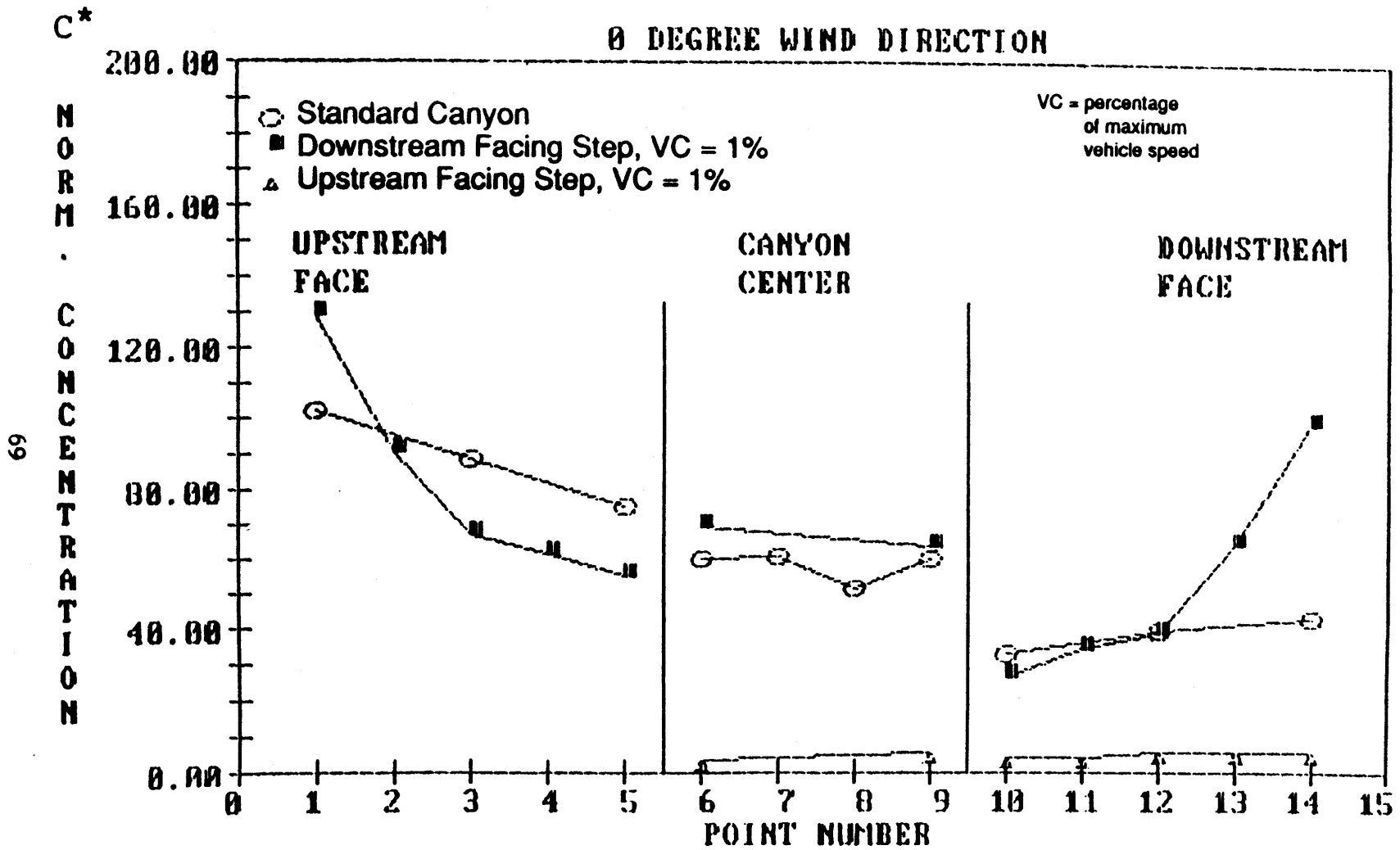


Figure 35. Effect of stepped terrain configurations.

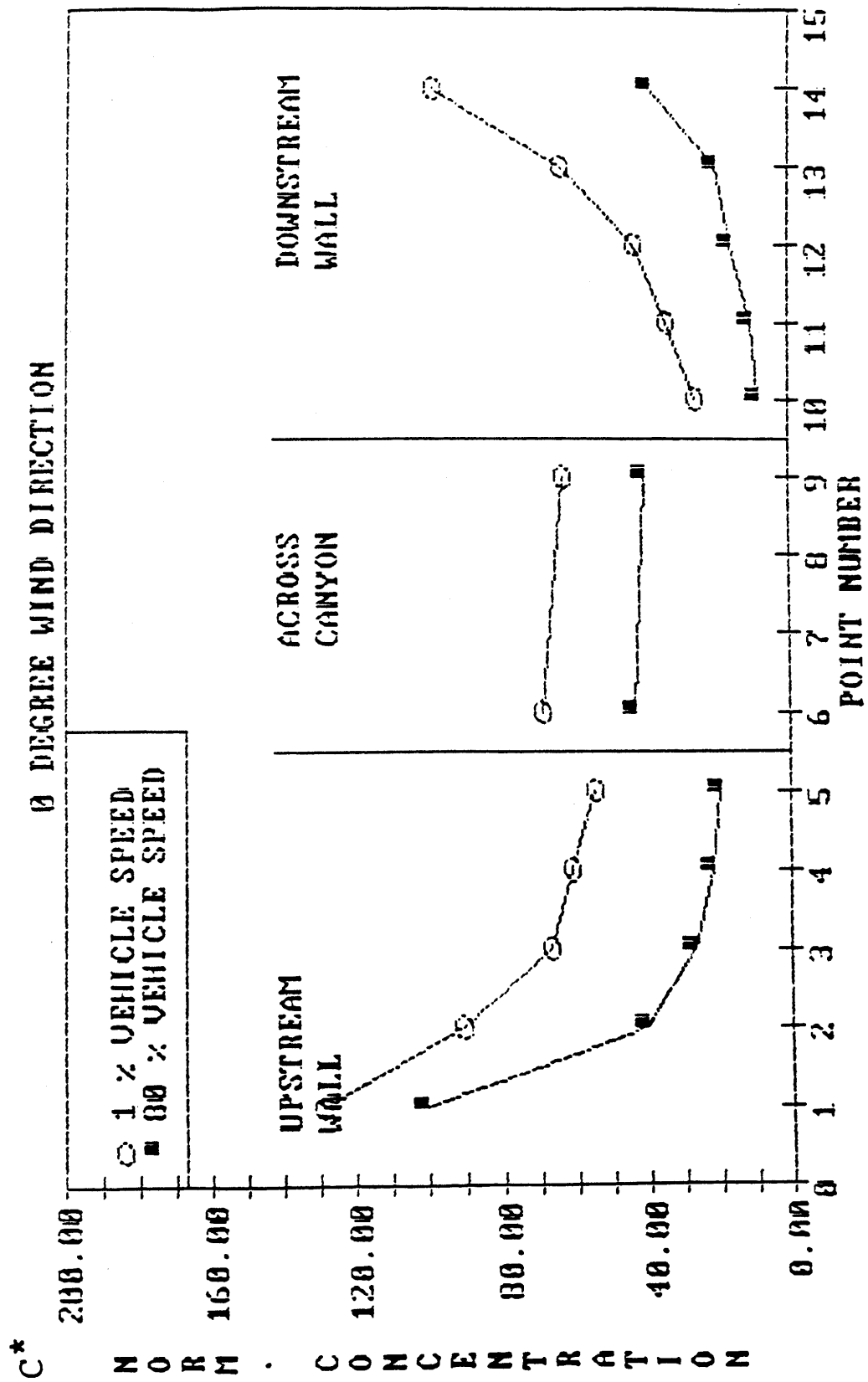


Figure 36. Effect of vehicles near a downstream facing step.

0° Wind Direction

X' IS DISTANCE FROM UPSTREAM WALL

C\*

○ X' = 1.00 \* H, 1 % VEHICLE SPEED  
 ■ X' = 1.00 \* H, 80 % VEHICLE SPEED  
 △ X' = 4.43 \* H, 1 % VEHICLE SPEED  
 ◇ X' = 4.43 \* H, 80 % VEHICLE SPEED

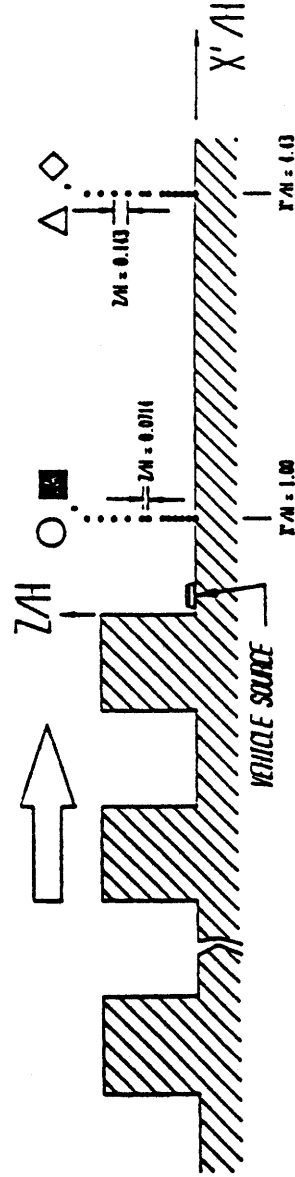
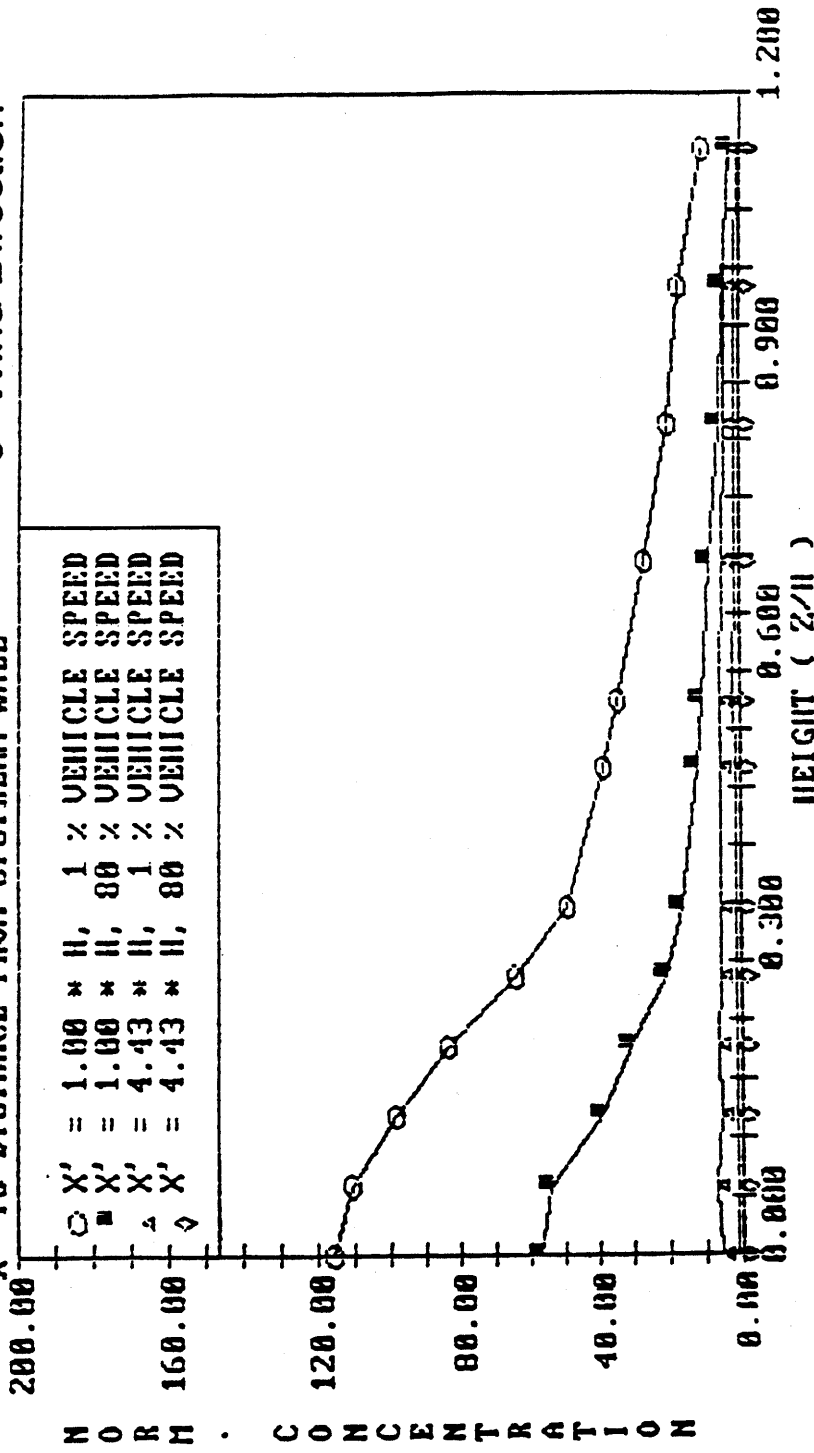


Figure 37. Vertical dispersion trends for downstream facing step.

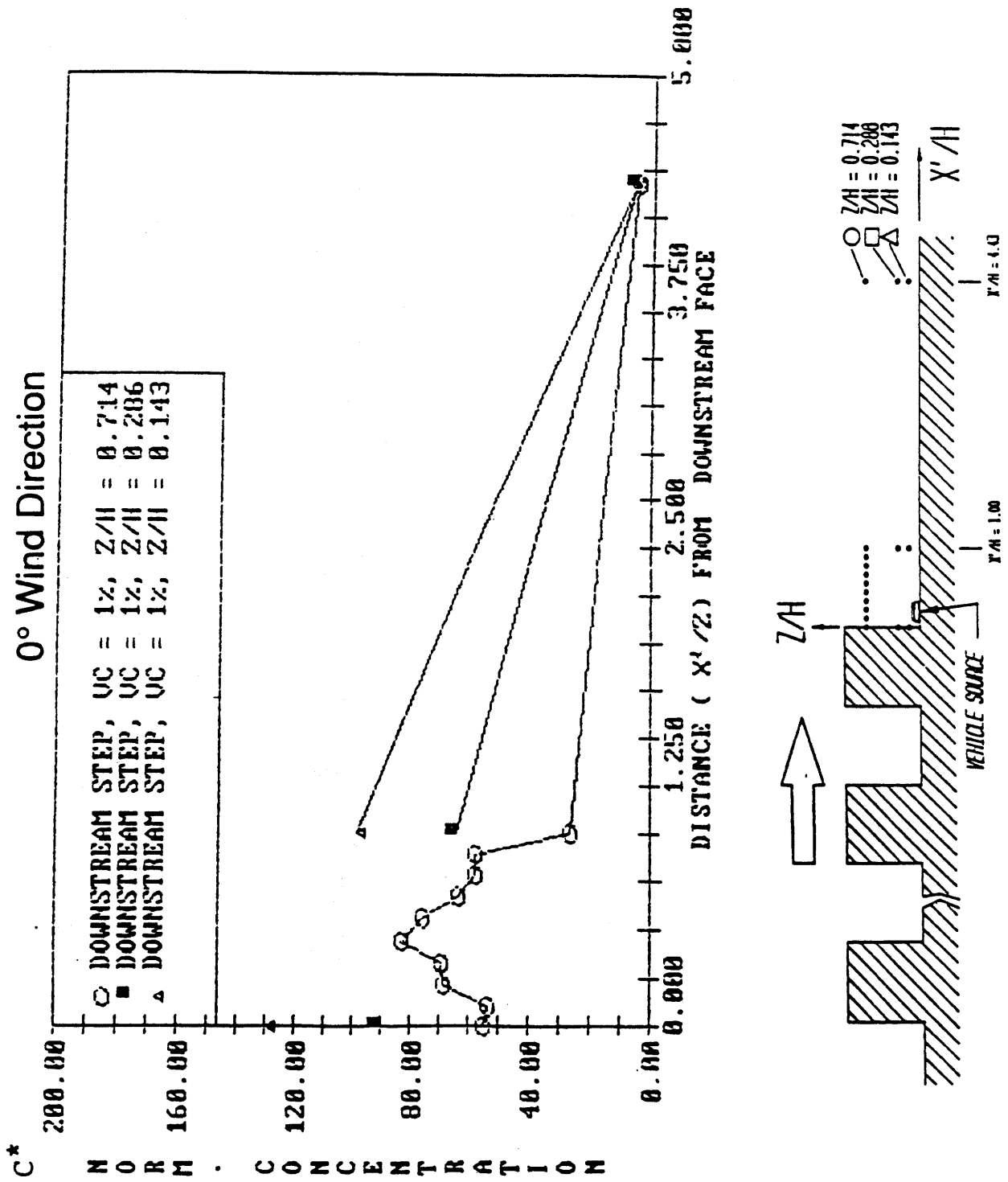


Figure 38. Lateral dispersion trends for a downstream facing step.

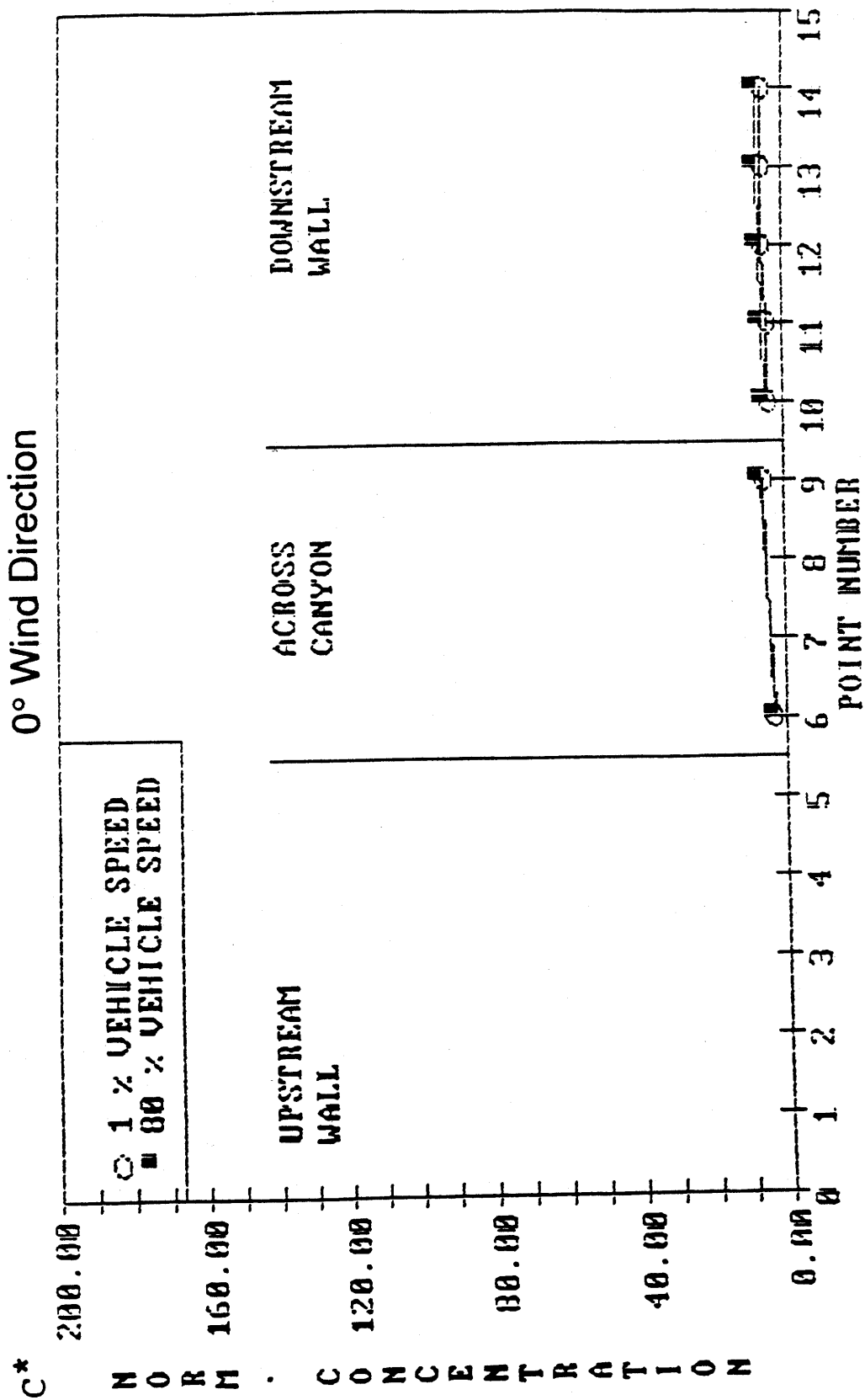


Figure 39. Effect of vehicles near an upstream step.

effect on this data because the source was located in an area of strong nonrecirculating flow.

### Open Highway

The dispersion downwind of an open highway is shown in figure 40. The highest concentrations are found at street level, with quickly decreasing concentrations above the roadway. The dispersion plume becomes an even profile at  $7H$  downstream from the first line source. These profiles are a baseline that will be used in a downstream facing step progression (Comparison of Open Highway and Stepped Highway).

### Uneven Height Canyon

- Effects of a Taller Upstream Wall;  $H1/H2 = 2$

Doubling the height of the upstream block reverses the concentration trends that are familiar in the standard 1:1 canyon (figure 42). In figure 41b, the flow visualization shows the vortex is much weaker and rotates counterclockwise. The receptors closest to the line source in the vortex path show highest concentrations.

It is of further interest that even with an apparently weaker circulating flow, the maximum and minimum concentration levels are surprisingly close to those in the 1:1 standard canyon.

- Effects of a Taller Downstream Wall;  $H2/H1 = 2$

This test was designed to determine the effect of a taller downstream wall. In this case, the downstream wall was twice as high as the upstream wall (figure 41c). In comparison to the baseline ( $W/H = 1$ ) canyon, the concentration values (shown in figure 42) were considerably lower, with the significant changes resulting throughout the canyon. The taller downstream wall directed more clean flow into the canyon, thus increasing the canyon ventilation. The mean flow speed at bottom center of the canyon recorded 1.7 times the value found in the corresponding baseline case.

When the vehicle speed is increased from 1 percent to 80 percent of the maximum speed, the values along the upstream wall increased (figure 43). This indicates the increased turbulence from the vehicles disturbs the strong flow in the immediate region, thus trapping more pollutants without influencing the overall strong vortex flow. This is thought to be a local effect, where the flow immediately along the upstream wall is drawn up and out before recirculating.

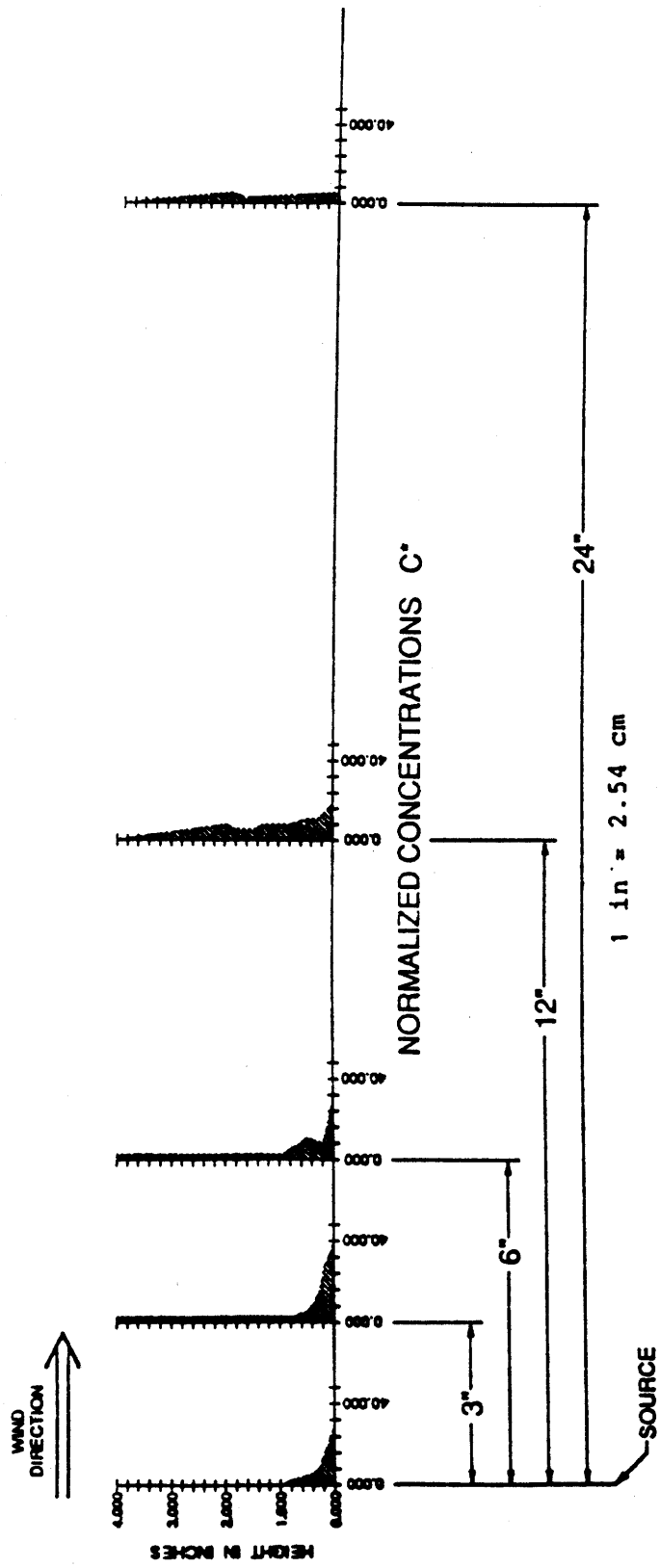


Figure 40. Pollution dispersion downwind of an open highway.

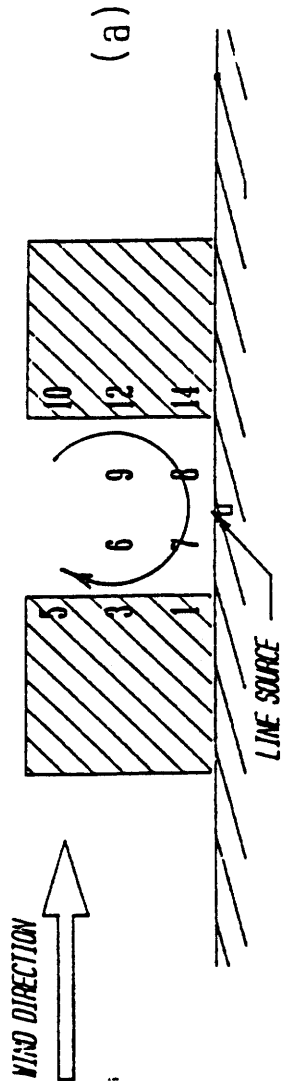


EFFECT OF DIFFERENT CANYON WALL HEIGHTS 0 DEGREE WIND DIRECTION

○ STANDARD CANYON

WIDTH / HEIGHT = 1.00

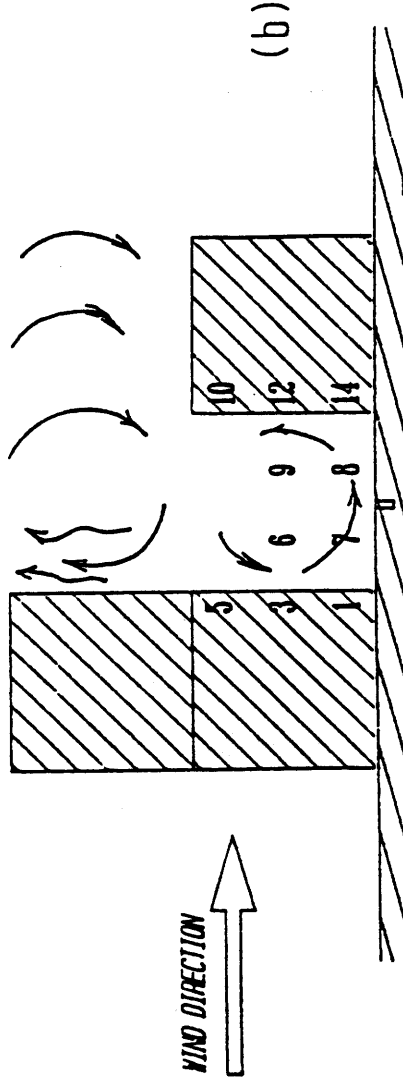
REFERENCE FILE : TEST RW3-0  
Data Base : TEST RW3-0



■ TALLER UPSTREAM WALL

H1 / H2 = 2.00

REFERENCE FILE : TEST RW3-31  
Data Base : TEST RW3-31



△ TALLER DOWNSTREAM WALL

H2 / H1 = 2.00

VEHICLE SPEED = 1%

REFERENCE FILE : TEST RW1-4  
Data Base : TEST RW1-4

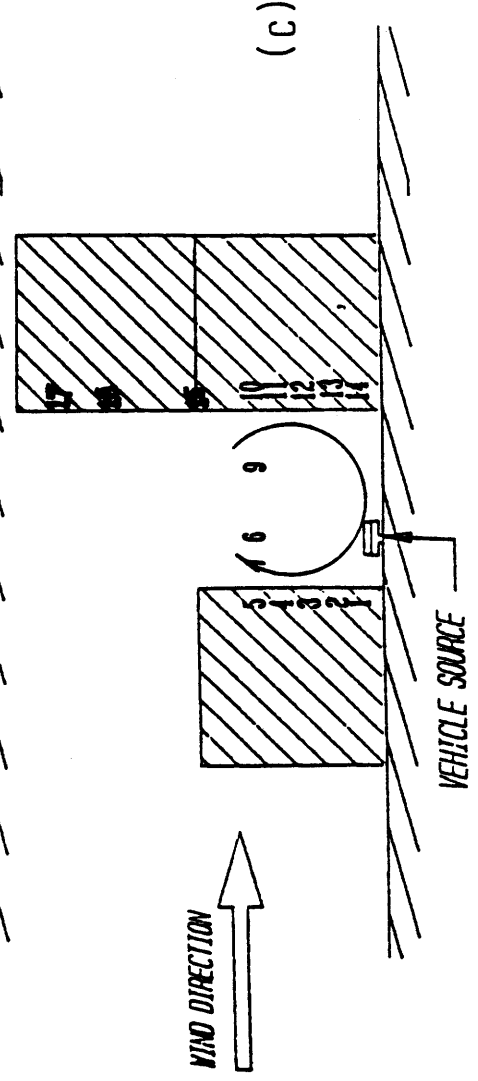


Figure 41, Test setup and point locale for uneven height walled canyons.

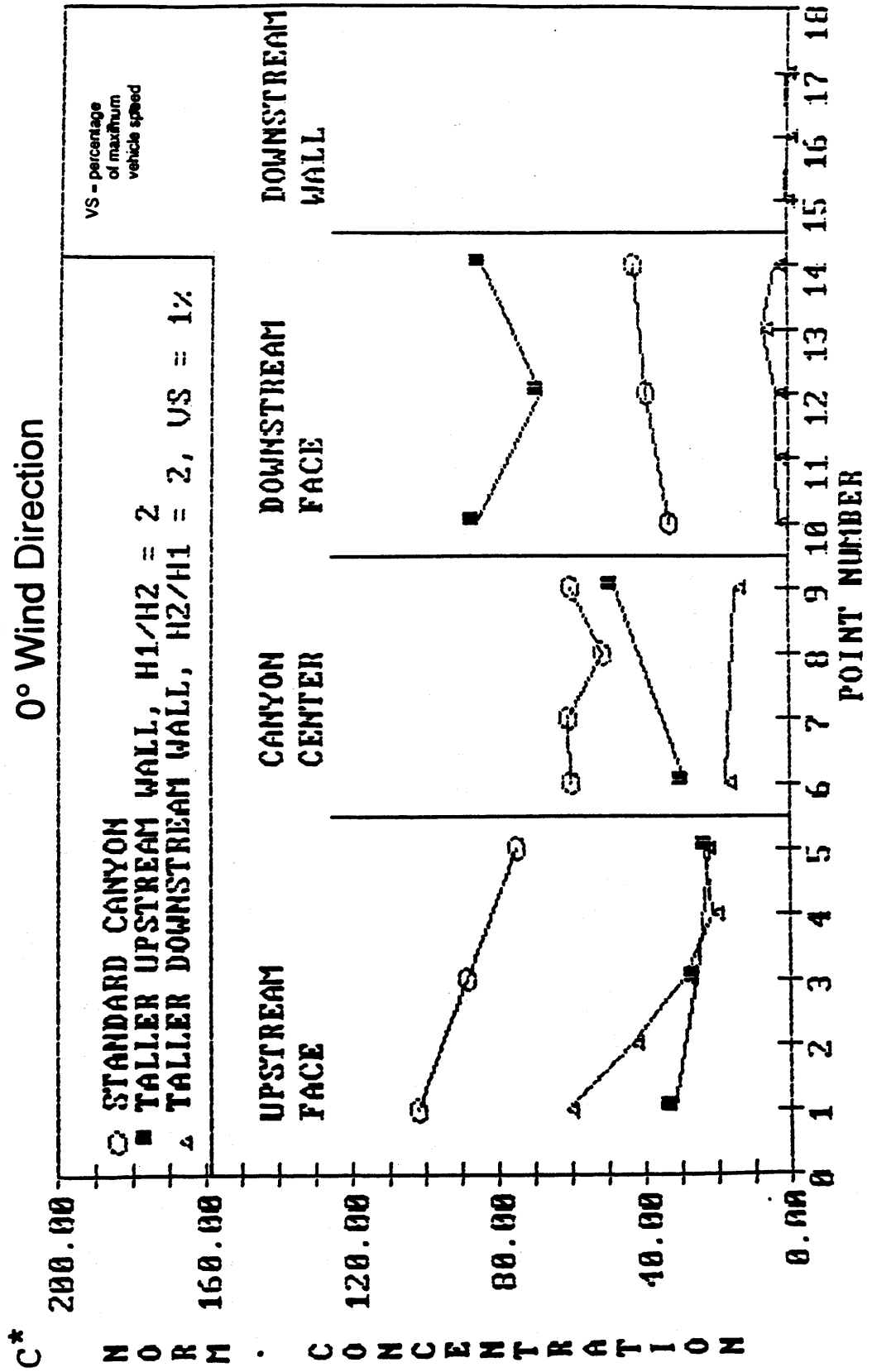


Figure 42. Effect of uneven height walled canyons.

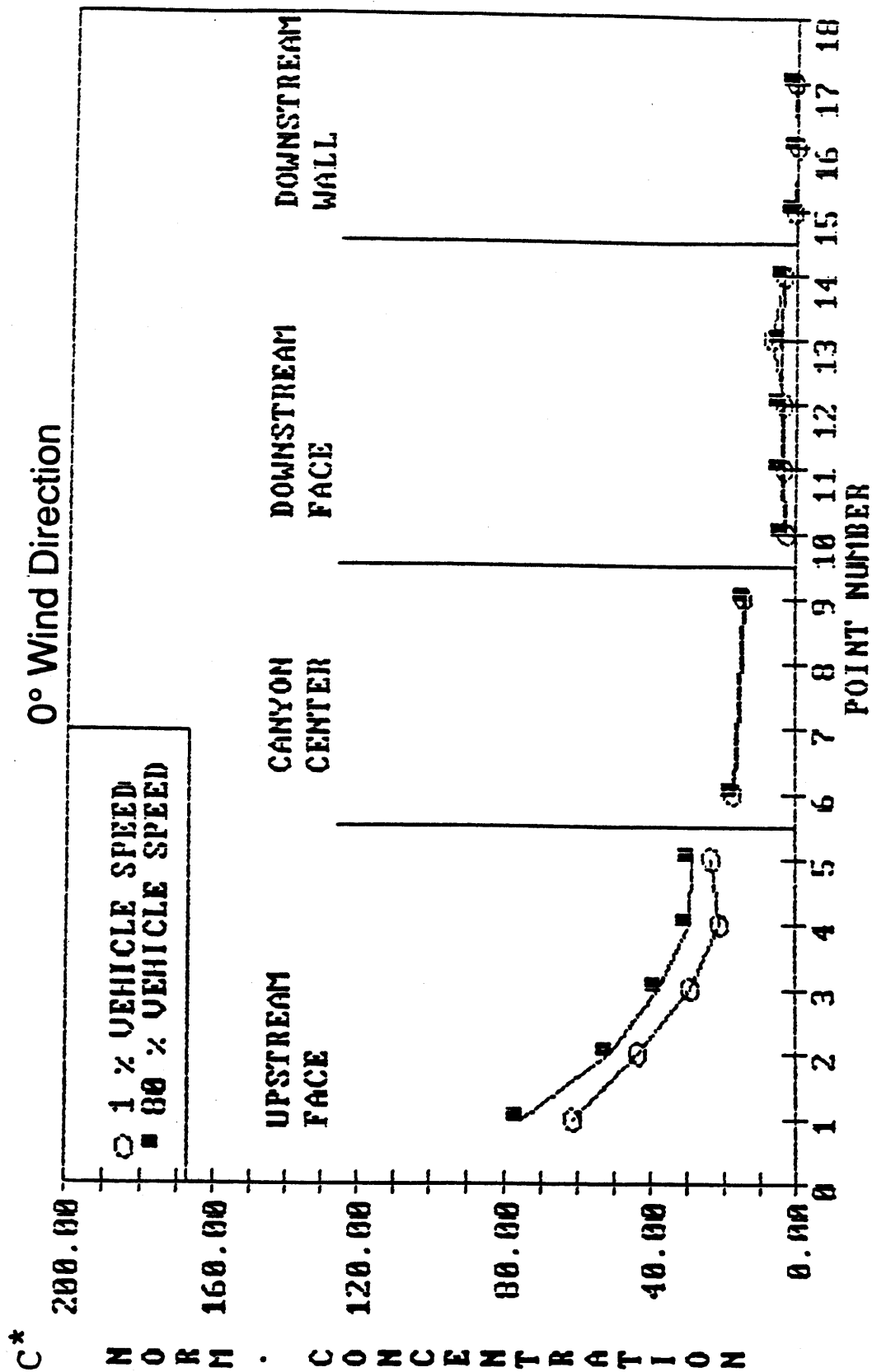


Figure 43. Effect of vehicles on a taller downstream walled canyon.

### Isolated Tall Building above an Otherwise 2-D Block

Figure 44 illustrates the flow field near a tall building placed in the center of an otherwise baseline  $W/H = 1$  canyon. Figure 45 shows the test configuration and receptor location. The presence of such an isolated tall building greatly affects the pollution dispersion in nearby canyons. This is mainly due to the pressure gradients along the building's surface. Behind the building, air is drawn out of the downwind canyon into the building's wake, while on the front (upwind) side of the building, the pressure gradient has the opposite sense, and clean air is driven down into the upwind canyon.

In the downstream canyon, where the pollutants are being drawn into the tall building's wake, the concentrations decreased along the downstream wall (see figures 46 and 47). A slight increase of concentration occurs along the upstream wall, and the mid-canyon receptors show an increase, since it is actually in a small stagnated zone created by the merging of along-canyon flows being induced by the "suction" of the tall building's wake. Thus, there is a hot spot directly downwind of the isolated tall building (figure 47).

At a 30' wind direction (figure 48), the stagnation pocket did not fully develop behind the building wake possibly due to the destabilizing lateral flow component. The concentration levels decreased dramatically in the center receptors behind the building. The suction along the downwind side of the building adds to the lateral flow component approaching the building and opposes it as the lateral flow passed the building. The highest concentration levels occur just before the building center. The clashing of flows past the building caused a greater mixing of flows and the concentration levels to be more evenly distributed.

### Sloping Canyons

Figure 49 illustrates the test configuration and the receptor locations. By sloping the walls of a canyon, the canyon is better ventilated (figure 50). For both 0 and 30' wind direction, concentration levels dramatically decreased. As the sloping canyon is widened, more fresh air is directed into the canyon and the concentration levels further decrease. In the case of the Katy Freeway Model (base/H = 7.0, top/H = 14.1), the ventilation is greater than the open highway case. This shows that sloping walls can effectively decrease the concentration levels.

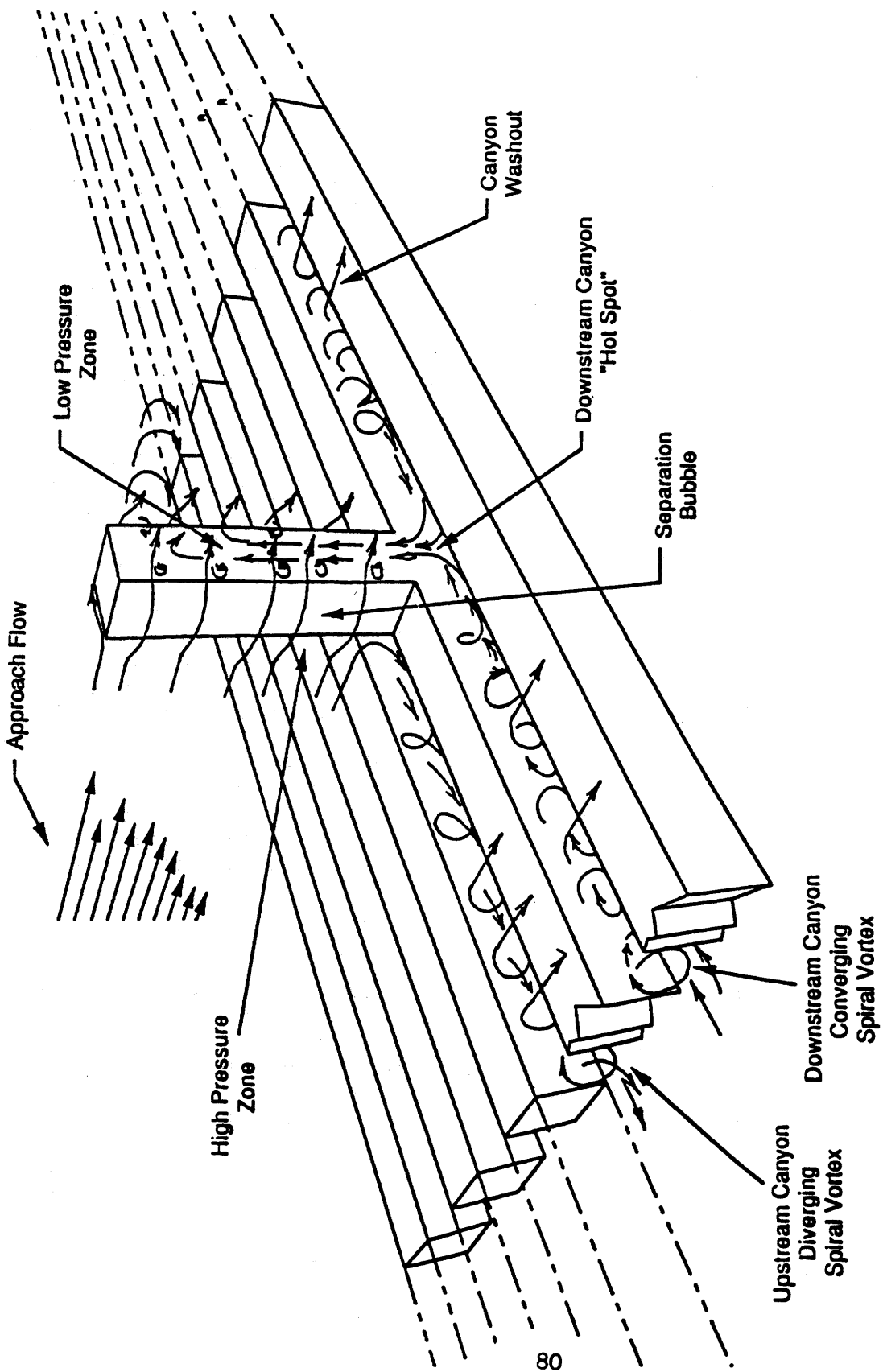


Figure 44. Flow visualization of a tall building placed with a standard canyon configuration.

# EFFECT OF A TALL BUILDING ( 4\*H ABOVE 2-D CANYON )

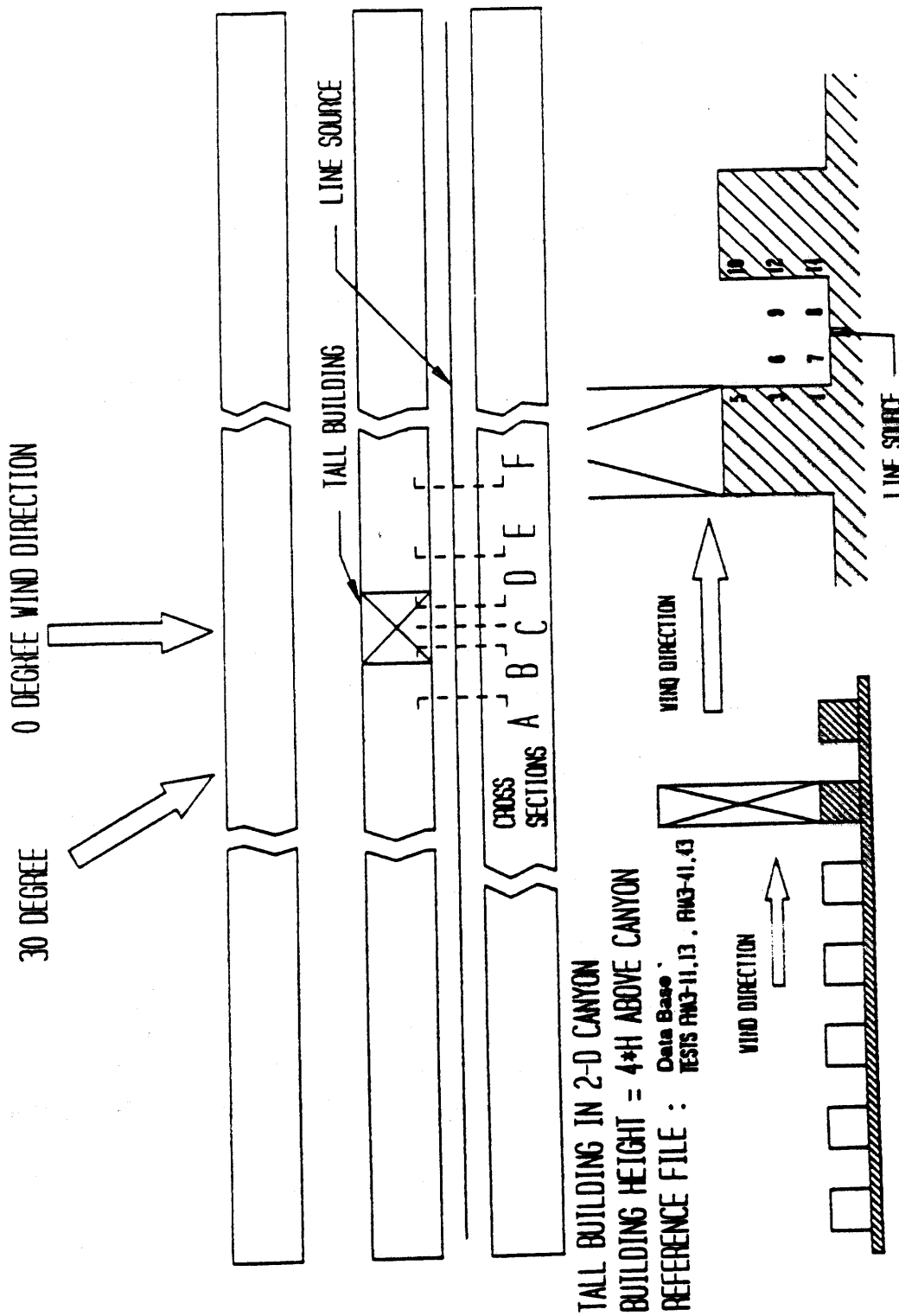
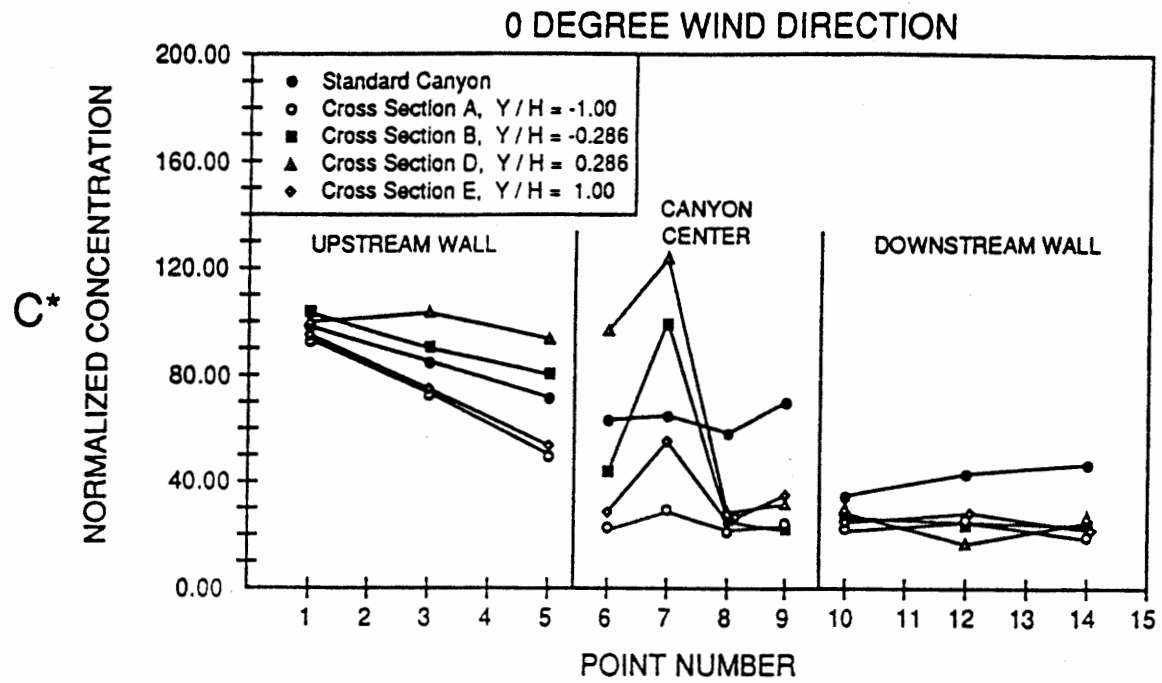
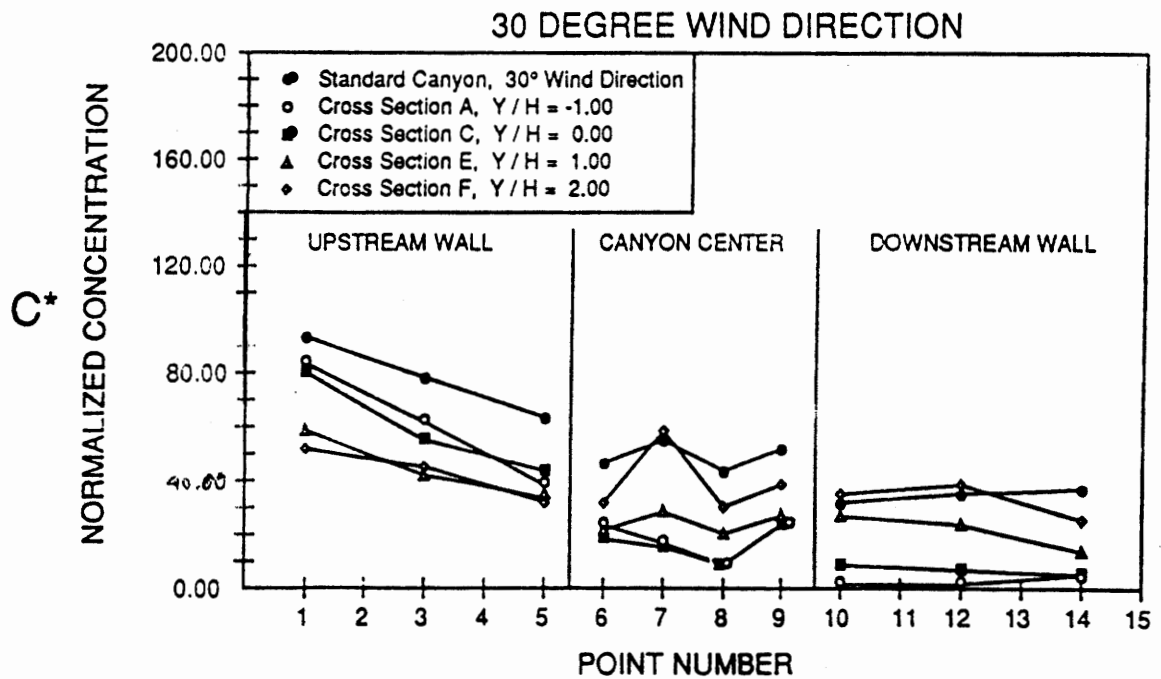


Figure 45. Plan view of cross sections behind a tall building at 0 and 30 degree wind direction.



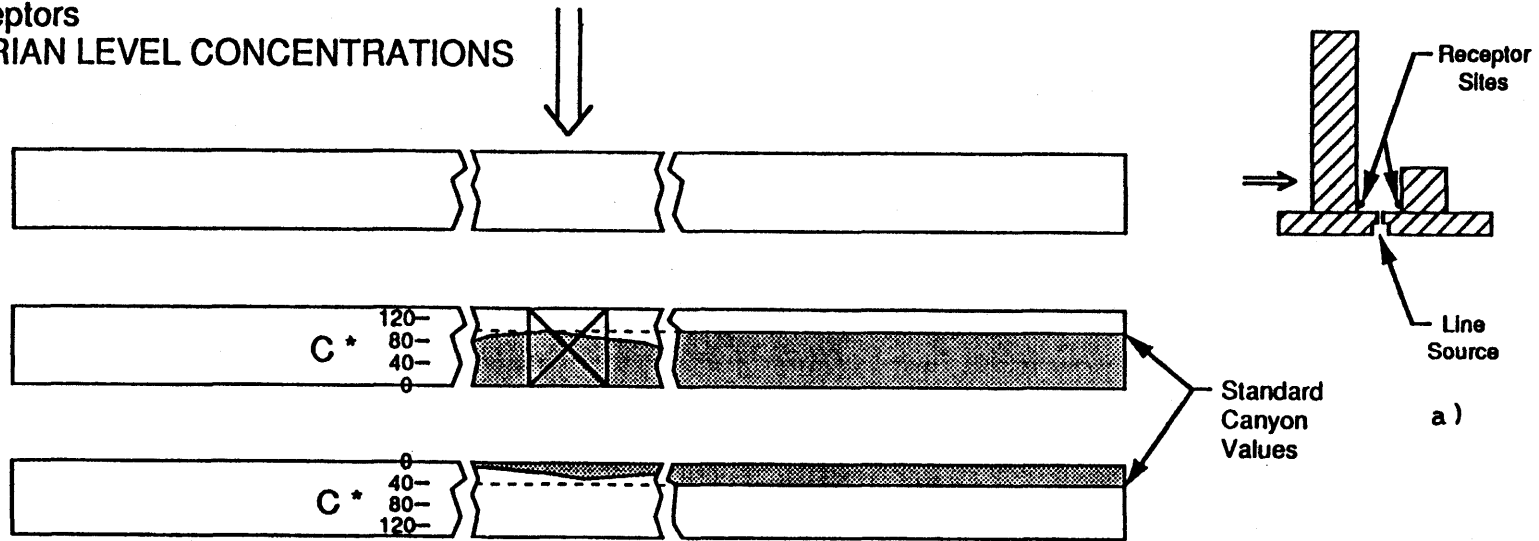
a)



b)

Figure 46. Comparison center and wall receptors at 0 and 30° wind direction for a tall building configuration ( $4H$  above  $W/H = 1$  canyon).

Wall Receptors  
PEDESTRIAN LEVEL CONCENTRATIONS



Center Receptors  
PEDESTRIAN LEVEL CONCENTRATIONS

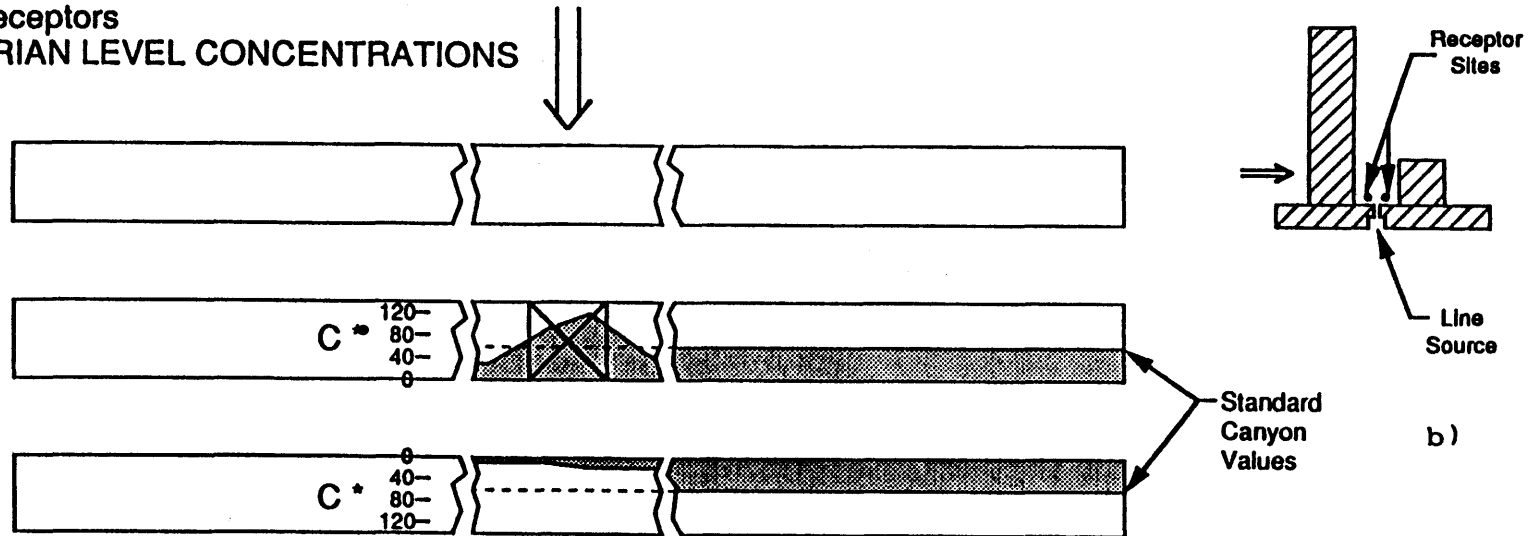


Figure 47. Concentration levels in a 2-D canyon near a tall building at 0 degrees.



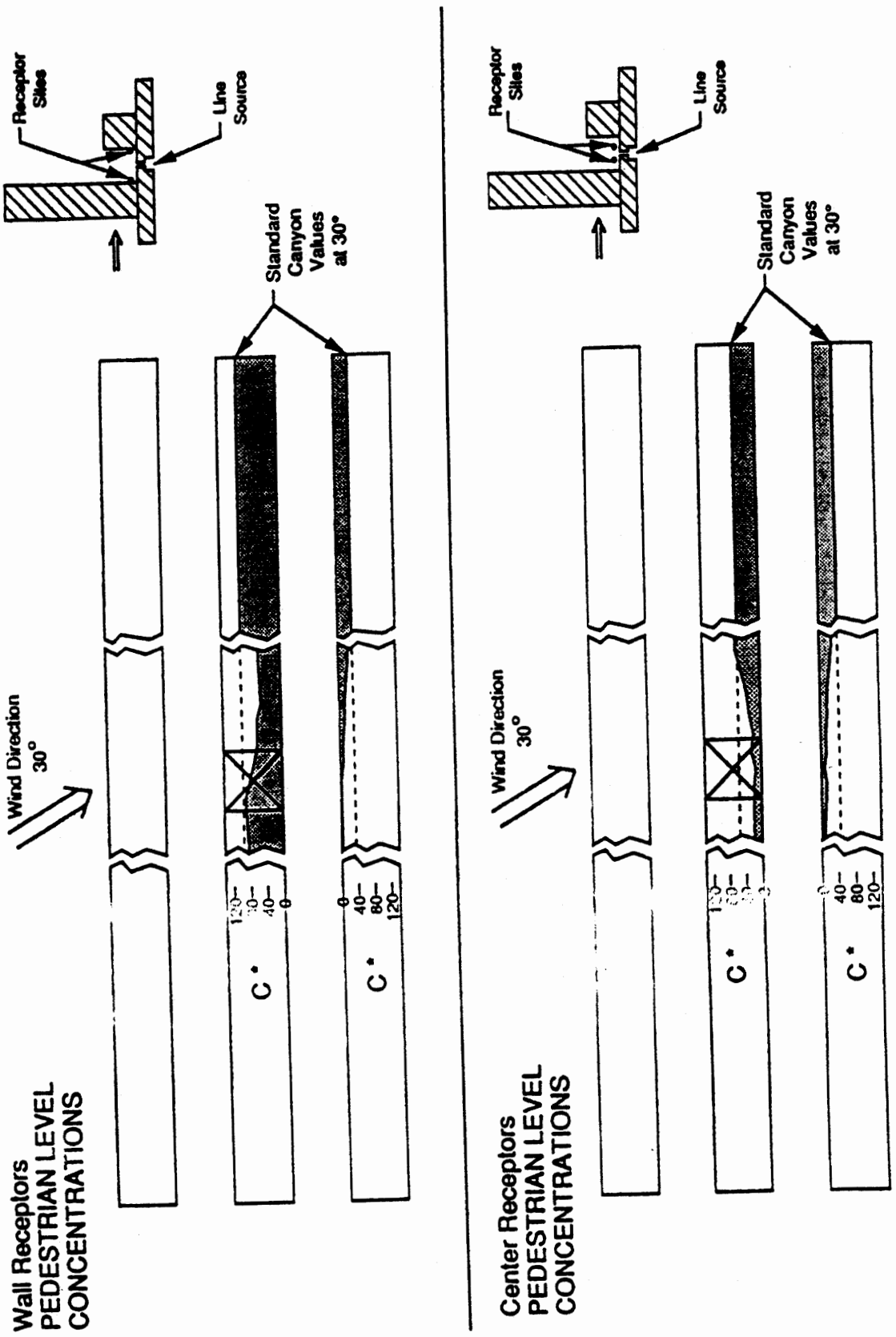


Figure 48. Concentrations of a 2-D canyon near a tall building at 30°.

# EFFECT OF A SLOPING WALLED CANYON 0 AND 30 DEGREE WIND DIRECTION

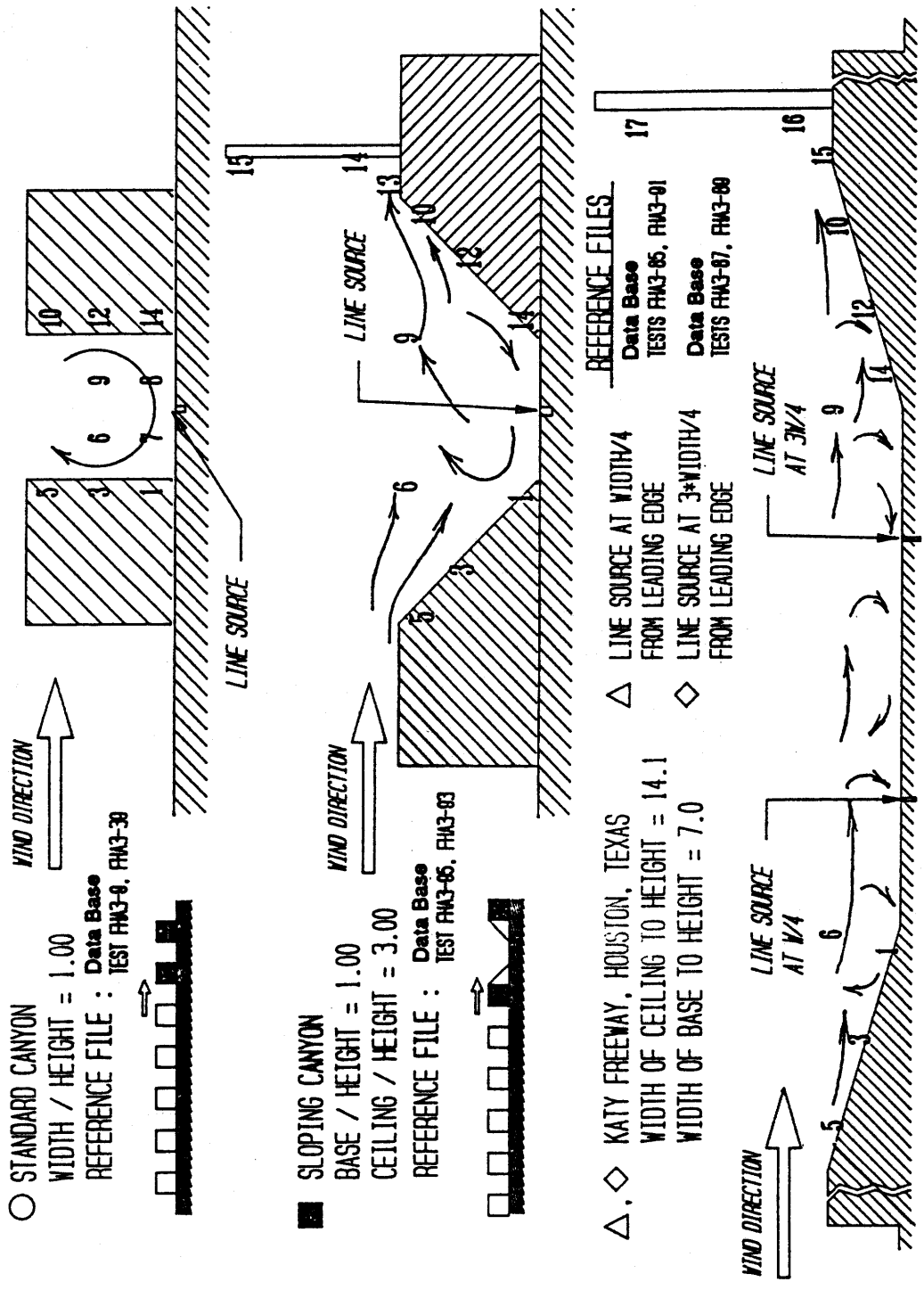
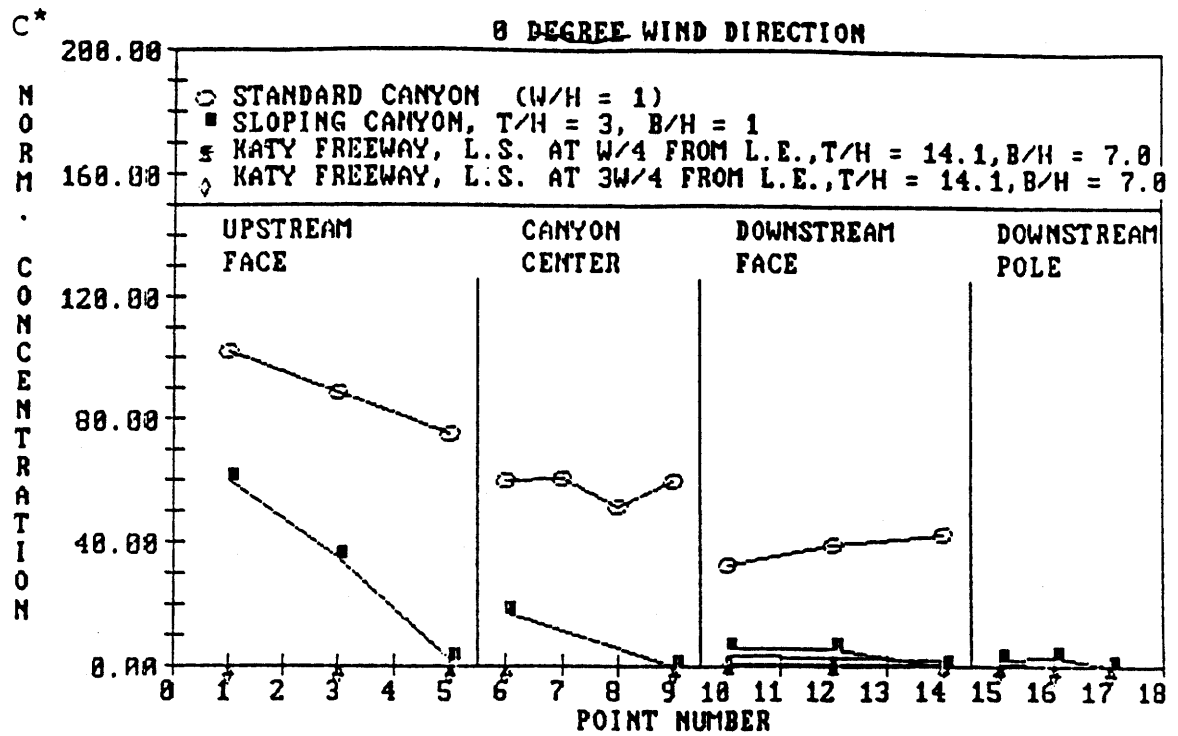
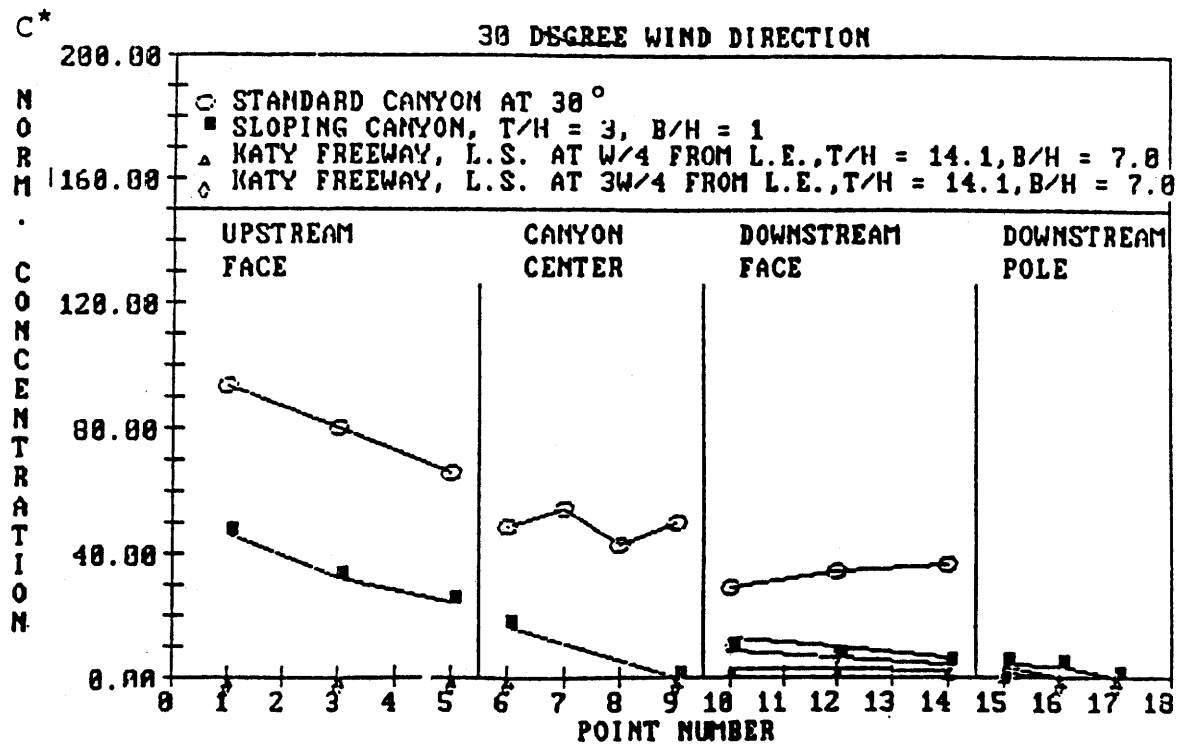


Figure 49. Test setup and point locale for sloping canyon configuration.



a)



b)

Figure 50. Effect of sloping canyon configurations at 0 and 30° wind direction.

### C. Summary of 2-D Straight Canyon Results

In the following section, the effect of stepped configurations and sloping walls is discussed, as well as a comparison of hot spots and averages in 13 different 2-D canyon geometries. The following highlights of the 2-D canyon tests should be kept in mind when reviewing data from the more complex configurations.

- The simplest 2-D flow in the standard canyon ( $W/H = 1$ ), is characterized by a strong recirculating vortex roughly centered in the canyon.
- Canopies increased concentration levels below the canopy near the canyon center by approximately one- and one-half times the baseline configuration ( $W/H = 1$ ).
- Slotted wall buildings increase the "fluid transfer" between adjacent canyons. More fluid transfers from the downwind canyon to the upwind canyon, and higher pollutant levels are found in the upwind canyon.
- By adding an isolated tall building above the standard canyon, a hot spot developed in the leeward canyon near the base of the building.
- The upstream facing step causes strong deflected flow with a small higher velocity recirculating zone near the base of the wall. The downstream facing step produces a large pocket of stagnant air in its wake and a recirculating zone reaching approximately  $4.H$  horizontally from the downwind face. This results in the lowest concentrations near the upstream facing step and very high concentrations behind the downstream facing step.
- Doubling the height of the upstream block reverses the direction and weakens the canyon vortex. In contrast, doubling the height of the downstream wall reduces the concentrations by increasing the flow into the canyon and increasing the vortex strength.
- As the canyon dimensions narrow or widen, a canyon vortex appears when the geometric bounds allow; rarely does the vortex elongate.

#### Comparison of "Hot Spots" and "Averages"

Figure 51 illustrates the highest and average concentration levels for the different 2-D geometries discussed in Analysis of Selected 2-D Straight Canyons. The "averages" and "hot

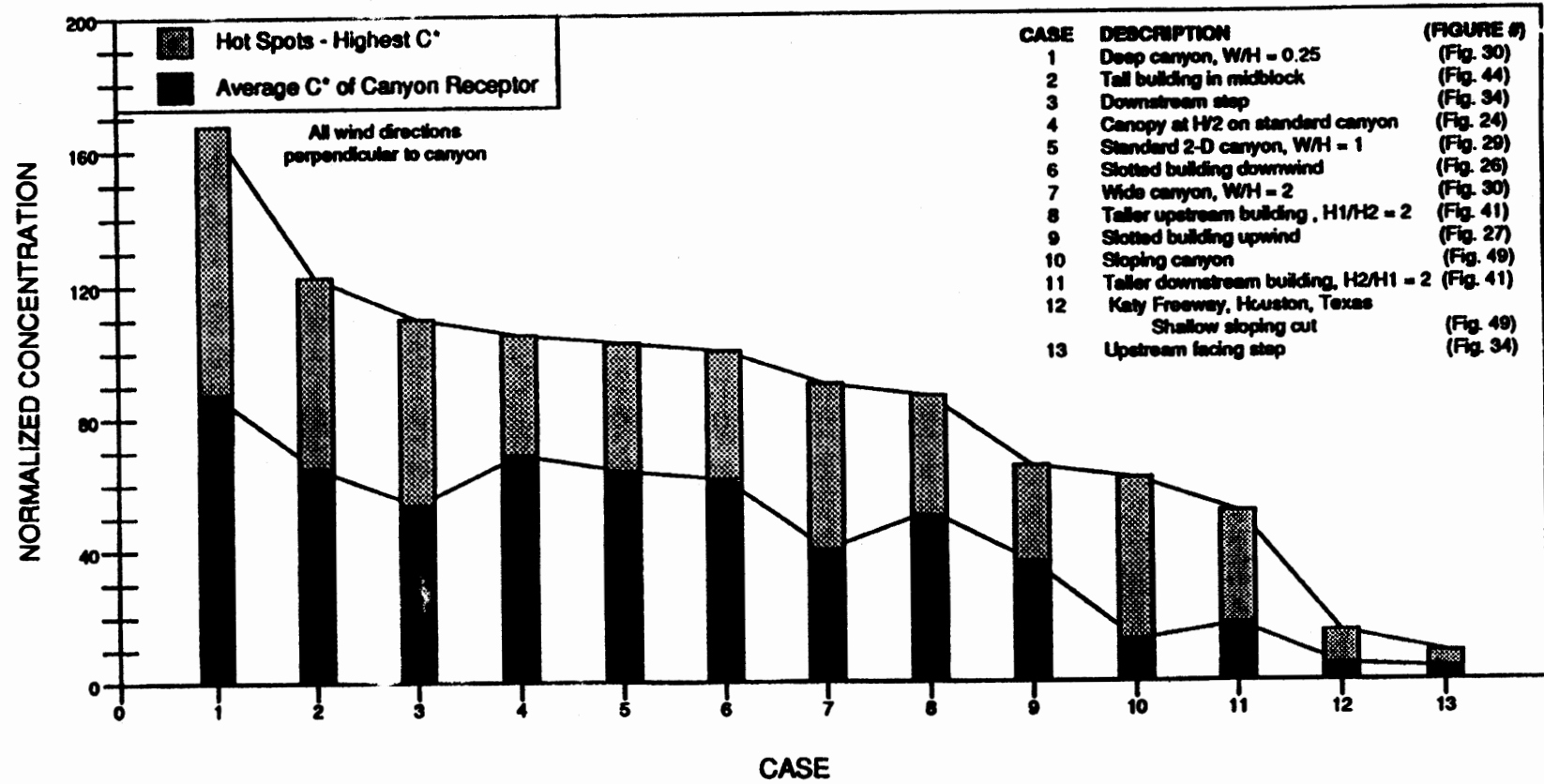


Figure 51. Comparison of "hot spots" and "averages" in different 2-D canyon configurations.

spots" were determined using only the receptors location presented in this document; therefore, the position and number of receptors is critical to proper interpretation of figure 51. To determine more comprehensive hotspots and averages, the appropriate database and data file should be reviewed. The points taken to calculate the average concentration values in figure 51 represent a characteristic sampling of each canyon, thus providing a base from which a comparison can be drawn. A vehicle source was used in Cases 3, 7, 11, and 13; therefore, correction factors had to be introduced in order to convert to the corresponding line source values. These correction factors were determined by comparing the "hot spot" and "averages" for standard canyon line source with a standard canyon vehicle source.

The data clearly illustrates that the basic trends of the "averages" closely follow the "hot spot" curve. For the first nine cases, the "average" values are within 45 percent to 65 percent of their "hot spots," but the "averages" drop to roughly 35 percent for Cases 10, 11, and 12. Note: Slotted upstream refers to the case where the line source is located upwind of the slotted building. Slotted downstream refers to the case where the line source is located downwind of the slotted building.

#### Comparison of Vertical and Sloping Walls

One of the most dramatic impacts on canyon concentration levels is sloping the canyon walls (figure 52). Figure 53 demonstrates that, the "hot spot" is reduced by 40 percent of its vertical walled counterpart, while the "average" concentration in the canyon dropped four to five times. By replacing vertical with sloping walls, the flow patterns dramatically change. Vertical walled canyons are characterized by stagnant air pockets and/or recirculating flow. In contrast, the mean flow over the sloping canyon drops into the canyon without establishing recirculating patterns, or causing areas of stagnation.

#### Trends of Different Width-to-Height Ratios

A clear pattern develops which can be used as a rough estimation of expected concentration levels for different width-to-height ratio canyons (figure 54). As the canyons change size, the flow patterns also change; therefore, it is difficult at this point to make general statements. For example, the deep canyon is characterized by a large pocket of height, whereas recirculating flow has a less steep concentration gradient and lower peaks.

# COMPARISON OF VERTICAL AND SLOPING WALLS 0° WIND DIRECTION

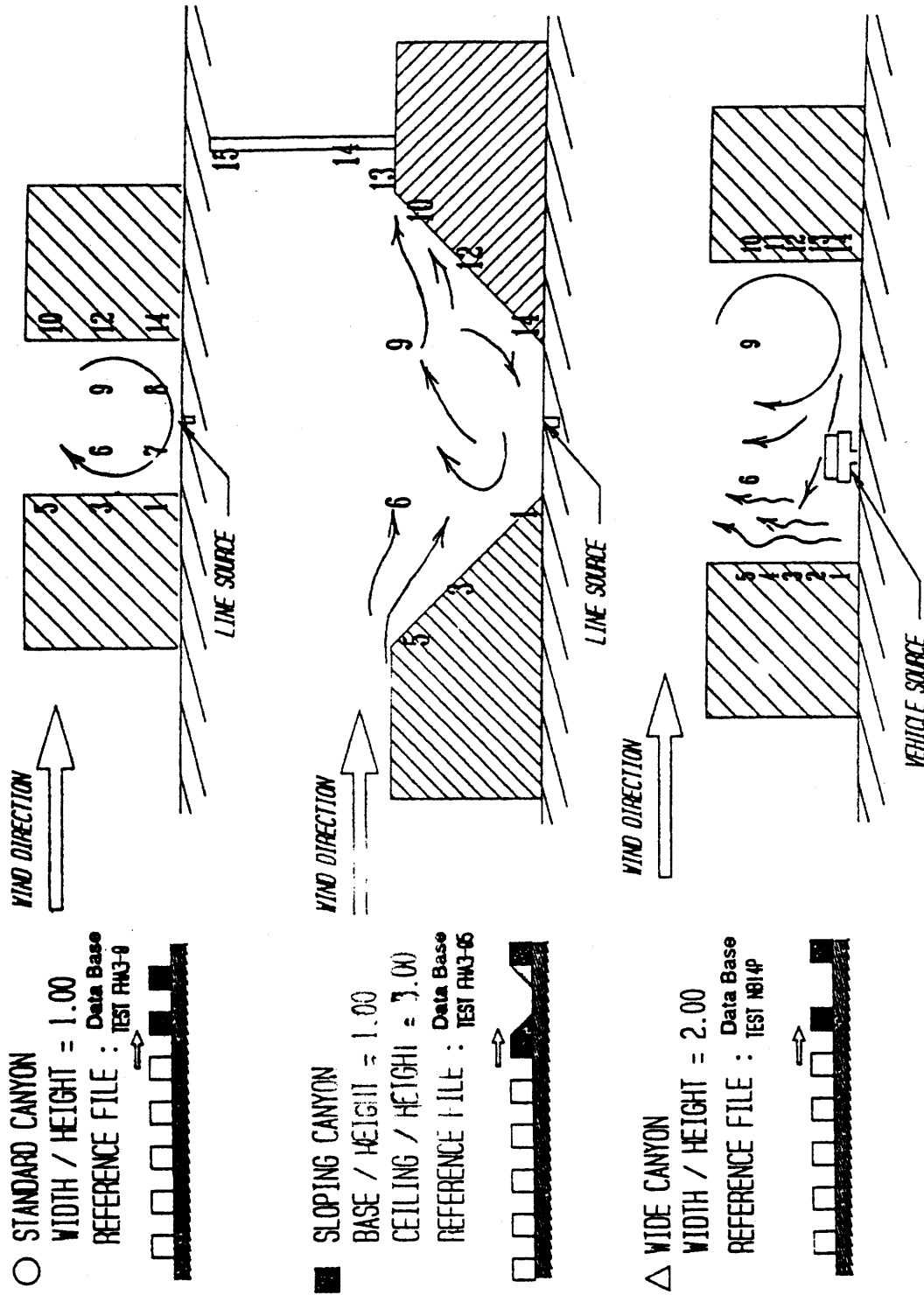


Figure 52. Test setup and probe locale for vertical and sloped walled canyon configuration.

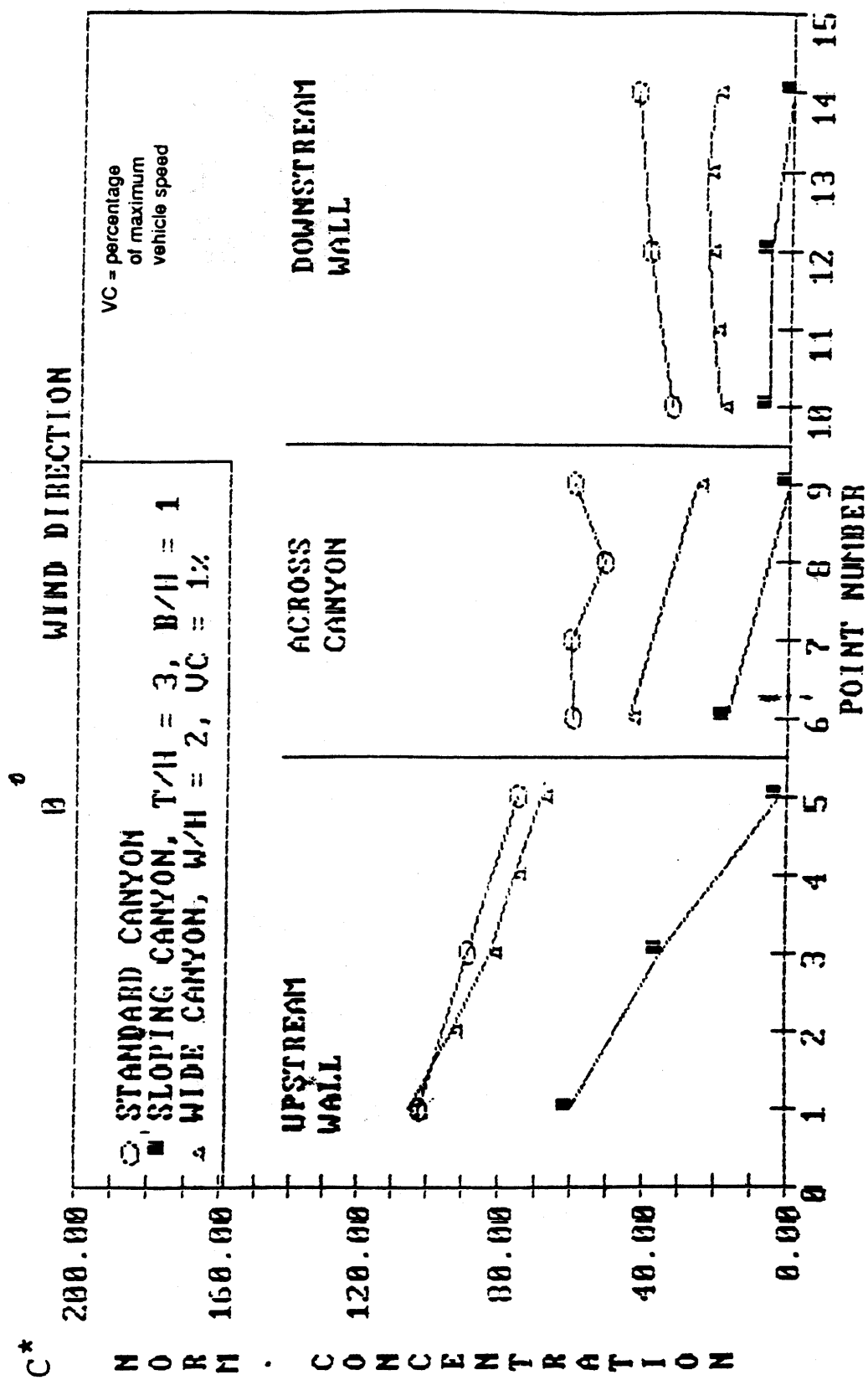


Figure 53. Comparison of vertical and sloped walled canyon configurations.



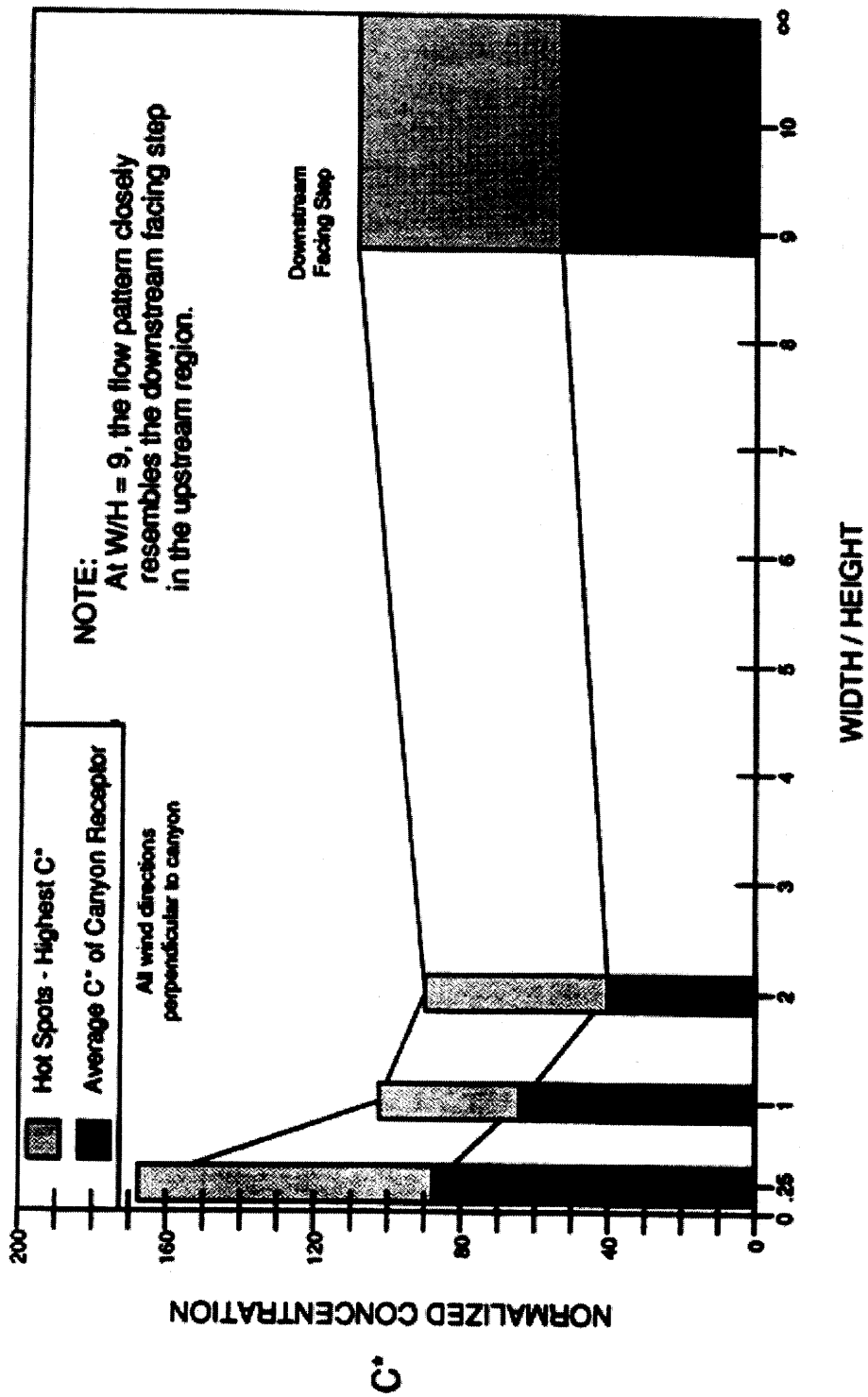


Figure 54. Comparison of different width to height ratios.

stagnant air; whereas a strong central vortex dominates the standard canyon ( $W/H = 1$ ).

Figure 54 should be used with careful consideration of the source position and flow structure to effectively predict concentration levels (refer to flow visualization drawing, figures 28 and 29 in Analysis of Selected 2-D Straight Canyons). For example, the standard canyon and deep canyon both were tested using a line source located at the canyon center, but the locations of receptors used were somewhat different due to the geometries. For the wide canyon, a vehicle source at 1 percent vehicle speed was located  $0.286H$  upwind of the canyon center, whereas the downstream facing step had a vehicle source located  $0.214H$  downwind of the downwind facing step. Once again, the location of receptors varied slightly due to the configuration. Therefore, two major variables must be considered when using figure 54. First, where is the source located, and what type of source is being used? Second, are the selection receptions, due to the limited number involved in testing, a fair representation of the "hot spot" and "averages"? The values plotted in figure 54 must be judiciously used as a reference and not as an absolute guide.

#### Comparison of Open Highway and Stepped Highway

The downstream facing step is often the predominant geometric characteristic that affects pollution dispersion. A detailed study with different height downstream facing steps reveals two separate mechanisms for dispersion behind the steps: first, the wake immediately behind the step and second, the dispersion plume further downstream (figure 55). The vertical axis in figure 55 represents the location of the rake of receptors, each set of receptors being at the same horizontal distance.

Immediately behind the steps, the concentrations appear to be inversely proportional to the volume of air behind the steps. Consider the recirculating flow discussed in Stepped Configurations: the volume/length of the air involved is roughly  $4H^2$ . Further from the steps, the pollutants mix into a downstream dispersion plume as in the open highway. The downstream facing step develops an area of lower velocity air directly behind its wake which effectively traps pollutants in a stagnant air pocket. The quantity of pollutants caught behind the step is greater than those found in the open highway dispersion and the strong recirculating flow of standard canyon geometries (figure 56). The shaded regions in figure 56b and c are truncated because additional data were not available above and below these receptor locations. Downstream facing steps are characterized by a sharply decreasing concentration with increased

height, whereas recirculating flow has a less steep concentration gradient and lower peaks.

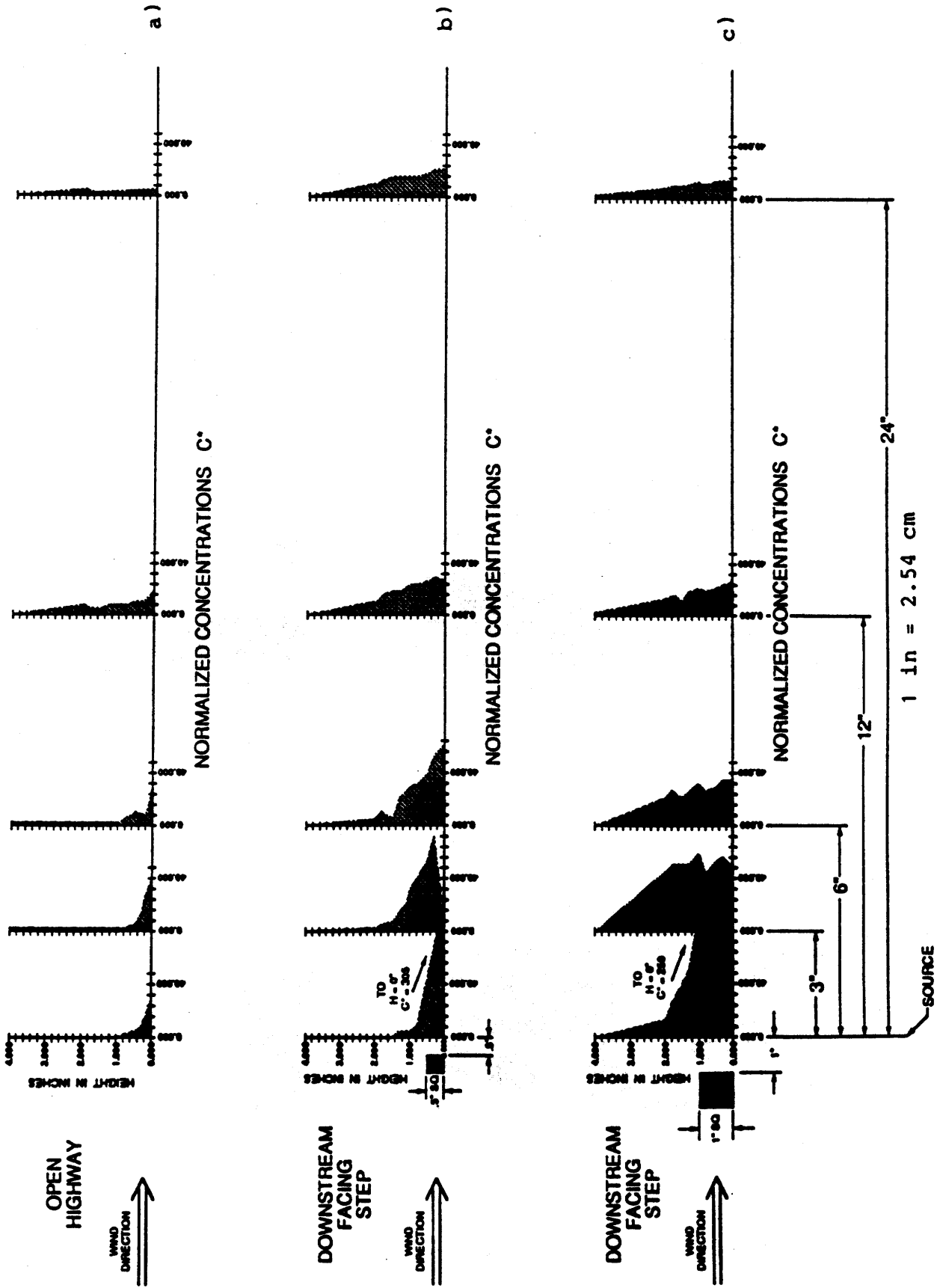


Figure 55. Comparison of open highway and downstream steps.

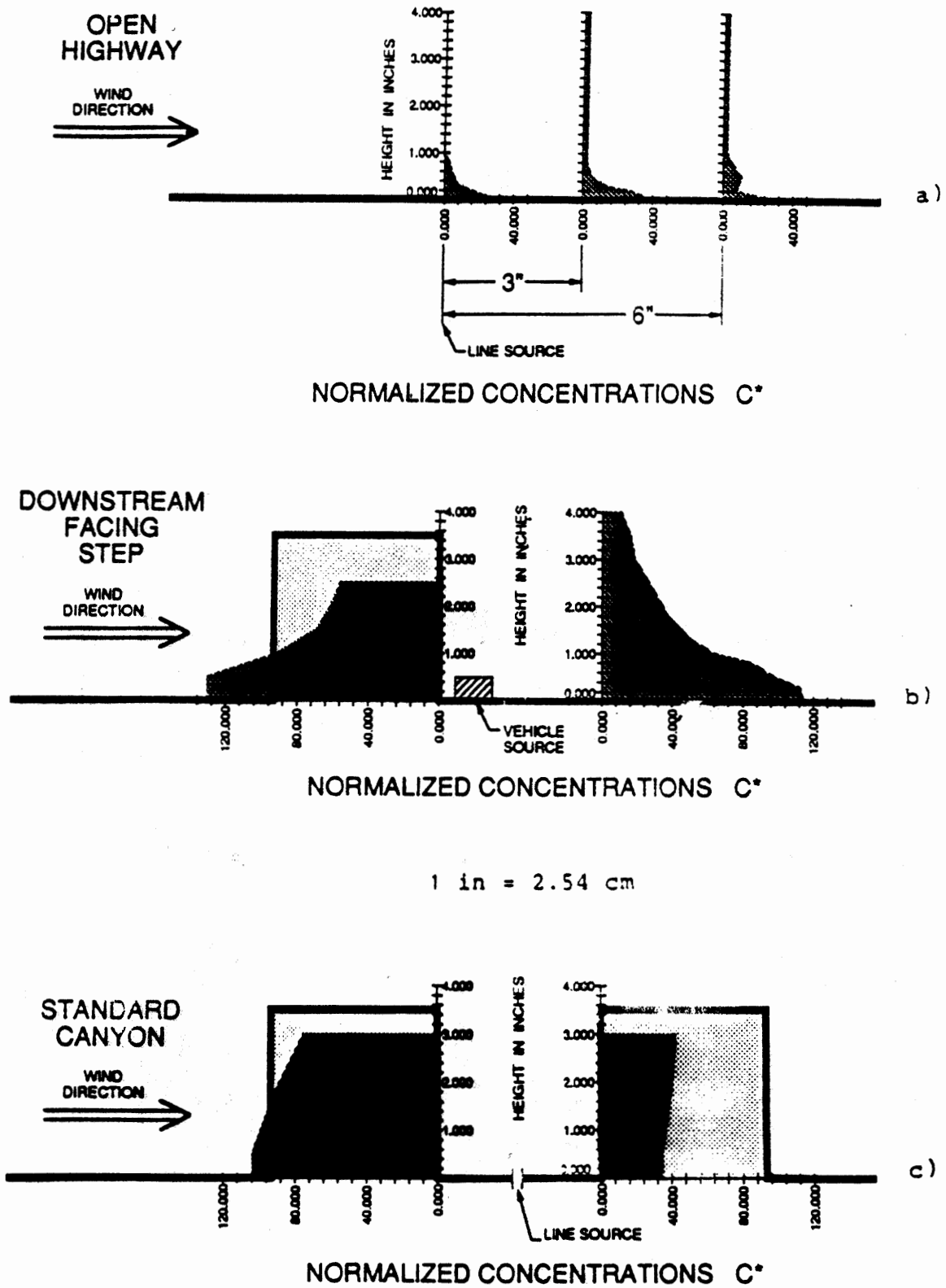


Figure 56. Comparison of open highway, downstream step and standard canyon.

#### 4. OBSERVATIONS AND RESULTS RELATED TO DISPERSION IN STRAIGHT CANYONS WITH CROSSCUTS AND INTERSECTIONS

##### A. Overview

The 2-D geometries described in section 3 were modified to simulate the effects of crosscuts and intersections. The emphasis was upon flow visualization to try to identify features which governed the dispersion phenomena at the intersection and upon obtaining trends which show the "correction" factor for intersections as compared with their 2-D canyon counterparts.

Table 7 summarizes the geometries tested and the data taken or observations made for each. The detailed data are all contained in Data Base 2, part 2 to this volume II.

##### B. Analysis of Selected Crosscut Cases

In this section variations on crosscut canyons are considered and concentrations graphed in the standard canyon format. In addition, the data will often be presented in a lateral concentration format in order to identify hotspots and trends. The source canyon as well as the upstream canyons are crosscut with intersections varying in widths of  $C/W = 0.5, 1, 2$ . Vehicles were run in the  $C/W = 1$  case and cross winds were tested for  $C/W = 2$ . A "T" intersection was made by eliminating the cross cut from the downstream wall of the source canyon.

##### 2-D Canyons With Crosscuts

Figure 57 illustrates the basic configurations studied.

With the wind direction parallel to the crosscut, figure 58 shows that the average pollution concentration is 40 percent lower in the canyon near the crosscut, compared to the 2-D canyon. Further from the intersection, the concentration rises and at four canyon widths from the intersection, the downstream and upstream wall concentrations are equal to the corresponding 2-D (nonintersected) canyon.

The flow visualization shows that the vortex flow is completely re-established for the intersection. The visualization also shows at each corner a vortex with a vertical axis located immediately adjacent to the crosscut. Figure 58 illustrates that these vertically-oriented corner vortices cause the average concentrations, immediately adjacent to the crosscut to be 70 percent of the corresponding standard canyon concentrations. Furthermore, the airflow that washes into the canyon reduces the concentrations about 1.5 canyon widths from the

**Table 7. Data file cross reference for data from crosscut and intersection tests.**

Headings:	wind angle	W/H	pollution concentration data file	flow visualization test #	tape
<b>"T" Intersection</b>					
Equal width canyons c/w = 1	0	1	FHA3-57, 59	32	B-23
Equal Width canyons c/w = 1	30	1	FHA3-55		
Narrow intersection c/w = 1/2	0	1		33	B-24
Wide intersection c/w = 2	0	1		31	B-22
<b>4-Way Intersection</b>					
Narrow intersecting canyon - c/w = 1/2	0	1	FHA3-61, 67	34	B-25
Narrow intersecting canyon - c/w = 1/2	45	1		39	B-30
Narrow intersecting canyon - c/w = 1/2	90	1		37	B-28
Wide intersecting canyon - c/w = 2	0	1	FHA3-63, 65	35	B-26
Wide intersecting canyon - c/w = 2	45	1	FHA3-69, 71,73,75	38	B-29
Wide intersecting canyon - c/w = 2	90	0		36	B-27

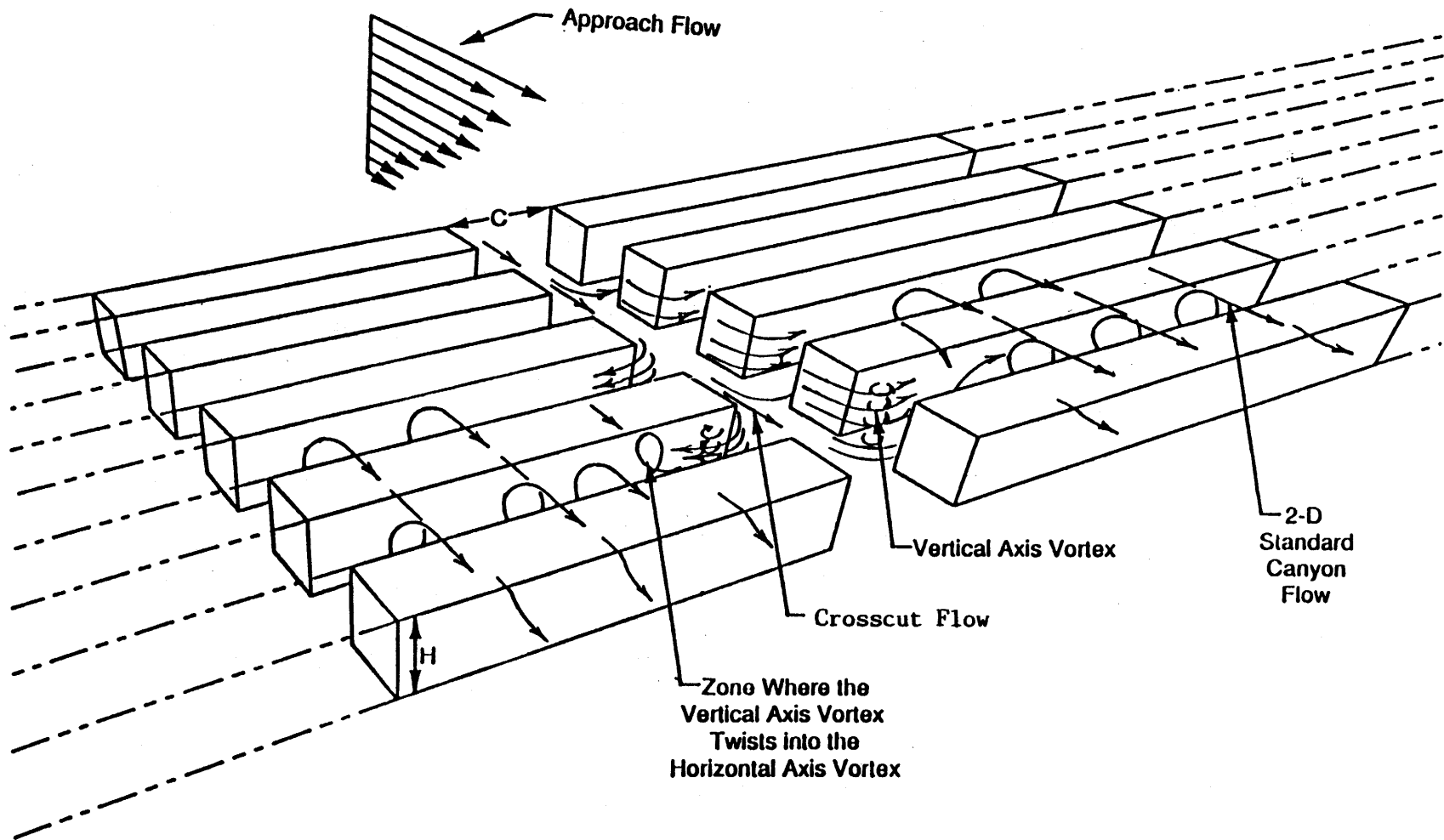
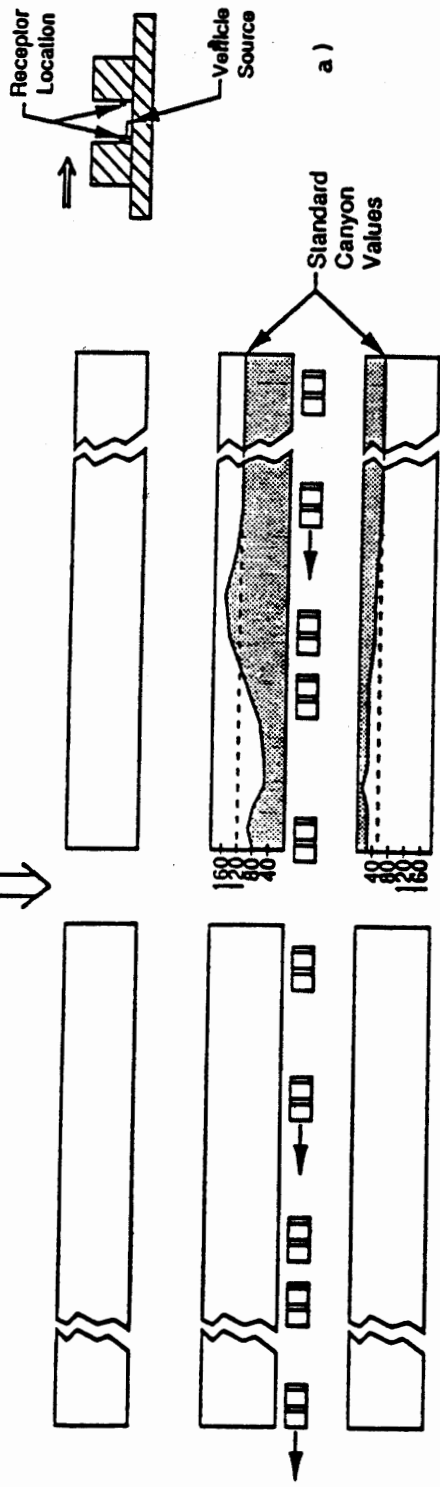


Figure 57. Flow visualization of an intersected canyon with crosscut twice the canyon height and width,  $C/H = 2.0$ .



1% Vehicle Speed  
PEDESTRIAN LEVEL CONCENTRATIONS



80% Vehicle Speed  
PEDESTRIAN LEVEL CONCENTRATIONS

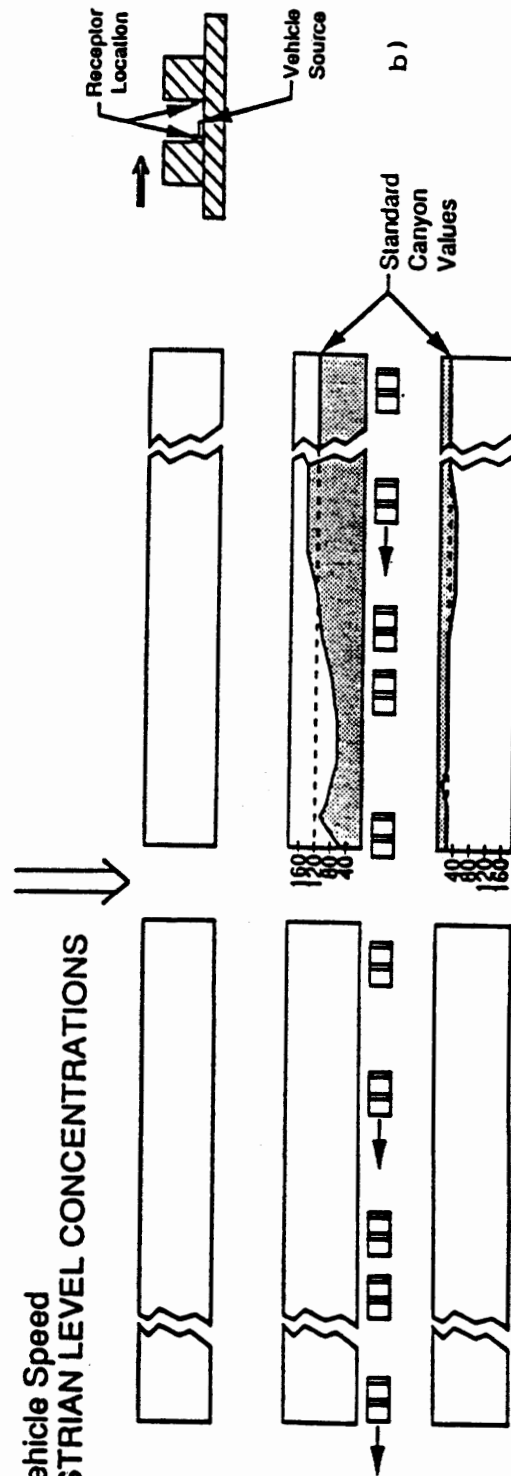


Figure 58. Concentration in a 2-D canyon with vehicles near a crosscut,  $C/H = 1.00$ .

intersection to only 30 percent of the standard canyon values for both the upstream and downstream walls.

Note that the reduction of concentrations near an intersection are attributed to the dilution of canyon pollutants rather than the canyon vortex washing out into the intersection.

#### Influence of Vehicle Speed

In this case, the vehicles are moving toward the intersection against the flow component from the crosscut ( $C/W = 1$ ). Very near the intersection the vehicle speed had little effect on concentration. On the downstream wall, the concentration decreased for 80 percent vehicle speed at three widths from the intersection (figure 59b). On the upstream wall, the concentration variation with vehicle speed is illustrated in figure 59a.

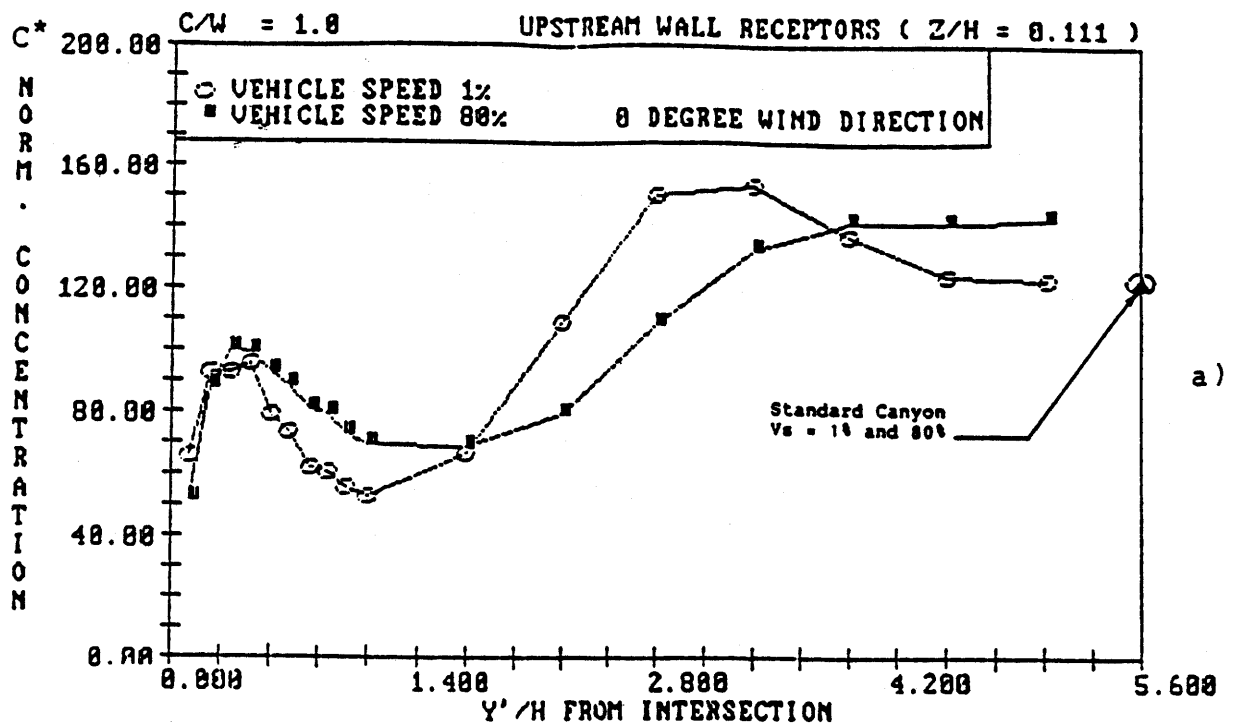
At four widths, the concentration levels on the upstream and downstream wall approach the standard canyon values. By comparing figures 59 and 60, the results show that vehicle source increases the amount of pollutant remaining in the canyon which may be the result of the vehicle direction into the crosscut.

#### Effect of Crosscut Width

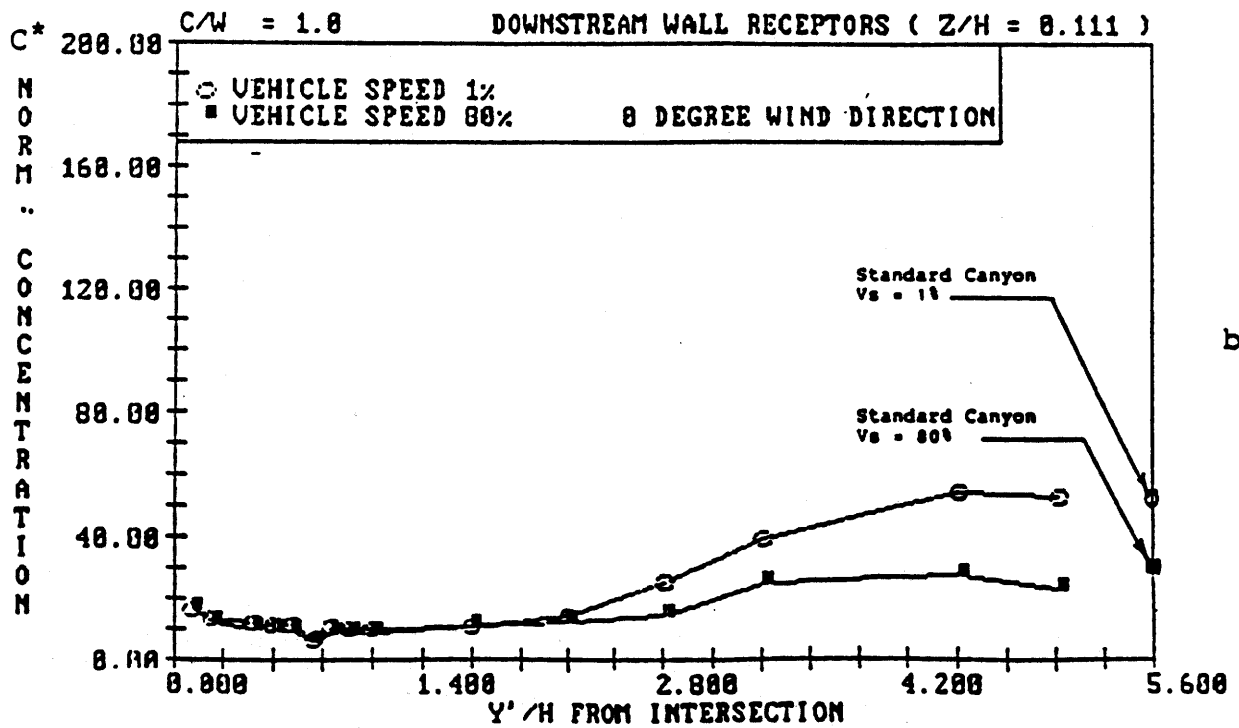
Figures 60a and 60b show the lateral concentration profile for the upstream and downstream walls at street level height of  $z/h = 0.143$ . Data show that the width of the crosscut slightly affects the concentrations along the upstream wall, but not the downwind wall. Figures 61a and 61b show the cross-section concentration profiles for the downstream and upstream walls as well as canyon center. Concentrations for the upstream wall are similar near the crosscut, but the canyon with a narrow crosscut ( $C/W = .5$ ) builds up concentrations along the upstream wall more rapidly than the canyon cut with a wider crosscut.

#### Effect of Cross Flows on Crosscut Intersections

As the flow approaches the intersected canyon from  $45^\circ$  (figure 62), the flow structure in the canyon is complex. The "standing" corner vortices that were discussed in the previous section are broken down by the longitudinal velocity component of wind (i.e., along the canyon axis). The corner vortices are replaced with randomly interacting vortices at each building corner. There is, however, one regular, very tight, vertical axis corner vortex that appears on the upstream corner of the intersection. Figure 62 shows a "hot spot" in that location.



a)



b)

Figure 59. Effect of vehicle speed near a crosscut.

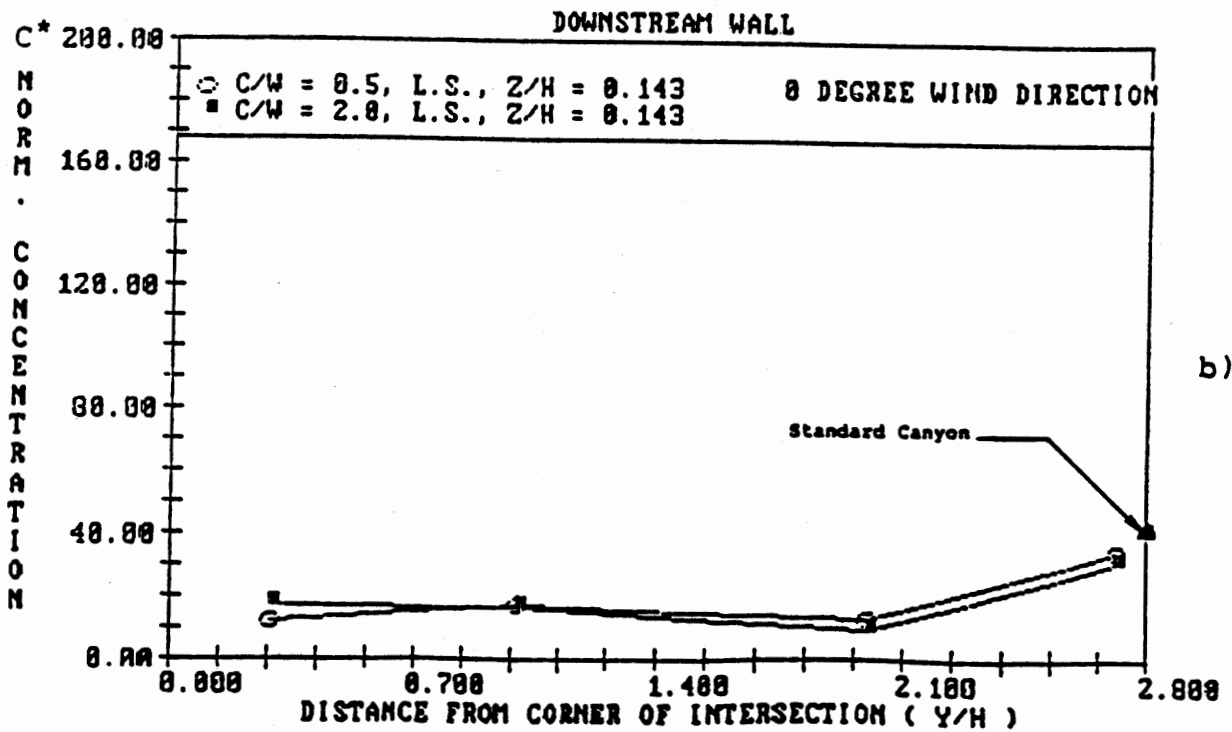
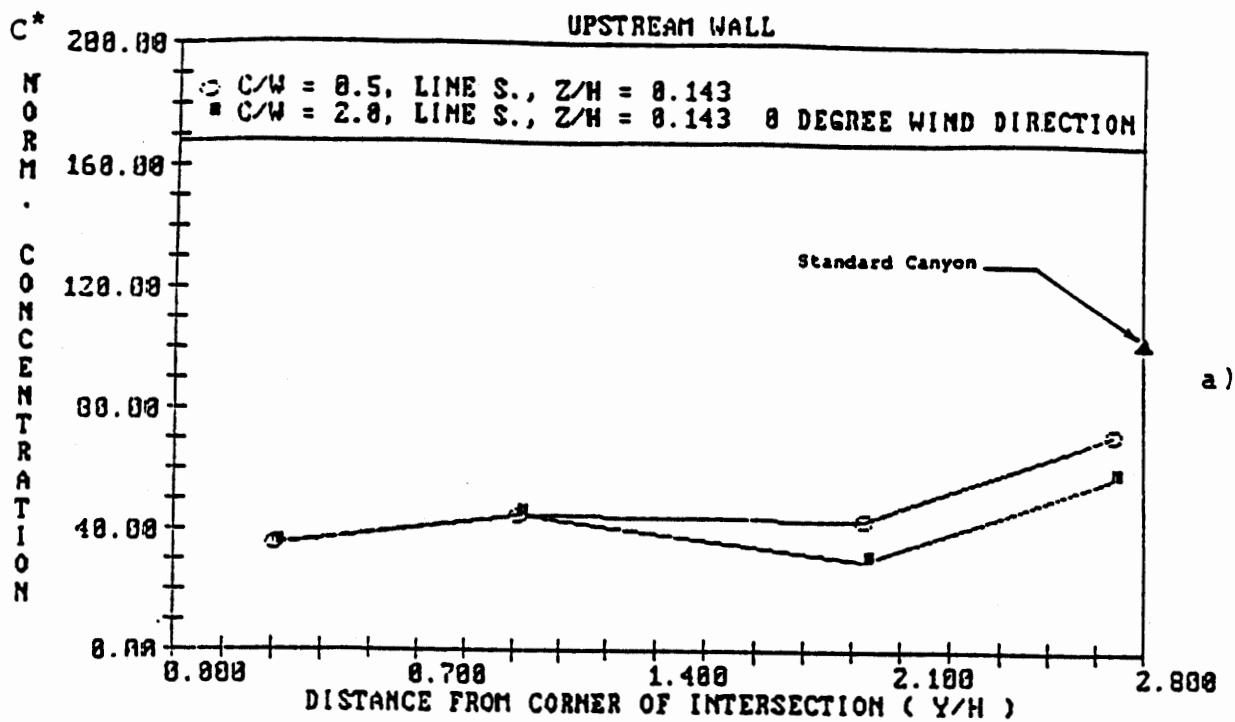


Figure 60. Effect of distance from a crosscut intersection, C/H = 0.5, C/H = 2.0.

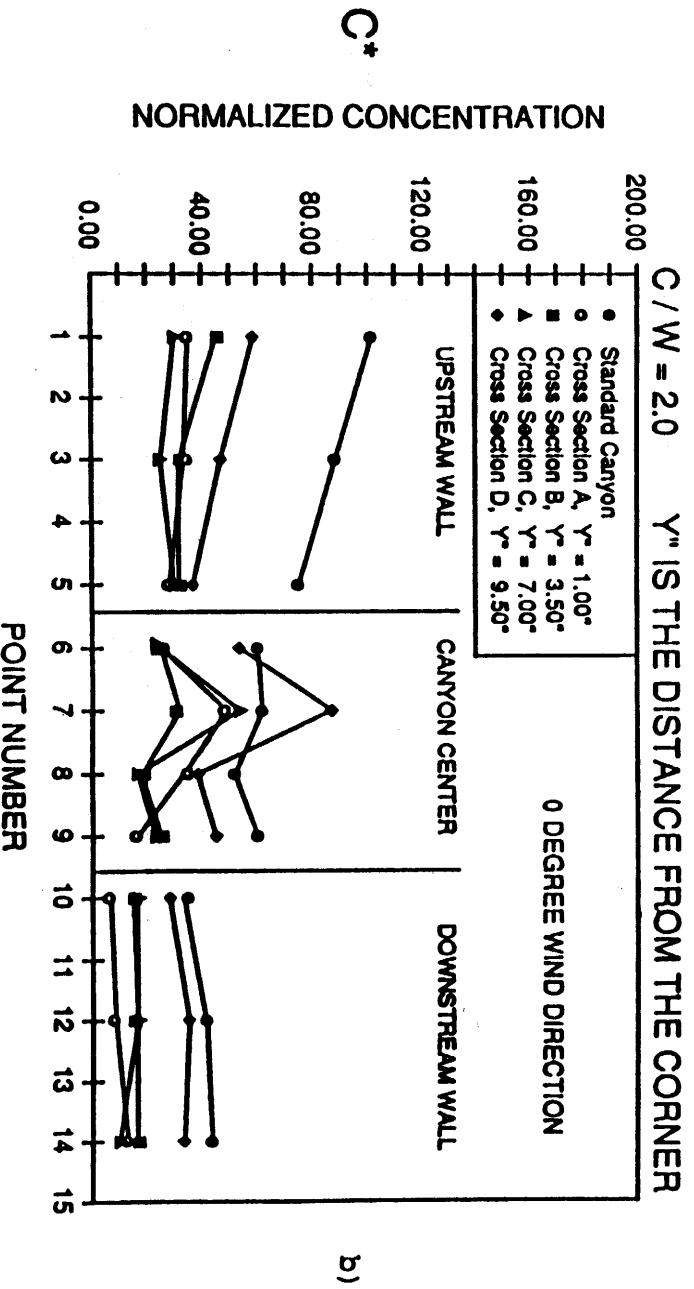
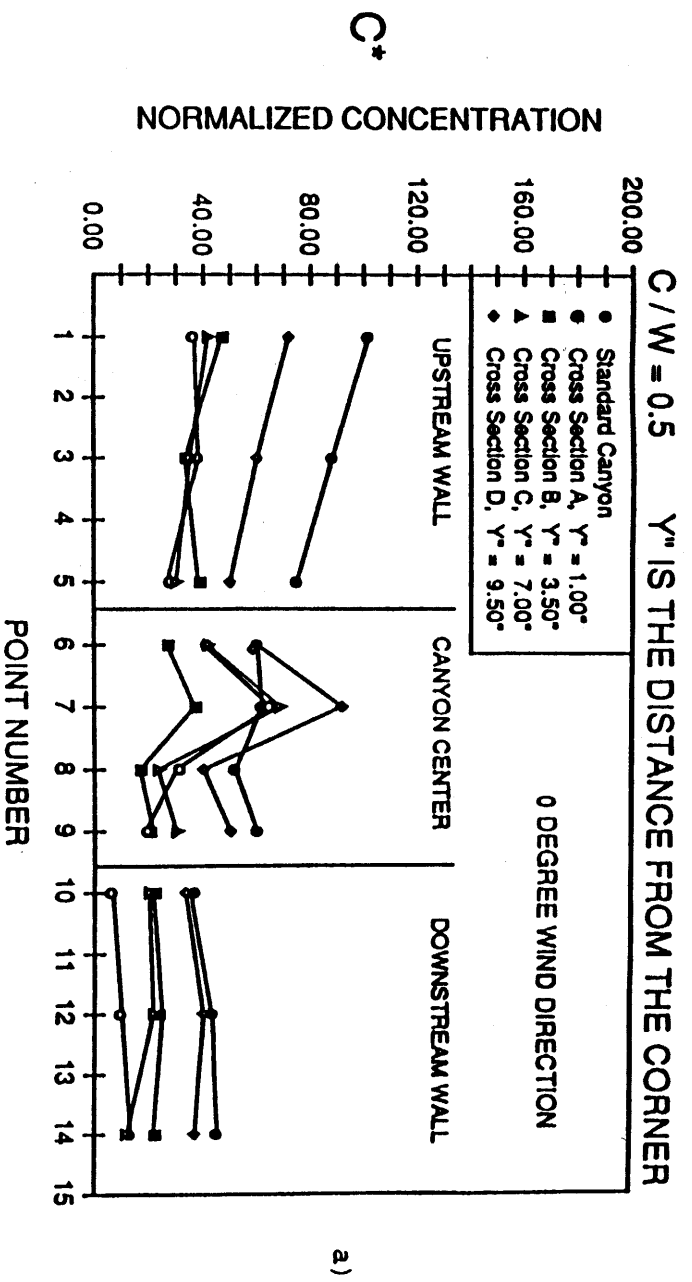


Figure 61. Comparison of cross section for crosscuts at  $0^\circ$ ,  $C/W = 0.5$ ,  $2.0$ .

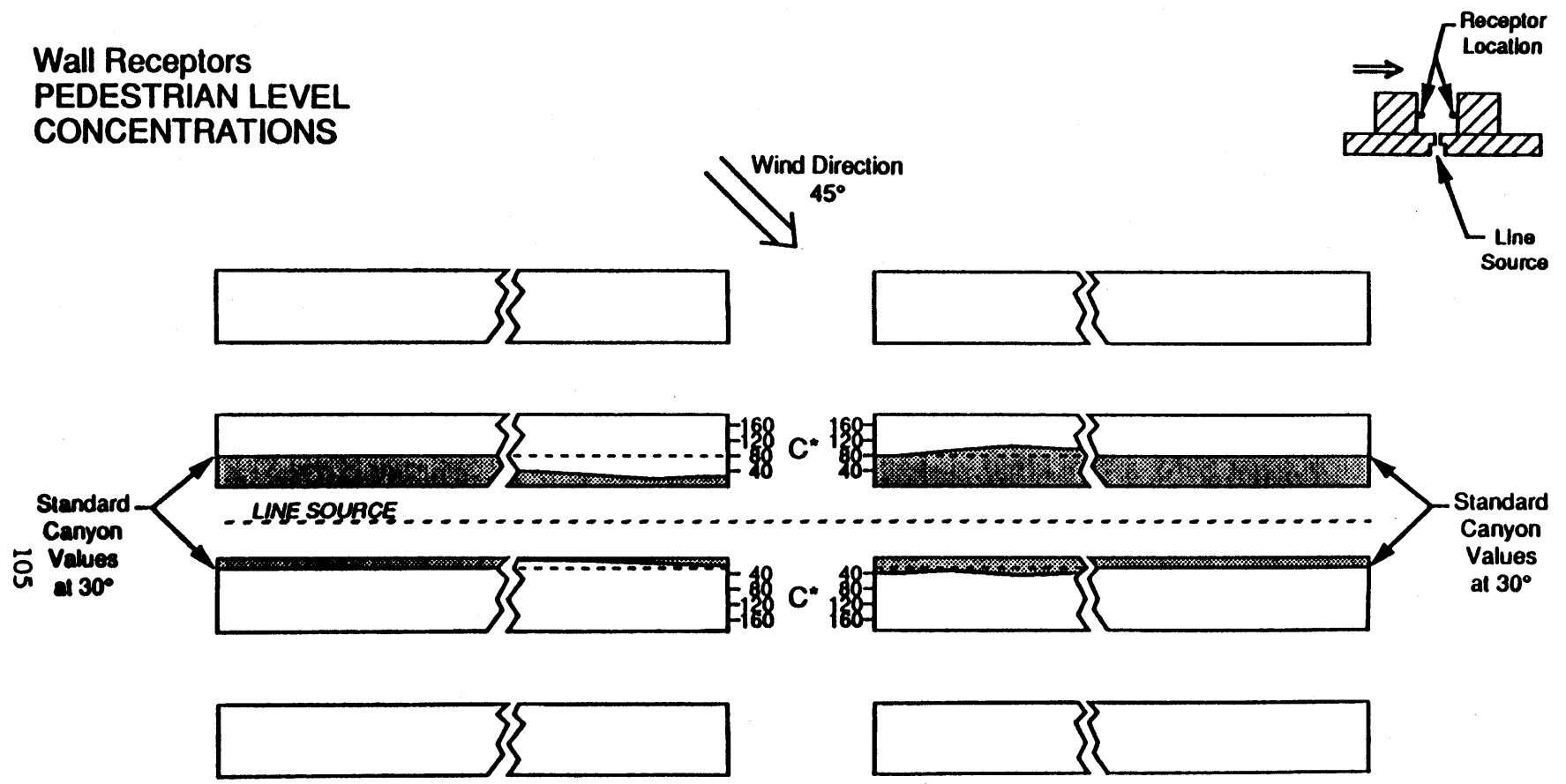


Figure 62. Concentrations in a 2-D canyon at 45° wind direction near a crosscut.

501  
105

The receptor across from the "hot spot" experiences very low concentrations.

Despite the seemingly random character of the flow, there is a distinct trend of concentration from downwind lateral side of the intersection to upwind lateral side. This appears to be due to the fact that the average flow of pollutants moves out of the upwind lateral side of the canyon into the intersection and continues to accumulate in the downwind lateral side of the canyon.

The pollutant levels increase for a distance of three canyon widths from the intersection and then stabilize. The pollutants maintain a concentration 25 percent greater than the corresponding nonintersecting canyons. In contrast, the upwind lateral side of the canyon has very low concentrations, 20 percent of the concentration of the downwind lateral side of the canyon.

At one canyon width back from the intersection, the pollutant concentrations along the downstream wall are 43 percent of those on the upstream wall for both upwind and downwind sides of the intersection. This is precisely the same ratio we observed between the upstream and downstream walls of the baseline,  $W/H = 1$ , nonintersected canyon. This shows a consistent trend far from the intersection at distances three canyon widths and greater. Closer to the intersection, there are very different concentration trends. Although there is not a clear explanation evident from the flow visualization, it is interesting to note the monotonic increase of pollutants along the upstream wall from the upwind lateral to downwind lateral side.

#### Effect of Three-way ("T") Intersections

The three-way ("T") intersection consists of a crosscut only in the upwind block and a parallel wind direction with the canyons upwind being full crosscuts. By blocking the parallel flow from passing through the intersection, a large quantity of flow is directed into the canyon, thereby increasing the dilution of pollutants.

The receptors were located on both sides of the intersection. The concentration levels were lower than those found in the standard canyon due to the additional "clean" flow channeled into the canyon by the intersection (figure 63). By comparing cross sections, figure 64a shows that the flow is very sensitive to this configuration.

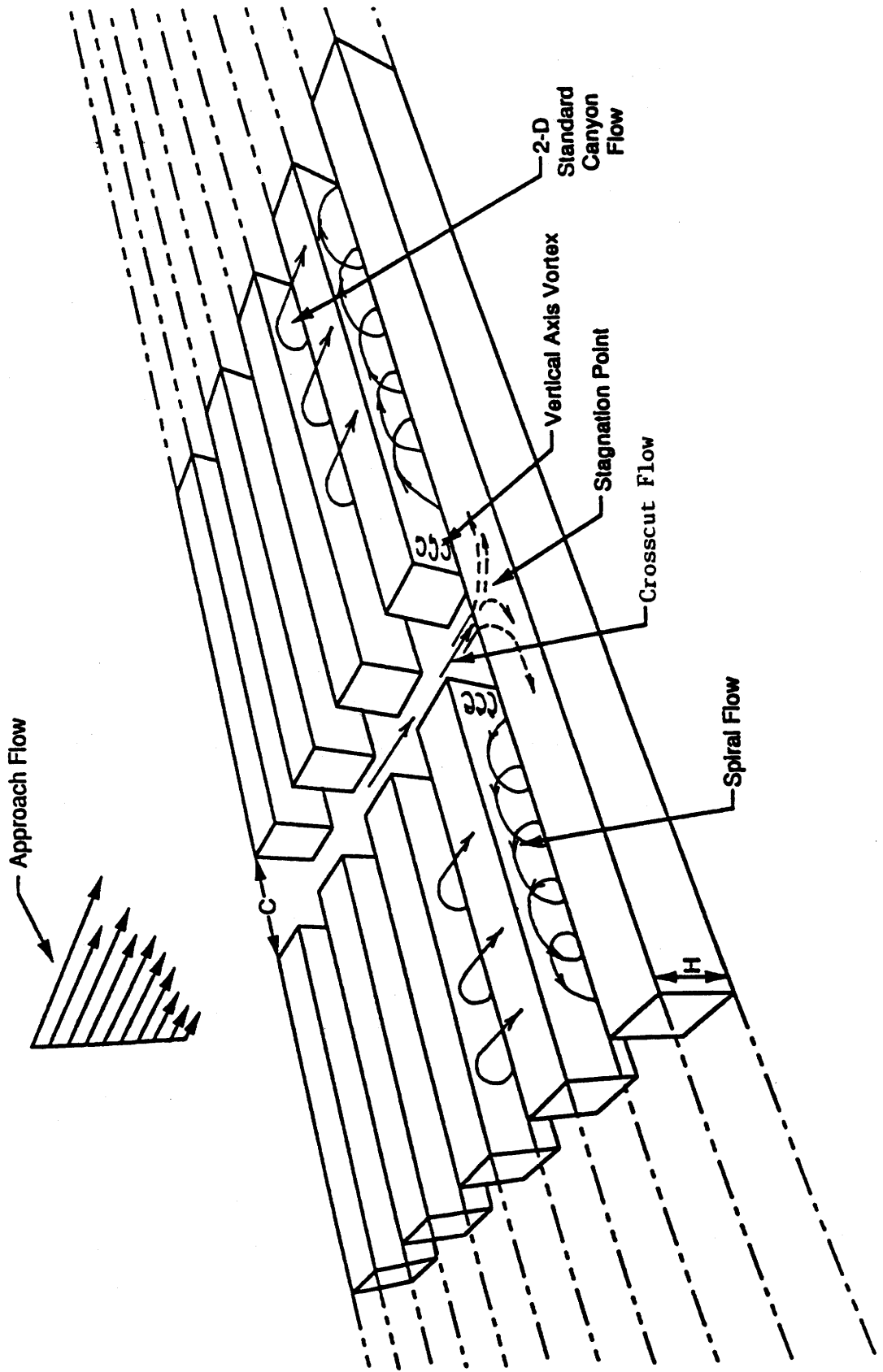


Figure 63. Flow visualization of a "T" intersection,  $C/W = 1.00$ .



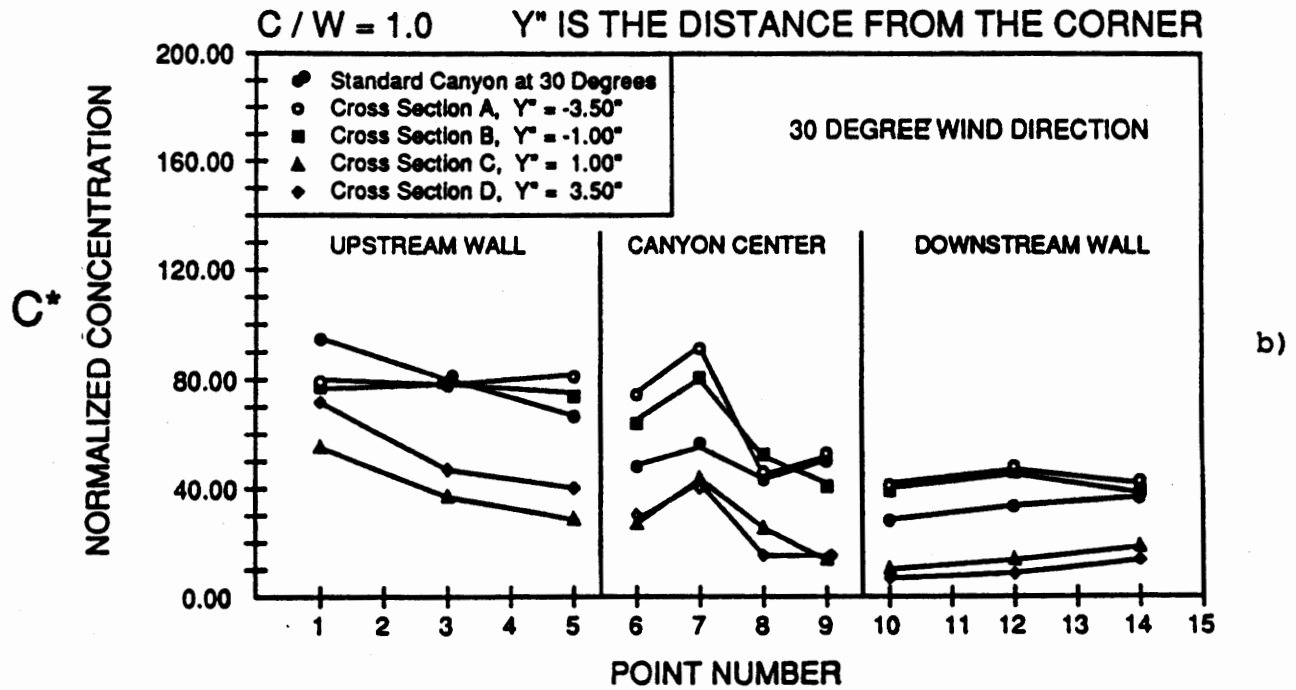
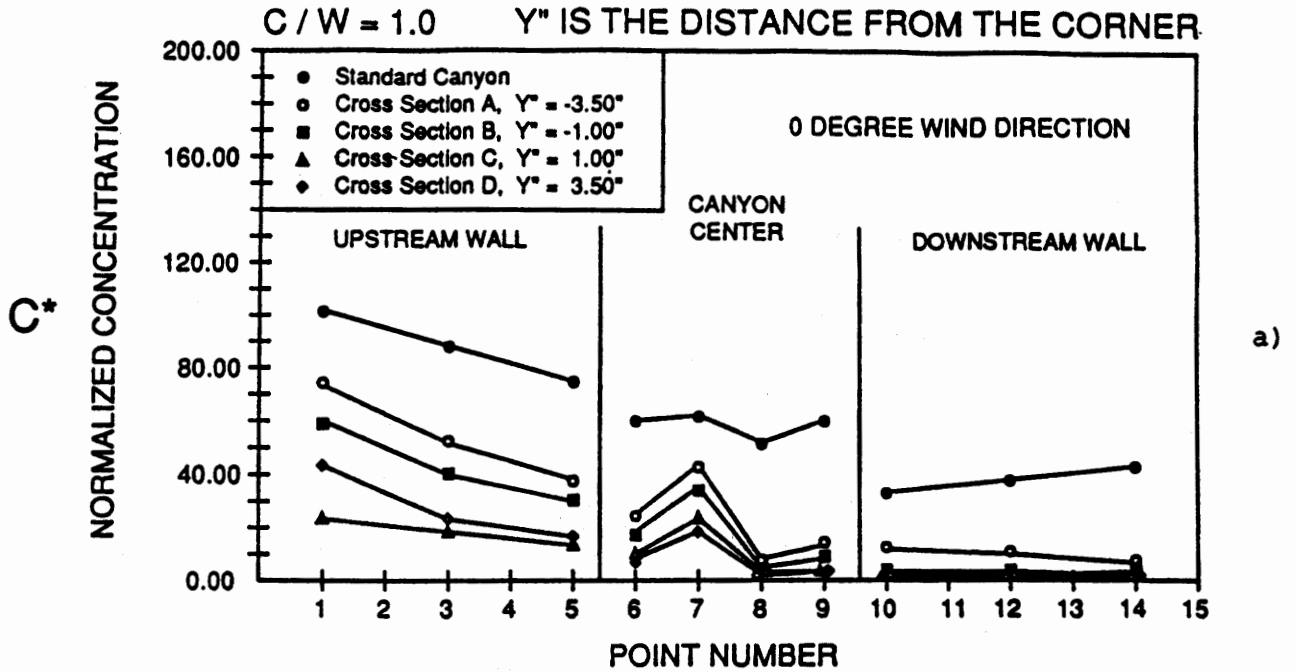


Figure 64. Comparison of cross sections in a "T" intersection.

When the wind direction has changed to 30°, the concentrations rose throughout the canyon (figure 64b). Upwind of the intersection in the lateral component direction, the upstream wall concentration levels were evenly distributed, and a dramatic increase occurred throughout the canyon (figure 65). In the downwind side of the intersection, concentration levels rose significantly on the upstream face and increased in the canyon center and on the downstream face. With a three-way intersection, the flow traveling down the crosscut was less for the 30° wind direction, thus decreasing ventilation and increasing concentration levels because the channel created by the crosscut is off angle with the wind direction.

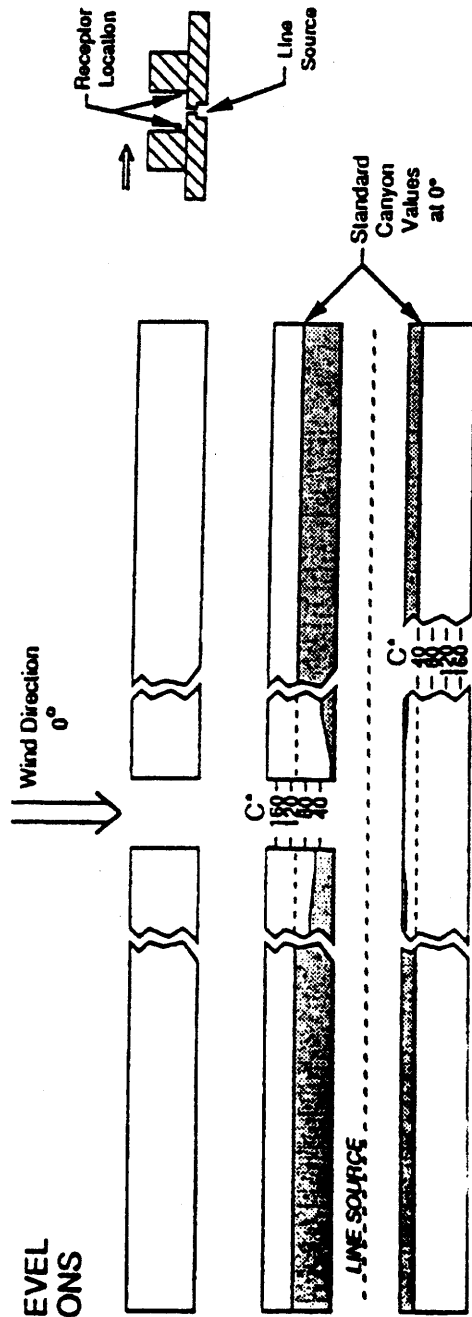
### C. Summary of Crosscut Results

Cross cutting a 2-D canyon results in the dilution of pollutants near the intersection when the wind is blowing at an angle to the canyons (45°), that is along the crosscut; the concentrations recorded in the downwind lateral side of the intersection exceed the level in the baseline configuration ( $W/H = 1$ ) at 30°. The air flow is driven into the 2-D canyon flow rather than washing out the end. This implies that for a "city block," the length between crosscut streets needs to be a minimum distance apart of eight canyon heights before 2-D flow dominates the dispersion process. For shorter distances between intersections there are interactions between the flows from the building sides and roof resulting in complex 3-D flows.

Narrow cross cuts cause establishment of 2-D-like concentration values nearer to the intersection than the wider cross cuts. The three-way intersections produce a large exchange of fluid air that results in a well-ventilated intersection, and attendant low concentrations.

The effect of vehicles appears to be due to the velocity component generated by the vehicles that mixes with the lateral flow component introduced into the canyon by the crosscut. The crosscut horizontal velocity components are further increased by crosswind situations. Although with crosswinds the flow structures in intersections are complex, there is a distinct trend of concentrations increasing downstream along the source canyon across the intersection.

**Wall Receptors  
PEDESTRIAN LEVEL  
CONCENTRATIONS**



**Wall Receptors  
PEDESTRIAN LEVEL  
CONCENTRATIONS**

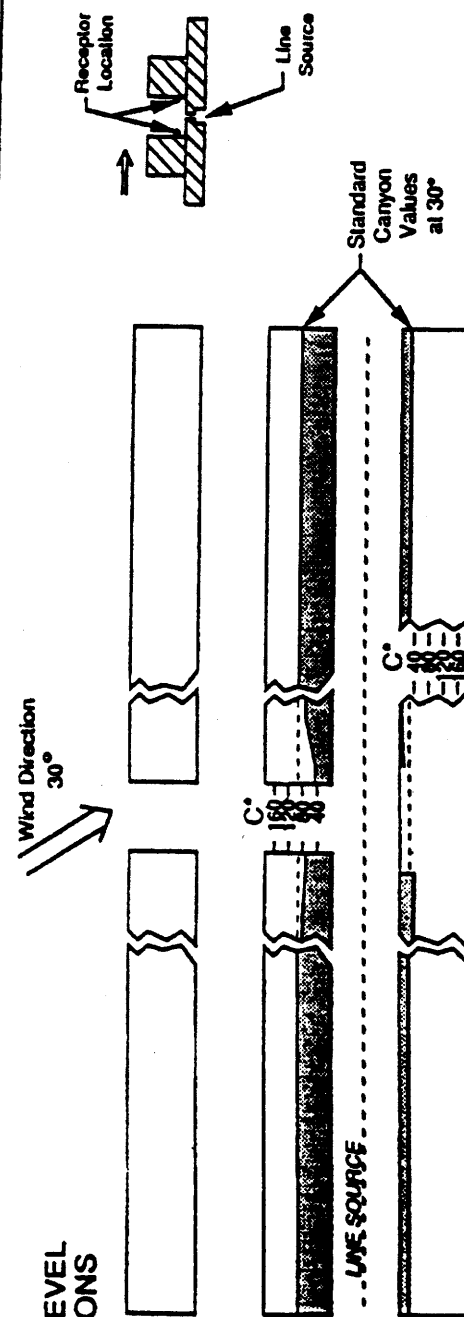


Figure 65. Concentration levels near a "T" intersection at 0 and 30°.

## 5. OBSERVATIONS AND RESULTS RELATED TO DISPERSION IN CURVED CANYONS

### A. Overview

Curved canyons are of interest since they occur in many congested areas, such as around airport terminals. The dispersion characteristics of several generic curved canyons were tested using a point source which was moved throughout the canyon. The configurations tested are summarized in table 8 and sample configurations illustrated in figure 66. Table 9 lists the x, z coordinates for the cross sections which are directly at the apex of the curved canyon. All cross sections are the same relative distance from the radius of curvature (canyon center) but rotated with respect to the tunnel centerline, as noted (5, 30, and 60° counterclockwise).

Receptors in the curved canyons were grouped at three cross sections: one cross section at the apex of the curve offset 5', one cross section at 30', and one cross section at 60'. Samples for each curved canyon were taken with the point source located at three different street-level locations. These three point source locations were at the apex of the curved canyon. A wind direction of 0° as defined to describe cases where the flow first approaches the curve apex and the cases in which flow approaches from the opposite direction defined the 180° wind direction (figure 67).

### B. Analysis of Selected Curved Canyon Data

The flow characteristics in the curved canyons were strongly influenced by wind direction and geometry. Thus, no universal trends were established. The data for these cases are contained in data base 3. To assist in gaining insight into curved canyon flows, a discussion of four major situations is provided below. Figures 68 through 71 provide detailed concentration information for three different cross sections. For each wind direction and canyon configuration, the figures illustrate the effect of source location on concentration distribution.

#### Narrow Curved Canyon (W/H = 1.0): 0° Wind Direction

At the curve apex, a strong vortex develops similar to the vortex observed in the standard 2-D canyon (W/H = 1.0) with a stagnation point on the downstream wall. Downwind from the apex, the vortex elongates in the direction of the curve (figure 72A) and a tightly wrapped spiral vortex filament develops.

**Table 8. Data file cross reference for data from curved canyon configurations.**

Headings:	wind angle	W/H	velocity data	pollution conc.	flow visualization test #	tape #
-----------	------------	-----	---------------	-----------------	---------------------------	--------

**Curved Canyons**

Large radius curves curves 1 & 2	0	1	FHA1-77 79	FHA2-6, 7,9	20	B-33
Large radius curves curves 1 & 2	180	1	FHA1-85	FHA2-19, 21,23	23	B-39
Large radius curves curves 1 & 3	0	2.43	FHA1-81	FHA2-31, 33,35	21	B-35
Large radius curves curves 1 & 3	180	2.43	FHA1-83	FHA2-25, 27,29	22	B-36
Medium radius curves curves 2 & 4	0	2.29	FHA1-87	FHA2-39, 41,43	27	B-37
Medium radius curves curves 2 & 4	180	2.29	FHA1-89	FHA2-45, 47,49,51	24	B-38
Small radius curves curves 3 & 4	0	0.86	FHA1-97			
Small radius curves curves 3 & 4	180	0.86	FHA1-99			

**Curved Canyons with Slotted Airport Terminal**

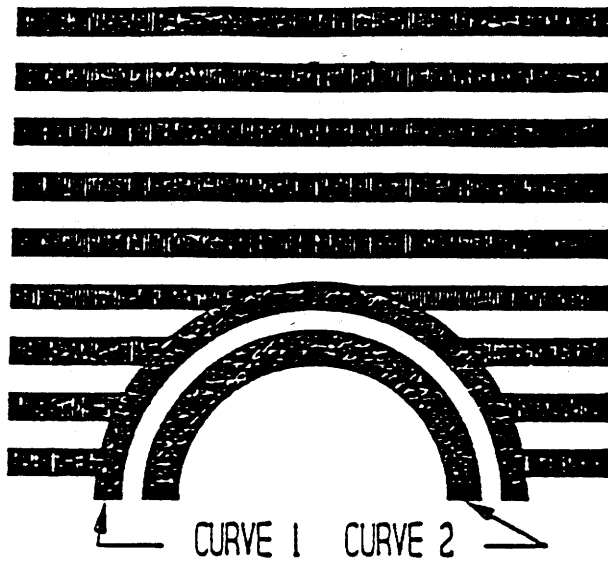
Curves 2 & 4 - curve 4 slotted	0	2.29	FHA1-95	FHA2-61, 63,65,67, 69,71	26	B-39
Curves 2 & 4 - curve 4 slotted	180	2.29	FHA1-93	FHA2-53, 55,57,59	25	B-40

Note: The medium radius curves are identical to the airport terminals without slots.

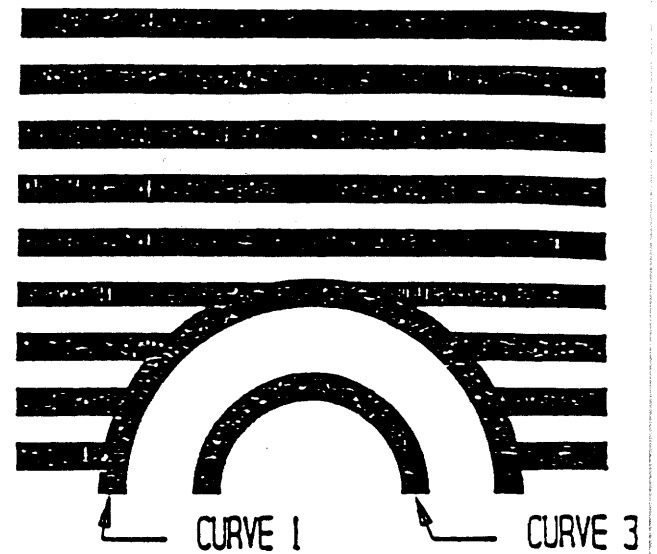
Table 9. Table of x,z coordinates for curved canyon test configuration(s)  
 curved canyon height (H) = 3.50 in.

POINT #	NARROW CURVE W/H = 1.00		WIDE CURVE W/H = 2.43		AIRPORT TERMINALS W/H = 2.29	
	<b>Along Upstream Wall Receptors</b>					
	X/H	Z/H	X/H	Z/H	X/H	Z/H
1	-0.500	0.171	-1.215	0.171	-1.145	0.171
2	-0.500	0.343	-1.215	0.343	-1.145	0.343
3	-0.500	0.514	-1.215	0.514	-1.145	0.514
4	-0.500	0.686	-1.215	0.686	-1.145	0.686
5	-0.500	0.857	-1.215	0.857	-1.145	0.857
	<b>Canyon Center Receptors</b>					
	X/H	Z/H	X/H	Z/H	X/H	Z/H
6	-0.180	0.514	-0.895	0.514	-0.825	0.514
7	-0.180	0.171	-0.895	0.171	-0.825	0.171
8	0.180	0.514	0.895	0.514	0.825	0.171
9	0.180	0.857	0.895	1.857	0.825	0.514
	<b>Along Downstream Receptors</b>					
	X/H	Z/H	X/H	Z/H	X/H	Z/H
10	0.500	0.857	1.215	0.857	1.145	0.857
11	0.500	0.686	1.215	0.686	1.145	0.686
12	0.500	0.514	1.215	0.514	1.145	0.514
13	0.500	0.343	1.215	0.343	1.145	0.343
14	0.500	0.171	1.215	0.171	1.145	0.171

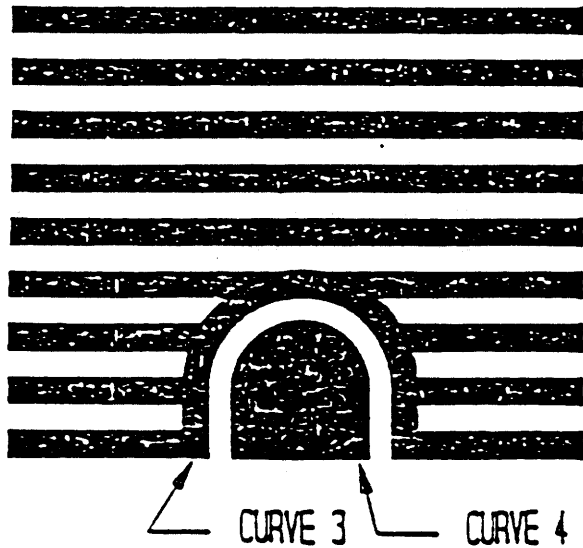
CURVES 1 AND 2, GENERIC CONFIGURATION



CURVE 1 AND 3, GENERIC CONFIGURATION



CURVES 3 AND 4, GENERIC CONFIGURATION



CURVES 2 AND 4, GENERIC CONFIGURATION

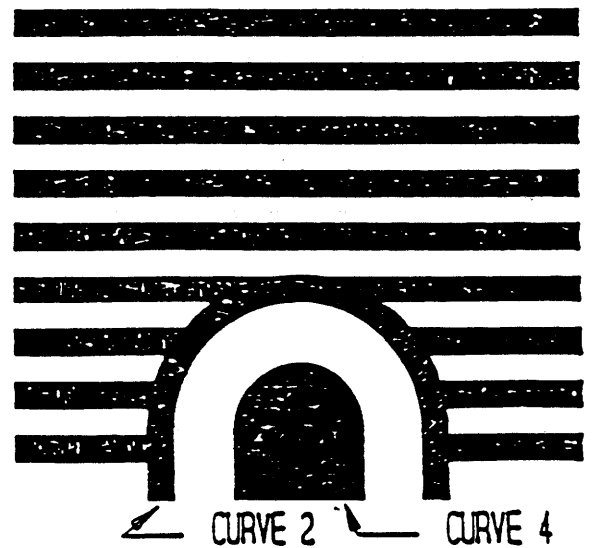


Figure 66. Plan view of different curved canyon configurations at 0°.

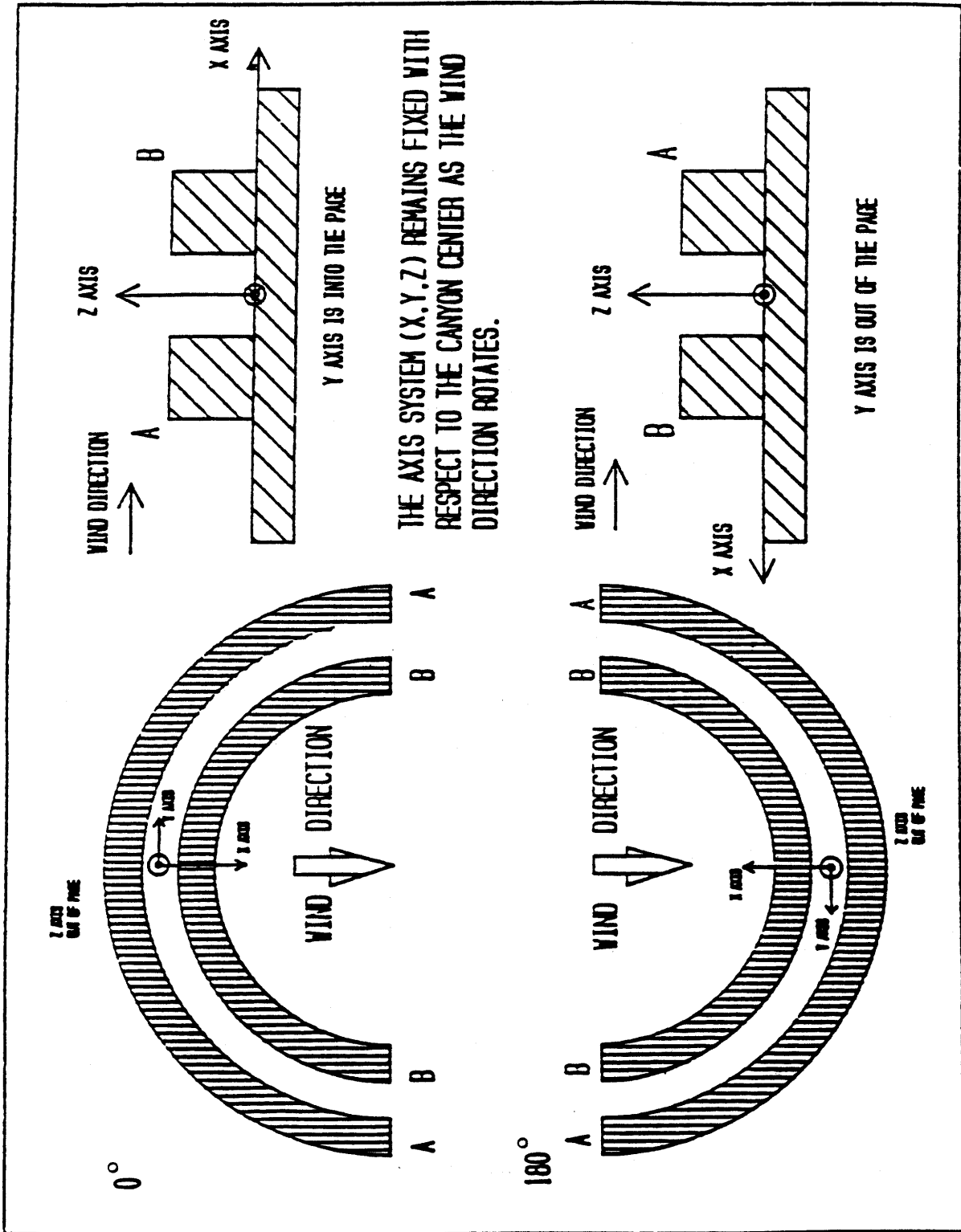
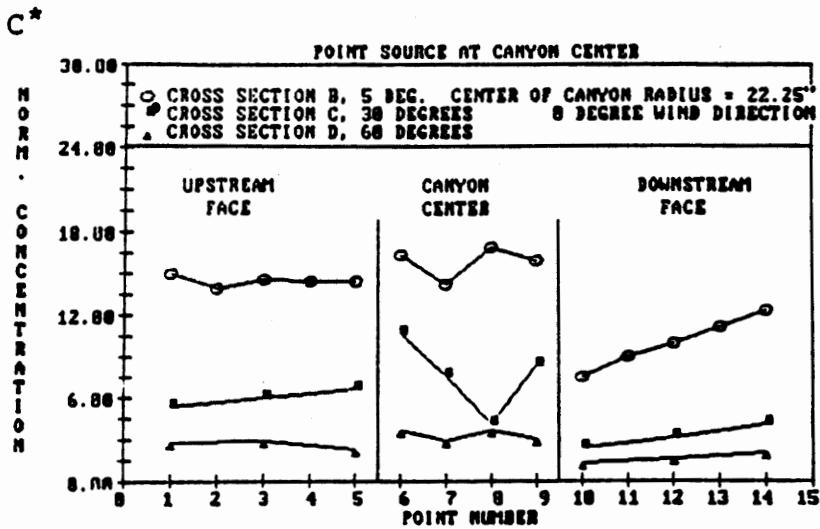
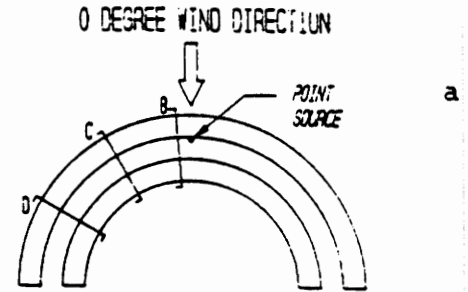
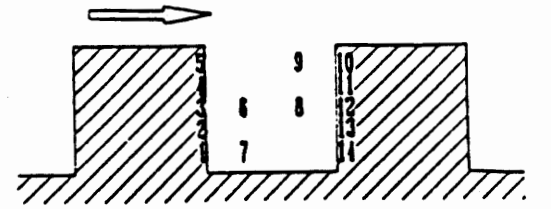
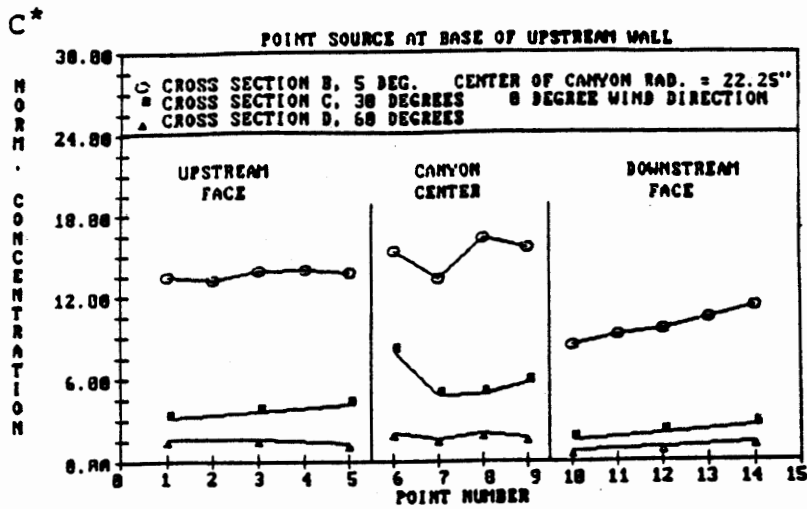
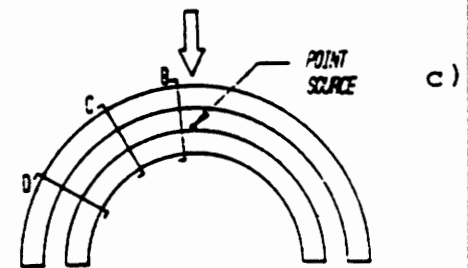
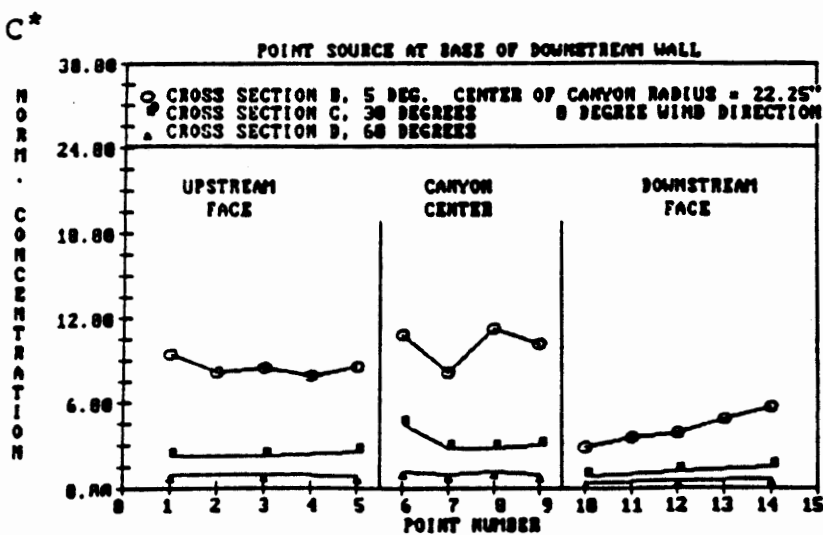
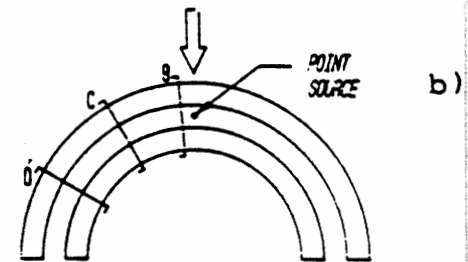


Figure 67. Coordinate system for curved canyons.





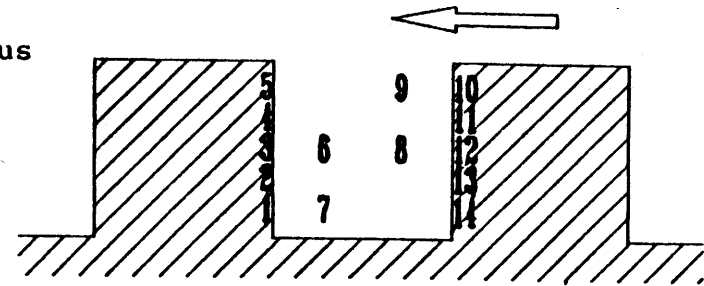
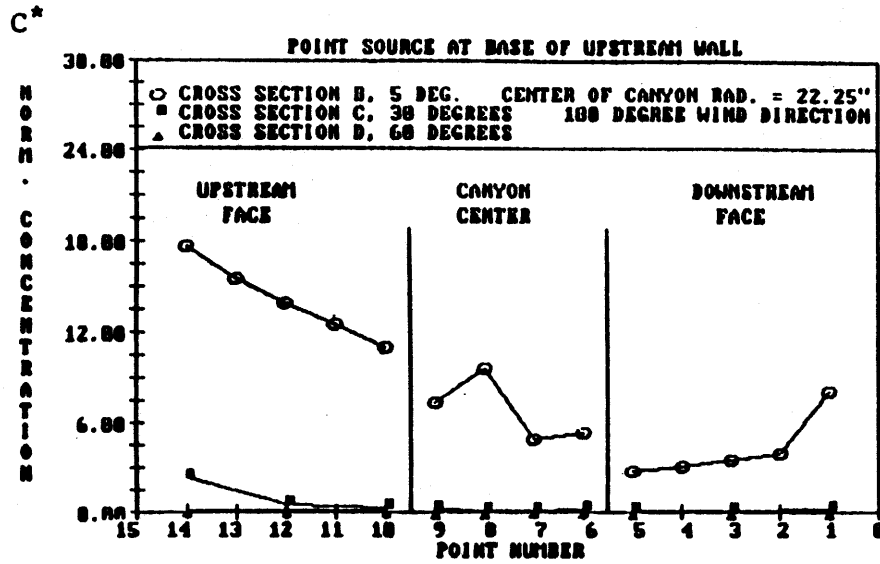
canyon width = 3.5 in  
 diameter = 2 times radius



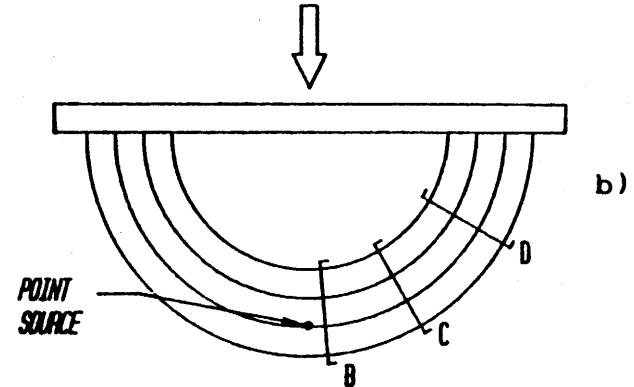
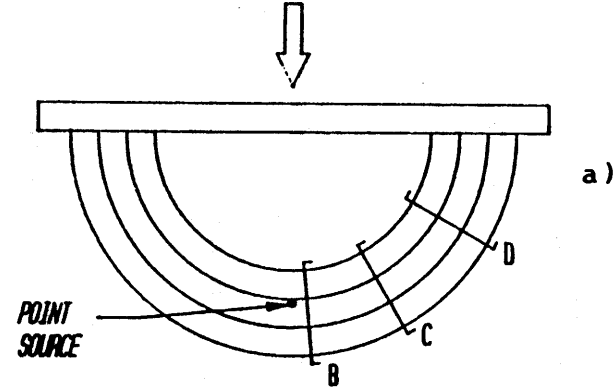
1 in = 2.54 cm

Figure 68. Concentrations in a curved canyon,  $W/H = 1.0$ , wind azimuth = 0° canyon.

canyon width = 3.5 in  
 diameter = 2 times radius



180 DEGREE WIND DIRECTION



1 in = 2.54 cm

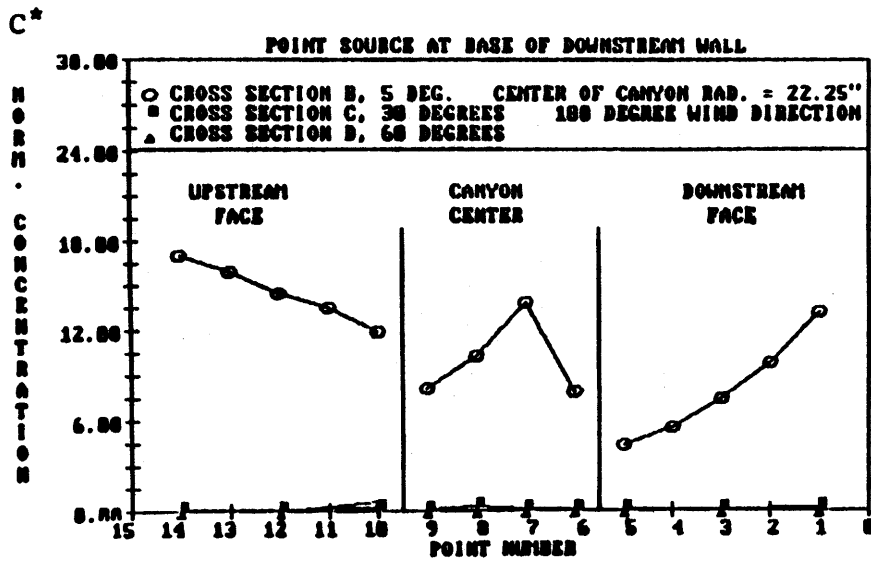


Figure 69. Concentrations in a curved canyon,  $W/H = 1.0$ , wind azimuth =  $180^\circ$ .

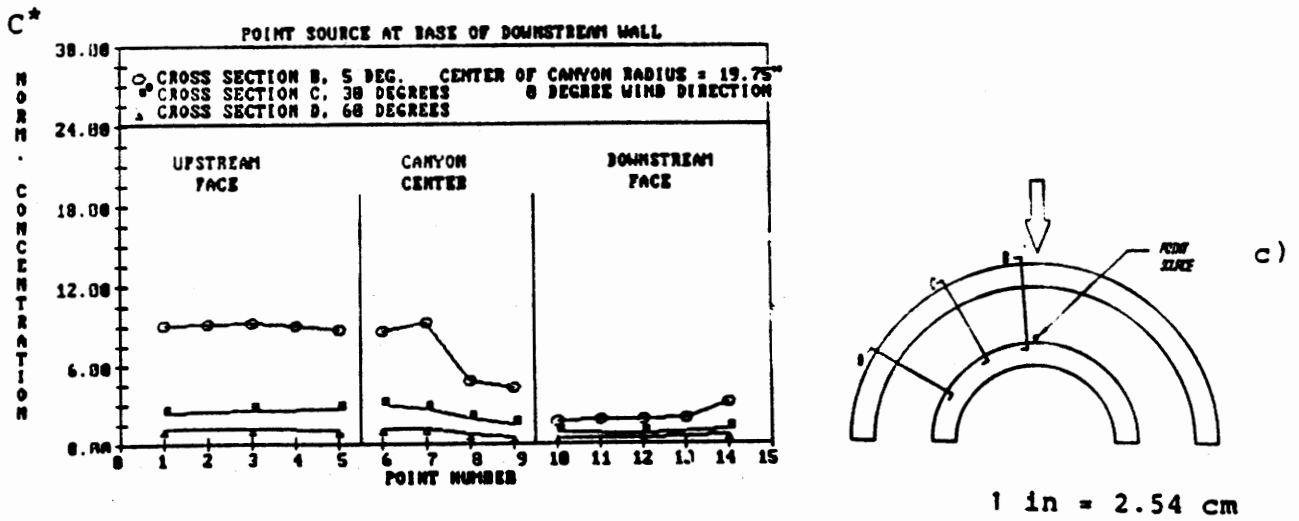
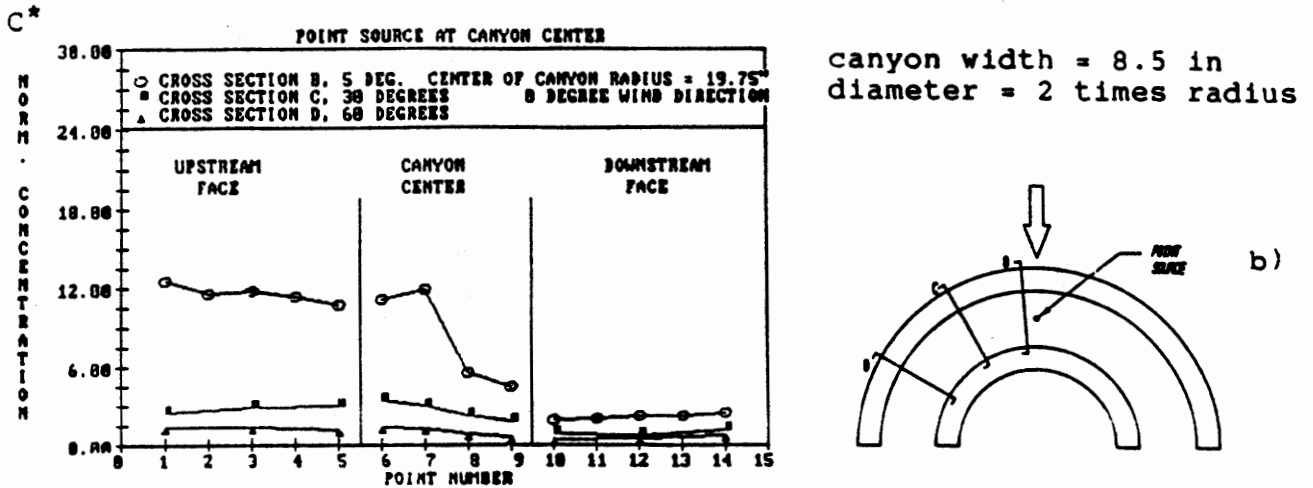
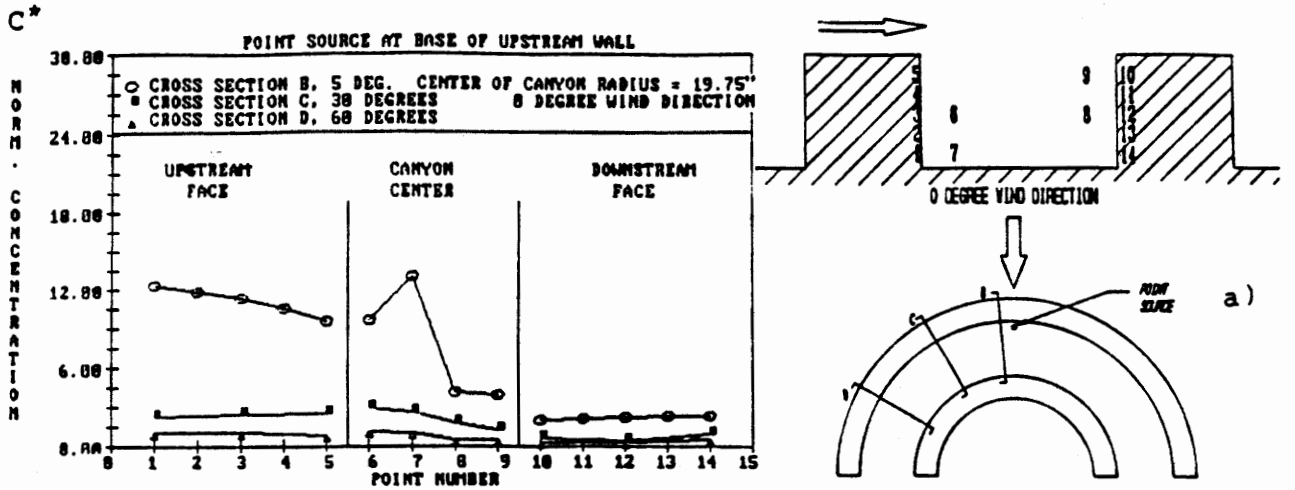
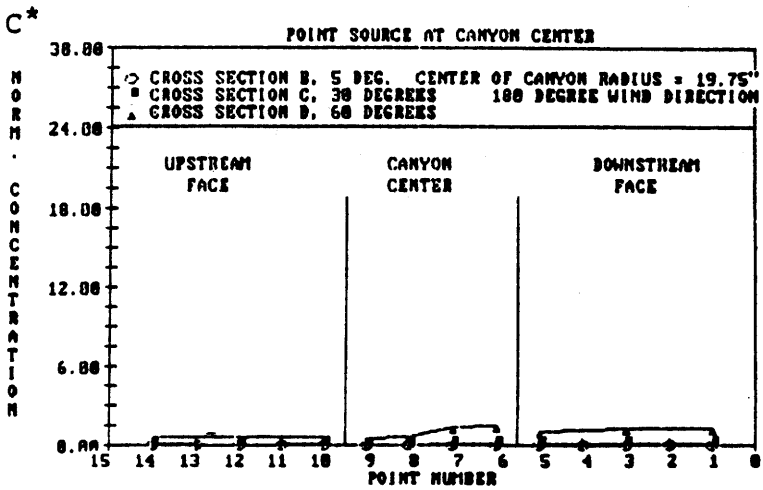
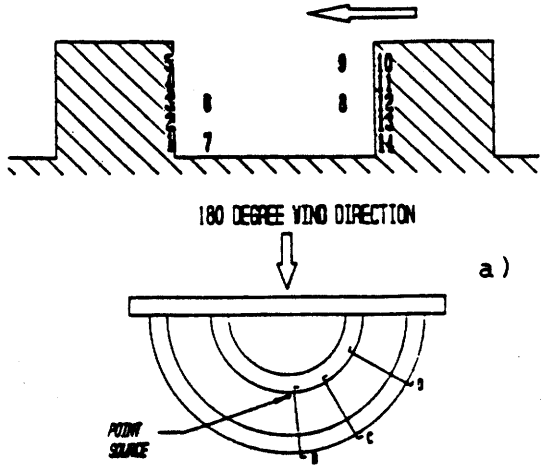
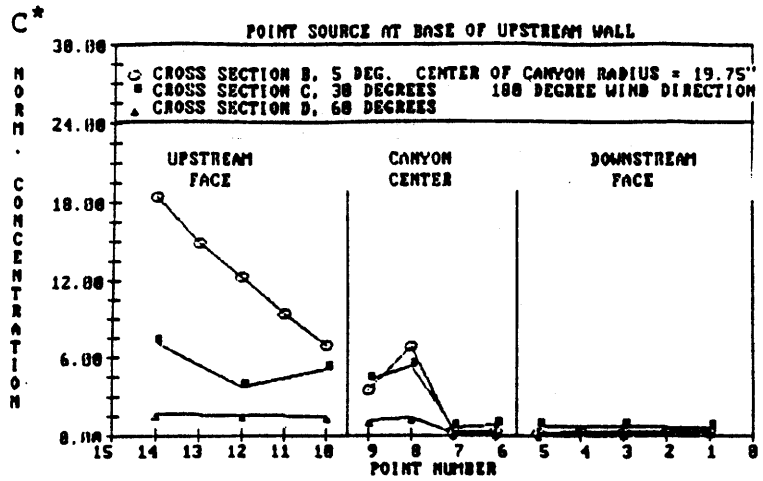
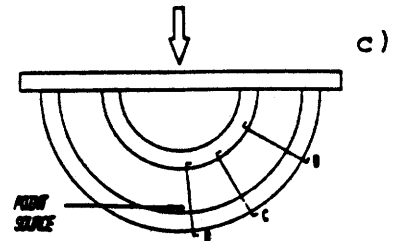
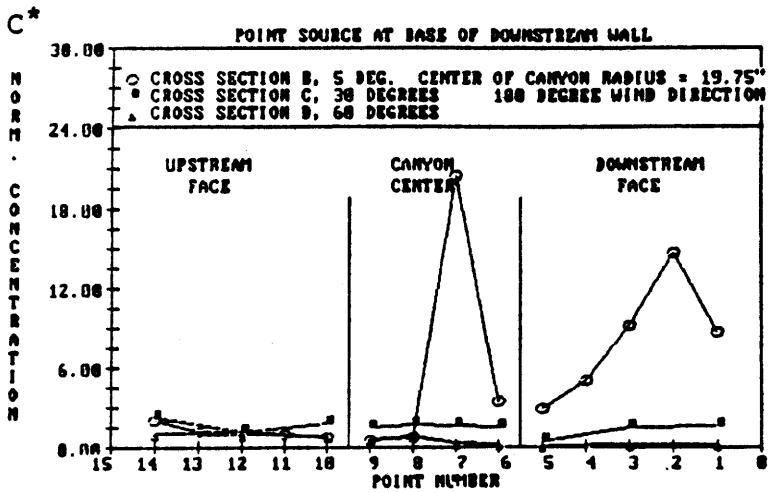
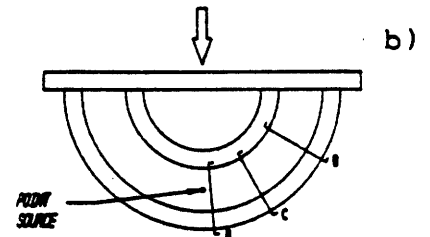


Figure 70. Concentrations in a curved canyon,  $W/H = 2.43$ , wind azimuth =  $0^\circ$



canyon width = 8.5 in  
 diameter = 2 times radius



1 in = 2.54 cm

Figure 71. Concentrations in a curved canyon,  $W/H = 2.43$ , wind azimuth =  $180^\circ$ .

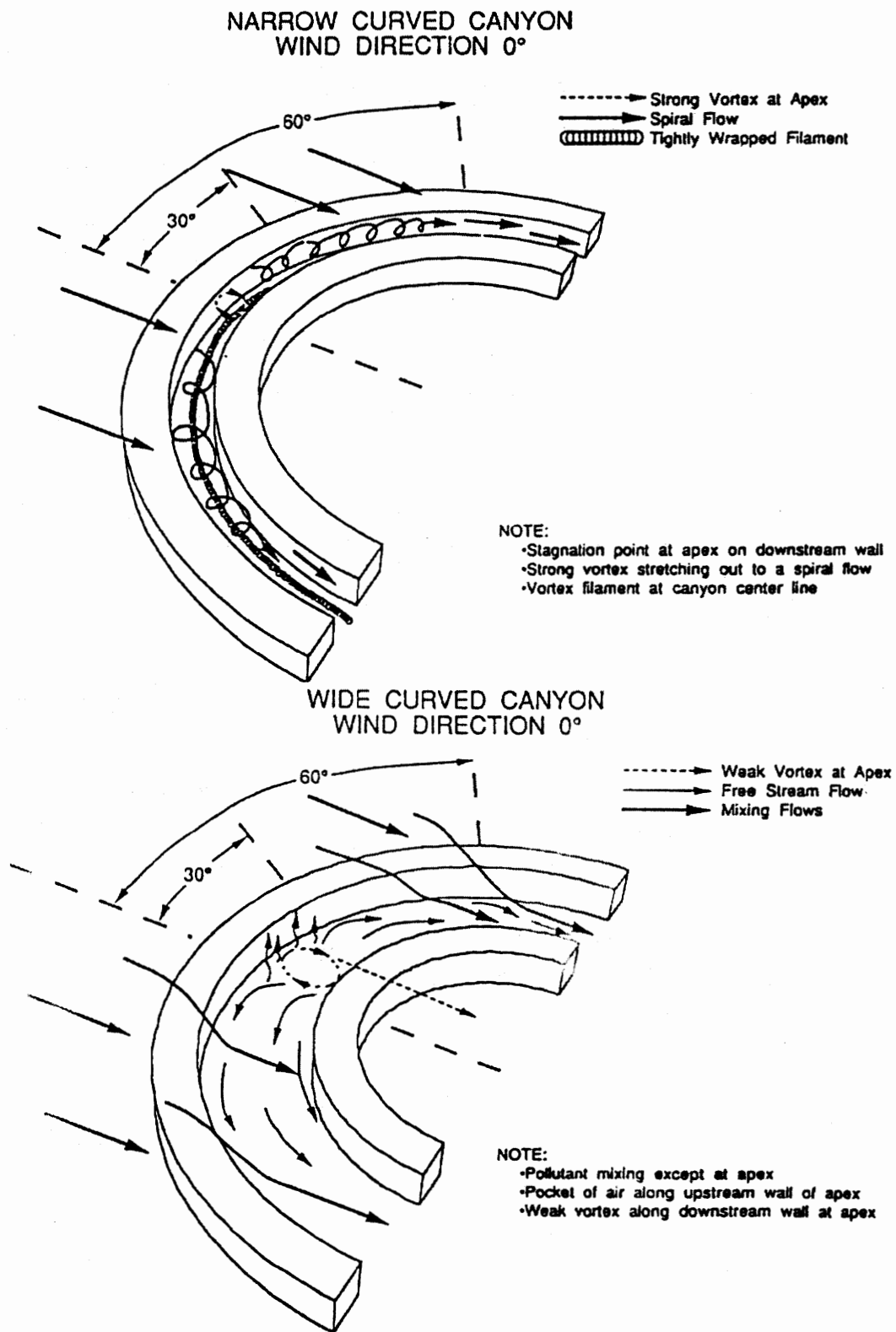


Figure 72. Flow visualization for narrow and wide curved canyons at 0° wind direction.

When the pollutants are introduced at the three different point source locations, the concentration distribution remains similar, but the magnitudes are different. The concentration levels are similar when the point source is located near the upstream corner or canyon center. A significant drop occurs when the point is moved near the downstream wall, due to lateral flow away from the stagnation point.

In all cases, the center receptors show the highest concentration level, demonstrating that the spiral vortex filament pulls the pollutants along the canyon. As expected, the concentration levels decrease as one proceeds along the curve (away from the source), due to the increasing lateral spiral component and the mixing of clean flow into the canyon.

#### Narrow Curved Canyon (W/H = 1.0): 180° Wind Direction

The narrow curved canyon, with wind from 180°, has a flow characterized by mixing of flows from the two legs. Figure 72a shows strong wall flows that collide at the apex of the canyon, where there is also a weak vortex. The flow then migrates along the center of the canyon away from the apex, between and in the opposite direction of the lateral wall flows. The mid-canyon flow continues until the 60' cross section, where it collides with the free stream flow and washes out of the canyon.

When the source is located along the upstream wall, the dispersion profiles are similar to the straight (W/H = 1) canyon vortex flow. With the source moved to the downstream wall, the concentration rises near the point source, but remains the same along the upstream wall. In both cases, the pollutants are trapped in the region near the apex where the two strong wall flows collide. The receptors at the 30 and 60' cross section detected little or no tracer gas concentrations.

#### Wide Canyon (W/H = 2.43): 0° Wind Direction

As a curved canyon widens, the ability to form strong vortices and spiral flows diminishes. At the curve apex, a weak vortex develops on the downstream side of the canyon (figure 72b), and a pocket of lower velocity flow develops on the upstream side. The flow is drawn towards the upstream wall and then is pulled around the curve, mixing with the flow coming over the canyon walls.

At the 5' cross section, higher concentrations were found along the upstream wall. The same trends occurred for all three point source locations, showing that most of the pollutants are drawn toward the pocket of lower velocity air along the

upstream wall near the apex. The lower concentrations along the downstream wall show that the flow is directed away from the downstream wall, and an extremely weak recirculation occurs.

As the flow passes the 30 and 60° cross sections, the flow has no coherent rotational velocity component. This flow is a turbulent mixing flow which causes greater dispersion along the upstream wall, thereby creating a more uniform dispersion across the canyon.

#### Wide Curved Canyon (W/H = 2.43): 180° Wind Direction

There is no evidence of a coherent vortex in the wide curved canyon with wind from the 180° direction (figure 73). There are distinct hot spots at the apex of the curve, both at the base of the upstream and downstream walls. These hot spots appear only when the source is located near the receptor location and do not appear when the source is located at mid-canyon. When the source is located at mid-canyon, the only significant pollutants observed are at the 60° cross section.

At the 30° cross section, there are also changes in the dispersion profiles as the source location is changed. This cross section and the apex cross section are both sensitive to the source location, due to the variation in the local flow characteristics and direction along the canyon. This is confirmed by the flow visualization which illustrates the downwind direction of the canyon center flow and the upwind direction of the flow along both walls. The insensitivity of concentrations to source location at the 60° cross section can be attributed to the full mixing of the along-canyon flows, and the upstream wall and downstream wall flows with the oncoming free stream flow.

It is interesting to note that the hot spot at the base of the upstream wall at the apex has the same  $C^*$  value as in the case of the 180° narrow curved canyon.

### **C. Comparison of Curved Canyon Results**

#### Effect of Canyon Width: 0° Wind Direction

By increasing the canyon width from 1.0 to 2.43, figure 74 indicates that the concentration levels decrease throughout the canyon. Due to a weak vortex near the apex, a dramatic drop occurred along the downstream wall in the wider canyon. As the width increases, the flow pattern changes from being mostly driven by shear flow across the canyon ceiling to being

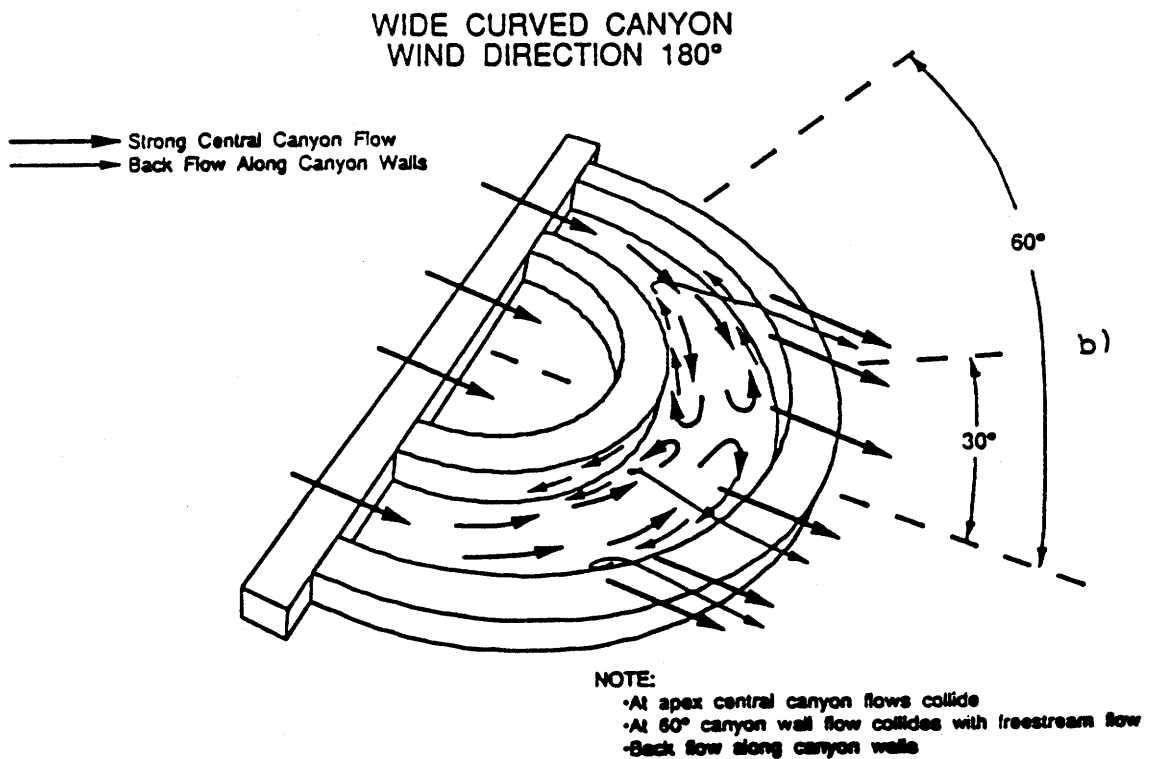
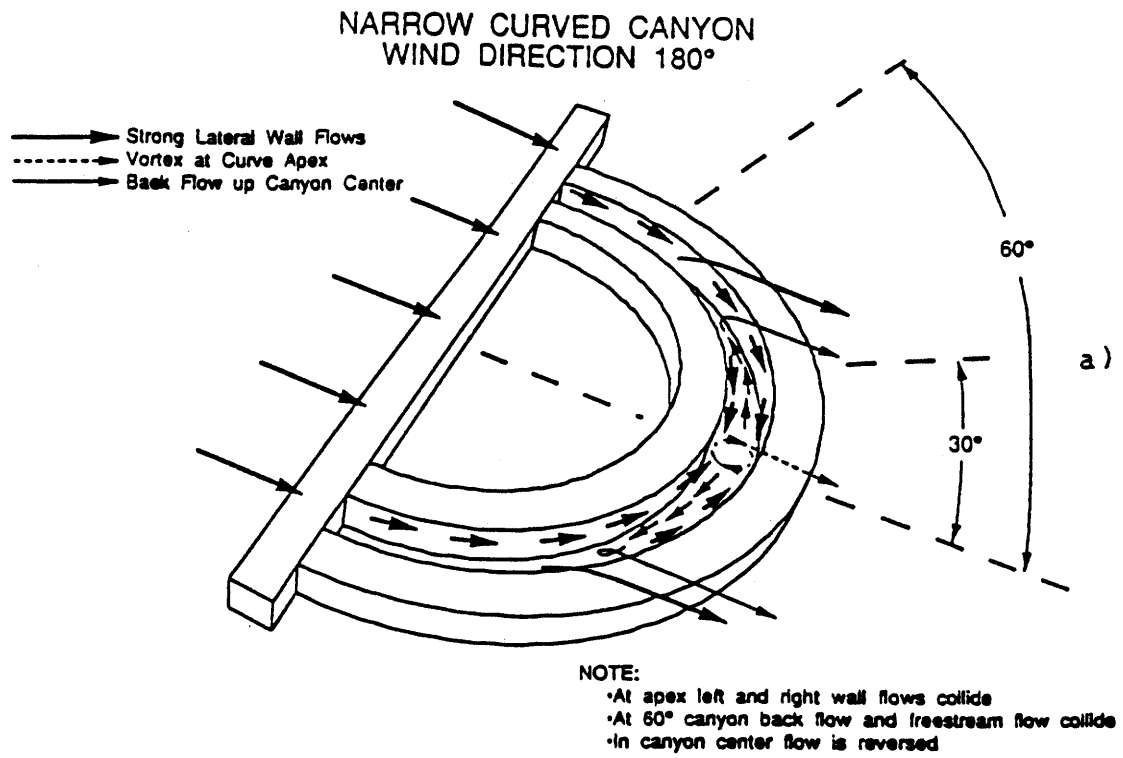


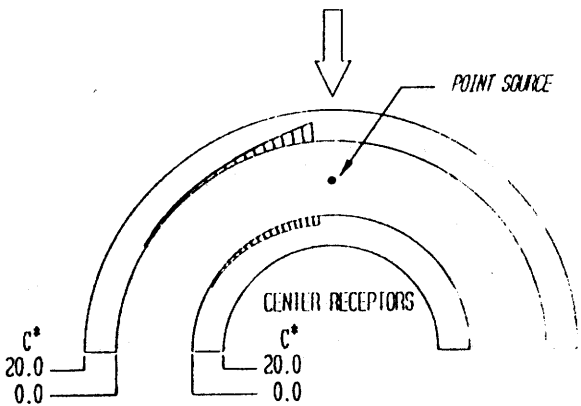
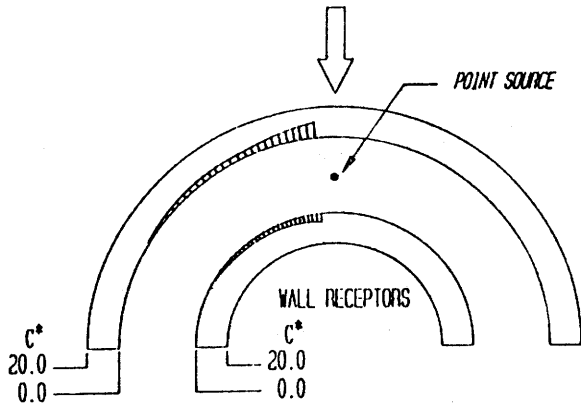
Figure 73. Flow visualization for narrow and wide curved canyons at 180° wind direction.



# 0 DEGREE WIND DIRECTION

WIDE CURVED CANYON  
WIDTH / HEIGHT = 2.43

REFERENCE FILE : Data Base :  
TEST FHA2-33



NARROW CURVED CANYON  
WIDTH / HEIGHT = 1.00

REFERENCE FILE : Data Base :  
TEST FHA2-7

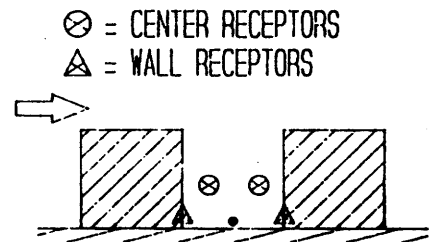
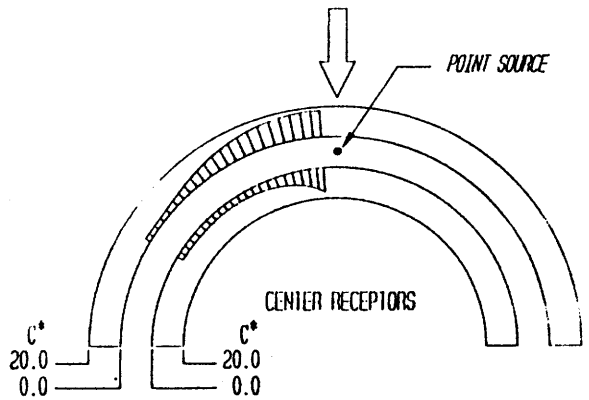
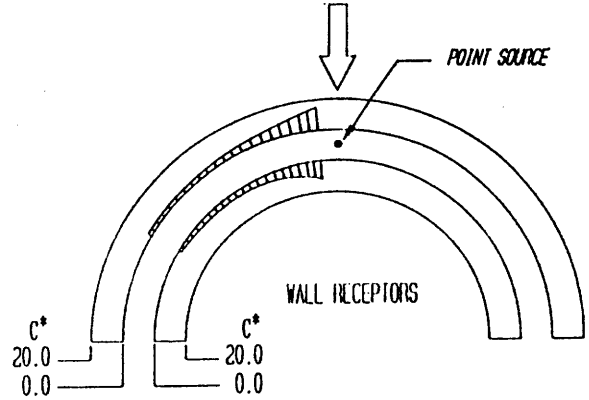


Figure 74. Concentration mapping for narrow and wide curved canyons at 0° wind direction.

dominated by turbulent mixing plunging into the canyon. This results in more clean air being pulled into the canyon and lower concentration levels.

#### Effect of Canyon Width: 180° Wind Direction

The narrow ( $W/H = 1$ ) and wide ( $W/H = 2.43$ ) canyons produce two extremely different types of flow when the wind direction is 180°. The narrow canyon develops a vortex at the apex with strong wall flow towards the apex and a reverse flow along the curved canyon center. In direct contrast, the wide canyon develops no apex vortex. Both upwind and downwind wall flows travel away from the apex, and strong canyon center flows travel toward and collide at the apex.

For the case of a point source located at the base of the upstream wall, figure 75 demonstrates that the wide canyon with flows attached to the upstream wall cause high upstream wall concentrations and almost nothing on the downstream wall. The narrow canyon produces significant concentration levels near the apex in the region where the vortex could be identified and little elsewhere.

#### Effect of Slotted Airport Terminal: 0° Wind Direction

An idealized airport terminal/parking garage configuration was modeled with a slotted parking garage as the inner wall of the curved canyon. Comparing the slotted airport terminal data to the nonslotted curved canyon setup, no significant changes in concentration are observed (figure 76). The fluid transfer through the garage slots observed in the straight 2-D slotted canyon is not prudent. Apparently, the depth and shape of the slotted garage produces the pressure gradients which are different from those which drove the fluid transfer through the 2-D slotted canyon. With the curved airport terminal, there is essentially no net flow through the garage.

#### Effect of Slotted Airport Terminal: 180° Wind Direction

Comparing the slotted to the nonslotted airport terminal garage (figure 77), the average concentrations at the 30 and 60° cross sections are lower in the canyon with the slotted garage. At the apex, cross section B, the high values are not as high and the low values not as low for the slotted case. Along the upstream wall, the center receptor concentrations are increased to the value of the wall receptors. This indicates more mixing at the canyon apex and weaker lateral flows due to the slots in the garage.

180 DEGREE WIND DIRECTION

WIDE CURVED CANYON  
 WIDTH / HEIGHT = 2.43  
 REFERENCE FILE : Data Base 2  
 TEST FHA2-20

NARROW CURVED CANYON  
 WIDTH / HEIGHT = 1.00  
 REFERENCE FILE : Data Base 2  
 TEST FHA2-23

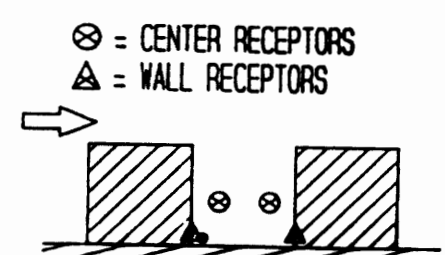
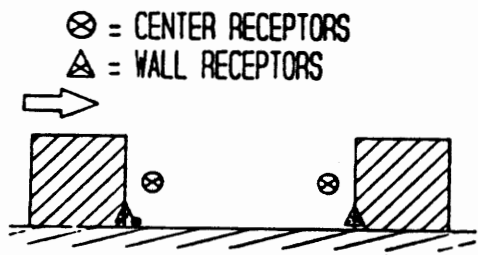
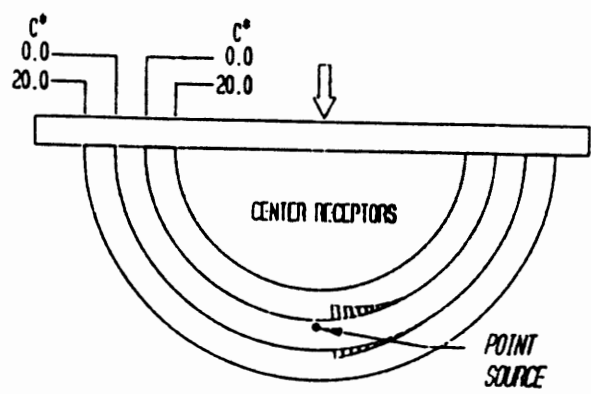
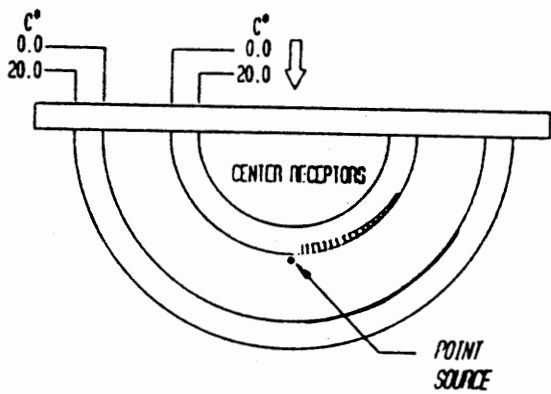
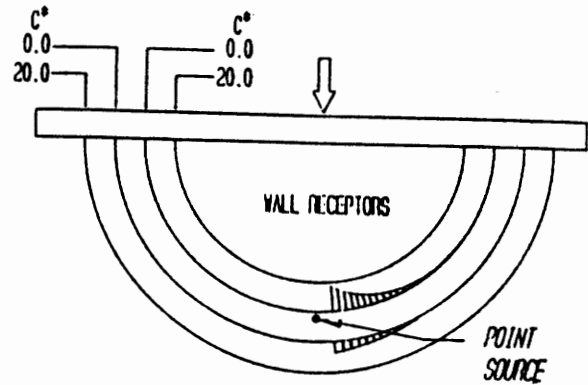
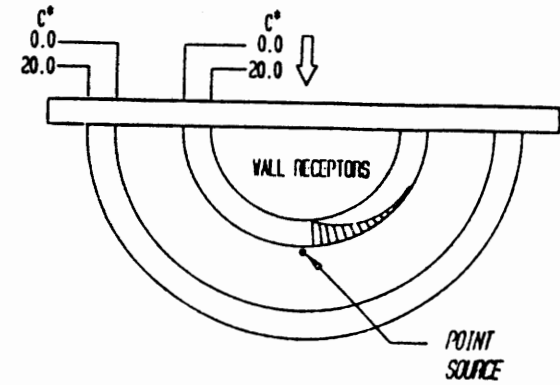


Figure 75. Concentration mapping for narrow and wide curved canyons at 180° wind direction.

# 0 DEGREE WIND DIRECTION

**OPEN WALL TERMINAL**  
 WIDTH / HEIGHT = 2.29  
 REFERENCE FILE : Data Base  
 TEST FH2-00

**CLOSED WALLED TERMINAL**  
 WIDTH / HEIGHT = 2.29  
 REFERENCE FILE : Data Base  
 TEST FH2-41

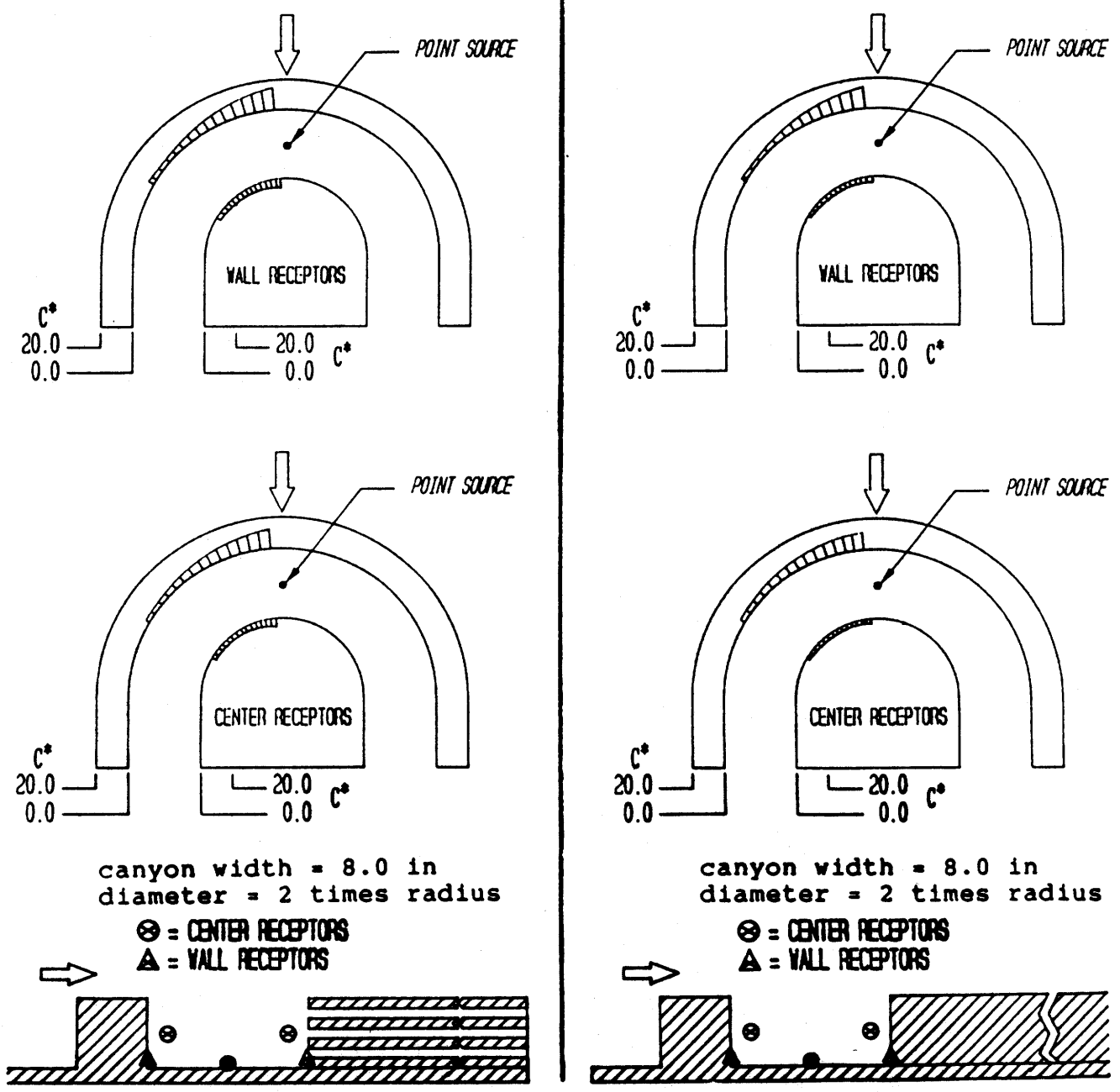


Figure 76. Concentration mapping for slotted and solid walled airport terminals at 0° wind direction.

# 180 DEGREE WIND DIRECTION

**OPEN WALL TERMINAL**  
 WIDTH / HEIGHT = 2.29  
 REFERENCE FILE : Data Base TEST FA42-55

**CLOSED WALLED TERMINAL**  
 WIDTH / HEIGHT = 2.29  
 REFERENCE FILE : Data Base TEST FA42-47

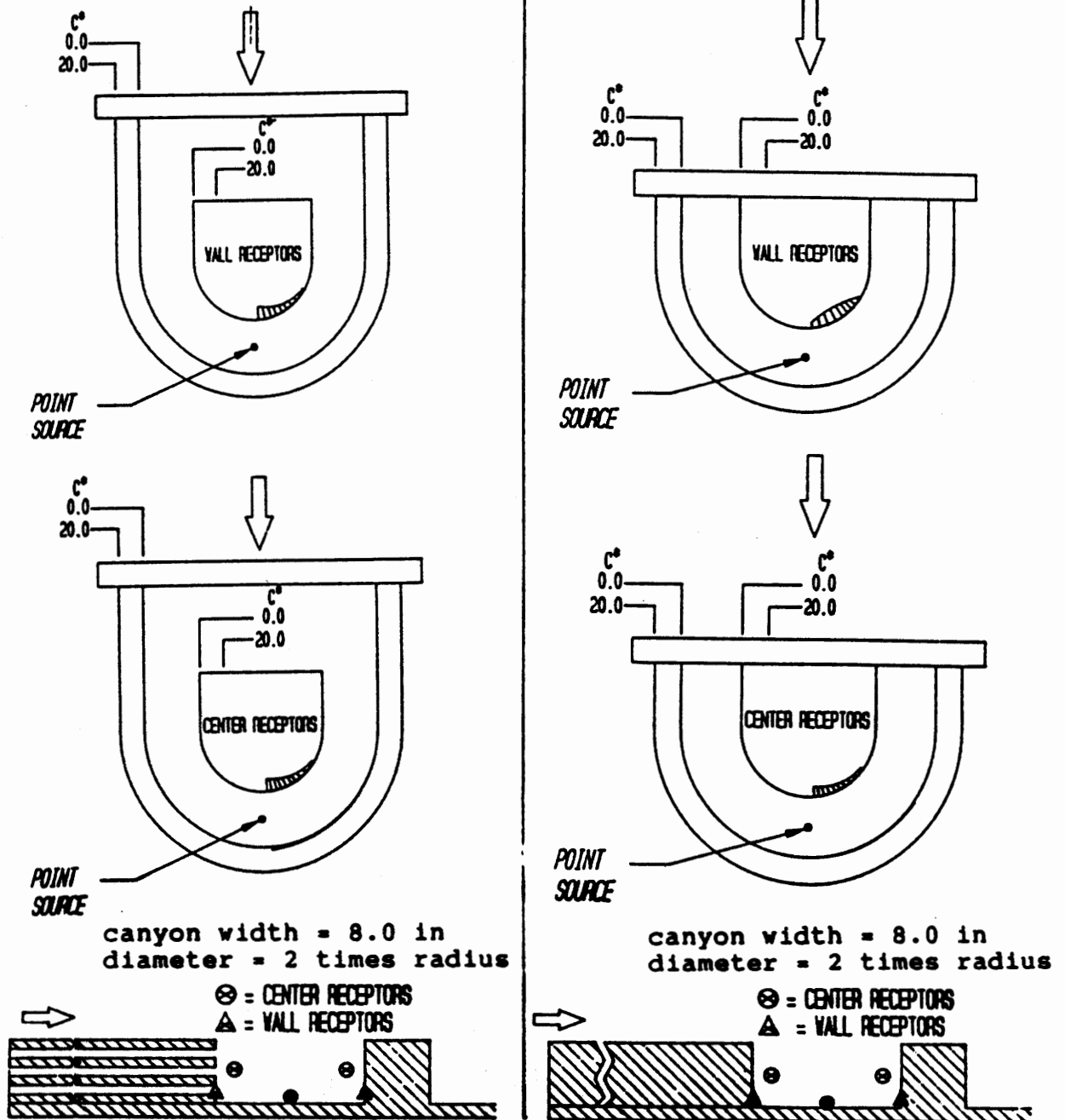


Figure 77. Concentration mapping for slotted and solid walled airport terminals at 180° wind direction.

#### D. Summary of Curved Canyon Results

The following section summarizes the effect of canyon width and slotted walls. As previously discussed, curved canyon flows are best understood by considering the 0 and 180° wind directions separately. The 0° wind produces diverging flows with the apex vortex behaving similarly to the 2-D straight canyon counterpart. In contrast, the 180° curves produce converging flows and lower concentrations. For the 0° wind direction case, slotted airport terminals/parking garages have little effect on concentration level and produce small amounts of fluid transfer between its faces. For the 180° wind direction case, more mixing occurred at the apex, and a more uniform distribution of pollutant was observed.

## 6. OBSERVATIONS AND RESULTS RELATED TO DISPERSION IN SPECIFIC URBAN SITES

### A. Overview of Tests on Nonspecific Urban Sites

Three sites were modeled in detail. Scale models were fabricated at scales ranging from 1/384 to 1/400 and tested with a line source located on a specific street. Wind directions were chosen with reference to the perpendicular line source - 0, 30, and 180 degrees. Receptors were placed at locations where full scale measurements had been made, as well as at other key locations. The concentrations were normalized using a reference length of 3.5 inches (8.89 cm), the same as in the idealized models.

### B. Analysis of Urban Sites

These three cityscapes include examples of wide canyons, deep canyons, intersections, tall buildings, etc. Diagrams of the urban sites illustrate the contrast in building sizes. St. Paul, MN has long city blocks with 2-3 story buildings (figure 78). Syracuse, NY has buildings and streets that result in close variations of the  $W/H = 1$  canyon (figure 79). In contrast, New York, NY is a series of tall buildings with frequent intersections (figure 80).

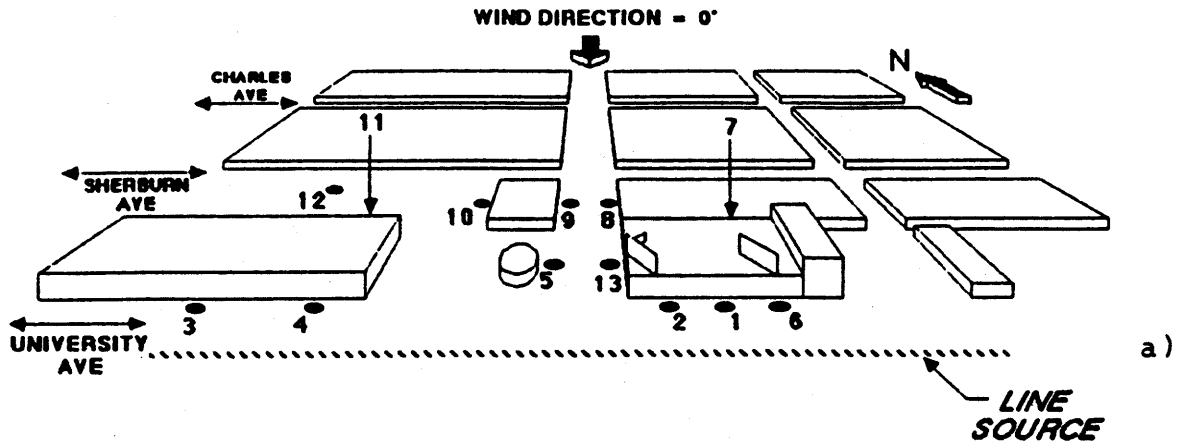
Table 10 summarizes the sites tested and identifies the data set which can be found in data base 4 of volume II.

#### University Avenue, St. Paul. Minnesota

The area of St. Paul, around University Avenue, is characterized by low buildings and wide streets. Receptor locations are illustrated in figure 81 as well as concentration levels recorded for two different wind directions. Table 11 lists the canyon cross sections at the point locations, wind direction relative to the line source, and other geometric parameters that are helpful in identifying the probable classification of the local flow.

This table lists the 10 highest concentrations observed on this site. The six highest are located at the base of the upstream wall in the wide canyons with  $W/H$  between 6.6 and 7.8. The remaining four points are located downstream from the line source in areas where the configurations resemble parking lots or open intersections.

FROM UNIVERSITY AVE LINE SOURCE FACING NORTH  
 FHA3-97  
 DATE OF TEST: MAY 27, 1987



FROM UNIVERSITY AVE LINE SOURCE FACING SOUTH  
 FHA3-97  
 DATE OF TEST: MAY 27, 1987

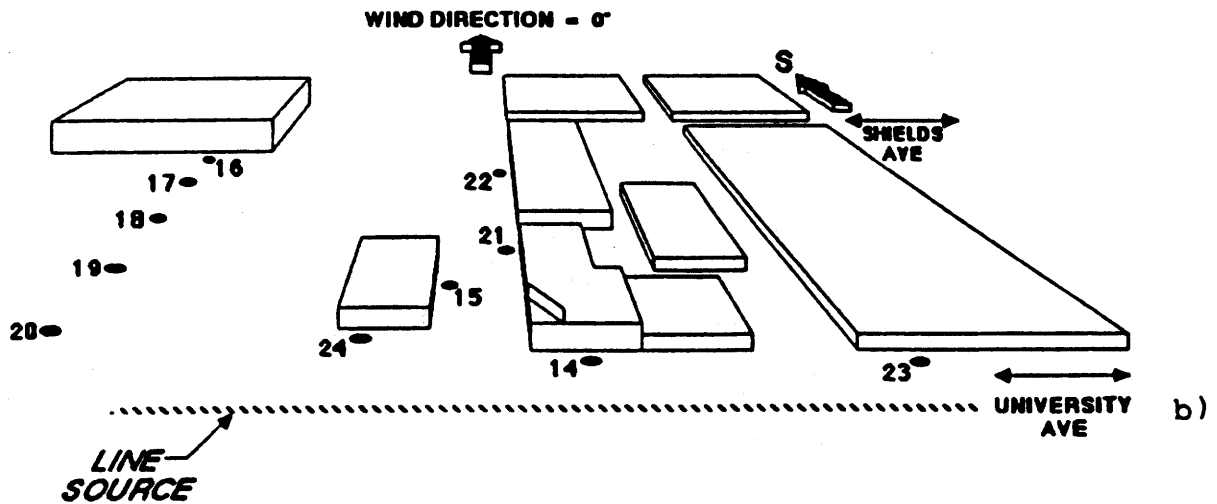


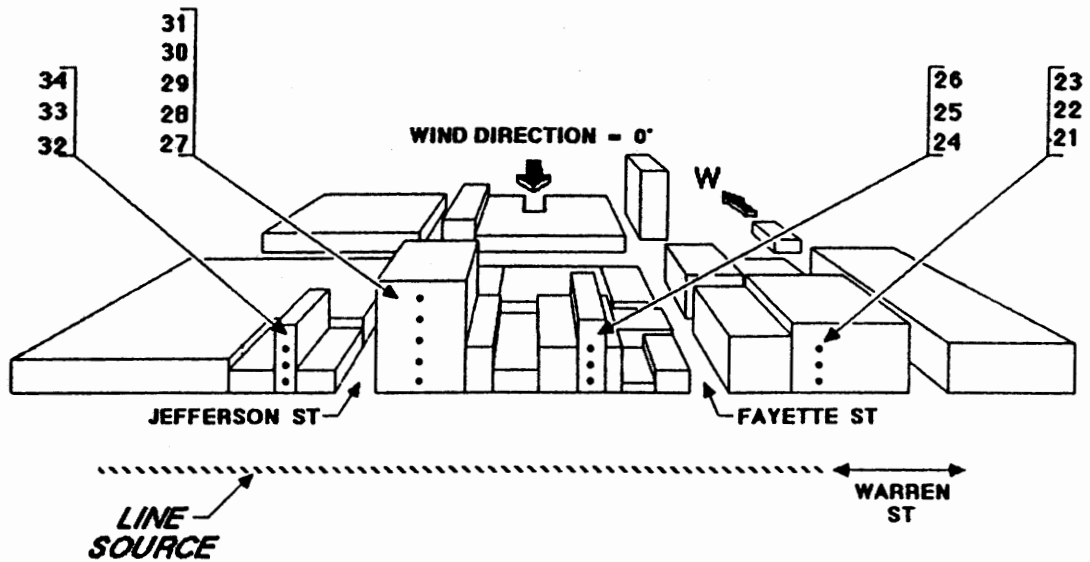
Figure 78. Perspective view of University Avenue, St. Paul, MN.



FROM WARREN ST LINE SOURCE FACING WEST

FHA3-121

DATE OF TEST: JUNE 16, 1987



FROM WARREN ST LINE SOURCE FACING EAST

FHA3-121

DATE OF TEST: JUNE 16, 1987

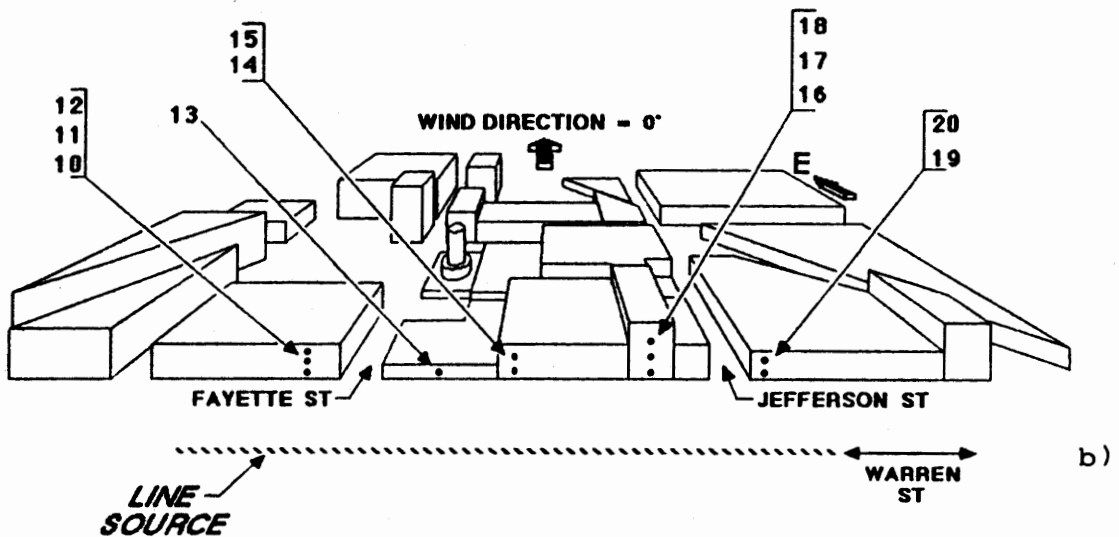
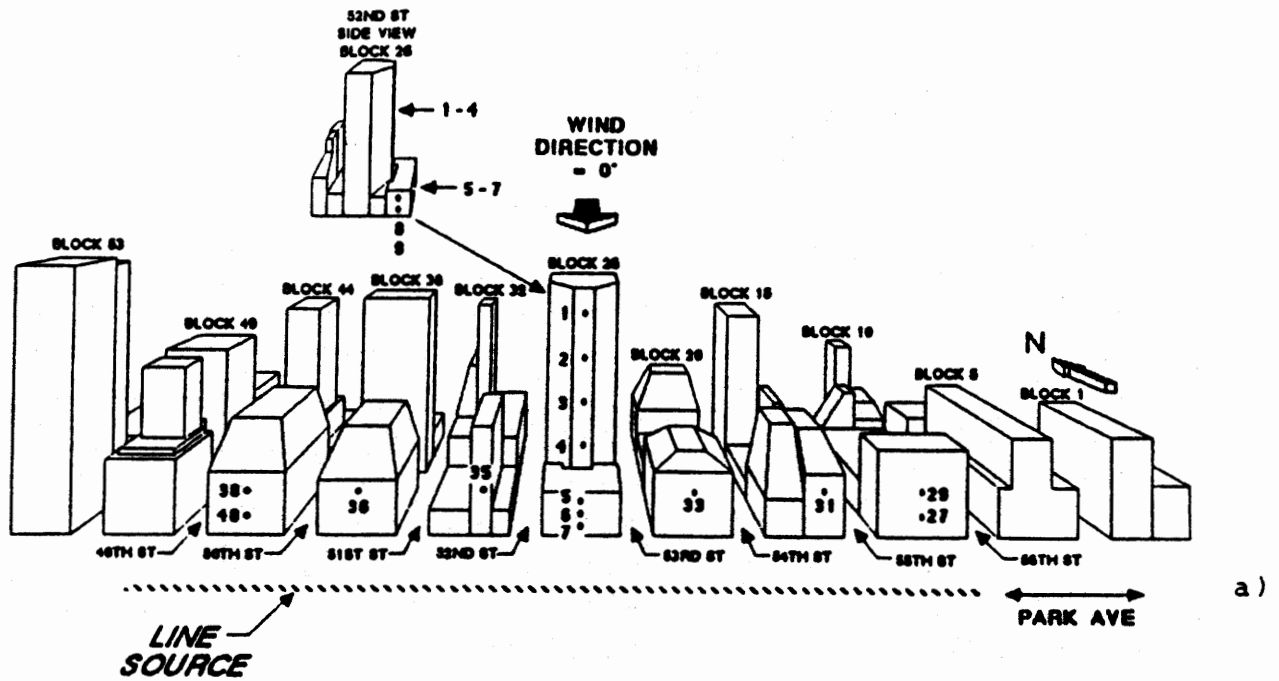


Figure 79, Perspective view of Warren Street, Syracuse, NY.

FROM PARK AVE LINE SOURCE FACING NORTH EAST

FHA3-111

DATE OF TEST: JUNE 4, 1987



FROM PARK AVE LINE SOURCE FACING SOUTH WEST

FHA3-111

DATE OF TEST: JUNE 4, 1987

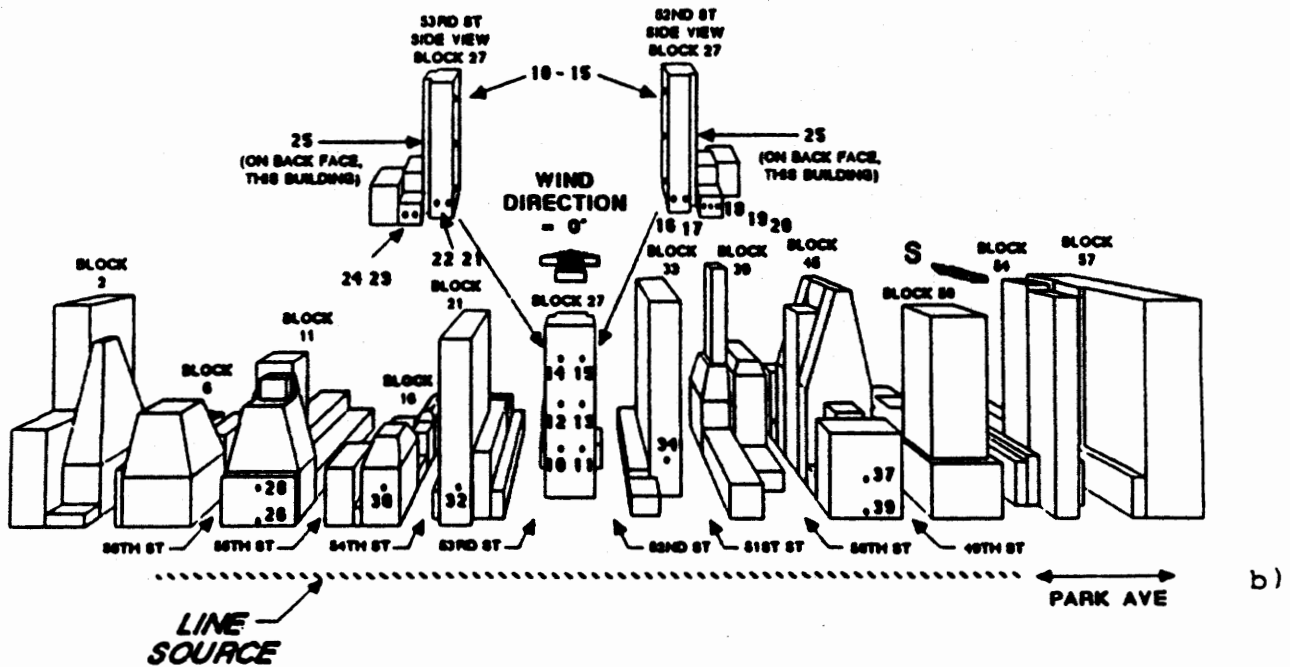


Figure 80. Perspective view of Park Avenue, New York, NY.

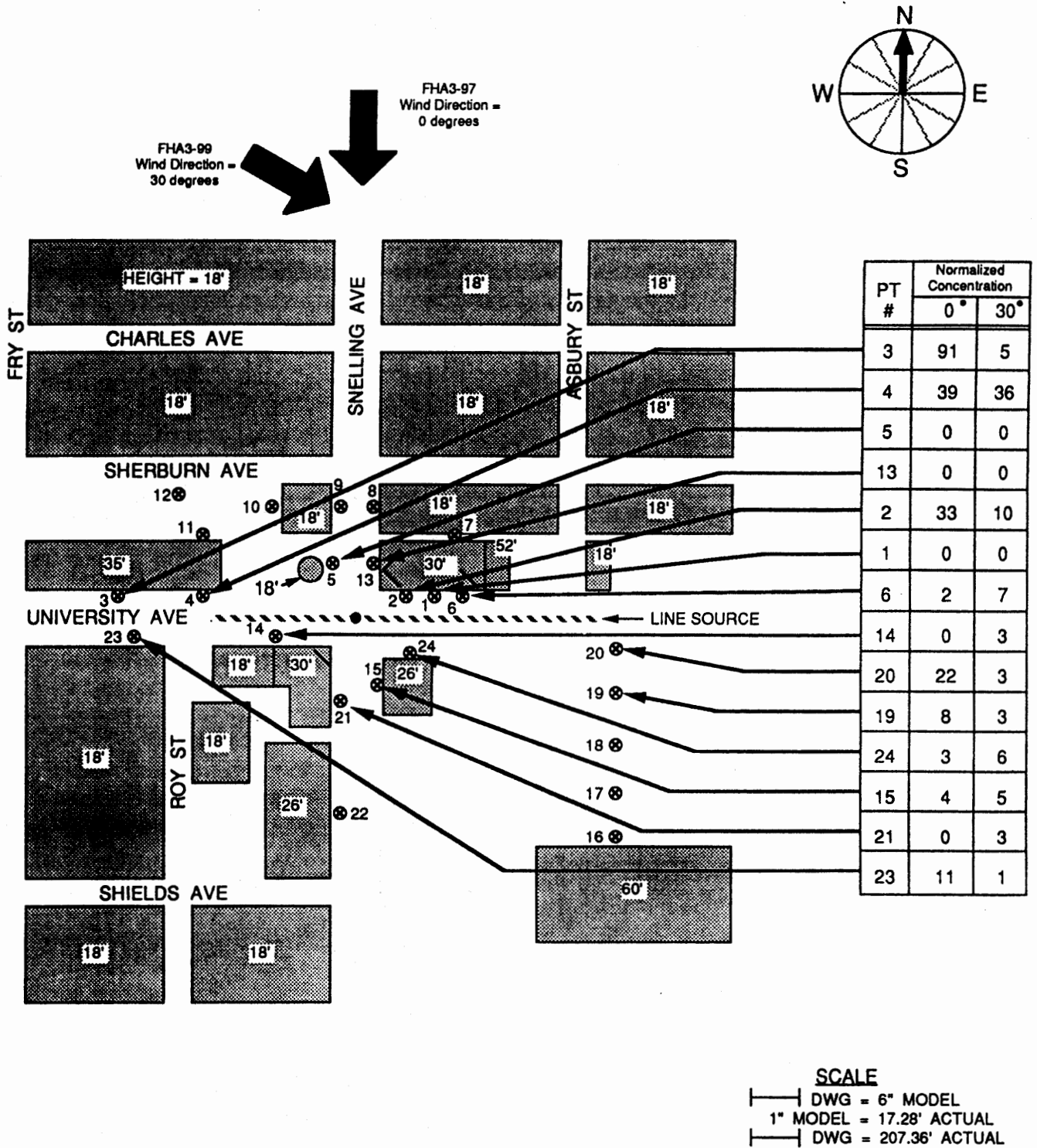


Figure 81. Plan view of St. Paul, MN with receptor concentrations and location.

**Table 10. Urban city configurations.**

Reference #	Test Description	Location
<b>St. Paul, MN</b>		
FHA3-97	0°	Line source along University Avenue
FHA3-99	+ 30°	" " " " "
FHA3-10	- 30°	" " " " "
FHA3-103	-120°	" " " " "
FHA3-105	-120°	Line source along Snelling Avenue
FHA3-107	-30°	" " " " "
FHA3-109	+30°	" " " " "
<b>Syracuse, NY</b>		
FHA3-119	+180°	Line source along Warren Avenue
FHA3-121	0°	" " " " "
FHA3-123	-30°	" " " " "
<b>New York, NY</b>		
FHA3-111	0°	Line source along Park Avenue
FHA3-113	+30°	" " " " "
FHA3-115	-30°	" " " " "
FHA3-117	180°	" " " " "

Table 11. University Avenue site, St. Paul, MN (10 highest concentrations).

Azimuth Degrees <sup>1</sup>	Conc C*	Pt#	Wind Dir. 2 Degrees	Z/H <sub>p</sub>	W/H <sub>1</sub>	W/H <sub>2</sub>	L/H <sub>p</sub>	B/H <sub>p</sub>	H <sub>1</sub> /H <sub>2</sub>	Cross Section	
1)	0	91	3	0	0.0	6.6	13.0	11.5	24.0	1.94	
2)	30	71	3	-30	0.0	6.6	13.0	11.5	24.0	1.94	
3)	30	47	2	-30	0.0	7.8	9.0	4.0	18.6	1.15	
4)	0	39	4	0	0.0	6.6	13.0	2.5	24.0	1.94	
5)	330	36	4	30	0.0	6.6	13.0	2.5	24.0	1.94	
6)	0	33	2	0	0.0	7.8	9.0	4.0	18.6	1.15	
7)	120	22	5	-120	0.0	--	--	--	--	--	
8)	0	22	20	0	0.0	--	--	--	--	--	
9)	120	19	13	-120	0.0	--	--	--	--	--	
10)	30	18	20	-30	0.0	--	--	--	--	--	

136

<sup>1</sup>Wind direction with respect to 0 degree northerly wind

<sup>2</sup>Wind direction with respect to the perpendicular of the line source

**Note:** C\* was determined using the same characteristic length as the idealized canyon, 3.5 in (0.0889 m).

W = Canyon width  
 L = Length from point to nearest intersection  
 B = City block length  
 H<sub>p</sub> = Height of wall at point of interest  
 H<sub>1</sub> = Upstream wall  
 H<sub>2</sub> = Downstream wall  
 Z = Height of point above street

The St. Paul site study shows the significance of 2-D canyons which are isolated from 3-D effects. With B/H between 18 and 24, a fully developed 2-D flow is illustrated by comparing two receptors, one near an intersection and one isolated from the effects. The first point, Number 3, has the highest concentration measured,  $C^* = 91$ . Point Number 4, which is within the 3-D effect of the corner, has a concentration only 43 percent of Point 3. This decreasing trend agrees with the results from the idealized intersection model, previously discussed in Analysis of Selected Crosscut Cases.

Other points of interest that reflect the trends of the previously-discussed 2-D models include the open parking lot (Points 16, 17, 18, 19, 20) which resemble the open highway configuration, and Point 14 which resembles an upstream facing step.

#### Warren Street Site, Syracuse, New York

The city blocks along Warren Street, between Onondaga Street and Washington Street in downtown Syracuse, were tested at a model scale of 1/226 for pollution concentrations at 34 different locations (figure 82). The length of the city block B/H range is between 3.9 and 19; the majority of the blocks being within the minimum  $B/H > 6$ , described in section, 2-D Canyons with Crosscuts, which allows 2-D flow to develop between the crosscuts.

The 10 highest concentrations measured on this Syracuse site are listed in table 12. Of the 10 points, 8 are located along the base of the upstream wall. The highest concentration recorded in Syracuse is Point 10 located near an intersection. This "hot spot" is thought to be caused by the combined 3-D effects of a tall building and an intersected 2-D canyon.

The second highest concentration, Point 24, is attributed to the leeward suction of a tall building above a 2-D canyon. Point 24 also recorded the third highest concentration, showing a reduction of pollutants due to a 30° wind direction and a true wind azimuth of North-Northwest 330°, which produces a lateral flow component in the canyon. This lateral flow component disperses the canyon pollutants as discussed in section Isolated Tall Building above an otherwise 2-D Block.

For the North-Northwest wind, receptors near the upwind end of the line source should be excluded due to the decrease of pollutants near the line source end. This would omit receptors 10, 11, 12, 21, 22, 23, since the source terminates near Washington Street.

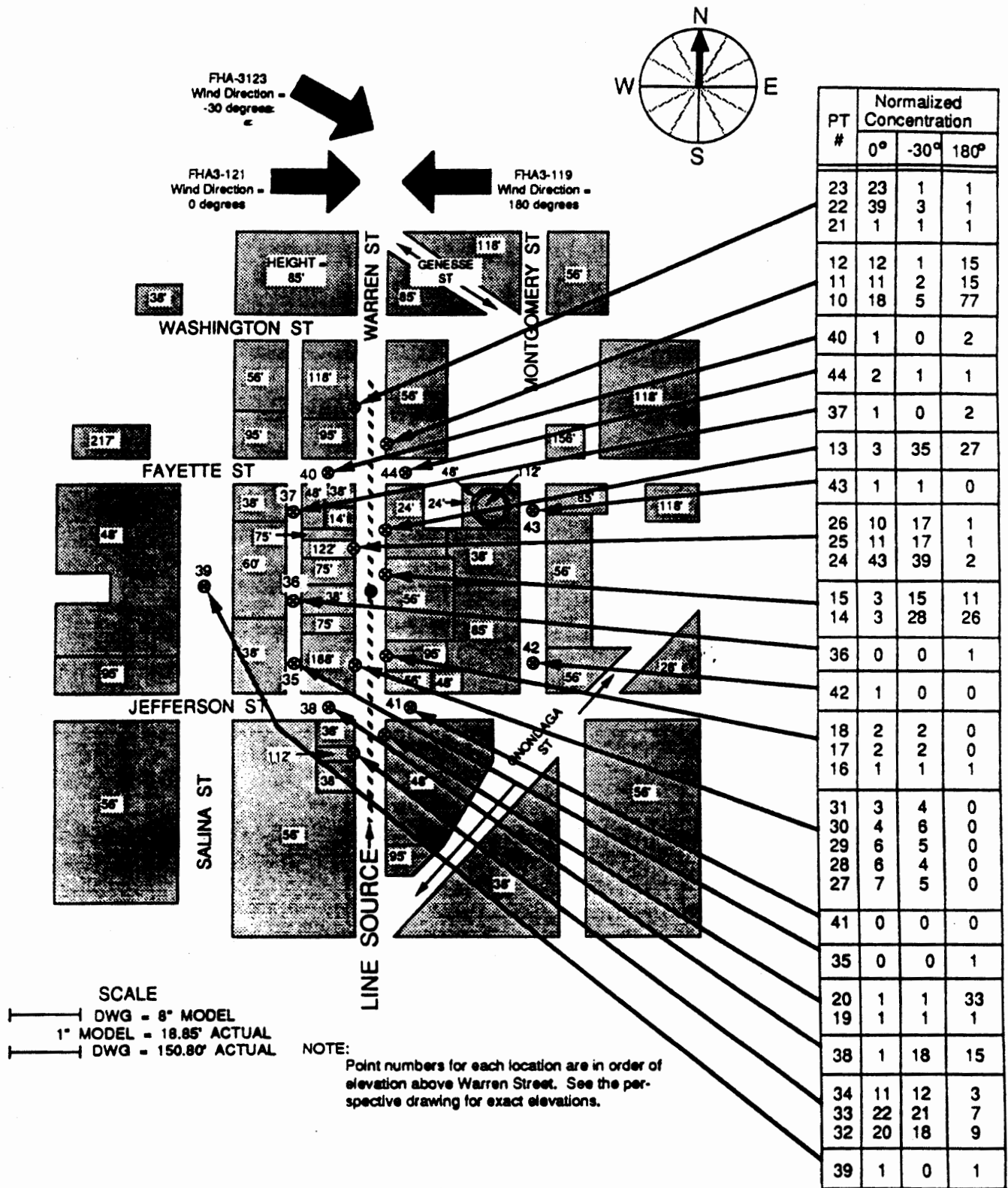


Figure 82. Plan view of Syracuse with receptor concentrations and location.

Table 12. Warren Street site, Syracuse, NY (10 highest concentrations).

Azimuth Degrees	Conc. C*	Pt#	Wind Dir. 2 Degrees	Z/H <sub>p</sub>	W/H <sub>1</sub>	W/H <sub>2</sub>	L/H <sub>p</sub>	B/H <sub>p</sub>	H <sub>1</sub> /H <sub>2</sub>	Cross Section
1) 90	77	10	180	0.164	1.1	0.65	0.9	4.9	0.59	
2) 270	43	24	0	0.076	0.5	2.6	1.3	3.9	5.0	
3) 330	39	24	-30	0.076	0.5	2.6	1.3	3.9	5.0	
4) 270	39	22	0	0.726	0.52	1.1	1.1	2.25	2.1	
5) 330	35	13	-30	0.575	0.8	2.5	3.5	19	3.1	
6) 90	33	20	180	0.575	1.3	0.55	0.7	7.4	0.4	
7) 330	28	14	-30	0.155	0.8	1.1	3.5	8.3	1.3	
8) 90	27	13	180	0.575	2.6	0.8	3.5	19	0.3	
9) 90	26	14	180	0.155	1.1	0.8	3.5	8.3	0.75	
10) 270	22	33	0	0.369	0.5	1.3	0.66	4.2	2.3	

Wind direction with respect to 0 degree northerly wind direction  
 Wind direction with respect to the perpendicular of the line source

W = Canyon width  
 L = Length from point to nearest intersection  
 B = City block length  
 H<sub>p</sub> = Height of wall at point of interest  
 H<sub>1</sub> = Upstream wall  
 H<sub>2</sub> = Downstream wall  
 Z = Height of point above street

NOTE: C\* was determined using the same characteristic length as the idealized canyon, 3.5 in (0.0889 m).



## Park Avenue and 52nd Street Site, Manhattan, New York

The pollution dispersion study in Manhattan was along Park Avenue, between 48th and 56th Streets, using a model scale of 1/384. Table 13 shows that 8 of the 10 highest concentrations are found along the base of the upstream walls. Figure 83 illustrates the receptor locations.

In contrast to the other site-specific studies, this section of Manhattan consists mainly of tall buildings. With short block lengths relative to building heights and B/H range between 0.3 and 1.5, there is little opportunity for 2-D flow to develop. Further inhibiting the evolution of 2-D flows is the variety of building heights and the relative close proximity of building corners with L/H ranging between 0.17 and 0.3.

The flow field in this section of Manhattan may be characterized by the interaction of 3-D flow fields created by flow around the many buildings. This makes it difficult to identify any specific idealized geometry that causes many of the high concentrations observed in the Manhattan model. Despite extensive mixing in the horizontal and vertical planes, "hot spots" still remain on the leeward side of many buildings.

### **C. Summary of Trends in Dispersion Measurements at Urban Sites**

Figure 84 illustrates the relative overall dispersion characteristics of the urban sites compared with some of the idealized canyon geometries. The average concentrations shown in figure 84 were calculated by selecting equal numbers of points on both sides of the street canyons in which the line source was emitting tracer gas. These near-street-level concentrations were averaged to establish a relative pollutant concentration for each site.

In the three urban sites shown in figure 84, the wind direction was always perpendicular to the street in which the line source was centered. In the 2-D cases shown, the wind direction was also perpendicular to the canyon but the position and type of source varied. The Katy Freeway (shallow sloping cut) had a line source located at width/4 from the bottom of the upwind slope. The tall building, standard canyon ( $W/H = 1$ ), and taller upstream building ( $H_1/H_2 = 2$ ) configurations had line sources located at the center of the canyon. The wide canyon ( $W/H = 2$ ) and taller downstream building ( $H_2/H_1 = 2$ ) configurations had vehicle sources located at  $0.286H$  upwind of the canyon center. The downstream-facing step was tested with a vehicle source located  $0.214H$  from the

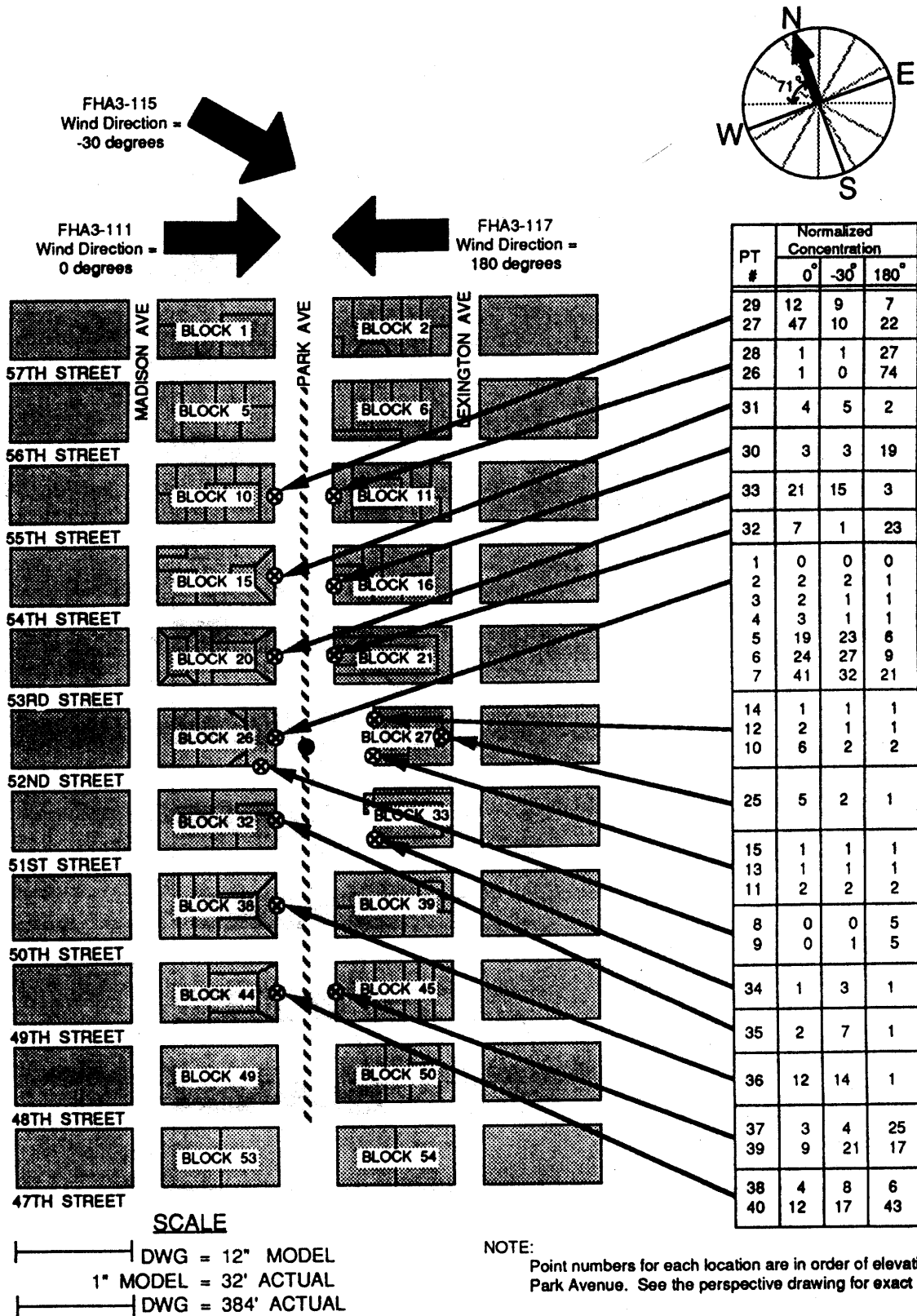


Figure 83. Plan view of Manhattan with receptor concentrations and location.

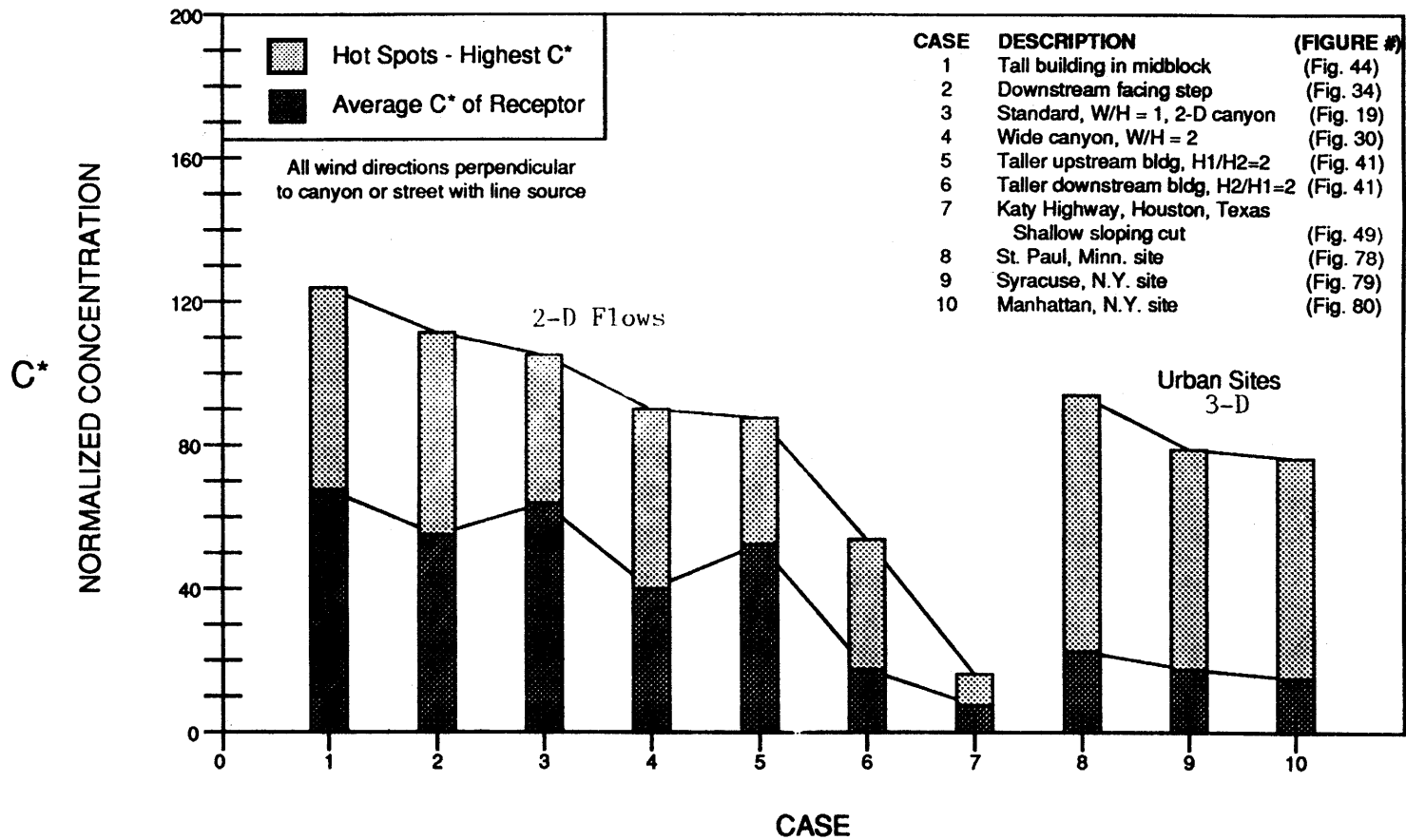


Figure 84. Comparison of concentration hot spots and averages in 2-D canyons and urban sites.

Table 13. Park Avenue site, New York, NY (10 highest concentrations).

Azimuth Degrees	Conc. C*	Pt #	Wind Dir. 2 Degrees	Z/H <sub>p</sub>	W/H <sub>1</sub>	W/H <sub>2</sub>	L/H <sub>p</sub>	B/H <sub>p</sub>	H <sub>1</sub> /H <sub>2</sub>	Cross Section
1) 109	74	26	180	0.063	0.6	0.9	0.3	0.6	1.4	
2) 259	58	27	30	0.083	0.9	0.6	0.47	0.9	0.75	
3) 289	47	27	0	0.083	0.9	0.6	0.47	0.9	0.75	
4) 109	43	40	180	0.063	0.9	0.6	0.47	1.0	0.75	
5) 289	41	7	0	0.030	0.7	1.0	0.17	0.34	1.5	
6) 259	36	7	30	0.030	0.7	1.0	0.17	0.34	1.5	
7) 319	32	7	-30	0.030	0.7	1.0	0.17	0.34	1.5	
8) 259	28	40	30	0.063	0.6	0.9	0.47	1.0	1.4	
9) 109	27	28	180	0.443	0.6	0.9	0.3	0.6	1.4	
10) 319	27	6	-30	0.093	0.7	1.0	0.17	0.34	1.5	

1 Wind direction with respect to 0 degree northerly wind  
 2 Wind direction with respect to the perpendicular of the line source

W - Canyon width  
 L - Length from point to nearest intersection  
 B - City block length  
 H<sub>p</sub> - Height of wall at point of interest  
 H<sub>1</sub> - Upstream wall  
 H<sub>2</sub> - Downstream wall  
 Z - Height of point above street

Note: C\* was determined using the same characteristic length as the idealized canyon, 3.5 in (0.0889 m).

face of the step. The table 10 (tables 11-13), averages and "hotspot" calculated for vehicle sources were normalized by using the ratio of values obtained from the standard canyon configuration with line source and vehicle source.

Intersections and varied building heights of the cityscapes increase the 3-D mixing and result in lower concentrations than the 2-D idealized canyons. There is also a wider range between average and "hot spot" concentrations in the urban sites than in the idealized configurations. As in the 2-D models, the trends of the average concentrations in the urban sites generally correspond to the trends of the "hot spots". Furthermore, the site which had the greatest tendency toward 2-D flow situations - St. Paul, MN - also showed the highest concentrations.

With respect to specific "hot spots," the following observations can be made from an examination of table 14:

1. The three concentration "hot spots" with the highest values are located in three different cities:
  - St. Paul  $C^* = 91$ .
  - Syracuse  $C^* = 77$ .
  - Manhattan  $C^* = 74$ .
2. The distribution of the top 10 "hot spots" are:
  - Manhattan 5 Points.
  - St. Paul 3 Points.
  - Syracuse 2 Points.
3. Along the base of an upstream wall near street level, 8 of the top 10 and 22 of the top 25 "hot spots" are located.
4. With winds perpendicular to the line source canyon, 7 of the top 10 occurred.
5. The remaining 3 of the top 10 occurred at wind direction of  $30^\circ$ , and two of these were at a location which was listed in the first seven for wind directions perpendicular to the line source.

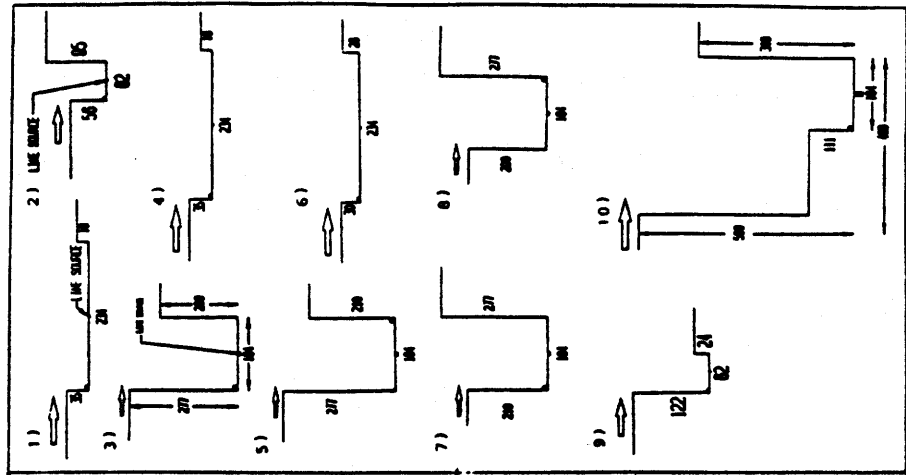
In addition to the "hot spots," many other concentrations along the upstream walls are higher than the downstream walls. This is clear in each of the cityscapes with the wind direction perpendicular to the source canyon. The concentrations along the source canyon are plotted in figures 85 (St. Paul), 86 (Syracuse), and 87 (Manhattan). The discontinuities in the

Table 14. "Hot Spot" summary.

City Point #	Asimuth Degrees	Wind Direction Degrees	L	B	H	Characteristic Flow	COMMENTS
91	St. Paul #3	North 0	11.5	24		(2-D) Wide canyon	Ideal 2-D geometry without flow obstructions or nearby cross cut.
77	Syracuse #10	East 90	0.9	4.9		(3-D) Intersected Canyon	Uneven wall canyon hot spot combined with a hot spot near a canyon intersection.
74	Manhattan #26	East 109	0.3	0.6		(3-D) Tall Building	Short city block with a taller building upstream results in a suction behind the large building.
71	St. Paul #3	NE 30	11.5	24		(2-D) Wide Canyon	Same point as highest concentration. The concentration is reduced by the introduction of the longitudinal velocity component due to the wind angle change of 30 degrees.
58	Manhattan #27	NE 49	0.5	0.9		(3-D) Combination	Introduction of 30 degree relative wind reduces suction of tall building. Possible counter rotating vortex in lower canyon causes hot spot across street.
47	St. Paul #2	NE 30	4.0	18.6		(2-D) Wide Canyon	Point location is far enough from canyon intersection so 2-D flow is predominant.
47	Manhattan #27	NW 289	0.5	0.9		(3-D) Combination	Complex tall building and intersection flow. Hot spot possibly due to pollutants being trapped by a local secondary vortex.
43	Manhattan #40	East 109	0.5	1.0		(3-D) Combination	Expected vortex in canyon similar to H <sub>2</sub> /H <sub>1</sub> = 2 but with 3-D interference due to intersection thus reducing the circulation.
43	Syracuse #24	West 270	1.3	3.9		(3-D) Tall Building	Base of suction side of exposed tall building in a city block. Although near intersection concentrations still high.
41	Manhattan #7	NW 289	0.2	0.3		(3-D) Tall Building	Base of suction side of tall building with a step locating the point nearer to the canyon center.

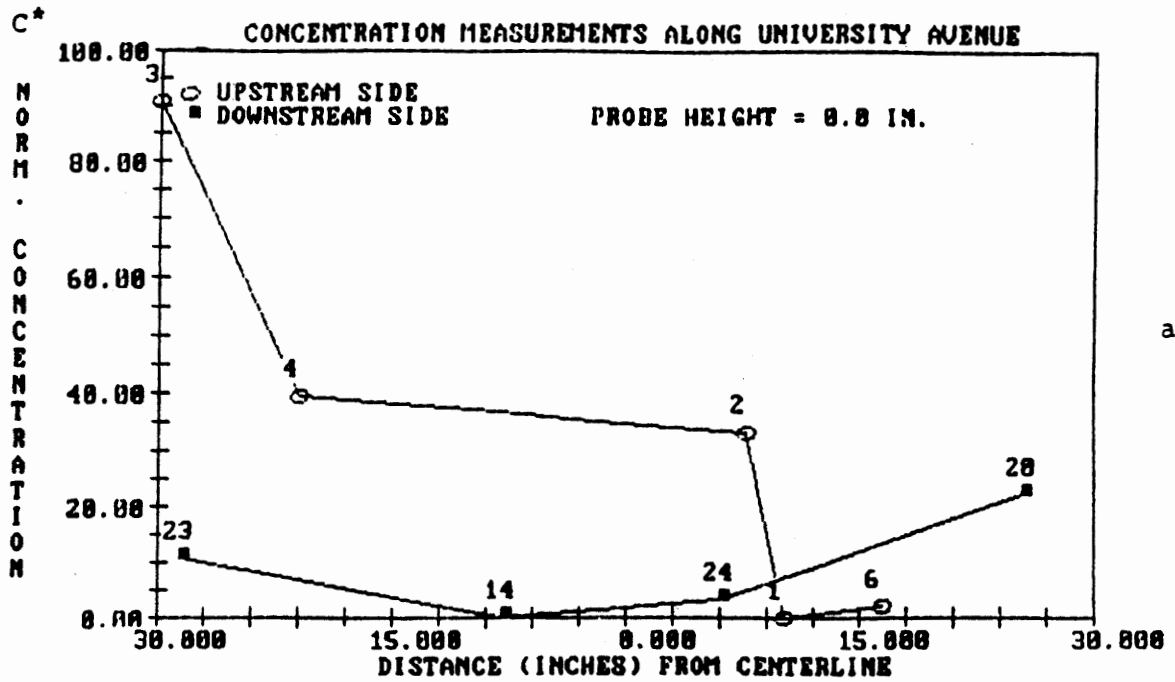
C: Normalized concentration  
 L: Length from point to nearest intersection  
 B: City block length  
 H: Height of wall at point of interest

Note: C\* was determined using the same characteristic length as the idealized canyon, 3.5 in (0.0889 m).



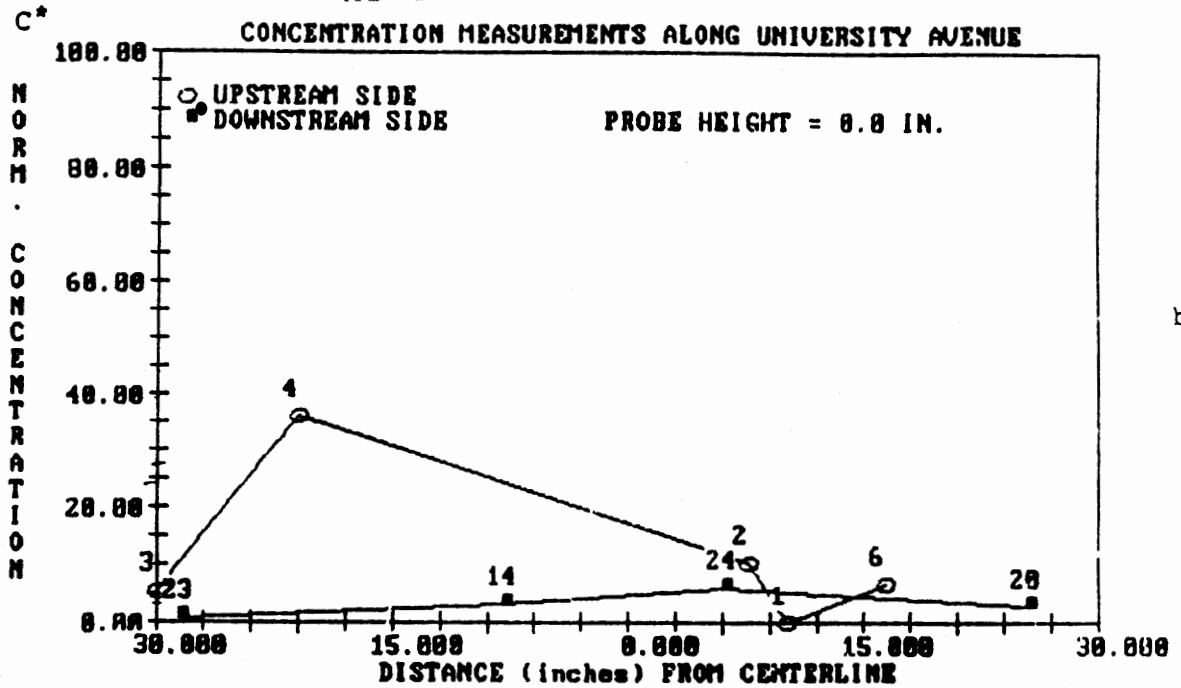
# ST. PAUL , MN

## AT 0 DEGREES



a)

## AT 30 DEGREES



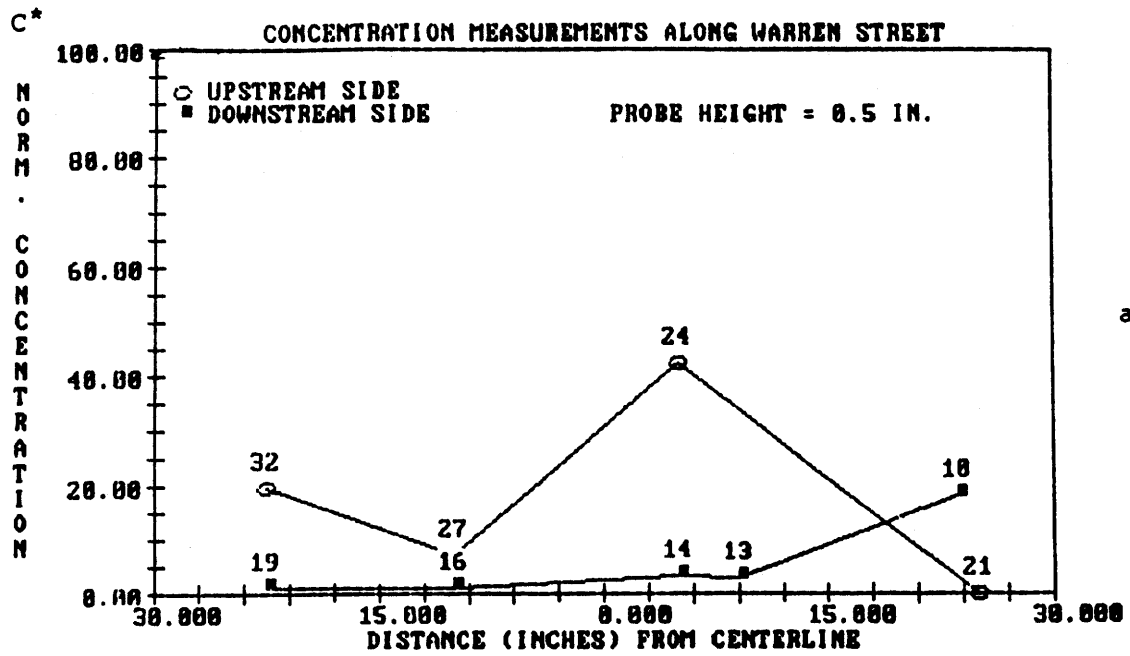
b)

1 in = 2.54 cm

Figure 85. Concentration levels near source in St. Paul at 0° and 30° wind direction.

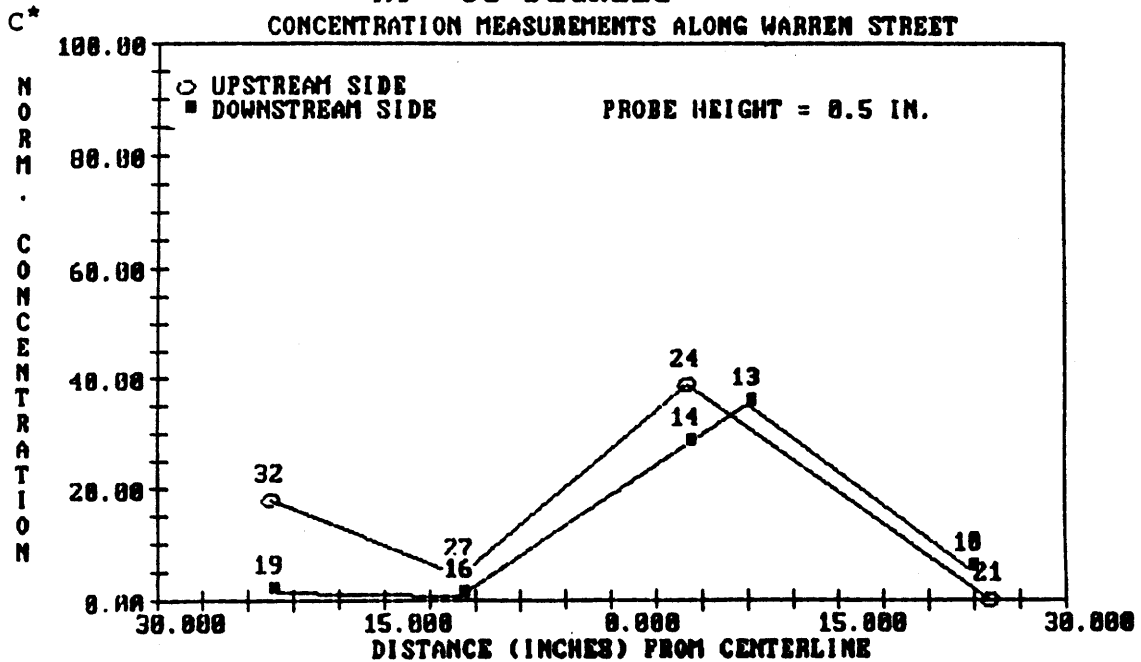
# SYRACUSE, NY

## AT 0 DEGREES



a)

## AT -30 DEGREES



b)

1 in = 2.54 cm

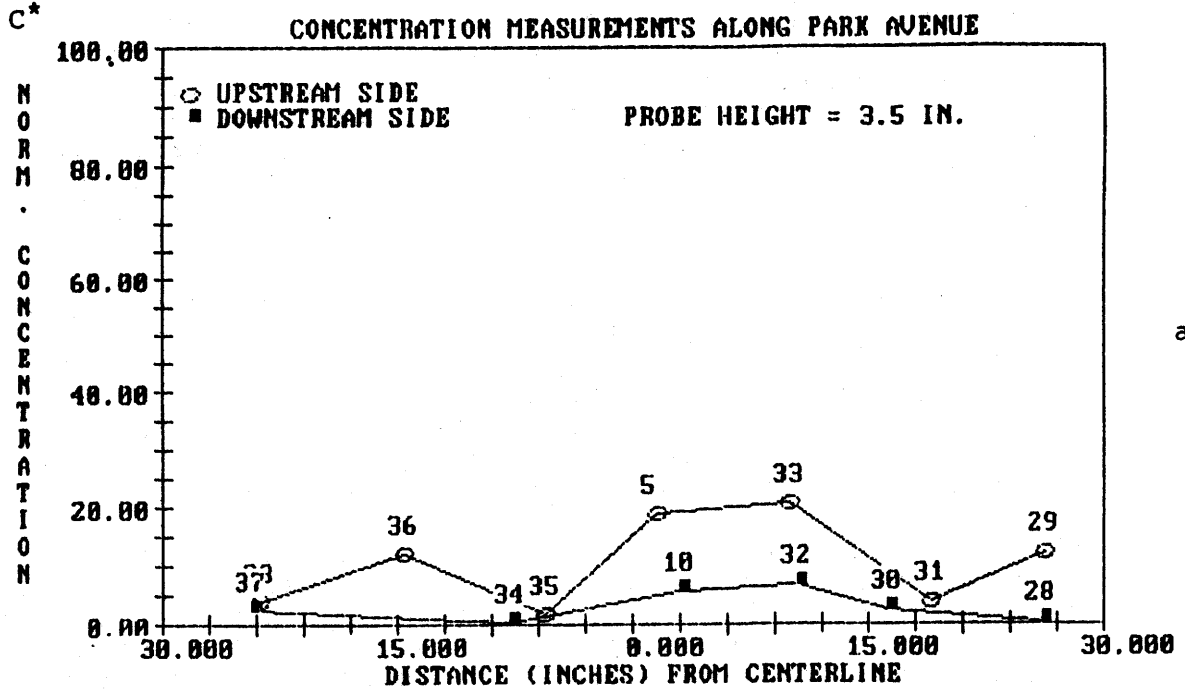
Figure 86. Concentration levels near source in Syracuse at 0° and -30° wind direction.



upstream wall curves (Points 35 and 31 for Manhattan, and Point 27 for Syracuse) are attributed to tall or unusually shaped buildings that affect the wind locally, so as to reduce the concentrations at those specific locations. In all three cities, the areas along the upstream walls show higher concentrations, and the concentrations are reduced with a 30° relative wind (figures 85b, 86b, 87b) in each case.

# MANHATTAN, NEW YORK, NY

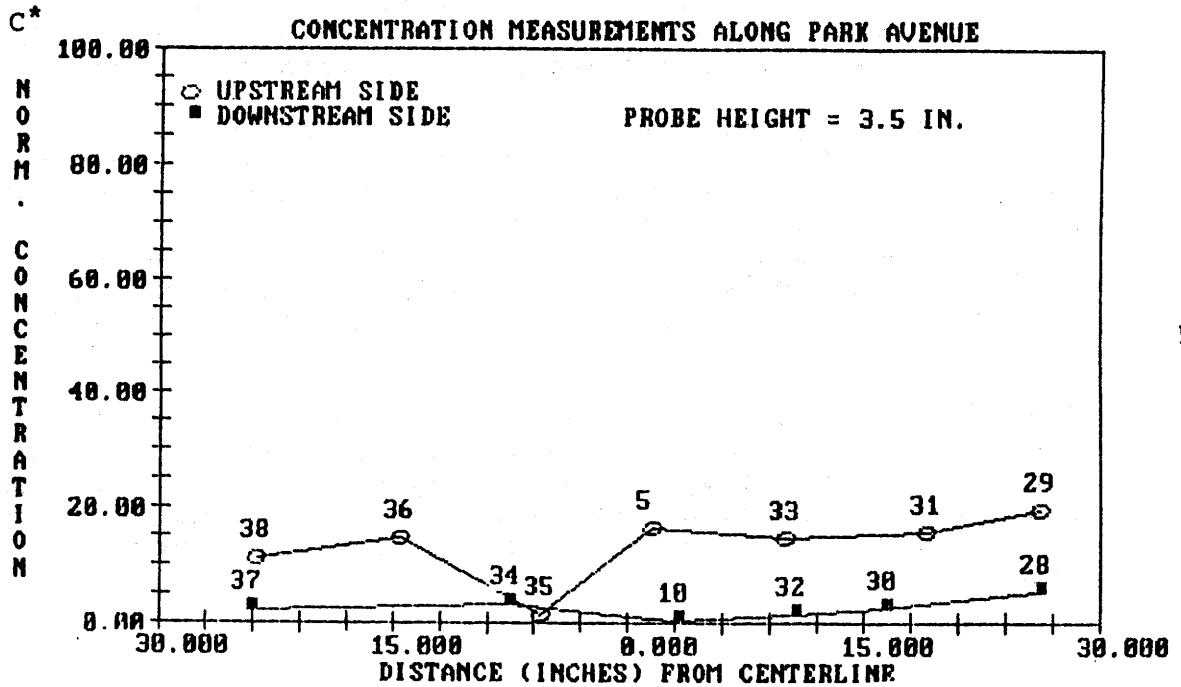
## AT 0 DEGREES



a)

## AT 30 DEGREES

1 in = 2.54 cm



b)

Figure 87. Concentration levels near source in Manhattan at 0° and 30° wind direction.

## 7. SUMMARY

### A. Conclusions

Wind tunnel studies provide a legitimate and valuable simulation alternative to costly on-site studies. The information obtained through accurate wind tunnel studies can provide a valuable data base from which computerized modelling, such as CPB-3, can be refined and improved. For geometries too complex for analytical modelling, such as site-specific cases, wind tunnel testing is the only viable alternative to full-scale studies.

The data and conclusions drawn from the body of this report also provide a valuable tool to improve the design of buildings and roadside topography to maximize the ventilation of pollutants. By determining possible high concentration configurations, one can avert problem areas by incorporating geometries which increase ventilation. These problem areas are avoided by increasing the volume of clean air channeled into the canyon.

The highest concentrations were recorded in four different types of flow geometries. First, the sheltered pocket of stagnant air at the base of a deep canyon produced the highest concentration areas. Due to the numerous intersections, varied building heights and shapes in large cities, such as New York City, a 2-D deep canyon is rarely encountered. The second highest "hot spot" occurred in the stagnant zone near the downwind base of a tall building at a perpendicular wind direction. Alleviation of the high concentration levels can be obtained by angling the building or wind direction, thus introducing a destabilizing effect in the stagnation area.

The two other geometries which produce high concentration levels consist of corners near intersections and downstream facing steps. Corner vortices form near intersections which pull pollutants into small circulating pockets and cause areas of high concentration. Downstream steps cause an area of stagnation directly behind the building. The pollutants are pulled down the street canyon into the stagnant area from up to four heights away.

Therefore, there is a potential for high concentration levels near the step, even when the pollutant source is located a sizable distance away from trailing edge. The downstream step and corner vortices effects continually produced some of the highest concentration levels recorded in the urban city configurations.

The lowest concentrations were recorded in geometries which channeled clean air into the canyon. The most effective geometries included: taller downstream buildings, upstream facing steps, and sloped walled canyons. By increasing the downstream building height, the upstream flow is forced into the canyon and increases the dilution of pollutants. The same effect is observed on the upstream face of a tall building where the pressure gradient drives the flow below the stagnation point downward into the canyon. Upstream facing steps deflect flow over the building and develop a strong, small vortex near the base of the building. The volume of clean air mixing with pollutants is large and therefore concentration levels are low.

One of the most effective methods to increase ventilation is by sloping the canyon walls. In comparison to its vertical walled counterparts, a sloped wall canyon reduces concentration levels on the order of 60 percent for "hot spots" and a 75 to 80 percent reduction in overall concentration measurements.

Therefore, introducing a sloping wall to the downstream facing step geometry would substantially reduce pollutant levels. The highest concentration zones are located in the lower velocity flow areas; thus methods for energizing flow activity in these areas should be incorporated into the design considerations.

Below are listed highlights of each section in a condensed form.

#### 2-D Flow Configurations

- Standard canyon is the most simplified 2-D flow with a strong central vortex and weaker secondary corner vortices.
- Concentration levels and distribution depend upon source location within the canyon.
- Maximum concentrations occur in the lowest velocity zones, such as near the street level on the upwind side of the canyon.
- Recirculating flow patterns produce lower concentration gradients than lower velocity, turbulent flow.
- Canopies on the upstream building increase concentration levels near the canyon center. Lateral wind components reduce concentrations in proportion to the standard canyon, approximately equal to the cosine of the wind angle.

- The presence of a slotted (or porous) wall or building on the upstream or downstream side of a line source leads to "communicated" pollutants through the slotted building; more pollutants travel from the downstream canyon to the upstream canyon than vice versa. By superimposing concentrations for a dual source configuration, the upstream canyon collects more pollutants than the standard canyon, whereas the downstream canyon is more ventilated.
- Width-to-height ratio has a profound effect on concentration levels and distribution. Five general categories of flow patterns exist:
  - Deep canyon ( $W/H < 1$ ): upper zone vortex with lower zone stagnant pocket.
  - Standard canyon ( $W/H \approx 1$ ): strong centralized vortex with intermittent secondary corner vortices.
  - Wide canyon ( $W/H > 4$ ): weaker downstream zone vortex and upstream zone stagnation pocket.
  - Downstream facing step: weak circulating flow between approximately  $2.5H$  and  $4H$  away from upstream face, large stagnant pocket upstream zone.
  - Upstream facing step: strong deflected flow with small recirculation zone.
- Downstream-facing steps trap pollutants inside a lower velocity zone in the building wake. Upstream-facing steps result in a high velocity, low concentration zone.
- Downstream buildings which are taller than their upstream neighbors channel more fresh air into the canyon and thus give rise to lower concentration levels. In comparison to the standard canyon ( $W/H = 1$ ), upstream buildings which are taller than their downstream neighbors reverse the direction and weaken the vortex; concentration trends are opposite that of the standard canyon.
- An isolated tall building in an otherwise 2-D canyon creates a "hot spot" at the base of the downwind side, and mitigates concentrations in the upwind canyon near its face. For  $\pm 30^\circ$ , the "hot spot" is substantially reduced, and the suction-induced flow caused downwind side pressure gradient adds and subtracts from the lateral flow component in the downwind canyon.

- Sloping canyon (or cut) walls create substantial ventilation of the canyon, leading to large reduction in concentration levels.
- The "average" concentration levels were approximately 50 percent of the "hot spot" for most 2-D flows; better ventilated flow configurations produced concentration averages which were a smaller percentage of the "hot spot" values.
- The highest "hot spots" and averages were the deep canyon ( $W/H = 0.25$ ), isolated tall building, and downstream step, respectively.

### 3-D Flow Configurations

- Intersections are better ventilated than their 2-D counterparts, and thus have lower normalized concentration levels.
- The effect of an intersection on the concentrations in the canyon is detected for a distance of approximately four canyon widths back from the intersection in a  $90^\circ$  crosswind in nonperpendicular crosswinds; the effect on the intersecting canyons is more-complex but still substantial.
- The three-way (or "T") intersection has better ventilation near the cut than the full crosscuts; the downwind wall records much lower concentration than the upwind wall.

### Semicircular (Airport Terminal/Parking Garages) Flow Configuration

- $0$  and  $180^\circ$  wind direction have distinct differences in flow patterns, and must be considered as distinct cases.
- 2-D vortices (similar to the standard canyon) appear at the apex in  $0$  and  $180^\circ$  narrow curved canyons; a vortex similar to the 2-D wide canyon appears at the apex in the  $0^\circ$  wide curved canyon; no vortex developed in the  $180^\circ$  wide curved canyon.
- Wider curved canyons provide greater ventilation than narrow curved canyons, and thus lower concentration levels.

- Concentration levels are highly dependent upon source locations and local flow characteristics. The 0' case concentration levels are less affected by source location than the 180' cases.
- Slotted inner curves (airport garage model) transmit little pollutants because the depth and shape of the curved building eliminates the sharp pressure gradients that drive the fluid transfer in the 2-D slotted canyon.

### Urban Site Results

- Katy Freeway, Houston, Texas, has an open sloping wall cut section and experiences low pollution levels relative to vertical walled sections.
- St. Paul, Minnesota is characterized by wide canyons with downwind facing steps. The city blocks are long with relatively few crosscuts. The concentration "hot spots" occur in areas where 2-D-like flow occurs.
- Syracuse, New York is characterized by variations of the  $W/H = 1$  canyon with height ratios among buildings in the 0.5 to 1.5 range. The canyons have relatively long blocks which promote local 2-D flow behavior, and associated concentration patterns. The "hot spots" are created by corner vortices of an intersection and taller upstream building configurations.
- Midtown Manhattan, New York, is characterized by tall buildings and "slab" buildings with frequent crosscuts; the city blocks are relatively short, which reduces the extent of 2-D flows and promotes 3-D flow. The majority of "hot spots" are found at the base of the downwind side of buildings. This is thought to be the result of corner vortices, suction on the downwind face of tall buildings, and deep canyon effects.
- Approximately 85 percent of the "hot spots" are located along the base of upstream wall.
- The "hot spots" track the "averages" calculated near the source at street level, that is, the road site with the highest "hot spot" has the highest "average."

8. REFERENCES

Builtjes, P.J.H., 1984. Determination of the flow and concentration fields in a street canyon by means of wind tunnel experiments. Draft TNO Final report.

Chock, D.P., 1982. Pollutant dispersion near roadways - experiments and modelling. The Science of the Total Environment, 25, 111-132.

Hoydysh, W.G., Griffiths, R.A. and Y. Ogawa, 1974. A scale model study of the dispersion of pollution in street canyons. APCA Paper No. 74-157, presented at the 67th Annual Meeting, June 9-1113, Denver, CO.

Kitahayashi, K., K. Sugawara and S. Isomura, 1976. A wind tunnel study of; automobile exhaust gas diffusion in an urban district. Proceedings of the Fourth International Clean Air Congress, Tokyo, April.

Leisen, P. and H. Sobottka, 1980. Simulation of the dispersion of vehicle exhaust gases in street canyons: Comparison of wind tunnel investigations and full scale measurements. IMA Conference on Modeling of Dispersion on Transport Pollution, Southend-on-Sea, England, March 17-186.

Lombardi, D.J., 1978. Steady state pollutant concentrations in an urban area. Master's Thesis, Colorado State University, Fort Collins, CO.

Skinner, G.T. and G.R. Ludwig, 1976. Experimental studies of CO dispersion from a highway model in the atmospheric simulation facility, Calspan Report No. NA-5411-A-1, Buffalo, NY.

Snyder, W.H., 1981. Guideline for fluiding modeling of atmospheric diffusion, EPA-600/8-81-009. U.S. Environmental Protection Agency, Environmental Sciences Research Laboratory, Research Triangle Park, NC, xiv and 185pp.

Sobottka, H. and P. Leisen, 1980. Vehicle exhaust gas emissions in city streets and their distribution; comparison of measurements and model aspects. IMA Conference on Modeling of Dispersion in Transport Pollution, Southend-on-Sea, England, March 17-18.



Sobotka, H. and P. Leisen, 1980. Pollutant dispersion of vehicle exhaust gases in street canyons. Proc. of the 5th International Clean Air Congress, Buenos Aires.

Wise, A.F.E., 1971. Architectural aerodynamics. 1: Effects due to groups of buildings. The Canadian Architect, 27, 467-468.

